THE COMPRESSIVE CREEP AND LOAD RELAXATION PROPERTIES OF A SERIES OF HIGH ALUMINIUM ZINC-BASED ALLOYS

MUHAMMAD ANWAR

Doctor of Philosophy

THE UNIVERSITY OF ASTON IN BIRMINGHAM

NOVEMBER 1997

THE UNIVERSITY OF ASTON IN BIRMINGHAM

THE COMPRESSIVE CREEP AND LOAD RELAXATION PROPERTIES OF A SERIES OF HIGH ALUMINIUM ZINC-BASED ALLOYS

MUHAMMAD ANWAR **Ph D 1997**

SUMMARY

A new family of commercial zinc alloys designated as ZA8, ZA12, and ZA27 and high damping capacity alloys including Cosmal and Supercosmal and aluminium alloy LM25 were investigated for compressive creep and load relaxation behaviour under a series of temperatures and stresses. A compressive creep machine was designed to test the sand cast hollow cylindrical test specimens of these alloys. For each compressive creep experiment the variation of creep strain was presented in the form of graphs plotted as percentage of creep strain (ε) versus time in seconds (s). In all cases, the curves showed the same general form of the creep curve, i.e. a primary creep stage, followed by a linear steady-state region (secondary creep). In general, it was observed that alloy ZA8 had the least primary creep among the commercial zinc-based alloys and ZA27 the greatest. The extent of primary creep increased with aluminium content to that of ZA27 then declined to Supercosmal. The overall creep strength of ZA27 was generally less than ZA8 and ZA12 but it showed better creep strength than ZA8 and ZA12 at high temperature and high stress. In high damping capacity alloys, Supercosmal had less primary creep and longer secondary creep regions and also had the lowest minimum creep rate among all the tested alloys. LM25 exhibited almost no creep at maximum temperature and stress used in this research work. Total creep elongation was shown to be well correlated using an empirical equation. Stress exponent and activation energies were calculated and found to be consistent with the creep mechanism of dislocation climb.

The primary α and β phases in the as-cast structures decomposed to lamellar phases on cooling, with some particulates at dendrite edges and grain boundaries. Further breakdown into particulate bodies occurred during creep testing, and zinc bands developed at the highest test temperature of 160°C.

The results of load relaxation testing showed that initially load loss proceeded rapidly and then diminished gradually with time. Load loss increased with temperature and almost all of the curves approximated to a logarithmic decay of preload with time. ZA alloys exhibited almost the same load loss at lower temperature, but at 120°C ZA27 improved its relative performance with the passage of time. High damping capacity alloys and LM25 had much better resistance to load loss than ZA alloys and LM25 was found to be the best against load loss among these alloys. A preliminary equation was derived to correlate the retained load with time and temperature.

Key Words: Compressive Creep, Zn-Al Alloy, Load Relaxation, Metallography.

DEDICATION

To my parents: for their great support and tolerance over the years.

ACKNOWLEDGEMENTS

I would like to express my thanks to my supervisor Dr. S. Murphy for his great help and guidance throughout the duration of this work, without whom it would not be possible to complete this project.

Acknowledgement is also made to the staff of Mechanical and Production Engineering Department of Aston University, Particularly David Farmer, Jim Jeffs, Paul Pizer, James Duggins and Keith Harrison for their valuable assistance.

I am also grateful to the Ministry of Education, Govt. of Pakistan for the financial support.

I am also grateful to my wife for her assistance in completion of my studies.

LIST OF CONTENTS

List of Tables

List of Figures

CHAPTER 1

1.0 INTRODUCTION

The Zinc alloys 2, 3, 5 and 7 became popular since their inception because they have many advantages over other types of alloys, like lower casting temperature, lower energy requirement for melting, longer die life, and superior as-cast surface qualities etc. The commercial zinc base alloys No3 and No5 have good mechanical and physical properties and therefore, are suitable for many applications e.g. in automotive applications, mechanical components, body hardware and trimmings, light fixtures, and scientific equipment, parts and frames in industrial machinery, domestic appliances and many other different applications. In recent years zinc alloys have found use in underbonnet applications where the high ambient temperature has caused some problems due to their low creep resistance. Therefore, efforts are being made to develop creep resistant alloys which could be used in such structural applications where conventional alloys are difficult to use.

Later on a new family of zinc-aluminum (ZA) high performance casting alloys was developed including ZA8, ZA12 and ZA27. Initially these alloys were used for gravity casting but now are being used in growing amounts for the manufacture of pressure die-cast components. Due to their superior properties i.e. high strength, hardness, improved creep resistance, excellent bearing and wear characteristics and lower densities as compared to conventional zinc and aluminum alloys, ZA alloys tend to be used in applications where zinc or aluminum alloys would otherwise not be used.

Due to excellent bearing and wear properties ZA27 especially can be used to produce bearings and wear components (within temperature limitation) i.e. bushing, bearings, wear plates, gears, cams etc. which can eliminate the need of costly bronze inserts, the copper based alloy used for bearing and bushing applications.

ZA alloys are general purpose casting alloys and can be cast by sand, centrifugal and permanent mould techniques. Because of their superior physical and mechanical properties, ZA alloys tend to be used in applications closer to the structural end of the application spectrum and less for decorative parts.

One property which must be taken into account is a comparatively low resistance to deformation when material is under a constant applied load, particularly at elevated temperatures which is known as creep. Creep tests are commonly performed by applying a constant stress to a specimen at certain temperature and creep data is obtained in the form of strain as a function of time. This data is used to find out the creep related parameters such as primary creep extension, secondary creep rate and time to fracture under given conditions.

At high temperatures creep becomes a major concern as a limiting factor in design. It is probable that ZA alloys can be used for service at elevated temperatures where application of conventional alloys is usually limited because of their poor creep resistance, so this need led to investigate the creep properties of these ZA alloys.

Some research has been carried out to determine the tensile creep strength of these ZA alloys in the past, but so far no attempt had been made to investigate the compressive creep behaviour of these alloys. Since compressive creep is also important in zinc alloys applications, especially when they are used in automotive applications where compression is common, it was therefore, considered of great interest to investigate the compressive creep properties of these alloys.

One important aspect of this research was also to compare the compressive creep behavior of the ZA alloys with high damping capacity alloys, Cosmal and Supercosmal, and also with aluminum alloy LM25.

For this research work a lever type compressive creep machine was designed and fabricated to carried out the creep tests, making this machine was a critical and important part of this research work.

The other important aspect of this research was load-relaxation tests of these alloys at different temperatures under constant initial preload. Castings of zinc alloys are widely used for automotive components due to their excellent mechanical properties and low manufacturing cost and screwed steel fasteners are commonly used to fix castings together or mount a casting onto another structure. However load relaxation is a problem in rivets and screw joints whenever the operating temperature is above ambient levels.

Load relaxation is the time and temperature dependent decrease in load in a fastener due to conversion of elastic into plastic strain. This data is not only important to evaluate the inelastic behaviour of a material, but can also be used to developed stress-relief heat treatments for reducing residual stresses and for the design of such mechanical elements like joints, gaskets, and springs.

Load relaxation is due to creep which allows a gradual loss in pre-load, and the low creep resistance of zinc-based alloys limits their use in certain applications. Only very limited theoretical and practical studies of these types of creep are known, so keeping in view the rising demand for zinc-based alloys, there is a need to find out the load relaxation behavior of these alloys along with other alloys at different temperatures.

The overall object of this research was to establish a better understanding of compressive creep and load relaxation behavior of zinc-aluminum sand cast alloys in general, in terms of creep kinetics and metallographic structure. Such understanding is essential for designers and will increase the scope for their application and further development.

CHAPTER 2

2.0 LITERATURE SURVEY

2.1 Creep and Creep Curve

Creep is time-dependent strain that occurs when a material is subjected to a stress for a prolonged period of time under given temperature.

Other definitions of creep by different authors are:

"Creep (elongation under load) is defined as the time dependent strain which takes place under a given constant load".(1)

"Creep may be defined as the time dependent part of the deformation which accompanies the application of stress to a solid" (2)

M S Loveday explains that creep is the name used to describe the manner in which a material deforms plastically over an extended period of time, when subjected to a stress which is normally less than its yield stress. He says that the essential thing to remember is that "Creep is time dependent deformation".(3)

Dowling(4) defines "Creep is deformation that accumulates with time. Depending on the magnitude of the applied stress and its time of application, the deformation may become so large that a component can no longer perform its function."

Conrad(5) says " Creep is the time-dependent deformation of materials which occurs under constant stress and temperature. Creep is not restricted to high temperature as is often believed but has been observed in metals down to 1.2K."

In general there are three stages in a creep curve, in addition to a stage which is considered as preliminary and is the almost instantaneous deformation obtained during the application of load.

A typical variation of creep strain with time for a specimen subjected to a constant stress is shown in *Figure 1.*

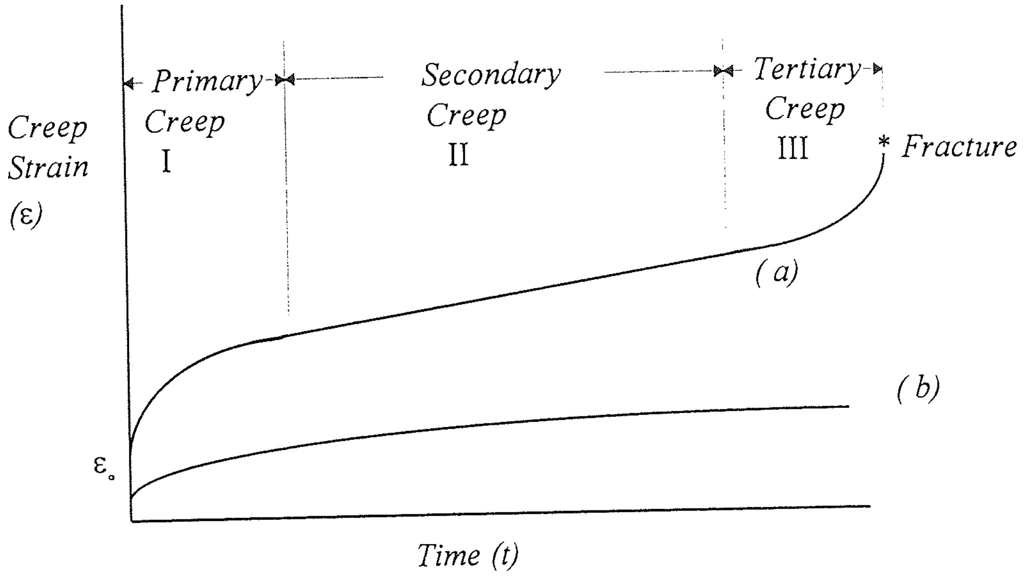

Figure 1. Typical creep curve, showing the primary, secondary and tertiary regions (curve (a) and logarithmic creep curve (b)).

Creep of metals and alloys is usually determined by a test in which a constant stress or load is applied to a specimen at a given elevated temperature, and the creep strain is measured graphically as a function of time. Creep involves plastic deformation, due to which the cross-sectional area of the specimen changes continuously.

Compressive creep is similar to the tensile creep except the load or stress applied is in compression. Compressive creep is common in industrial applications, and during the study of materials, it is therefore important to investigate the effects of compressive loads. It has been observed that the mode of failure in compressive loading is likely to be tensile or shearing failure in all materials except the most plastic materials(6). If the test specimen is relatively long, i.e. L/D > 3, failure will probably occur by buckling, as shown in *Figure2(a)*. If the length of test piece is small (L/D < 3), the plastic specimen will barrel *Figure2(b)*, because the specimen end faces are frictionally restrained by the loading faces. If the test piece material is not plastic, or if it has low shear strength, then failure may occur by shearing along a plane direction, as can be seen in *Figure2(c)* since the associated shear stress component of a compressive stress is always half the intensity of the compressive stress.

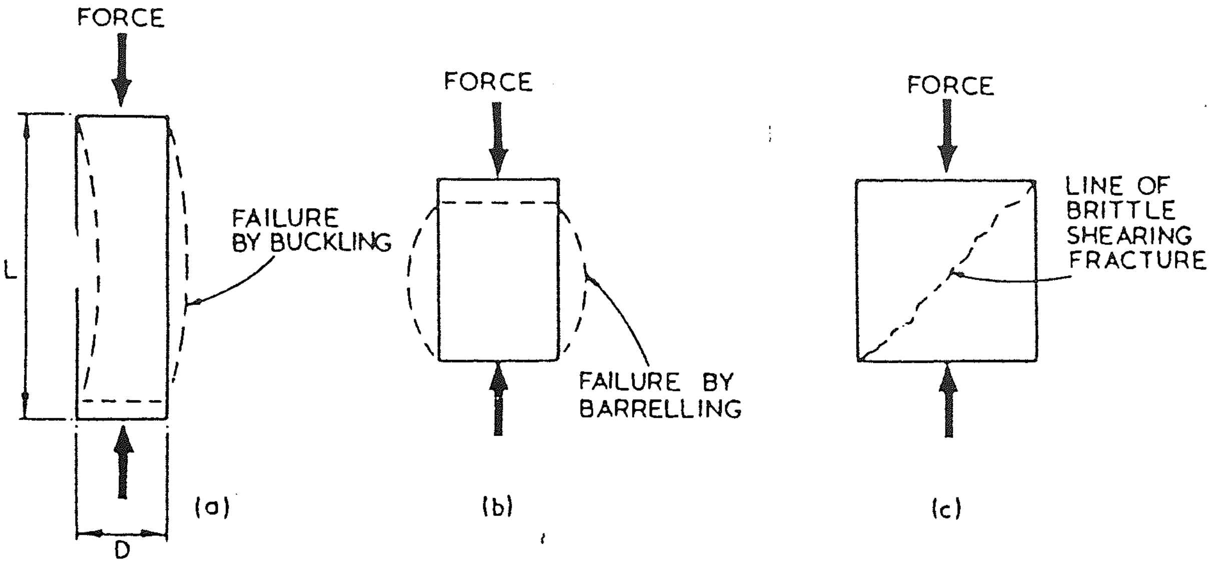

Figure 2. Failure modes in compression; (a) instability (b) bulging under frictional restraint (c) brittle shearing.

Fatigue and creep effects in compression are likely to be similar to those in tension for reasonably plastic materials except that failure is much less likely. However, in brittle materials, the difference may be large because these materials have good compression fatigue and good compression creep properties but very poor complementary tensile properties. Change of temperature is likely to have effects on compressive properties similar to those on tensile properties, except that malleability will not decrease as rapidly as ductility as the melting temperature of a material is approached(6).

The three stages of creep are:

Primary creep

The period of an initial decrease in rate to a constant value is termed as primary creep.

Secondary creep

The period of constant or steady state creep rate is known as secondary creep.

Tertiary creep

The final, accelerating stage, which usually precedes fracture, constitutes tertiary creep.

For some materials the primary stage may be absent or have an inverted form but the conventional shape shown in *Figure 1* is that most frequently found. Similarly, the extent of tertiary creep stage may be limited in some relatively brittle materials and very extensive in ductile ones. For this general description we shall consider only the classic, three-stage creep curve of *Figure 1* where the duration of each stage is roughly the same.

Generally, the creep curve of metallic alloys in compression is similar to that in tension, and has the same three characteristics, i.e. a decelerating primary stage, a secondary stage having steady-state creep rate, and a third or tertiary stage which has accelerating rate. However, there is a major difference between compressive and tensile creep beyond the initiation of tertiary creep stage, since in the latter case, the creep rate accelerates continuously until the fracture of the specimen; whereas, in compressive creep, the creep rate generally goes through successive stages of acceleration and deceleration, and fracture does not occur.

The two main differences between the results of compression and tensile creep tests were studied by Sully(7). Firstly, the initial or primary creep extension was larger in the compression test than in the tension test. Secondly, the creep results of relatively brittle materials have shown that these materials may initiate failure under axial tensile load due to the presence of stress concentrations, such as casting defects and grinding cracks, etc. On the other hand, these defects have relatively little effect on materials which are under compressive stress, and therefore the compression creep test is a better measure of the intrinsic creep resistance of these materials.

A wide variety of forms of creep curves are obtained from the creep tests, but they all include the essential stages of the typical creep curve. Generally the shape of the creep curve always depends on the stress (load) applied or temperature level, e.g. the creep curve may consist of only two stages at very low stresses for a fixed temperature. Secondary or steady-state creep, with almost constant creep rate, lasts for a very long time and neither failure nor tertiary stage with accelerated creep rate may occur at all. It is also shown that the secondary creep rate is very small at low stresses(8). Contrary to low stresses at higher stresses, the failure occurs after a short period of test. In this case, steady-state creep may be non-existent, or of very short duration because the tertiary creep or failure may be observed almost immediately after the primary creep(8).

Another important characteristic of the creep phenomenan is that the longer the creep test, the smaller the total creep extension is obtained. The creep phenomenon has two aspects, one is concerned with deformation, while the other with creep rupture or fracture. Both deformation and creep rupture are considered as important factors in many applications.

2.2 The Three Main Types of Creep

The creep observed in a test may be classified as belonging to one of the three well-defined types. The type of creep depends upon the test temperature and applied stress. The temperature-stress diagram of *Figure 3* indicates the region in which each of these types is to be found.(9)

Two different metals may be treated on the same footing if temperature is plotted as T/T_m rather than simpley T, and stress is plotted as σ/μ instead of simpley σ; where

T= Test temperature, T_m= Melting Point,
σ= Applied Stress, μ= Shear Modulus

Once temperature and stress are modified by dividing them by T_m and μ, the different types of creep of different metals and alloys fall roughly in the same regions on the creep diagram even though metals/alloys tested differ widely in their melting points and elastic constants.

The upper limit of the diagram is set by the theoretical shear stress which represents the stress required to cause shear of one plane of atoms over an adjacent plane, and the bottom limit is set by critical resolved shear stress which represents theoretical stress below which the amount of dislocation motion is slight. Extensive dislocation multiplication and motion of dislocations can take place if the stress is above the critical resolve shear stress σ_{crss} thus more plastic deformation take place at this stress as compared to the stress below σ_{crss}.

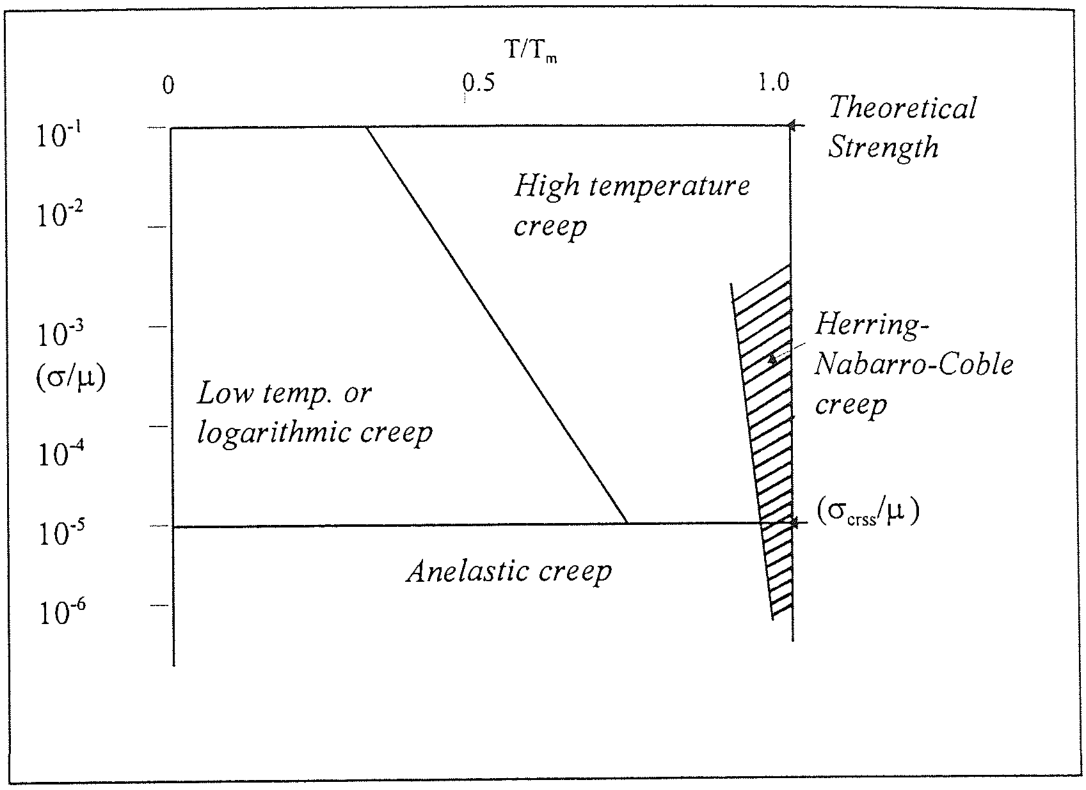

Figure 3. The creep diagram: the conditions of temperature and stress which produce the three principal types of creep, and under special circumstances, Herring-Nabarro-Coble creep.

The creep due to stresses smaller than the σ_{crss} arises through mechanisms other than large scale of motion of dislocations(9). Although this creep contributes to the process of creep in the region above σ_{crss} but this contribution to the strain is negligible compared to the dislocation contribution. *Figure 3* represents two regions, one embraces the high temperatures in which dislocations have two degrees of freedom, whereas other corresponds to temperatures (low temperatures) which permit only one degree of freedom. The boundary between two regions will shift to the right for a short-time tests and to the left for a very long-time tests.

2.2.1 Logarithmic or Low-Temperature Creep

When a sample is deformed by a stress which is more than the critical resolved shear stress and the test temperature is relatively low, i.e. below about 0.5 of the absolute melting temperature of the metal, it will be difficult for edge dislocations to move perpendicular to their slip planes. The applied stress causes deformation by producing dislocation multiplication and moving dislocations over long distances. Recovery does not take place due to lack of thermal activation at low temperatures and causes an unrelieved work-hardening mechanism, which makes motion of dislocations on slip planes more difficult and eventually causes the dislocation multiplication to stop. This reduces the creep rate almost to zero.

Since diffusion is slow at low temperatures, therefore, the motion of dislocations in directions other than parallel to their slip planes is also slow. It can be predicted that creep of a transient nature occurs in the low-temperature region of the creep diagram. In this region of the creep diagram, thermal stress fluctuations help in the process of deformation and, therefore, creep strain is produced. However, with the increase of deformation, the stress fluctuations also increase the hardening of the sample. As a result, the more a sample is deformed, its further deformation becomes more difficult. Therefore, the rate of creep deformation decreases with increasing time and the contribution of low-temperature creep to total creep strain is also comparatively small. This type of creep is called low-temperature creep or logarithmic creep because the strain depends logarithmically on time.

Low-temperature creep is of a transient nature because creep rate decreases to zero as the inverse of the time. The creep equation determined from measurements at low temperatures is given by(9):

$$\varepsilon = \varepsilon_e + \varepsilon_p + \varepsilon_o \log(1 + \nu t) \qquad (2.1)$$

which gives the creep rate as:

$$\dot{\varepsilon} = \frac{\varepsilon_o \nu}{1 + \nu t} \qquad (2.2)$$

where, ε_e is the elastic strain, ε_p the instantaneous plastic strain, and ε_o and ν are constants which depend on stress and the test temperature.

Logarithmic creep has been observed in polycrystalline aluminium and copper below 200K, some hexagonal metals at low temperatures, and some other materials such as rubber and glass(10). Some form of transient creep always occurs at all temperatures but it does not necessarily to obey the logarithmic law(10).

2.2.2 High-Temperature Creep

Creep is considered principally a high-temperature phenomenon in most of engineering materials(11). It is recognised that the melting point of the alloy or metal under creep test is important and the temperature at which creep becomes significant, is related to the melting point. Creep deformation can be observed at low temperatures but it is not very important for all practical purposes when test temperature is between zero and $0.3T_m$, where T_m is the melting point of the material in degrees Kelvin. On the other hand, when the test temperature is raised above $0.3T_m$ (according to some researchers $0.4T_m$(17) and $0.5T_m$(12)), creep deformation becomes significant(11).

At high temperatures, the dislocations acquire a new degree of freedom. The dislocations can climb as well as glide and they are no longer restricted to move only in their original slip planes. Since slip occurs on new slip planes, the rate of work hardening is reduced. It is recognised that at these temperatures, large creep strains can be produced in some tests without specimen failure. The creep strains are also much greater than the relatively small strains found in the anelastic and low-temperature portions of the creep diagram.

Unlike low-temperature creep, high-temperature creep is not due to the effect of thermal stress fluctuations on the dislocation structure of a work-hardened metal. Therefore, high-temperature creep deformation is a unique deformation mechanism and it always is considered separately from creep which occurred at low temperatures. The relative amount of transient creep in the high-temperature field of creep diagram depends on the exact temperature and stress.

2.3 High Temperature Creep Mechanisms

The secondary or steady state creep stage is the most important and the mechanisms or theories of high temperature creep are therefore concerned with the steady state part of the creep curve.

2.3.1 Climb-Controlled Glide Model

The theory for dislocation-climb for steady-state creep was first proposed by Weertman(14). It was based on the climb of edge dislocations. First, Weertman used Mott's mechanism of dislocation-climb to develop dislocation-climb theory. This theory was a major advancement in the rationalisation of the mechanical behaviour of metals at high temperatures(13,15), however, it was limited only to pure metals or simple alloys(14). According to this theory, the rate-controlling process during steady-state creep is the diffusion of vacancies between dislocations which create vacancies and those which destroy them. The proposed creep equation is(14) :

$$\text{Creep rate} = \text{constant}\,(\sigma^{\alpha} / kT)\exp(-Q / kT) \qquad (2.3)$$

where σ is the applied stress, α a constant ($\alpha =$ 3 to 4), k Boltzmann's Constant, T the absolute temperature and Q is the activation energy of self-diffusion. This process usually exhibits an activation energy equal to that for lattice self-diffusion (Q_d) at temperatures above $0.5T_m$, but there are number of cases where values of Q_c of ~ 0.5-$0.6Q_d$ have been observed over a limited range of temperature below $0.65T_m$.

Later on, Weertman(16) proposed another dislocation-climb model for steady-state creep which was slightly different from the first model. According to this second model, the production of immobile dislocations was not required(16)

The relation between creep rate and stress can be expressed by power laws in both models. However, for polycrystals, the first model gives a power of 3 and the second model a power of 4.5. But later on, it was revealed that only the second model was in reasonable agreement with experimental results(16,17). Weertman considered a case where dislocation loops were emitted from fixed and more or less uniformly distributed sources and were confined to their glide planes. The leading dislocations were eventually arrested at obstacles and, after a sufficient number of dislocation loops had been emitted, the back stress (elastic in nature) prevented further source operation(16). For a constant stress, this situation would rapidly lead to a discontinuation of dislocation motion and therefore, of deformation. However, the leading dislocations of the pile-ups would continue to climb and annihilate. After the annihilation, a new dislocation loop might be emitted from the source(17) and therefore, creep would continue. In this case, the climb rate was assumed to be controlled by diffusion because at high temperatures, dislocations can climb with the help of a diffusional mass transport of atoms(19). It was also assumed that every atomic position on the climbing dislocation line would absorb or emit vacancies efficiently(15). On this basis, Weertman expressed the creep rate ($\dot{\varepsilon}$) by the following equation (20)

$$\dot{\varepsilon} = \frac{3\pi^2\sigma^2 D}{2\sqrt{2}\mu^2 b^2} Sinh\left(\frac{\sqrt{3}\sigma^{2.5} b^{1.5}}{8\mu^{1.5}\sqrt{MkT}}\right) \qquad (2.4)$$

where σ is the measured stress, D the self-diffusion coefficient, $D = D_A D_B / D_A C_B + D_B C_A$, where C_A and C_B are the fractional concentrations of the alloy species and D_A and D_B are their diffusion constants, b the length of the Burgers vector, μ the shear modulus, M the density of Frank-Read sources on one slip system, k Boltzmann's constant, and T is the absolute temperature. This equation reduces to the power law equation at low stresses(20).

$$\dot{\varepsilon} = \frac{3\sqrt{6}\pi^2\sigma^{4.5} D}{2^5\sqrt{b}\sqrt{M}\mu^{3.5} kT} \qquad (2.5)$$

This equation predicts a stress exponent of 4.5. The model has been proved experimentally and is valid for various alloy systems(20). The main characteristic of this model is that it correlates quite well with most of the mechanical data on high-temperature creep and, therefore, is considered as one of the major mechanisms which operate at high temperatures. However, the stress exponent (n) depends on the content of alloys over the stress levels where the power law is valid. The results show that the value of exponent decreases from 4.5 for pure metals towards close to 3 by increasing the alloy content(20).The same trend was also reported for many solid solution alloys due to the increase of stress(21).

This suggests that there is a transition in creep behaviour from climb-control at low stresses to control by viscous glide at high-stress levels(21).

2.3.2 Viscous Glide Model

During the process of dislocation-climb, it has been experienced that dislocations glide and climb alternately. Since dislocation-climb and viscous-glide are two sequential processes, the measured steady-state creep rate is controlled by the slower process(21). This has led to the development of a model based on viscous glide, which applies only to solid solution alloys and the deformation is governed by one of the micro-creep mechanisms proposed by Weertman. This mechanism suggests that there is the possibility of a transition to control by viscous glide as the stress is increased.

According to the viscous-glide mechanism, dislocation motion under stress is controlled by solute drag of the dislocation line which controls its velocity. The creep rate ($\dot{\varepsilon}$) is then given by the following equation(20):

$$\dot{\varepsilon} = \frac{0.35\sigma^3}{\mu^2 A^2} \qquad (2.6)$$

where A is a constant which depends upon the solute-dislocation interaction that is viscously retarding dislocation glide and it can be evaluated from the particular micro-creep mechanism. The equation for creep rate shows that the creep rate of solid solution alloys is proportional to the third power of stress which indicates that viscous glide is a slower process than dislocation-climb mechanism. This glide behaviour, however, is different from the low-temperature glide behaviour of yield because due to the diffusion available at elevated temperatures, the dislocation structure recovers as rapidly as the deformation proceeds, thereby allowing steady-state creep deformation to be measured(23).

Among the different viscous drag processes so far proposed(20-22), the major force retarding the glide of dislocations is the presence of impurity atmospheres(24) or atoms. It has been observed that viscous glide of dislocations occurs due to interactions with impurity atoms. These interactions include(12):

(i) Elastic or Cottrell interaction between the stress field of a dislocation and the stress field caused by the misfit of solute atoms in the lattice.

(ii) Short- and long-range order interaction arising from the energy change as order is destroyed by a moving dislocation.

(iii) Electrostatic interaction between the conduction electron distribution near a dislocation and the screened charge of solute atoms.

(iv) Chemical or Suzuki interaction arising from the segregation of solute atoms to stacking-faults of extended dislocations.

(v) Snoek ordering interaction between dislocations and interstitial atoms.

These interactions also play a role in the resistance of an alloy to recovery. Once a dislocation distribution is established by deformation , recovery tends to change such a distribution through dislocation rearrangements. The overall effect of the interaction between solute atoms and dislocations is to resist such rearrangements and therefore recovery.

2.3.3 Dislocation-Jog Model

A jog is defined as a point where a dislocation jumps from one plane to another. The jogs on a screw dislocation are always edge jogs. If the screw dislocation is forced to move, it is observed that jogs can not maintain their positions in the dislocation by glide in their own slip planes, and it is possible only by climb of the jogs.

There are two types of jogs(17) :

(i) Vacancy-emitting jogs and (ii) Vacancy-absorbing jogs.

Since the jog is only a small piece of edge dislocation, it can move sideways along the screw dislocation conservatively and also attach itself to an edge component of the dislocation. Therefore, jogs on edge dislocations do not restrain the motion of an edge dislocation materially because the orientation of the slip planes of the jogs is such that they can move along the dislocation by slip(17).

The jog-dragging process and the climb-controlled process are considered as two quite different concepts of creep mechanism(18). The dislocation-jog model is also considered a high-temperature steady-state creep mechanism(25), where the jog-dragging-screw dislocations control the creep rate(19).

The jogs on dislocations will be saturated with vacancies, whereas the rate of emission and absorption of vacancies will fix the rate of movement of the dislocations, and this in turn, will depend on the rate of vacancy diffusion(18). Therefore, there are two regimes of creep; (i) when the jog density is less than the density of vacancies (except at very high stresses) and in this case, the creep rate is controlled by vacancy self-diffusion, and (ii) when the jog density is greater than the density of vacancies where the creep rate is controlled by interstitial self-diffusion.

Due to the high energy of formation of interstitials (the equilibrium concentration of interstitial is negligible), it is generally agreed that the vacancy mechanism is the much more probable(15,17,25). According to this mechanism, when a screw dislocation moves due to the applied stress, the jogs can accompany the dislocations only by the emission of vacancies. As a consequence, the local vacancy concentration near the jog increases and this gives rise to a chemical force (dragging force) that counteracts the motion of the dislocation. The steady-state velocity is attained when the chemical force is equal to the driving force (applied stress). On the other hand, for the vacancy-absorbing jogs, the rate of the process is controlled by the vacancies which diffuse to jogs and cause a decrease in vacancy near the jog, producing dragging force on the jog.
For dislocation-jog mechanism, the secondary creep rate is given by(25):

$$\dot{\varepsilon}_s = 2\pi\rho_s D\alpha\left(\frac{b}{a_o}\right)^3 Sinh\left(\frac{\sigma b^2\lambda}{2kT}\right) \qquad (2.7)$$

where ρ_s is the mobile screw dislocation density, D the self-diffusion coefficient, α the number of atoms in a cell, b the Burgers vector, a_o the lattice parameter, λ the average spacing between jogs, and k is Boltzmann's constant.
Assuming that the number of both types of jog are equal, the creep rate is given by the following expression(17):

$$\dot{\varepsilon} = BD_s\rho Sinh\frac{\sigma b^2 l}{kT} \qquad (2.8)$$

where the numerical constant B ~ 20, and ρ is the density of mobile dislocations.

The dislocation velocity contribution to the creep rate is usually taken as weighted sum of the velocities of jogged screw dislocations containing only a single jog type, that is, either vacancy absorbing or vacancy emitting. When the weighting is equal, the velocity contribution is related to the stress through a hyperbolic sine law such that at constant temperature, $v \propto \sinh\left(\frac{\sigma b^2 l}{kT}\right)$(27).

Nix and Barrett(25) pointed out that in general both jog types exist along screw dislocations. On this ground, Holmes(26) derived the relation between dislocation velocity and stress in the form of $v \propto \tanh\left(\frac{\sigma b^2 l}{kT}\right)$.

There are some imperfections found in the jog-dislocation model which are in many respects similar to those of the dislocation-climb theory. For example, the uncertainty of the mobile dislocation density (ρ), is great, with respect to both the magnitude and dependence on the stress. The stress-dependence of l is also not considered(17).

2.3.4 Recovery-Creep Model

All theories of recovery creep are based on the fact that materials while being heated, harden with strain and soften with time. If these two processes occur simultaneously, deformation is bound to take place, and it can be observed during high-temperature creep.

Recent formulations by McLean(28) and Lagneborg(29,30) have considered the recovery mechanism in some detail. The recovery creep theories proposed by them were based on the commonly observed presence of a three-dimensional dislocation network in steady-state creep. The creep process consisted of consecutive events of recovery and strain-hardening, and the strength was provided by the attractive and repulsive junctions of the network. Some of these junctions would break due to thermal fluctuations and those connected with the longest dislocations would break most frequently. The released dislocations would move a certain distance until held up by the network, and thereby give rise to a strain increment with an increase in the internal stress, i.e. strain-hardening, since at the same time, the expanding dislocation increases its length and, therefore, the dislocation density. Dislocation network recovery takes place simultaneously and it is assumed to occurs by a gradual growth of the larger meshes and a shrinkage of the smaller meshes.

It has been proposed that during the recovery process, the dislocation motion occurs essentially by the driving force due to the line tension of the curved dislocation meshes. The recovery process would tend to increase the average mesh size of the network, i.e. to decrease the density of dislocation. Eventually, some links would be long enough for their junctions to break due to the effect of thermal fluctuations and the applied stress, and the consecutive events of recovery and strain-hardening would repeat themselves.
The recovery-creep model also explains the processes during transient or primary creep. According to the model, at short creep times, the recovery rate can not catch up with the rate of strain-hardening for the low dislocation densities and therefore, the creep rate in the primary region is high and decreasing. However, if the dislocation density is increased, the driving force for recovery will increase which also increases the rate of recovery. Eventually, a stage is attained where recovery and strain-hardening balance each other. At this point, the creep rate and the dislocation density will remain constant. McLean formulated the recovery-creep process quantitatively by means of the classical expression(28):

$$\dot{\varepsilon} = \dot{\varepsilon}_o \exp\left[-\frac{bA(h\varepsilon - rt)}{kT}\right] \tag{2.9}$$

where ε_0 is the initial creep rate, b the Burgers vector, A the activation area, h the strain-hardening coefficient, r the recovery rate, and t is the time.

The refined recovery-creep model based upon the earlier theories of recovery-creep, proposed by Lagneborg(29), takes into account the variation in strain-hardening and the recovery with dislocation density, which the simple recovery-creep models do not consider. This refined model provides an improved description of the strain versus time relation in the primary and secondary stages, gives information regarding the dislocation density versus time variation and also the constant dislocation density that is reached in the secondary stage of creep.

According to this refined model(29), the steady-state creep rate is given by:

$$\dot{\varepsilon}_s = \frac{2M\tau\rho_s^2}{C} \tag{2.10}$$

where M is the mobility of climbing dislocations, τ the dislocation-line tension, ρ_s the steady-state dislocation density, and C is a constant which relates ε and ρ. Another inadequacy of the recovery-creep models was that they did not distinguish between the athermal (internal stress) and thermal (effective stress) components of the applied stress and to cover this deficiency, Lagneborg(30) formulated another modified recovery-creep model. This model takes into account the separation of the applied stress into an effective stress and an internal stress and the stress-dependence of the activation area. It describes the time and stress-dependence of the creep rate in the primary and secondary stages.

The model under normal conditions predicts that the ratio of the internal stress (σ_i) to the applied stress (σ) increases at the expense of the effective stress (σ^*), as the applied stress is decreased and the temperature is increased. Finally, a stage is reached where the internal stress is approximately equal to the applied stress. The steady-state creep rate at this stage is given by(30)

$$\dot{\varepsilon}_s \sim 2b\bar{l}M\tau\left(\frac{\sigma}{\alpha G b}\right)^4 \qquad (2.11)$$

where $\bar{l}$ is mean free path of dislocation motion and M is the mobility of climbing dislocations. This expression is in close agreement with empirical observations.

According to this modified model(30), the apparent activation energy should represent the activation energy for the recovery process when $\sigma_i \cong \sigma$. The simulation of the strain/time relationship according to the theory has shown that the creep curves produced are in good agreement with the experimental curves.

The model describes that the recovery creep is due to two processes, i.e. recovery and glide, which are thermally activated. It is assumed that recovery occurs by a climb-controlled increase in size of the meshes in the network-like dislocation structure. The glide process is assumed to be controlled by the junction breakages in the dislocation network.

Barrett et al(31) also proposed the recovery work-hardening theory of creep in terms of the co-operative relationship between dislocation glide and recovery. They concluded that the measured recovery and hardening rates were in accordance with the combined glide-recovery theory of steady-state creep only when the internal stress was an appreciable fraction of the applied stress. When the internal stress was much smaller than the applied stress, it was observed that the measured recovery and hardening rates were appreciably larger than the actual values. However, the predicted steady-state strain rate was still in agreement with the actual strain rate.

2.3.5 Nabarro-Herring-Coble Creep

Nabarro-Herring-Coble Creep is a special kind of steady-state creep which can occur at high temperature in specimens of very small size or of very fine grain material(9). For this type of creep, the stress levels are too low for dislocation processes to be significant. Nabarro-Herring-Coble Creep can be observed in Creep Diagram(9) *(Figure 3)*.

Creep can occur at high temperature when an appreciable number of vacancies are transported from one side of a grain to another under stress for a specimen of fine-grained structure. The mass transport of atoms and vacancies has been indicated in *Figure 4a.* The stress-directed flow of atoms and vacancies changes the shape of the grain which becomes longer in the tensile direction *(Figure 4b).* This type of creep was first proposed by Nabarro(32) and subsequently Herring(33) developed an analysis from which the creep rate produced by this mechanism can be calculated. The Nabarro-Herring creep is perhaps the best understood of all creep theories.

The original theory developed by Nabarro and Herring considers that diffusion occurs only through the crystal lattice, however, material can also be transferred along grain-boundaries(18). Grain-boundaries can accommodate or release atoms or, in other words, generate or annihilate vacancies. It has been observed that the energy required to form a vacancy at the top or bottom surface of the grain *(Figure 4a)* is different from the energy needed to form a vacancy at a side surface if a tensile stress is applied to the grain vertically. When there is a net flow of vacancies in one direction, an equal net flow of atoms occurs in the opposite direction. Therefore, atoms are removed from the side faces of the grain and transferred to the top and bottom faces. As a result, the grain changes its dimensions, as shown in *Figure 4b*(9).

For diffusion creep, if the rate-controlling step is the diffusion over distances of the order of the grain size (d), while the applied stress (σ) is the driving force, then, according to Nabarro and Herring(32,33), the creep rate is proportional to the applied stress and inversely proportional to the square of the grain size (d), and given by the following expression:

$$\dot{\varepsilon} = \frac{\alpha_v \sigma \Omega D_v}{kTd^2} \qquad (2.12)$$

where Ω is the atomic volume, D_V the diffusion coefficient in the grains, k the Boltzmann's constant, and α_V is a dimensionless numerical factor (constant), the magnitude of which depends on the grain geometry. In a uniaxial tensile or compressive test, α is in the range of 5⁽¹⁹⁾. In contrast to dislocation creep, Nabarro - Herring creep varies with stress linearly and occurs at T ≈ 0.8 T_m with applied stress (σ) ≈ 10^6N/m^2.

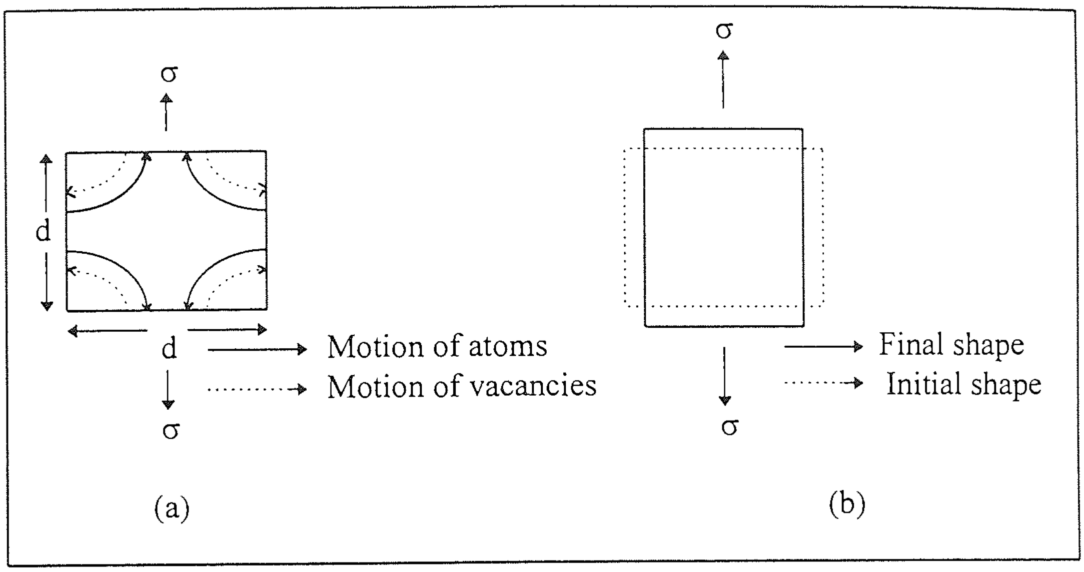

Figure 4. Nabarro-Herring creep. (a) Mass motion of atoms and vacancies across a small grain of dimension d under an applied stress. (b) Change in shape of a grain under the mass motion shown in (a).

According to Nabarro and Herring theory, diffusion occurs only through the crystal lattice. However, Coble(34) revealed that the diffusion path was not only confined to the interior of a grain but could occur along grain-boundaries. The temperature range over which vacancy-diffusion creep is significant may be extended to much lower temperature, i.e. T ≈ 0.5 T_m, if the vacancies flow down the grain-boundaries instead of the grains. In this case, the creep rate is also proportional to stress, but inversely proportional to the cube of the grain size, and is given by(34):

$$\dot{\varepsilon} = \frac{\alpha_{gb}\sigma\Omega\delta D_{gb}}{kTd^3} \qquad (2.13)$$

where $\dot{\varepsilon}$ is Coble or grain-boundary diffusion creep, D_{gb} the grain-boundary self-diffusion coefficient, α_{gb} a constant which has a value of around 40(34), and δ is the effective thickness of a grain-boundary.

Burton and Greenwood(35), later on analysed the creep rate by the stress-directed diffusion of vacancies along surfaces or grain boundaries of crystals having cylindrical and cubic shape, by using the Coble mechanism. It has been shown that a complete analytical solutions can be obtained which satisfies all physical conditions of the problem.

The formulae derived for the creep rates are as follows:

(a) for an axially stressed cylinder;

$$\dot{\varepsilon} = 64 D_g \omega\sigma\Omega / kTLD^2 [1 + (4L/3D)] \qquad (2.14)$$

where T is temperature, L the length of cylinder, D the diameter, D_g the coefficient of self-diffusion, Ω the atomic volume, ω the grain boundary width, and k is the Boltzmann's constant.

(b) for a cube uniaxially stressed perpendicular to a pair of faces;

$$\dot{\varepsilon} = 16 D_g \omega\sigma\Omega / kTL^3 \qquad (2.15)$$

So above equations indicate that creep rate is proportional to the applied stress.

2.3.6 Creep Theory for Particle-Hardened Materials

Only a few attempts have been made so far to describe the creep quantitatively in materials hardened by second-phase particles(17). Ansell and Weertman(36) were the first to develop a quantitative creep theory for particle-hardened materials. The model proposed by them is somewhat similar to that for steady-state creep in pure metals(12) and it was assumed that the rate-controlling process over the second-phase particles was the climb of dislocations. The details of this mechanism may differ slightly from those of pure metals, depending on the stress level.

The model suggests that at low stresses, the dislocations climb over the particles and there is no pile-up or bowing of dislocations at the particles. In this case, the creep rate (ε) is given by the following expression⁽³⁶⁾:

$$\dot{\varepsilon} = \frac{\pi\sigma b^3 D_s}{2kTd^2} \qquad (2.16)$$

where D_S is the coefficient of self-diffusion and d is the diameter of the particle. When the stresses are greater than the Orowan stress, G b/A, where A is the inter-particle spacing, the dislocation moves past the particles by bowing out and pinching off loops around the particles. This process continues until the back stress applied by the loops around the particles stops new dislocations from bowing out between the particles. The creep rate is then governed by the rate at which the dislocation loop which is nearest to the particle climbs to the top of the particle and is annihilated; the other loop then moves inwards, and a new loop is formed by bowing and pinching off an arrested dislocation. For this process, the creep rate is given by⁽¹⁷⁾:

$$\dot{\varepsilon} = \frac{2\pi\sigma^4 A^2 D_s}{dG^3 kT} \qquad (2.17)$$

Equation 2.17 shows that the creep rate decreases due to: (a) decrease of inter-particle distance, or (b) increase in the particle size.

From *equations 2.16* and *2.17*, it is expected that the stress/creep rate relation obeys a first-power law at low stresses, and a fourth-power law at high stresses. However, this type of stress-dependence is not always in agreement with experimental results.

Generally, the stress exponent (n) is found to be much higher than 4, which also implies that the stress exponent of materials hardened by second-phase particles considerably exceeds that of solid solutions and pure metals.

Lagneborg⁽³⁷⁾ has given a semi-quantitative explanation to show the high stress sensitivity of the creep rate for particle-hardened materials. By introducing a back stress which the precipitate particles exert on the dislocations, he showed that the stress exponent has high values when the creep rate is represented by a power function of the applied stress.

2.4 Grain Boundaries and Superplasticity in Creep Deformation

At low and intermediate temperatures, the polycrystalline metals deform essentially due to the deformation of the grains. Each grain of the metal deforms in approximately the same manner as the specimen as a whole, to maintain continuity of the specimen. However, the deformation will be inhomogeneous to some extent, which means variations may occur from grain to grain and from point to point within a grain, to maintain continuity of stress throughout the specimen. This inhomogeneity has been observed by many investigators for coarse-grained structures(38). Urie and Wain(38) have examined coarse-grained aluminium specimens to check this effect. They observed that the deformation in the vicinity of the boundaries was less than the average deformation of the grains. However, across the boundaries, no discontinuities in strain were reported. The smaller deformation in the vicinity of the boundaries shows that the grain-boundaries at low-temperatures, are a source of strength. It was supported by the fact that with the decrease in grain size, the yield stress of metals is increased. Carreker and Hibbard(39) have shown the effect of grain size for copper.

At high temperatures, the case is reversed because grain boundaries are a source of weakness, and a fine grain size reduces the creep strength of material, especially when the rate of testing is low(11). During the creep of materials having polycrystal structure, the grain boundaries play an important role in the deformation process at high temperatures, because they may;
(i) slide passing each other, or (ii) create vacancies.
Both processes involve an activation energy for diffusion and therefore, may contribute to steady-state or secondary creep stage(10).

2.4.1 Grain Boundary Sliding

If the test temperature of creep is raised approximately to $0.5T_m$, significant sliding is observed along the grain boundaries. At this temperature, the grain boundaries are considered as a source of weakness rather than strength. The contribution of grain boundary sliding to total creep strain is always a debating point. Some researchers regard sliding as a major factor in creep deformation, while others consider it something which is used only to accommodate inter-crystalline deformation(11).

Grain boundary sliding was studied by a number of investigators. The study of grain boundary sliding in aluminium by Hanson and Wheeler(40) from the early work on this subject is considered especially important because it paved the way for the later research. They investigated the movement of grain boundaries in polycrystalline aluminium which was strained slowly at 250°C.

The sliding is generally limited to the immediate vicinity of the grain boundary for small displacements. However, when creep strain is increased, the width of sliding zone increases with time. Weinberg(42) studied this effect for aluminium bicrystals. He found that the width of sliding zone for Al was about one-hundredth of the measured shear. It was observed that the shear was relatively uniform over the entire length of the boundary during the early stages of deformation, but when time was increased, the displacement often varied from point to point along the boundary and therefore, the flow would also occur in the grains.

It has been experienced that the rate of sliding increases with the increase in angle of misorientation between the conjugate crystals, or if angle is increased between the active slip planes and directions(43,44).

A number of polycrystalline metals and alloys were studied for grain boundary sliding and their sliding was measured quantitatively. The main purpose of these investigations was to find out the nature of the sliding at individual grain boundaries and also to determine the contribution of the grain boundary sliding to the total deformation of the creep specimen.

According to McLean and Farmer(41), the grain boundary displacement is directly proportional to the total elongation of the specimen during the creep test. To estimate the contribution of the grain boundary sliding to the total strain during creep, scratch mark experiments are usually used.

The contribution of grain boundary sliding to the total strain is shown in *Table 1*(46) for zinc alloys and some other materials.

Table 1. Contribution of Grain Boundary Sliding to the Total Axial Strain.

	$\varepsilon_{gb}/\varepsilon_t$ (%)		
Material	**Region I**	**Region II**	**Region III**
Zn-22% Al	30	60	30
Pb-Tl		50	33
Mg-Al eutectic	12	64	29
Pb-Sn eutectic		70	
Pb-Sn eutectic	21	56	20
Mg-1.5% Mn-0.3% C	33	41-49	30
Al-9% Zn-1.0% Mg		63	26
Zn-0.4% Al	42	48	28

It was observed by Valiev and Kaibyshev(47) that the amount of grain boundary sliding (GBS) was strongly dependent on the angle between the axis of the creep specimen and the sliding boundary trace on the surface. It was noted that in Region I, sliding was mainly at the transverse boundaries, whereas in the other two regions (region II and III), the largest amount of sliding was observed at boundaries situated at 45° to the axis of the specimen. In all three regions, the boundaries which showed the highest sliding, were also the most active in boundary migration.

The proportionality between grain boundary displacement and total creep strain gives a constant, i.e. $\varepsilon_{gb} / \varepsilon_t =$ constant (2.18)

where $\varepsilon_{gb} =$ Grain boundary displacement,

and ε_t = Total creep strain

The ratio $\varepsilon_{gb}/\varepsilon_t$ increases if temperature is increased(41) and stress is decreased(48) However, below a critical stress, the ratio decreases if stress is further decreased(49).

According to Fazan et al(45), $\varepsilon_{gb}/\varepsilon_t$ remained constant and independent of temperature for a constant stress. Martin et al(50) also found that for a constant stress, $\varepsilon_{gb}/\varepsilon_t$ was independent of temperature for β brass. It was observed that for alloys, this ratio increased with decrease in stress more rapidly than for the pure metals, which meant that at lower stresses, alloys had greater values of $\varepsilon_{gb}/\varepsilon_t$. The data for Al and Al alloys(51) indicated that grain boundary sliding might contribute 50 to 80 percent to the total creep strain.

According to Gibbs(52), the total tensile strain of a polycrystalline aggregate is equal to the mean strain of individual grains in the aggregate, i.e. $\varepsilon_t = \varepsilon_{gb}$, provided the number of grains per unit length is unchanged. When there is deformation due to diffusional processes, the total aggregate strain may be resolved into two parts, i.e. (i) contributions from grain displacements normal to their boundaries, and (ii) sliding displacements parallel to the boundaries. Since it has been experienced in many practical cases that the ratio $\varepsilon_{gb}/\varepsilon_t$ is approximately constant during creep tests, the effect of stress and temperature on the sliding rate ($\dot{\varepsilon}_{gb}$) should be the same as on the total creep rate ($\dot{\varepsilon}_t$).

2.4.2 Superplasticity in Zinc-Aluminium Alloys

It may be defined as the ability to deform at small stresses to exceptionally large strains at elevated temperatures. The superplastic behaviour in materials may be observed(53-55) if ; (i) the temperature is above approximately $0.5T_m$, where T_m is the absolute melting point of the material, while the strain rates are in the vicinity of about 10^{-3} s^{-1}, and (ii) the grain size is small, typically (but not necessarily) less than about 10μm in size. The grains should be fine, stable and equiaxed. It has been observed that the strain rates for superplasticity are much lower than those for conventional hot-working processes. The optimal superplastic materials are either two-phase eutectic or eutectoid alloys because in these alloys, the grain growth is limited by the presence of two phases(54) or alloys having a fine stable dispersion of a second phase which refines the grains.(55,56) Considering the two requirements for superplasticity, the binary Zn-Al system is an excellent choice for producing superplastic alloys. The Zn-Al eutectoid (Zn-22% Al) is preferred due to its equiaxed fine-grained structure for superplasticity. This alloy exhibits optimum superplasticity at 520-540 K, and has been investigated in great detail, in terms of temperature, stress, grain size and deformation rate.(57-60) It was found that the maximum attainable ductility of this alloy increased with temperature increasing and / or decreasing initial grain size, and occurred at intermediate strain rates.

The effects of phase composition and structure on superplasticity were also studied by Keybyshev(61) in a composition range from 0.4% Zn to 50% Zn. This research showed that the appearance of superplasticity was strongly dependent on the original grain size, the stability of the structure and the quantative ratio of the zinc and aluminium rich phases. Experiments were carried out at different temperatures from 20°C to 250°C at a constant deformation rate of 10^{-2} s^{-1}. These tests revealed that at 250°C, only the quenched sample of eutectoid composition showed superplasticity.

The results for Zn-Al alloys in the quenched and rolled conditions have been shown in *Figure 5.* It was observed that the eutectoid alloy had the minimum flow stress as shown in *Figure 6.* The flow stress was minimum for 18% and 2% Al at temperatures of 150 and 20°C, respectively. *Figure 5* also showed that the plasticity dropped rapidly when the Aluminium content went down above the eutectoid composition. It was also shown that for alloys with Aluminium contents above 10%, plasticity decreased with decrease in temperature (*Figure 5).* The plasticity of the alloy with 0.4% Al increased with decreasing temperature, and at room temperature, this alloy had the highest plasticity, whereas it decreased to a minimum at 250°C.

Cook and Risebrough(62) found that the superplasticity of an alloy with 0.2% Al was associated with a very high strain rate sensitivity (m) of 0.72 at a very low temperature of 23°C. At this temperature, the eutectoid was not superplastic, and values of m were less than 0.1. Therefore, in the absence of the higher melting point phase (Al-rich), the Zn-rich phase itself was superplastic at much lower temperatures compared with the eutectoid alloy.

It has been found experimentally(58-60) that for superplastic deformation of the eutectoid alloy, there are three distinct regions for the relation between stress and strain rate, and the fine-grained microstructure was equiaxed throughout the deformation. The maximum deformation was observed over an intermediate range of stress and strain rate, and the strain decreased at both high and low values of stress and strain rate. Region II was therefore considered to be responsible for superplasticity. The rate-controlling mechanism in Region III is due to climb of edge dislocations as well as slight grain-boundary sliding.(53,63) The mechanisms proposed for low stress region (Region I) are Coble creep(63,64), Nabarro-Herring diffusion creep(59) or diffusion accommodated flow of grain-boundaries(64).

It has been verified by the models proposed for deformation mechanism that grain-boundary sliding (GBS) plays the main role in the superplastic deformation process. Many researchers(62,66,67) have investigated the contribution of GBS to total strain in Zn Al alloys. The results of these investigations are given in *Table 1.* This table shows that the contribution of GBS to total strain is significant although results of Sheriat et al(67) are different, giving much lower values. Their research(67) also revealed that the maximum sliding occurred at Zn-Zn intercrystalline boundaries, slightly less sliding at the Zn-Al interphase boundaries and the least sliding at Al-Al crystalline boundaries.

2.5 Correlation of Creep Data

When creep tests are performed to find out how some parameters, such as, time spent to produce a certain creep strain, varies with stress and temperature for any material, simple graphical representation of the creep curve is adequate. However, for many practical and theoretical purposes, using only a graphical representation of the creep curve does not fulfil the requirements and it is often desirable to develop equations which show the strain rate accumulation with time. In this way, graphical representation can be replaced by analytical procedures which allow the creep curves to be presented in terms of a set of parameters. Other equations can also then be formulated which describe how these parameters vary with temperature, stress, or material details. Therefore, the creep characteristics of a material can be expressed in terms of one or more constitutive equations which relate stress-strain-time and temperature.

2.5.1 Stress-Dependence of Secondary Creep Rate

The influence of stress on the creep rate is an important experimental variable. The possible rate controlling processes and the variables that control the creep rate are usually considered significant in three stress ranges.

(i) Low Stress Creep Range:

The relation between the steady-state creep rate ($\dot{\varepsilon}_s$) and stress is usually linear at very low stresses and is given as follows(68):

$$\dot{\varepsilon}_s = K\sigma \qquad (2.19)$$

where σ= stress and K= constant.

It is generally believed that creep in this stress range is due to a process of stress-directed diffusion (Nabarro-Herring-Coble Creep) and not due to dislocation motion.

(ii) Intermediate Stress Creep Range:

In a range of intermediate stresses, the stress dependence of secondary creep rate is usually described using the following power law equation.

$$\dot{\varepsilon}_s = A\sigma^n \qquad (2.20)$$

where A and n are independent of stress within the region considered but A, and to some extent n, depends on the test temperature(12). Depending on the material and test conditions, generally, the stress exponent (n) ranges between 4 and 6 for pure metals, and between 2 and 4 for alloys(12).

At intermediate stresses, the creep behaviour of solid solution alloys depends upon several factors, which include the solute concentration, the solute-solvent size difference and the test temperature(70).

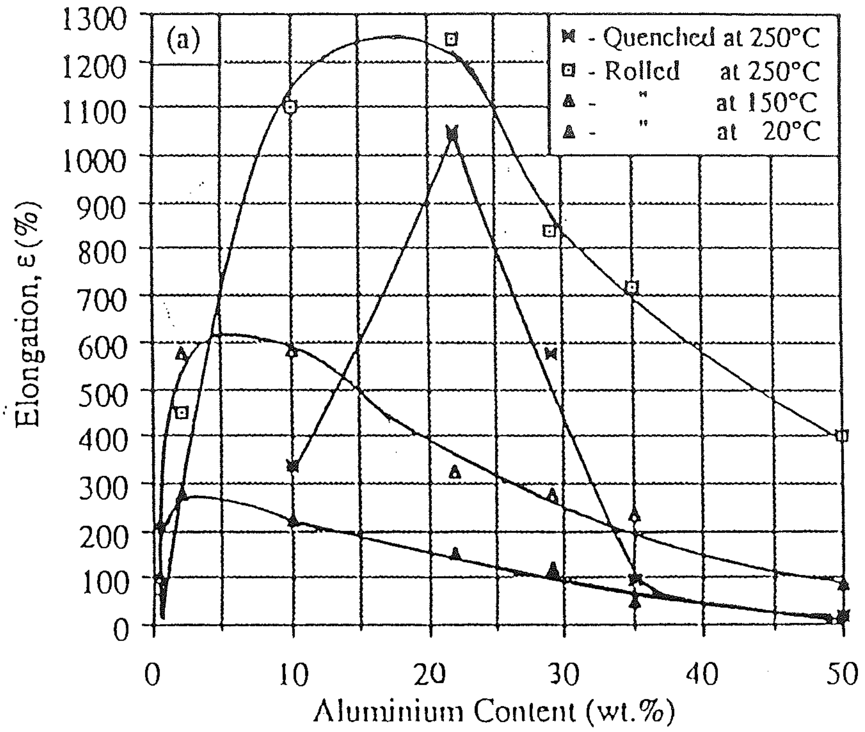

Figure 5. Plasticity of Zn-Al alloys at different temperatures.

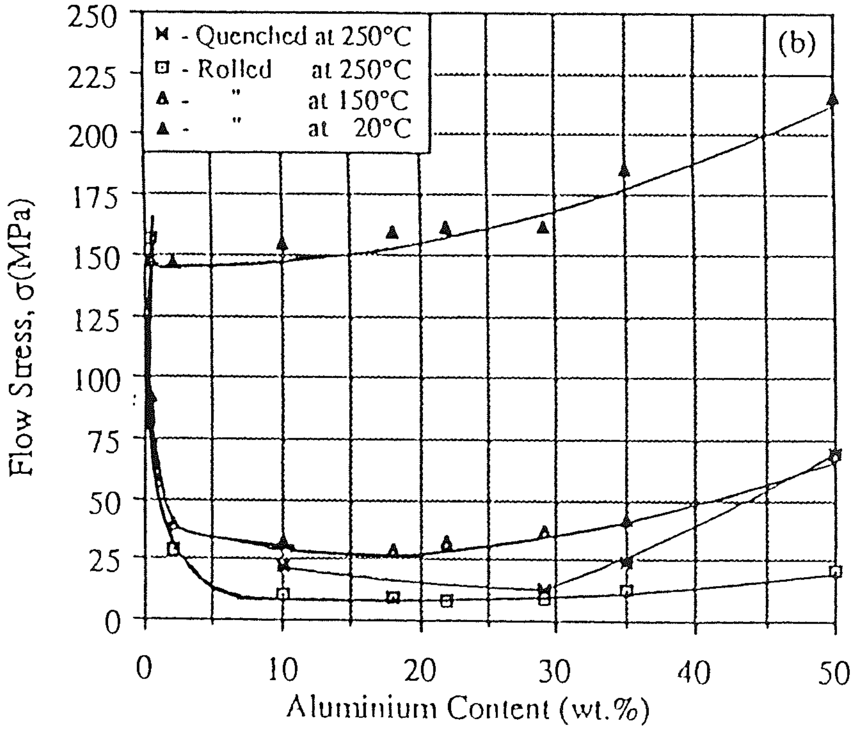

Figure 6. Flow of stress of Zn-Al alloys at different temperatures.

(iii) High Stress Creep Range:

At high stress levels, the secondary creep rate increases more rapidly than predicted by the power-law equation(15). This phenomenon is described as the power-law break-down. Therefore, at higher stress levels, the secondary creep rate is better expressed by an exponential expression which agrees well with experimental data(12,69):

$$\dot{\varepsilon}_s = A'\exp(\beta\,\sigma) \qquad (2.21)$$

where A' and β are constant at constant temperature and for constant stress tests, both are independent of stress within the ranges of stress examined. This relation can be used for single crystals and polycrystals of annealed metals and alloys, also A' and β depend on temperature for these materials.

There are various empirical relationships which have been proposed to describe both the intermediate- and high-stress range in one expression. For this purpose, Garofalo(69) has suggested the following relation:

$$\dot{\varepsilon}_s = A''(\sinh \alpha\sigma)^n \qquad (2.22)$$

where A'' and α are constant at constant temperature. For values of $\alpha\sigma < 0.8$, *equation (2.22)* reduces to power law *equation (2.20)* and the value of $A = A''\alpha^n$. For values of $\alpha\sigma > 1.2$, *Equation (2.22)* reduces to the exponential *expression (2.21)*,
where $A' = A''/\,2^n$ and $\beta = n\alpha$.

Equation (2.22) can satisfy creep results of both metals and alloys, but to evaluate the value of α, results at both high and low stresses must be known(12), e.g. this relation agrees well with experimental creep results over wide range of stresses and temperatures for copper, aluminium, an Al-3.1% Mg alloy, and an austenitic stainless steel(69). *Equation (2.22)* also satisfies the linear relation, $\dot{\varepsilon}_s = K\,\sigma$, at low stresses, where the test temperature is close to the melting point of material(69)..

Evans and Harrison(72) have proposed the following universal equation to describe the stress dependence of the secondary creep rate:

$$\dot{\varepsilon}_s = B\{(\sigma - \sigma_o/\sigma_{0.05})\}^{3.5} \tag{2.23}$$

where the value of B is 2.5 x 10^{-5} s^{-1} and it is both structure and temperature-independent for a range of T/T_m ratios of 0.5-0.8. It has been shown that the relation is valid for Nimonic 90, H46 steel, MAR-M246, α-iron, Nimonic75, and many other single and two-phase alloys. The equation can also be used immediately to simplify the evaluation of new engineering materials, while with some development, it can be adapted to situations where component creep behaviour under complex stresses is being analysed.

2.5.2 Temperature-Dependence of Secondary Creep Rate

Experimental results show that creep is a thermally activated process, and normally the temperature sensitivity of the creep rate is presented in terms of an Arrhenius-type equation with a characteristic activation energy (Q_c), which is considered as the rate controlling mechanism(17,68):

$$\dot{\varepsilon}_s = K \exp(-Q_c / RT) \tag{2.24}$$

where K is a constant for a given creep stress and creep strain, and may be slightly dependent on temperature. The exponential factor shows the rate at which a controlling mechanism allows the process to carry on, where Q_c is the activation energy for creep. R is the universal gas constant and T is the test temperature in degree Kelvin.

It has been proved experimentally that the activation energy for creep is often independent of strain(73,77). Under some test conditions, Q_c is found to be a function of temperature and stress(75,17). The activation energy for creep does not change with increasing temperature and also its value usually approaches the activation energy for self diffusion for temperatures above ~ 0.5 T_m(9,17,68), e.g. the activation energy for creep of Al has been found to be nearly equal to the activation energy for self diffusion Q_d =

34000 cal/mol)(68). Therefore, it is believed that the most likely mechanism of creep in that region may be dislocation climb(16) or non-conservative motion of jogs in screw dislocations(25). However, it has been shown by Poirier(78) that the region where activation energies for creep and self diffusion coincide is limited. It usually starts only at about 0.6 or 0.7 T_m and does not always extend to the melting point of the material. To prove his point, Poirier made a detailed re-examination of all published data of creep for 5 pure metals. It was observed that the results of 4 metals showed that the values of Q_c and Q_d were not similar above 0.5 T_m(78).

If both stress and temperature are considered as major factors which influence the creep rate, especially at low temperatures, then both stress and temperature dependence terms can be incorporated in one equation for secondary creep rate, as given below:

$$\dot{\varepsilon}_s = C \sigma^n \exp(-Q_c / RT) \tag{2.25}$$

or

$$\dot{\varepsilon}_s = C'(\mathrm{Sinh}\ \alpha\sigma)^n \exp(-Q_c / RT) \tag{2.26}$$

2.5.3 Time-Dependence of Creep Strain

The time-dependence of the creep strain in the primary and secondary stages is based on Andrade's $(\mathrm{time})^{1/3}$ law(17,12). This equation is given as follows(12):

$$\varepsilon = \varepsilon_0 + \beta t^m + \dot{\varepsilon}_s t \tag{2.27}$$

where ε_0 is the instantaneous strain, β and m are constants independent of time, t the time, and $\dot{\varepsilon}_s$ is the secondary creep rate.

For many metals and alloys, the value of m has been found in the range of 0.03 to nearly 1.0, and it depends on both temperature and stress(12). Very often m takes the value of approximately 1/3(5,9), and it generally increases with decrease in stress and increase in temperature. The value of β generally increases exponentially with stress and temperature(5). Within certain limits, this relation satisfies experimental results obtained on a large number of metals and alloys (with fcc, bcc, hcp structures) and ceramic oxides(79).

Brinson & Argent(80), and Davies et al(81) have shown the agreement with this relation *(equation 2.27)* of creep strain and time. However, this expression has been found to predict an infinite initial creep rate and it can not produce a true steady-state(17,76).To overcome these deficiencies of creep-time relationship, the following exponential expression is used which was found adequate over wide ranges of deformation(12,76).

$$\varepsilon = \varepsilon_0 + \varepsilon_t(1 - e^{-rt}) + \dot{\varepsilon}_s\ t \qquad (2.28)$$

where ε_0 is the strain observed upon loading, ε_t the limiting transient strain during the primary stage of creep and r is the ratio of transient creep rate to the transient creep strain. $\dot{\varepsilon}_s$ is the secondary creep rate. The initial creep rate is given by $r\,\varepsilon_t + \dot{\varepsilon}_s$.

Equation 2.28 has been used successfully in describing the time dependence of creep strain for ferritic and stainless steel within the temperature range of 0.4 to 0.6 T_m(12), tungsten(82), copper-aluminium alloys(83), Nimonic 80A(84), a nickel-chromium alloy and many other metals and alloys. Although the relation gives an adequate description for most of the creep life, a general deviation over the first 10-15% of the primary creep also occurs, due to which the actual creep rates are larger than those predicted(85.87).
An important finding of these investigations was that the initial creep rate, the duration and shape of the primary stage and the steady-state creep rate, all showed the same stress-dependence which suggested that the mechanism controlling the creep rate was the same throughout the primary and secondary stages(85,87).

The phenomenon that the mechanism of creep remains same throughout the primary and secondary stages provides a justification for the fact that the most fundamental studies on creep have concentrated exclusively on the experimental determination and the theoretical interpretation of the ways in which secondary creep rates of materials vary with stress, temperature. When the test temperatures are close to the melting point of the material, the creep curves become essentially linear at low stresses and thus has been found for Al, Au, Cu, and δ-Fe at 0.96 to 0.99 T_m . In these cases, primary creep does not exist and the creep curve is described by the following relation(12):

$$\varepsilon = \varepsilon_0 + \dot{\varepsilon}_s\ t \qquad (2.29)$$

Evans et al(88-90) have recently proposed a new creep life prediction method, i.e. the θ - projection concept in order to quantify the changes in the creep curve shape with stress and temperature. This concept envisages normal creep curves as the sum of a decreasing primary and an accelerating tertiary region, whereas a steady-state does not exist. There is also an increase in creep strain with time which may be described by the following expression(88):

$$\varepsilon_c = \theta_1\left(1 - e^{-\theta_2 t}\right) + \theta_3\left(e^{\theta_4 t} - 1\right) \qquad (2.30)$$

where θ_1 and θ_3 are scaling terms defining the extent of the primary and tertiary stages of creep with respect to strain, while θ_2 and θ_4 are the rate parameters which govern the curvatures of the primary and tertiary components, respectively.

Equation (2.30) presents the creep curve as an addition of decelerating and accelerating exponential functions of time in which θ plays the important role of governing the shape of the creep curve. This can be observed readily by differentiating *equation (2.30)* (90), which gives the creep rate at any instant:

$$\frac{d\varepsilon_c}{dt} = \theta_1\theta_2 e^{-\theta_2 t} + \theta_3\theta_4 e^{\theta_4 t} \qquad (2.31)$$

and the rate of change of creep rate is:

$$\frac{d^2\varepsilon_c}{dt^2} = -\theta_1\theta_2^{\,2} e^{-\vartheta_2 t} + \theta_3\theta_4^{\,2} e^{\theta_4 t} \qquad (2.32)$$

when θ_2 and θ_4 are increased, it rapidly increases the deceleration of creep rate in the primary and acceleration in tertiary stage. *Equation (2.32)* shows that the function f{θ , t} has a minimum gradient for positive values of θ_i (i = 1-4), whereas this minimum creep rate occurs at time t_m, given by the equation(87):

$$t_m = \frac{1}{\theta_2 + \theta_4} \ln \frac{\theta_1 \theta_2^2}{\theta_3 \theta_4^2} \qquad (2.33)$$

Since by using different θ relationships, the minimum creep rate ($\dot{\varepsilon}_m$) can be calculated for any stress and temperature, it is therefore very easy to compute the values of n and Q_c for a wide range of stress and temperature. It has been observed during θ analysis for copper that both n and Q_c decrease gradually with decreasing stress and temperature(90),which quantifies the dependence of creep curve shape on stress and temperature. Although it has been claimed that θ - projection concept offers numerous theoretical and practical advantages, it can only be used to describe the creep curves under a constant stress(88), and at present only a few reports are available to confirm the applicability and validity of the concept.

2.6 Phase Diagrams

2.6.1 The Binary Zn-Al System

The binary phase diagram of Zn-Al system has been one of the most investigated equilibrium diagrams over a period of more than 80 years(91). Many phase diagrams have been published during this period but are now obsolete except the liquidus curves and temperatures of three phase equilibria. The most attention was given to determine;

(i) the solidus curve, (ii) the solid solubility of Zn in Al, which includes the boundary of the closed miscibility gap above 275°C, and also (iii) the solid solubility of Al in Zn. The major dispute among the researchers for many years was the possibility of a peritectic reaction in Zn-Al system.

The earliest investigators(92-94) proposed equilibrium diagrams of Zn-Al system which showed the following similarities: (i) these diagrams exhibited an intermediate phase of variable composition around 78%, generally denoted as β, and formed by a peritectic reaction of the melt (at about 443°C) with the aluminium based solid solution α, containing about 70% Zn, (ii) a eutectic of β and also the zinc-based solid solution η at

95% Zn, at temperature 380°C, and (iii) a eutectoid decomposition of β, whereas the eutectoid point was situated at 270-280°C. Later, Owen and Pickup(95) and Elwood(96,97), studied the system by high temperature X-ray camera method, but could not confirm the existence of a peritectic reaction.

Fink and Willey(98), by using resistivity and microscopic techniques, concluded that the peritectic reaction was not present. Later on, Gayler and Sutherland(99), on the basis of thermal, microscopic and dilometric evidence, reached the same conclusion. The thermal arrest which was found by them at 443°C was due to a rapid change in composition of the α' solution along the solidus. The Zn-Al phase diagram compiled by Hansen and Anderko(100), is shown in *Figure 7*. The Figure has been drawn from the results of Elwood and earlier workers, and does not show the peritectically formed intermediate phase β.

Figure 7. Zinc-Aluminium phase diagram compiled by Anderson and Anderko(100).

The consecutive work of Presnyakov et al(101) and Goldak and Parr(102) has produced a binary diagram of *Figure 8* which is considered as perhaps the most accurate representation of the Zn-Al system proposed in recent years. The diagram accounts for all the experimental facts.

Presnyakov et al studied the Zn-Al system in detail to find out whether a peritectic reaction existed. The alloys were prepared from 99.99% aluminium and 99.96% zinc by crucible melting and cast into graphite moulds. The alloys were then homogenised at 350°C for 168 hours, deformed to 50% cross-section by rolling, and finally heated at 350°C for 2 hours. A back-reflection, high-temperature camera was used to measure lattice parameters in alloy filings, whereas air was used as the camera atmosphere. The temperatures were controlled to ± 2°C. The estimated error in the measurement of parameters was 0.0004 kX. They studied a small portion of the phase diagram in great detail and discovered a very narrow two-phase field. From this investigation, they concluded that; (i) the peritectic reaction, in fact, existed at about 443°C, (ii) another phase, known as β phase, distinct from the α phase, existed and also involved a discontinuity in the solubility, and (iii) a second eutectoid decomposition of the α' phase into $\alpha + \beta$ occurred at about 340°C, with the eutectoid point at about 70% Zn.

Later, Goldak and Parr(102) confirmed the work explicitly by high temperature X-ray diffractometer study of the Zn-Al system in the region 40-75 wt.-% Zn. In this study, aluminium and zinc of 99.999% purity were used for the preparation of alloys. The alloys consisted of 70% zinc and 30% aluminium. As specimens of the highest possible purity were required during this investigation, the levitation-melting technique was therefore adopted. The size of ingots produced was ~ 30mm long, 10mm wide, and 3mm thick. Before X-ray analysis, a thin layer of surface was machined off from all sides of the specimen. A wet chemical method accurate to one part in one thousand was used to analyse one finished alloy.

The phase diagram of Presnyakov et al, confirmed by Goldak and Parr, is considered probably the most accurate representation of the binary diagram for Zn-Al system to date, and has been reproduced in *Figure 8*. In this phase diagram, α is the Al-rich terminal solid solution, α' is the part of it which lies on Zn-rich side of the monotectoid,

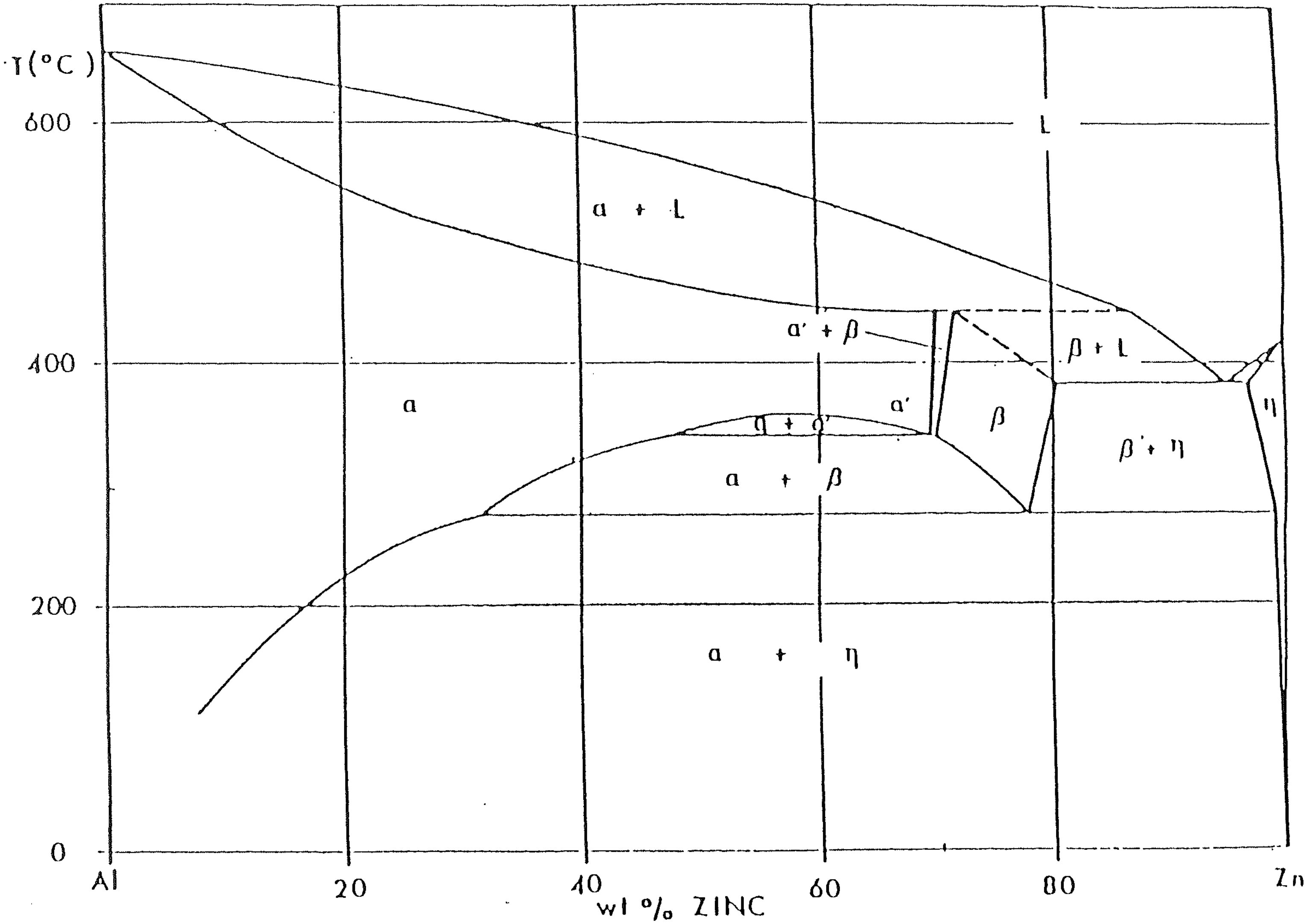

Figure 8. Accepted phase diagram of binary Zinc-Aluminium system.

β is the Zn-rich eutectoid phase and η is the Zn-rich terminal solid solution. The invariant transformations observed in solidification are given as below:

a peritectic, liquid + α → β at approximately 70% Zn, 443°C;

and a eutectic, liquid → β + η at 94.9% Zn, 382°C

The solid solubility of zinc in aluminium at different temperatures has been determined and given in *Table 2*(103).

In the temperature range of 340°C and 351°C, the Al-rich solid solutions break down into two phases α and α′, which are both a solid solution of zinc in aluminium having different percentages of zinc. At 340°C, this gap of miscibility extends from 49% to 69.5% Zn and regularly shrinks on heating to reach the single point at 351°C. It can be observed that α′ + β is a very narrow field nearly equal to 1 wt.% wide(102), extending from an eutectoid point at 69.5% Zn to the peritectic point at 443°C. At the zinc end, the solidus and liquidus slopes down to the eutectic sharply. Aluminium is soluble in zinc in small amounts, approximately 1.1 percent aluminium at 380°C(104), which decreases to 0.65% at eutectoid temperature (275°C) and 0.42% Al at 227°C(107). At 340°C, β phase is f.c.c. with its lattice parameter decreasing from 4.04Å at 70% Zn to 4.03Å at 76% Zn(101). It decomposes by an eutectoid reaction into α + η at 275°C with

Table 2. The solid solubility of zinc in aluminium at different temperatures

Temperature (°C)	Solubility (% wt.)
77	2.5
127	6.2
177	11.5
227	18.0
275	31.6
327	43.5
340	49-69.5
351.5	61.3
443	70.0

the eutectoid point at 78% Zn. At 25°C, the lattice parameter of pure aluminium is 4.0414Å$^{(105)}$ and it decreases almost linearly to 4.0000Å at 65% Zn in the α region$^{(97)}$. Zinc has a hexagonal close packed (h.c.p.) crystal structure with the following lattice parameters$^{(105)}$:

a = 2.6595Å, c = 4.9368Å when it is pure,

and a = 2.6650Å, c = 4.9870Å when saturated with aluminium.

2.6.2 The Binary Zn-Cu System

The phase diagram of binary Zn-Cu system is presented in *Figure* 9$^{(106)}$. This diagram can be regarded as very well established. It differs only slightly from that compiled by Hansen and Anderko$^{(100)}$. Five peritectic reactions are shown in this Figure. There are also four intermediate phases, i.e. β, γ, δ, and ε existing in the system, and have broad ranges of solid solubility except δ phase.

(i) α + Melt $\Leftrightarrow$ β.

The reported temperatures vary between 890 to 906°C. The most reliably determined points are 32.5 wt. (31.9 at.)% zinc and 36.8 wt. (36.1 at.)% zinc.

(ii) β + Melt $\Leftrightarrow$ γ.

The temperatures for this phase may vary between 833 and 840°C, where as 834 ± 1°C is considered as the most reliable point. Almost all investigators agree that the composition of the melt and γ within the limits of experimental error, is identical. The most accurately determined point is 56.5 wt. (55.8 at.)% Z.

(iii) γ + Melt $\Leftrightarrow$ δ.

According to different investigators, the temperatures vary between 685 to 700°C. The most reliable compositions were determined by using micrographic analysis, located at 69.8 wt. (69.2 at.)% Zn and 73.0 wt. (72.45 at.)% Zn.

(iv) δ + Melt $\Leftrightarrow$ ε.

The temperatures recorded are varied from 585 to 600°C. The points located at 76.5 wt.% Zn and 78.6 wt.% Zn were found out by using micro-graphic method.

(v) ε + Melt $\Leftrightarrow$ η.

The temperature for this phase was variable between 421 and 426°C. The maximum solubility of Cu in Zn occurred at 97.3 wt.% Zn being the most reliable point$^{(100)}$.

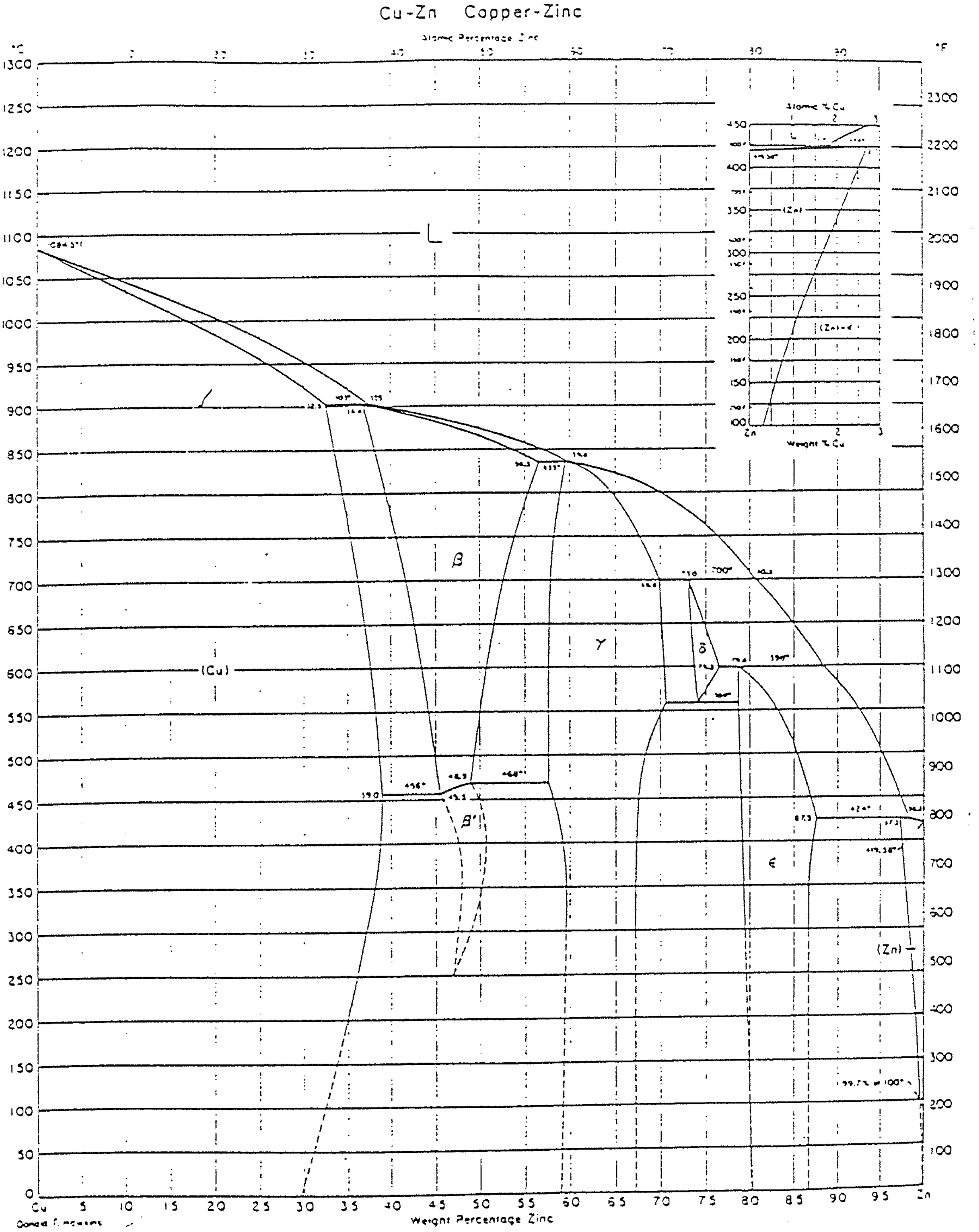

Figure 9. The equilibrium phase diagram of the binary Zn-Cu system.

2.7 Creep in the Ternary and Higher Alloys

Although it has been experienced that Zn-Al binary alloys possess good forming and mechanical properties, these alloys have a low resistance to creep due to their superplastic characteristics. Due to poor creep strength, these alloys have limited commercial use in applications where high creep resistance is required.

In order to improve their creep strength, many researchers have studied the effect of alloying additions on Zn-Al alloys. Naziri and Pearce(107) checked the effect of copper additions of up to 1% on creep properties of slightly hyper-eutectoid alloys (20% Al). They found that copper additions did not have a significant effect above about the temperature of 150°C. However, it was observed that at room temperature, the addition of up to 1% copper continuously improved the creep resistance of the alloy and for 1% addition, the improvement was by a factor of 140.

Later on, Nuttall(108) investigated the creep properties of three eutectoid-based ternary Zn-Al alloys, one with 4% Cu, the second with 0.2% Mn and third with 1% Si. The alloy containing 1% silicon cracked on hot rolling or swaging and little further research work was carried out on this alloy. However, the steady-state creep resistance of other two alloys was measured at a stress of 35 MPa after various heat treatments. The results indicated that the room temperature creep resistance of the alloys was significantly increased due to the copper additions of up to 1%, but there was no further improvement in the creep resistance of alloys when the copper content was added from 1 to 4%. Whereas, the creep resistance of a manganese containing alloy was observed to be substantially better than that of any of the alloys containing copper. In as-quenched condition, the steady-state creep rate of Zn-Al-0.2Mn was $8.1 \times 10^{-6}h^{-1}$ as compared to $9.0 \times 10^{-5}h^{-1}$ for Zn-Al-1Cu and $8.0 \times 10^{-5}h^{-1}$ for Zn-Al-4Cu.

Other researchers such as Mulvania et al(109) also tried to modify the composition of eutectoid alloys in an attempt to improve the creep resistance by adding single elements; titanium, chromium, manganese, copper and magnesium. They found that generally the creep resistance of alloys was improved by alloying even when tested at room temperature. It was observed that manganese, titanium and chromium had little effect in improving the creep strength. However, the additions of magnesium and copper showed a significant improvement in creep resistance of alloys. Copper additions of up to 0.5% enhanced the creep resistance, but additional copper was not beneficial. It was also noted that the addition of 0.018% Mg produced the highest creep strength overall and showed a much greater improvement than 0.06% Mg. The optimum combination of high creep strength and low super plastic flow stress was observed in an alloy with 0.42% Cu and 0.002% Mg, which had the creep resistance equivalent to that of a commercial zinc die-casting.

Savaskan and Murphy(110-112) investigated the creep behaviour of one eutectoid and two near-eutectoid alloys, containing 3 and 4% Cu in both as-cast and heat treated conditions, over a range of stress and temperature. The alloys were heat treated by homogenising them for three hours at 350°C, and then quenching and ageing at 200°C for two hours.

The results showed that the alloys containing 3 & 4% Cu, in both as-cast and heat treated conditions, had much lower secondary creep rates than the binary alloys; and as cast alloy, in turn, had substantially lower secondary creep rates than heat treated alloys of the same composition. In the as-cast condition, the alloy with 4% Cu exhibited a lower creep rate than that with 3% Cu among the ternary alloys. However, these results were reversed in heat treated condition. This was due to the overall copper content which increased the creep resistance of as-cast alloys, whereas, in the case of heat treated alloys, it was attributed to the matrix copper content.

Savaskan and Murphy in their first two works(110,111) also showed that the secondary creep rates of these alloys in both as-cast and heat treated conditions could be correlated using an equation of the form:

$$\dot{\varepsilon}_s = A \sigma^n \exp(-Q_c / RT) \qquad (2.34)$$

where n = 3, and a mean value of Q_c = 87 kJ/mole.

Later on, Murphy et al(112) modified the *equation (2.34)* and correlated the creep data more satisfactorily by the following empirical equation:

$$f(e) = C\,t\,\sigma^n \exp(-Q_c / RT) \qquad (2.35)$$

where f (e) is some function of creep deformation, C a constant, t the time, σ the stress, n the stress exponent, Q_c the activation energy for creep, T the absolute temperature and R is the universal gas constant. They found the stress exponent of 3.33 for alloys tested in the stress range of 10 to 60 MPa, whereas the activation energies for these as-cast alloys were similar, with a mean value of 122 kJ/mole and for heat treated alloys, these varied in the range 60-107 kJ/mole.

2.8 Experimental Zinc-based Zn-Al Alloys

A total of six alloys have been used for compressive creep and load-relaxation experiments, which include alloys ZA8, ZA12, ZA27 COSMAL, SUPERCOSMAL and LM25.

2.8.1 The Background and General Properties of Zinc-based Alloys

In order to improve the properties of zinc, its alloying with aluminium, copper and other metals was started early in this century. Zinc-rich alloys were first developed and utilised in some pressure die-castings as a substitute for tin and lead alloys because tin was expensive and lead had low strength. One of the earliest zinc-rich alloys developed for use had 5% Cu, 6% Sn, 0.5% Al and the balance zinc(116). Although the early die-castings of zinc alloys seemed satisfactory, but it was observed that in many cases rapid deterioration set in after a few months of service and results were not according to the standards. It was found that these problems were due to intercrystalline corrosion in these alloys because of some impurities, such as lead, tin and cadmium; whereas, the over ageing was due to the high copper content(116,117).

With the availability of high-purity zinc (99.99%) and advancements in casting technology, the New Jersey Zinc Company introduced two pressure die-casting zinc alloys, i.e. Zamak 3 and 5 (known as Mazak 3 and 5 in the United Kingdom)[1] between 1930-40(117). Both alloys can be used to produce widely-used engineering materials having reliable properties, when properly alloyed, cast and applied. These alloys have a unique combination of properties which allows the rapid, economic casting of strong, accurate and durable parts and hence, have dominated the market since their introduction.

The zinc-based alloys have many advantages over other non-ferrous die-casting materials such as, aluminium, magnesium and copper alloys because zinc alloys can be easily cast, and are stronger and more ductile. They also require less finishing, can be held to lower tolerances and can be cast in thinner sections. The die life for zinc die-castings is also longer than that for other die-casting materials due to the low casting temperatures required for zinc-based alloys. The production rate (shots/hour) is also much higher than other alloy systems. They are used in a variety of applications, ranging from the simplest drawer handle to the most complex precision automotive part(118). The nominal compositions of the alloys are given in *Table 3*(1). Alloys No3 and No5, however, have poor resistance to creep in applications where sustained loads are applied at temperatures above 100°C(118), and therefore do not always meet the design requirements. ILZRO[2], therefore, started research to develop a die-casting alloy that would have higher creep strength without sacrificing the other excellent properties of alloys No3 and No5.

---

[1] *Mazak 3* and *5 corresponds to the specification of BS1004A and BS1004B respectively, in British Standards (1972). They have been designated as alloys No3 and No5 in this text.*

[2] *ILZRO: International Lead Zinc Research Organisation*

In the mid 1960s, ILZRO developed a cold-chamber pressure die-casting alloy with some additions of titanium. This alloy was named as ILZRO.14, which was later on superseded by ILZRO.16. This is a special-purpose creep-resistant alloy which also meets the requirements of structural applications and its creep strength is markedly superior to that of alloys No3 and No5 at all testing conditions. For example, it was observed that when an aged sample of No3 was tested at room temperature, it showed about the same creep resistance as an aged sample of ILZRO.16 tested at 177°C(119). It is shown that higher creep resistance of ILZRO16. is due to its alloying constituents of chromium and titanium. Since these elements have high melting points, due to which they form a fine eutectic inter-growth of inter-metallic compounds with zinc, e.g. $TiZn_{15}$ in Ti alloys(120,121). It was observed that these particles created an effective barrier to grain growth, but the most important factor was that it increased the structural stability and creep resistance by eliminating a substantial number of high energy, mobile grain boundaries(120,121). However, the other mechanical properties of ILZRO.14 and ILZRO.16 at room temperature are inferior to those of alloys No3 and No5(1,119) and unlike alloys No3 and No5 , they cannot be die-cast in a hot-chamber die-casting machine in which the injection plunger sleeve and gooseneck are continuously immersed in molten zinc in the machine part or furnace. Due to the low aluminium content of ILZRO.14 and 16, it would slowly dissolve iron if left in contact with the

Table 3. Chemical Composition of zinc-based alloys (% by weight).

Alloy	Al	Cu	Mg	Ti	Cr	Zn
No3	3.5-4.3	0.25 max.	0.02-0.05	-	-	Balance
No5	3.5-4.3	0.75-1.25	0.03-0.08	-	-	"
ZA8	8.0-8.8	0.8-1.3	0.015-0.03	-	-	"
ZA12	10.5-11.5	0.5-1.2	0.015-0.03	-	-	"
ZA27	25.0-28.0	2.0-2.5	0.01-0.02	-	-	"

steel plunger sleeve and cast iron goose-neck. Therefore, both alloys must be cast in cold-chamber die-casting machines. These alloys have limited use on the market due to the above mentioned disadvantages. The typical mechanical properties of the alloys are given in *Table 4*.

In view of these limitations, high aluminium, high strength zinc-based (ZA) alloys were developed. The first alloy which was developed had 12% Al, was proposed by ILZRO in 1962(116) and was named ILZRO.12. Later on, the Al content as reduced to 11%, which together with other changes gave improved properties. This improved alloy is now known as ZA12.(114).

Two other alloys, ZA8 and ZA27 were developed in the late 1970s by ILZRO Inc(114). The chemical composition of these three alloys according to ASTM B 669-82 ingot specification is shown in *Table 3* (115).

These new ZA alloys were rapidly introduced and become popular in the market. Each alloy was designated specifically to meet market needs, and the family collectively provides alternatives to other well developed alloy systems, such as Al-based alloys, brasses, bronzes and cast-irons. The advantages of ZA alloys include good mechanical properties, excellent bearing characteristics, ease of finishing, non-sparking properties, and also pollution-free melting(117,1).

Originally, these alloys were developed as sand and gravity casting alloys, but later on they were used in a wide range of casting processes including pressure die-casting. They can be die-cast in cold-chamber machines, but ZA8, due to its low Al content and lower melting point could even be used in conventional hot-chamber machines.

Of all three ZA alloys, ZA27 has the highest strength and hardness, followed by ZA12 and ZA8. There is no significant effect of casting techniques on the tensile strength of ZA27, whereas the hardness and tensile properties of ZA8 and ZA12 are significantly higher in die-cast condition.

Murphy et al(122) investigated the effect of elevated temperatures in the range of 20°C to 260°C on the tensile properties of the die-cast alloys No3, ZA8 and ZA27. They found variations in ultimate tensile strength, proof stress and elongation with temperature. It was observed that ZA27 had the highest strength, about 60% greater than that of alloy No3, followed by ZA8 which had 30% higher strength than No3. It was also found that the ultimate tensile strength and proof stress of the alloys decreased with increasing temperature and the rate of decrease was proportional to the Al content. ZA27 also showed quite a sharp decrease with temperature. Elongation results gave a very pronounced temperature dependence. Below 100°C, the ductility of ZA27 increased very slowly, then at an increasing rate with increasing temperature up to the maximum temperature tested, exhibiting an expected characteristic of superplasticity of the alloy. Alloy No3 showed different behaviour from ZA27 because initially there was a rapid rise in elongation, but this increase was the highest between 150-200°C and decreased thereafter. The elongation in ZA8 occurred in a similar way to that of ZA27 in the temperature range of 20 to 150°C, then it was the highest at about 200°C and decreased in a similar manner to that of alloy No3.

Similar research work was carried out in a more limited temperature range of up to 150°C on alloys No3, No5 and ZA alloys by Loong(123). His results for alloys No3, ZA8 and ZA27 were in close agreement with those of Durman(124) for same alloys. It was found that the tensile strength of alloys No5 and ZA12 were between those of No3 and ZA8, and of ZA8 and ZA27, respectively. The elongations in ZA12 and alloy No5 were also very similar to that of ZA27 and ZA8, respectively.

At the eutectoid point, the zinc-aluminium binary alloy has been known to have high damping capacity but due to its low strength it has not been utilised. Cast iron is the only high damping metallic material which has ever been used because of its low price and therefore could be used in large quantities. Recently, efforts have been made to develop light and cheap alloys having high damping capacity.

Table 4. Typical mechanical properties of zinc-based alloys.

Mechanical Property	No3	No5	ZA8	ZA12	ZA27
Ultimate Tensile Strength (MPa)	283	328	374	404	426
Yield Strength 0.2% offset (MPa)			290	320	371
Elongation (%)	10	7	6-10	4-7	2.5
Hardness (BHN)	82	91	100-106	95-105	116-122
Shear Strength (MPa)	213.7	262	275	296	325
Fatigue Strength (MPa)	47.6	56.5	103		145

Table 5. Chemical Composition of the High Damping Alloys Cosmal-Z.

	Al	Si	Cu	Mn	Mg	Fe	Pb	Sn	Cd	Zn
ZM-11	22	1.5	0.5	0.3	0.005 max.	0.1 max.	0.003 max.	0.001 max.	0.001 max.	Bal.
ZM-3	40	3.0	1.0	0.3	0.005	0.1	0.003	0.001	0.001	Bal.
Super-Cosmal	60	6.0	1.0	0.3	0.005	0.2	0.003	0.001	0.001	Bal.

Mae and Sakono-oka(113) developed Zn-Al alloys for die casting (Trade Mark Cosmal-Z) by alloying it with Si, Cu and Mn to strengthen without lowering the inherent high damping capacity. Among these ZM-11 has superior strength and damping capacity at room temperature while ZM-3 and supercosmal up to 100°C and 150°C respectively. In addition these alloys have good castability in die casting. The chemical composition of the high damping alloys is shown in *Table5* (113).

Mae and Sakono-oka found that it was possible to select alloys from a wide range of chemical compositions in the Zn-Al system because it was an alloy system with no intermediate phases. *Figures 10 and 11* show the relationship between aluminium content at the Zn-Al binary system , internal friction and tensile strength of die castings. (113)

Mae found that it is not difficult to produce products with high damping capacity in the as die cast condition when Cosmal-Z alloys were cast under the appropriate conditions. Physical and mechanical properties of Cosmal-Z in the as die cast condition are shown in *Table 6 and 7* (113) respectively.

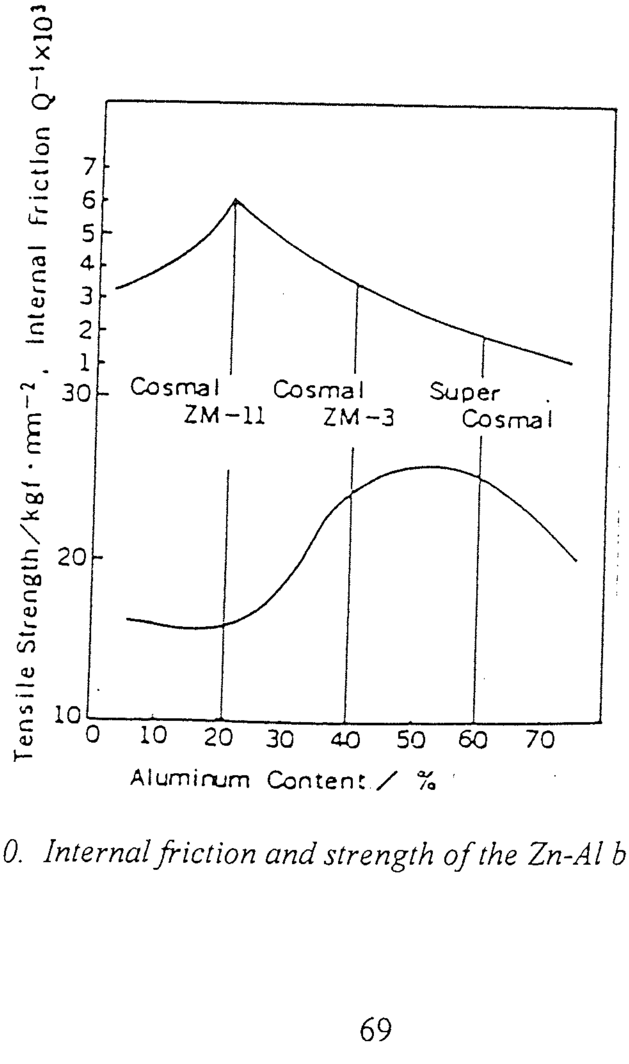

Figure 10. Internal friction and strength of the Zn-Al binary system.

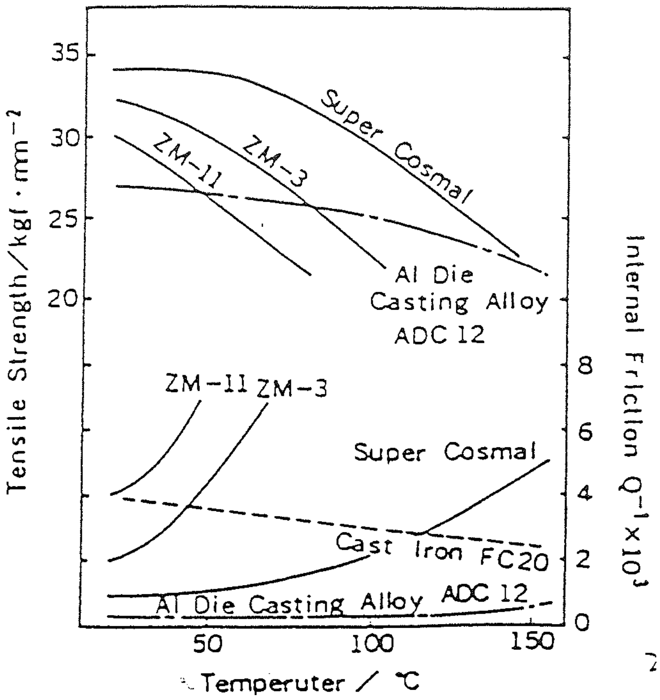

Figure 11. Tensile strength and internal friction of Cosmal-Z at elevated temperature.

Table 6. Physical properties of the high damping alloy Cosmal-Z.

Alloy / Item		Cosmal-Z			Al Die Casting Alloy ADC12	Cast Iron FC20
		ZM-11	ZM-3	Super Cosmal		
Density	g/cm^3	5.0	4.1	3.4	2.7	7.2
Electric Conductivity	%IACS	30.1	27.4	21.5	25.5	3.0
Melting Point	°C	477	516	549	580	1168
Specific Heat	J/Kg/°C	500	590	660	963	627
Coefficient of Thermal Expansion	10^{-6}/°C	28.4	25.6	24.8	21	11.1

Table 7. Mechanical properties of the high damping alloy Cosmal-Z.

Alloy		Cosmal-Z			Al Die Casting Alloy ADC12	Cast Iron FC20
Item		ZM-11	ZM-3	Super Cosmal		
Young's Modulas	kgf/mm^2	8,300	7,500	8,400	7,900	11,800
Tensile Strength	kgf/mm^2	24	30	34	26	23
0.2% Offset Yield Strength	kgf/mm^2	15	24	30	17	18
Elongation	%	3	1	0.5	1	2
Vickers Hardness	kgf/mm^2	100	120	130	110	80

2.8.1.1 The Effect of Alloying Elements on General Properties of Zinc Alloys

Copper and magnesium are the main alloying elements of zinc-based alloys. It was found that the effect of increasing Cu between 0 and 1% was most influencial on creep strength of the alloys ZA8, ZA12 and No5(114). Copper additions up to 2 or 2.5% significantly increased the tensile strength and hardness of the alloys. However, due to excess copper, ductility is reduced, and more than 1% Cu can cause dimensional growth on ageing. In both ACuZinc alloys (ACuZinc 5 & ACuZinc 10) the improved strength, hardness, ductility and wear properties are attributed to the Cu-rich epsilon phase(126).

Additions of magnesium are also very effective in small amounts of up to 0.01% in increasing the hardness and tensile strength, but at the expense of ductility. It was shown that the effect of 0.01% Mg on tensile strength of alloys is similar to that of a 2% Cu addition(114). Magnesium is also useful in preventing intergranular corrosion, which may occur when low levels of impurities, such as, lead, tin and cadmium are present(114).

2.8.2 The Creep Characteristics of Zinc-based Alloys

The commercial zinc alloys were studied over the years to find their creep behaviour but most of the published data of these alloys was derived from the actual creep tests combined with limited extrapolation of the creep data of the experiments.

Figure 12(1) shows the tensile creep data for alloy No3 at 25°C for different times ranging from instantaneous to ten years. This creep data was obtained after the test continued up to five years, and the data for ten years was achieved from the extrapolation of the five years test. From this data, it is possible to compute the permissible design stress at 25°C for allowable design strain up to approximately 0.8% in desired service life up to ten years.

In order to determine the creep properties of ZA alloys in die-cast condition the Noranda Corporation (115) initiated a program to establish the design stress of the alloys ZA8, ZA12 and ZA27 as defined by the ASME pressure vessel code for steel, in which the design stress was specified as the stress to produce 1% creep strain at given temperature over 100,000 hours. Zinc alloys differ in that they suffer creep at room temperature, and results have become available at 20°C for these three alloys. Inverse creep rate (days/% elongation) versus stress have been shown in *Figure 13*.

From these results all three alloys have approximately the same creep resistance at room temperature, thus the design stress according to ASME Boiler Code for these alloys would be three times greater than Mazak 3(115). The design stress for ZA27 will be much less at 100°C because it showed poor creep resistance at 100°C as compared to 20°C and it was expected that the other two alloys (ZA8 and ZA12) would also behave similarly.

Murphy et al (112) found the creep strength of Mazak3, ZA8, ZA12 and ZA27 at 120 °C using the time to a total creep elongation of 1% . He noted that ZA8 has best creep resistance followed by ZA12 and then ZA27. ZA27 was slightly better than Mazak3 but both were ten times weaker than ZA8.

The creep strength of Cosmal-Z alloys was also studied by Mae and was compared with ZA27, ZDC2 and ADC12. ZDC2 is the existing die-casting Alloy No 3 with the composition of Zn- 4%Al -0.03%Mg., and it showed the same creep behaviour as the newly developed alloy (ZA27) *(Figure 14)* at 60°C against different stresses while supercosmal and ADC12 had almost no creep and ZM-3 was between ZDC2 and ADC12 (113). *Figures 15 and 16* were derived at 100°C and 150°C against different stresses and graphs showed that ZM-3 creeps most followed by Supercosmal and then ADC12. These results show that in case of specific application it is necessary to select alloys taking into consideration the application temperature, damping capacity, tensile strength and creep strength.

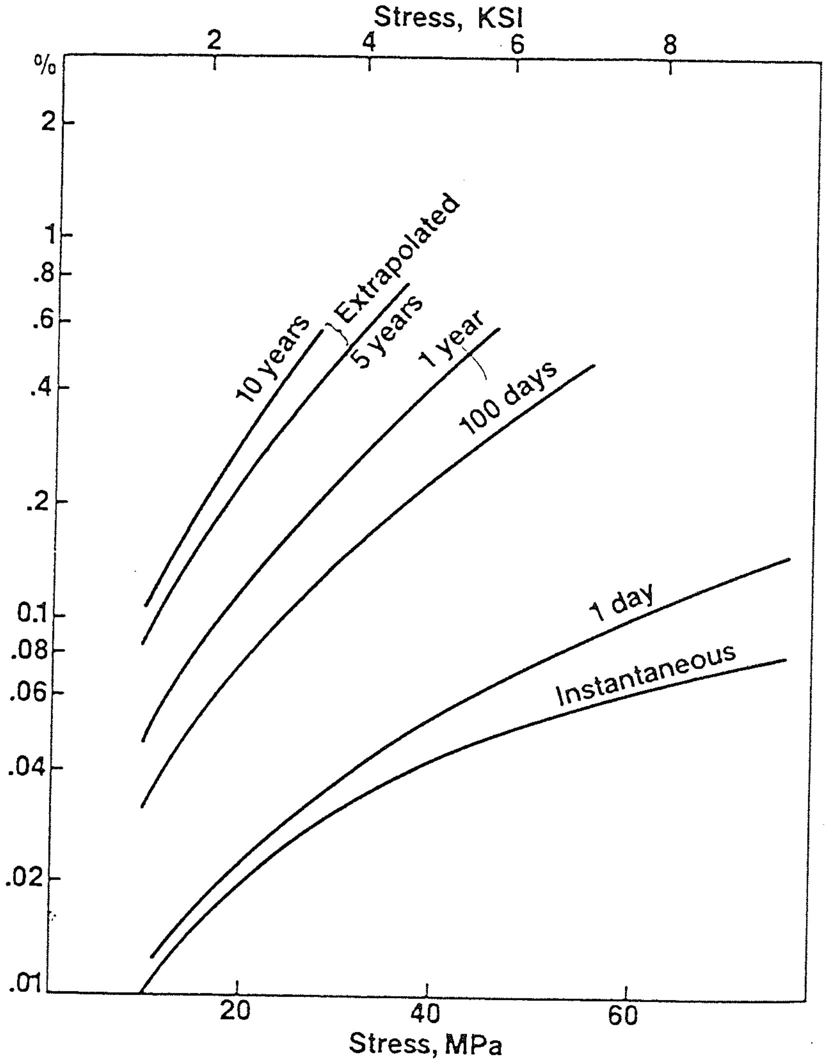

Figure 12. Tensile creep properties of alloy No3 at 25°C (% allowable strain in indicated time versus allowable stress)(1).

Figure 13. Inverse secondary creep rate of ZA alloys as a function of stress at 20 and 100°C[(123)]

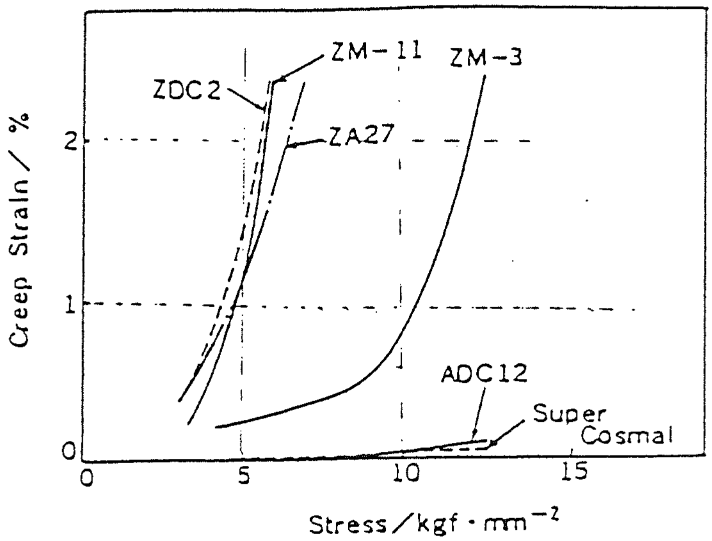

Figure 14. Creep stress-strain relationship at 60°C, 96 hour creep test.

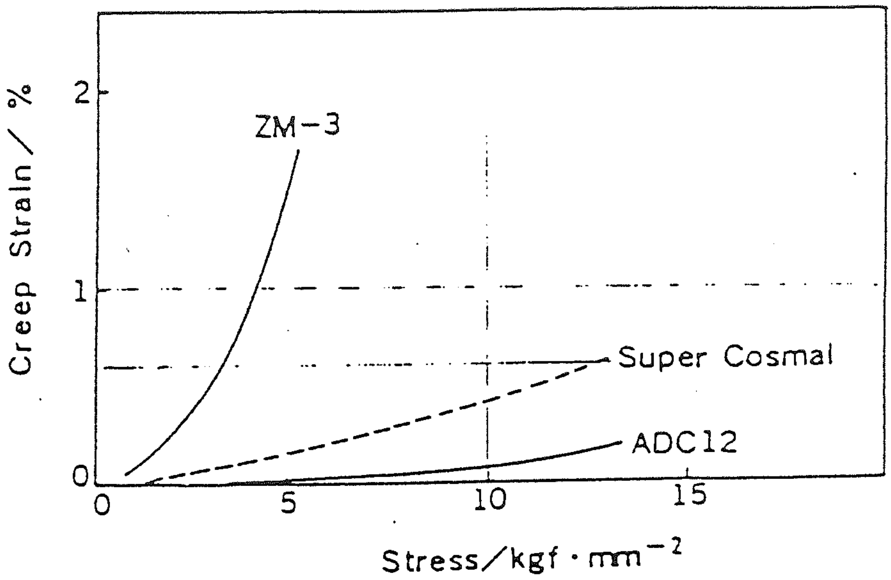

Figure 15. Creep stress-strain relationship at 100°C, 96 hour creep test.

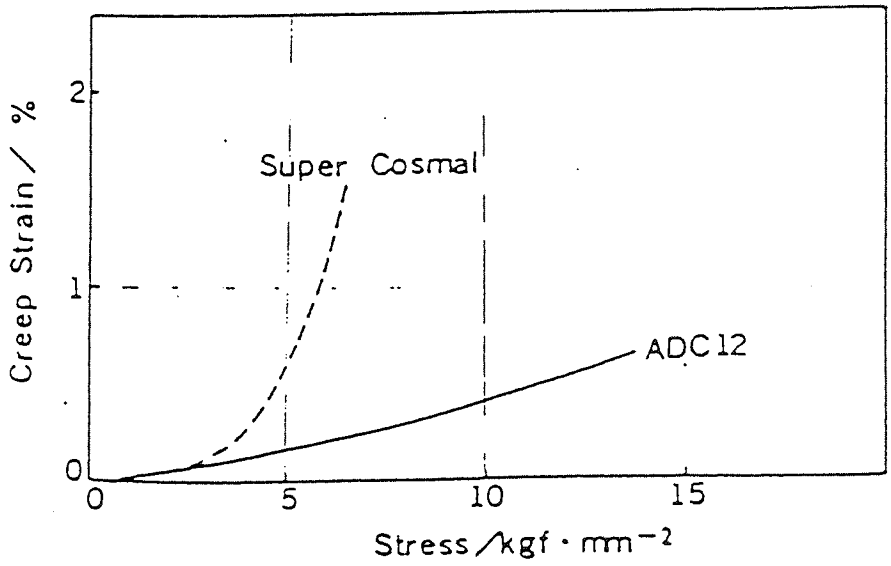

Figure 16. Creep stress-strain relationship at 150°C, 96 hour creep test.

2.9 Load Relaxation

Load relaxation is the time and temperature dependent decrease of load in a material due to conversion of elastic into inelastic (plastic) strain(127). Therefore, during this process, the total strain is kept constant while the load applied initially decreases with time(12). A common example of this phenomenon is the relaxation of load (stress) in the bolts of joints in a 'hot' environment. The rim of a gas-turbine disc which works with a cooling system, is another case where relaxation may cause a marked redistribution of stress(128). The phenomenon is related to creep and seems to exhibit the characteristics of logarithmic creep(12). The data obtained from load relaxation tests can be used to develop stress-relief heat treatments for reducing residual stresses, and also for the design of such mechanical elements as joints, bolted flanges, press-fit elements, gaskets and springs(127,129). The data obtained is also an important source to evaluate the constitutive relations governing a material's inelastic behaviour(127).

A greater creep rate is expected during constant stress creep than during stress (load) relaxation which involves creep under a decreasing stress(12). For a specimen in a tension test, the load relaxation depends upon the conditions of loading during the test as well as on the elastic and inelastic properties of the material.

It has been observed that load or stress relaxation is a problem in rivet and screw joints, particularly in automobile components where the temperature is usually high. It is also considered important in other stressed components, such as wheel rims and consoles for spring brackets in cars which are used in a warm climate(130).

2.9.1 Load Relaxation Properties of Zinc-Aluminium Alloys

The load relaxation behaviour of zinc-based alloys was studied only in recent years. Murphy and Haines(131) investigated the load relaxation characteristics of commercial zinc alloys, i.e. No3, No5, No2 and ZA8.

During the load relaxation tests, they used a new device to continuously monitor preload loss in these zinc-based pressure die castings. A load cell was used to monitor load loss in an ISO metric 6 x 1 steel screw set into castings made from these alloys, and tightened to give an initial preload of 5900N (1320lbf). Each casting was held at a constant temperature in an oil bath and the tests were conducted for periods of up to 100 hours. The test temperature range was 22-80°C.

All test specimens were produced using a single impression die on the same hot-chamber machine, whereas a central hole in the boss of the casting was formed during die casting using a tapered core. The residual load was measured continuously and plotted as a function of test time for all alloys. In all experiments, the initial load loss was high, diminishing gradually with time, but not ceasing. It was also observed that the amount of loss increased rapidly with test temperature, and all curves approximated to a logarithmic decay of preload with time. There was some variation in the initial part of the curves.

The results showed(131) that commercial zinc alloys had clear differences in the comparative resistance to preload loss. Generally, alloy No2 had the best resistance, with alloy No5 next and No3 worst at all testing conditions. The variation of 50 hour load was plotted as a function of copper content for three hypoeutectic alloys. There was little difference in behaviour at room temperature, but at higher temperatures of 60 and 80°C, a linear dependence of retained load on copper content was displayed.

ZA8 showed different behaviour from other alloys. It had poor resistance in comparison with the higher zinc alloys at low temperatures, but improved its relative position as the test temperature was increased to become comparable to alloy No2 at 80°C. Therefore, the retained load curve of ZA8 reduced less rapidly with increasing temperature than the other alloys.

Later on, Murphy and Goodwin(132) examined the preload loss of steel fasteners set into zinc alloy pressure die castings. The load loss was continuously monitored over a period of 150 hours using a calibrated load cell. The tests were conducted at 50 and 80°C on alloys No3, No5 and ZA8.

Commercial high-strength zinc-coated steel screws were used for the majority of the tests. The base design was an ISO-metric M 6 x 1 steel fastener of 10mm engagement length set in a roll-threaded casting which had a boss diameter of 12.7mm, and torqued to give an initial preload of 6000N.

The following variations were engineered in the base configuration and tested:
- Changing the engagement length from 10 to 25 mm.
- Thread pitch was varied from 0.75mm to 1.25mm.
- Reducing the external diameter of the boss from 12.7mm to 10.0mm.
- Changing the way the casting thread was produced by replacing a roll-threaded casting by,

(i) a casting having a thread made by a cutting action tap, and
(ii) a casting where the thread was provided by a self-tapping screw.

The results showed(132) that for the common combination of an M 6 x 1 steel screw set into a 10mm hole pre-threaded by a roll-forming tap in an alloy No3 pressure die casting, an initial load of 6000N decays to about 17% of its initial value over the first 150 hours at 80°C, with very little change thereafter. Alloy No5 which contains a small copper content, retains more than 25% of its initial load after the same time, and ZA8 retains about 30%. At lower test temperature of 50°C, the proportions of retained load are approximately 35% for No3, 55% for No5 and 60% for ZA8.

It has been found that a change in engagement length had significant effect on the retained load. Improvements in long-term retained loads of 100% for No3, and 60% for No5 and ZA8 at 80°C, while 55% for No3 and 30% for No5 & ZA8 at 50°C were observed by increasing the engagement length by 50% from 10 to 15mm. Further increases were beneficial for certain materials, but might lead to unacceptable weight penalties for small improvements.

It was also observed that thread pitch had a smaller but still important effect on load relaxation. When the pitch of a 6mm screw was changed from 0.75 to 1.25mm, it increased the long-term retained load by an average of 22%, although alloy No3 showed no improvement and alloy No5 a 46% improvement at 80°C.

The effect of reducing the external diameter of the boss was not large. The research(132) revealed that most of the preload relaxation was due to thread-related effects rather than compressive stress on the boss, and doubling the compressive stress resulted in an average load reduction of only 20%, with alloy No3 least sensitive to this variable.

Another important factor was the way the thread was formed in the hole. It was found that a cut-threaded casting gave on average a long-term preload retention 42% & 33% better than the standard roll-threaded casting at 80°C and 50°C, respectively, while the use of self-tapping screws gave worse results when compared with ordinary metric screws in roll-threaded holes. It was also observed that the reductions were modest, particularly at the higher temperature where an average reduction of just 7% was measured. By taking the average long-term retained loads for all of the load relaxation tests, it was found that an increase of 41% could be obtained by replacing alloy No3 with No5, and 59% by substituting ZA8. These improvements were similar for both test temperatures.

CHAPTER 3

3.0 EXPERIMENTAL TECHNIQUE

Two types of experimental technique were used in this research work:

1. Compressive creep testing, for which a compressive creep machine was designed and fabricated and zinc-base alloys were tested under different test conditions.
2. Load-relaxation testing of the same materials under different test temperatures at a constant initial pre-load.

3.1 Design of Compressive Creep Machine

The compressive creep machine was designed to test the hollow cylindrical test specimens of any material. The coaxial force was applied on the test piece to avoid any bending which may give inaccurate results.

The schematic diagram of a compressive creep machine is shown in *Figure 17*. The machine is of the standard weighted lever-arm type, with a lever-arm ratio 10:1. The machine has been designed for compressive creep testing of different materials, whereas during the current research, zinc-base alloys were tested to find out their compressive creep behaviour at different temperatures under different stresses. The machine consists of the following parts:

1) A base frame and a steel plate, fitted over this frame.
This whole structure represents the base of the machine which was placed on the flat surface and it was aligned/leveled precisely, as a slight difference in its level may affect the performance of the machine, giving inaccurate results.
2) Three vertical supporting columns of steel, fitted on the base of the machine in a triangular shape and a lever was placed on the top of these columns.
3) Three plates of mild steel, fixed between the two front columns with support flanges at different locations and heights from the base of the machine as shown in *Figure 17*. The prime purpose of the top plate was to support the hydraulic jack. At the start of the experiment the applied load was sustained by the hydraulic jack, and opening the

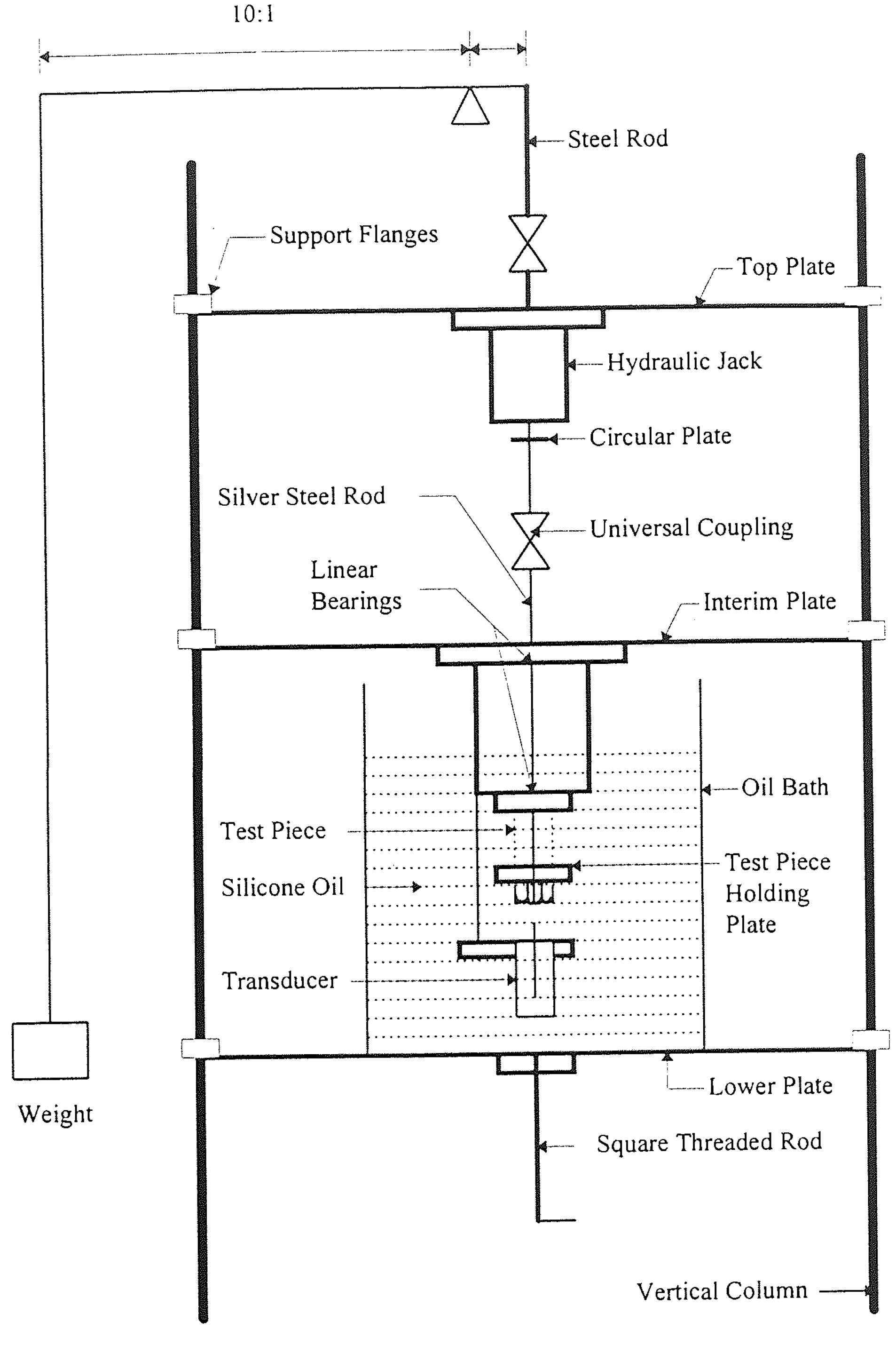

Figure 17. Schematic Diagram of a Compressive Creep Machine

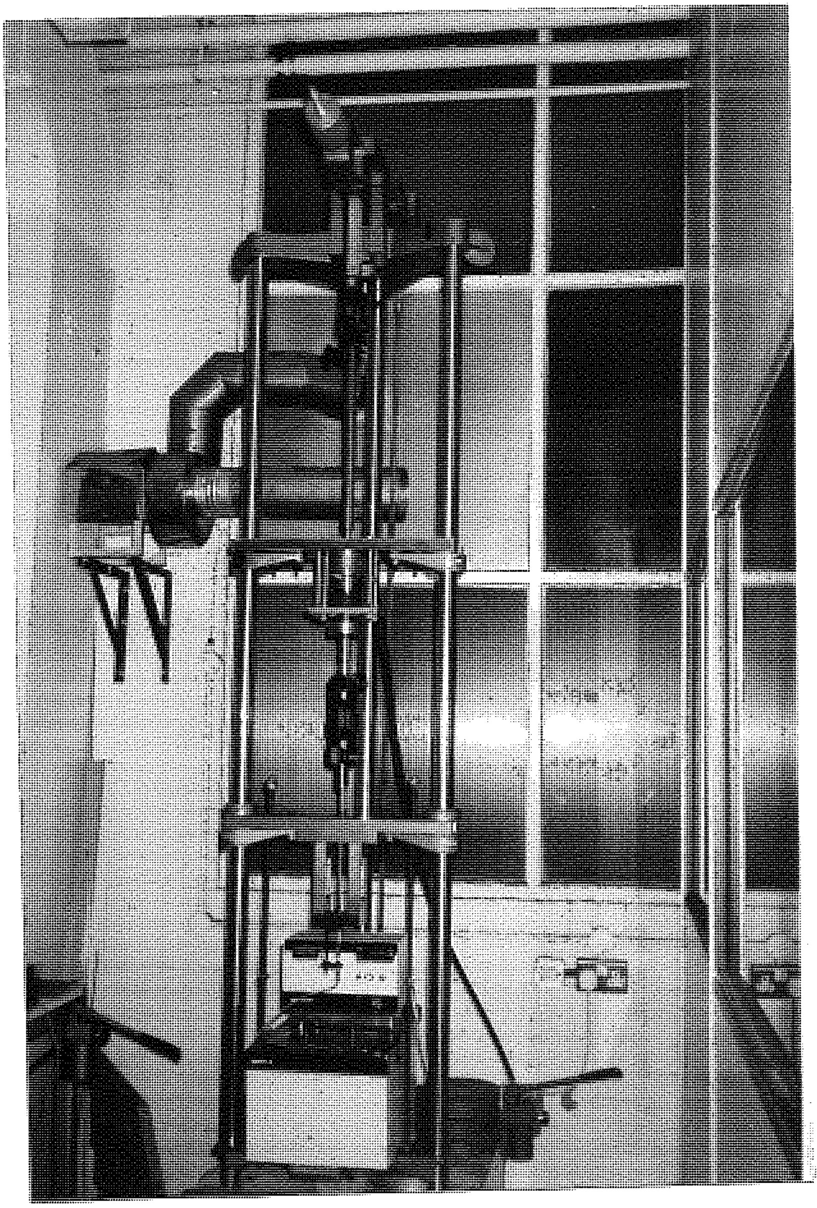

Figure 18. Compressive Creep Machine

bleed valve on the jack allowed a smooth transfer of load to the test specimen so it saved the test piece from a jerking load which may have affected the test data and produced unreliable results.

The second plate was between the other two plates which hold the rectanglar type structure of mild steel plates assembled together which was ultimately used to compress the test specimen during test. The third major plate holds the oil bath and can move up and down between two front columns.

4) A hydraulic jack was used to apply and remove the load on the test specimen. A hand pump was connected to the hydraulic jack and was bolted to the frame of the machine base.

5) Two linear bearings were fixed in two different plates in the rectangular type structure. These bearings assist in the alignment of the loading arrangement.

6) Two highly finished small plates which served as platens were used to compress the test specimen.

7) An oil bath was used to heat the test specimen to a required temperature and maintain it constant during the test. The range of operating temperature of the oil bath was 45°C to 300°C and an extended temperature range with additional cooling was -100 to 300°C. There was a temperature controller which formed a part of the oil bath having a temperature control accuracy of +/-0.03°C.

8) A load scale and appropriate loading weights which were loaded manually according to required load/stress for given test. The loading rod with a circular plate at its lower end to holds the weights was connected to the rear end of hanging lever at its upper end through a pin.

9) A steel rod, passing through the hydraulic jack whose one end was connected to the lever through a universal joint while the other end was jointed to the circular plate. This circular plate moves downward with the application of load on the jack.

10) Two universal joints which are helpful in the alignment.

11) A silver steel rod, 8mm diameter passing through the linear bearings.

12) Two rubber rings, used to align the test piece in a proper position coaxially with the loading rod.

13) A LVDT displacement transducer, used for the measurement of creep strain.

14) A square threaded rod which was used to move the whole oil bath up and down manually.

15) A microprocessor-based transducer conditioner was used to measure the deformation taking place during a test.

16) A light spring, used to keep the test piece in touch with the polished surface plates so that prior to the application of a load the test piece must be in contact with the platen plates, otherwise the deformation shown by the transducer conditioner will not be accurate.

Most of the fabrication and machining work of creep machine was done in the manufacturing and production laboratory of Aston University.

Some parts of the machine were purchased from the market which included:

i) The hydraulic jack with hand pump
ii) The oil bath
iii) The silicon oil (Sil 300), which is used in the oil bath to heat the test piece up to required test temperature.
iv) A displacement transducer.
v) Nuts, bolts and washers used during the assembly of the creep machine.
vi) Two linear bearings of 25.4mm long and 8mm bore
vii) Measurement and control software "Windmill", on a PC-type computer.

3.1.1 Heating Equipment (Oil Bath)

The oil bath was a very important part of the compressive creep machine. The main purpose of the oil bath was to heat the test specimen to the required test temperature and keep it constant during the test. The oil bath was manufactured by Haake (Germany) and its technical specifications are according to the German standard DIN 58966.

The size of oil bath was 380x300x425mm while the bath could be filled up to 200mm of depth. The weight of oil the bath was 17kg. The oil used was Sil 300 whose specifications were:

Temperature range = 80/270°C, Flash point = 280°C , Freezing point = -35°C,
Colour = Transparent colourless. The flash point was much higher than the maximum test temperature of 160°C.

This oil bath was selected for the following reasons:

1) Sufficient capacity to contain the test sample and loading/measurement systems.
2) Excellent temperature control during test.
3) The oil used fulfills the test temperature requirement due to its high flash point.

3.1.2 The Data Acquisition System

The data acquisition system consisted of the following parts:

1) A LVDT displacement transducer
2) A E525 CYPHER transducer conditioner
3) Data acquisition software "Windmill"
4) IBM Compatible Computer.

The linear variable differential transducer (LVDT) DC-DC D5 series from RDP Group used for this research provides one of the most reliable and accurate means of measuring displacement, position, dimensional tolerance etc. over a range from a few microns to 25mm.

The initial value of creep deformation is set close to zero by rotating the transducer core and by moving the transducer holding plate up and down before the application of load on the test sample. At the start of the experiment when load was applied the test specimen began to compress and creep began to occur. This compression displacement was measured by a transducer and was shown on E525 CYPHER transducer conditioner which was directly connected to the transducer. The values of creep strain were recorded after a particular time interval set in the data acquisition software "windmill". This software was designed especially for creep testing so that creep strain could be recorded precisely up to 4-significant figures (e.g. 0.0000).

The Windmill software can be set for data recording according to the required time interval. In this research work the time interval set for recording data in the beginning was 5 seconds, and this was gradually increased, as creep slowed down and ultimately the maximum time interval was 1 hour.

The test sequence gave a different number of readings at each interval of time set in the software.

Time (Sec)	Interval (Sec)	No of Readings
0	0	0
60	5	12
120	10	12
300	20	15
600	30	20
1200	60	20
3600	300	12
7200	900	8
14400	1800	8
2592000	3600	720

The data shown on the computer was in the form of creep strain verses time (s). The data files were automatically saved on hard disk and then copied for further analysis.

3.1.3 Testing of Compressive Creep Machine

After the assembly the creep machine was tested to check its performance. First, two experiments were carried out on test specimens of ZA8 and ACuZinc10 . These tests were performed at 100 MPa stress and 100°C. The creep deformation was recorded on the plotter which was already available and in use for tensile creep testing. The experiment was run for a few hours and then analysed. The creep shown on the plotter was compared with the actual test piece shortening and both were compared and found to be the same value. The plotter was then replaced by a direct data acquisition system.

Another creep test was performed on a mild steel test specimen at 100 MPa and 160°C which was run for 4 days. Mild steel should suffer negligible creep under these test conditions, and this sample exhibited almost no creep during that time. The results of these initial tests showed that the working of the machine was according to the requirements of this research programme and the resulting graphs could be used for creep analysis of these zinc-base alloys.

3.2 Load Relaxation Testing Technique

Load relaxation is the time and temperature dependent decrease of load in a solid due to conversion of elastic into inelastic strain. Load relaxation data can be used to develop stress-relief heat treatments for reducing residual stresses and for the design of such mechanical elements as joints, gaskets, and springs. Load relaxation for a specimen in a tension test depends upon the conditions of loading in the test, as well as on the materials elastic and inelastic properties.

3.2.1 Load Relaxation Tests

In a load relaxation test the specimen is first subjected to some desired elastic extension or equivalent load level. Typically a steel screw holding two members together is tightened, so that the screw is in ealstic tension and the members in compression. If creep occurs the screw or member deform inelastically, and the applied load gradually relaxes. The material used for load relaxation included ZA8, ZA12, ZA27, Cosmal, Supercosmal and LM25. Tests were performed at 80, 100 and 120°C under a preload of 6kN for 10,000 minutes.

3.2.2 Load Relaxation Testing Procedure

The testing equipment used for load relaxation tests consisted of the load monitoring cell, oil bath and data acquisition system. A 6kN preload was applied initially to a 6mm diameter ISO metric threaded screw inserted to a depth of 16mm into a threaded hole in sand-cast test piece. The whole assembly was dipped into the oil at constant temperature and loss of pre-load was monitored continuously for a period of 10,000 minutes.

Further description follows in *Chapter4* in detail.

CHAPTER 4

4.0 EXPERIMENTAL WORK

4.1 Experimental alloys

A group of commercial zinc alloys designated as ZA8, ZA12, and ZA27, were provided by Britannia Alloys & Chemicals Ltd. U.K. in the form of ingots with guaranteed composition.

To investigate the detailed effects of different phases present in higher-aluminium zinc alloys, Cosmal and Supercosmal which are known as high damping capacity alloys, were also tested for creep and load relaxation. Supercosmal was supplied by Britannia Alloys & Chemicals Ltd. U.K. in the form of ingots with guaranteed composition, while Cosmal was prepared locally in the Departmental foundry with exact composition. The calculated amount of zinc and aluminium along with small quantities of other alloying elements were melted in a gas-air furnace at temperature 600°C and was stirred vigorously and then poured into a sand mould to acquire the resultant casting.(See *Table 9* for composition).

LM25 was also supplied by Britannia Alloys & Chemicals Ltd. U.K. in the form of ingots with guaranteed composition. It was also used for creep and load relaxation testing under the same temperature and stress conditions.

4.2 Casting of Alloys

There are four major factors which should be considered during the development of moulding and casting methods. These are the Size of moulding, Composition of alloys, Mechanical properties of materials and Production and economic factors.

Different methods are commonly employed to cast the zinc-base alloys studied here, which include sand casting, investment casting, die-casting, permanent-mould casting, etc. Sand casting was used to cast all alloys used in this research work because it was suitable for all the alloys being investigated, with low tooling costs.

Table 8. Standard Composition of Alloys (wt %)(1,113)

Material/ Elements	ZA8	ZA12	ZA27	Cosmal	Supercosmal	LM25
Al	8-8.80	10.50-11.50	25-28	40	60	Balance
Mg	0.0150-0.030	0.0150-0.030	0.010-0.020	0.0050	0.0050	0.20-0.450
Cu	0.80-1.30	0.50-1.20	2-2.50	1.0	1.0	0.10
Fe(max.)	0.0750	0.0750	0.0750	0.10	0.20	0.50
Pb (max.)	0.0060	0.0060	0.0060	0.0030	0.0030	0.10
Cd (max.)	0.0060	0.0060	0.0060	0.0010	0.0010	
Sn (max.)	0.0030	0.0030	0.0030	0.0010	0.0010	0.050
Ni						0.10
Si				3	6	6.50-7.50
Mn				0.30	0.30	0.30
Ti						
Zn	Balance	Balance	Balance	Balance	Balance	0.10

Table 9. Composition of tested Alloys (wt %)

	Cu (%)	Mg (%)	Si (%)	Fe (%)	Zn (%)	Al (%)
ZA8	1.07	-	-	-	88.9	9.89
ZA12	0.79	-	-	-	87.1	12.0
ZA27	2.02	-	-	-	70.7	27.2
COSMAL	1.03	-	NA	-	57.0	40.1
SUPERCOSMAL	1.02	-	NA	-	33.0	57.0
LM25	-	0.38	7.35	0.44	-	90.9

However it is not a precision process, and sand castings have the lowest surface finish quality, but since test samples had to be fully machined, this was not a disadvantage. The slow cooling rate of sand casting did however produce relatively coarse microstructures compared with other forms of casting.

The pattern used for the preparation of moulds was 18mm in diameter and 100mm long made from a metal which consists of two identical parts as shown in *Figure 19* so that it could be easily extracted after the sand was properly packed around it. It had two small pins in one part to locate the other part properly over it and could be separated easily when required. It was prepared in the Production Engineering laboratory.

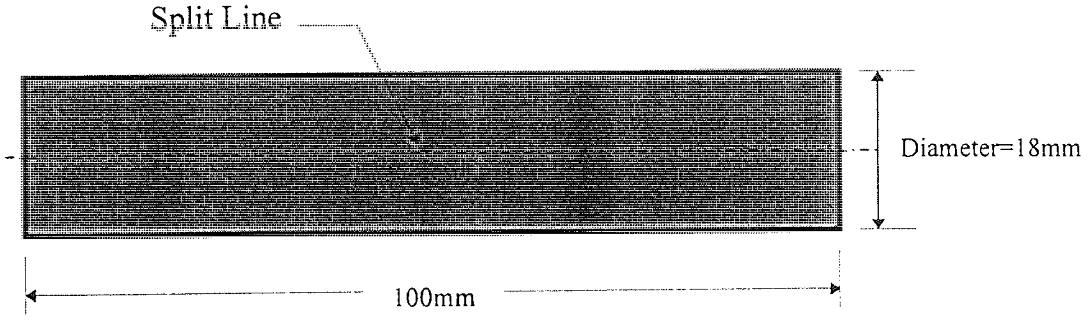

Figure 19. Metal pattern used for casting

Silica sand bonded with a small amount of clay was used for the preparation of mould. For conventional moulding, a typical range of moisture content recommended is 3-3.5%[(2)]. It was very important to maintain the amount of moisture content, because it controls all the the strength properties of the sand mix and can markedly affect the sand-castings.

The steps involved in the preparation of the mould were as follows:

a) The bottom halves of the metal pattern were placed on a mould board in the bottom half of the flask, and two bronze chills were placed on one side of each pattern. The chills play an important role to prevent shrinkage cavities and also promote soundness in the casting.

b) The bottom half of flask was filled with moistened sand which was prepared in sand miller and rammed to achieve the correct degree of sand compaction. The excess sand was struck off the flask.

c) It was rolled over and the top of the pattern and flask were placed in position.

d) Parting powder (talc powder) was applied on the prepared bottom half of the mould so that the two halves could be separated easily without disturbing the facing sand. It was also helpful in achieving smooth extraction of the metal pattern from the mould.

e) The top half of the mould was prepared in the same way and the feeder (sprue) was placed at a proper position to receive the molten alloy.

f) The upper half of the flask was separated from the lower half, and the pattern removed. Feeding gates were prepared very carefully to feed the mould. With a simple top poured mould, the metal falls vertically inside the mould with the consequent risk of splashing and sand erosion. To avoid this, the metal was introduced at the lowest point of the mould, i.e. bottom-gating, and to prevent the adverse temperature gradients produced by this procedure, ingates were provided which became inoperative in turn as the molten metal rose in the mould. The upper half of the mould was refitted back after cutting of the ingates. Most metals contract during solidification so risers were utilised to supply molten metal to the casting and avoid the formation of shrinkage cavities. The risers were cut with a tapered pipe. To be effective, the size of risers was made sufficient to provide extra metal, and ensured that it stayed molten until the casting itself had solidified. The risers also remained open to atmospheric pressure. The runner was prepared using a brass pipe to cut away the sand.

4.2.1 Sand Casting Procedure

Once the moulding box had been prepared, it was ready for casting. The required amount of ingot material was placed in a clay-graphite crucible and melted in a gas-air furnace. The temperature was raised to about 50°C above the melting point of the alloy so giving a reasonable degree of preheat. The metal temperature was measured with a standard Pyrotenax Chromel/Alumel thermocouple which was connected to a digital indicator with working accuracy of +/-2°C. The crucible was taken out from the furnace with the help of lifting tongs, stirred vigorously and then the molten metal was poured into the mould through the feeder and left to cool for about half an hour. After cooling the casting was broken out of its mould. Now it was ready for the remaining processes, i.e. cleaning and fettling.

Basically the same procedure was used to cast each material used in this research work.

In the case of LM25, degassing was required, so the tablets of hexachlorine were used as a degasser. Chlorine liberated from this compound reacts with hydrogen and forms gaseous HCL, which evaporates into the air. Any oxygen present in the molten metal reacts with aluminium and forms alumina, which floats up to the surface of liquid and can be easily removed.

4.3 Test Specimens

Two types of test specimens were prepared from the above castings, totalling about 300 in number from all six materials. These test specimens had to be machined in such a way as to avoid any deformation or surface defects and ensure that the metallurgical structure and mechanical properties of the test pieces were representative of the original test material.

Cylindrical creep test specimens were machined from the above castings in the Manufacturing and Production workshop at Aston University with surface finish, CLA (Centre line average height)=1.14 μ m. The finished test pieces were of cylindrical shape with dimensions shown in *Figure 20.*

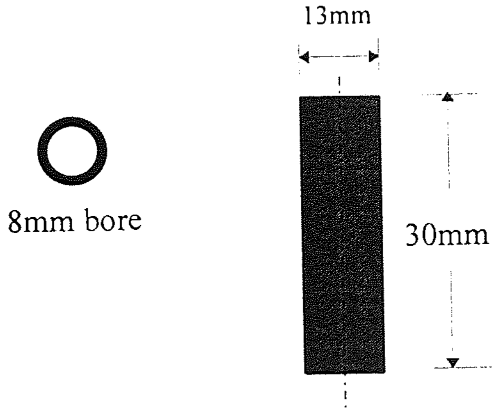

Figure 20. Creep test piece

The load relaxation test specimens had the same dimensions (length and diameter) but differed in internal bore. These specimens had a threaded bore of nominally 6mm diameter (ISO metric thread with cutting tap), shown in *Figure 21.*

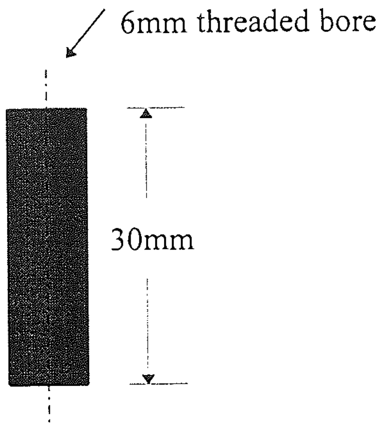

Figure 21. Load relaxation test piece

4.3 Compressive Creep Testing

The compressive creep tests were performed on the conventional zinc alloys ZA8, ZA12, and ZA27, and also on two high damping-alloys, Cosmal and Supercosmal. Some tests were also performed on LM25.

The tests were carried out at 70°C, 100°C, 130°C and 160°C and at stress levels from 20 MPa to 100MPa. Most of the tests were done in duplicate in order to obtain a better precision in measuring the compressive creep behaviour of the alloys. Some of the tests were done in triplicate or more where duplicates showed significant variation. The temperature and stress levels were chosen to test the alloys at lower and comparatively higher range of stress and temperature.

The compressive creep machine described in *Chapter 3 Figure 18* was used for compressive creep testing.

4.3.1 Creep Testing Procedure

The LVDT transducer was fixed in the plate shown in *Figure 17* connected with transducer conditioner and a check of its working made by moving the transducer core up and down. The transducer conditioner was connected with the computer.

Two rubber rings, (Bore=5mm, Thickness=1mm) were set on a 6mm silver steel rod at test piece location at two different points so that test piece should be aligned exactly in the centre and could not move either side. The test piece was pushed over these rubber rings and a circular plate was placed under it to hold it and a nut was tightened under this plate. The test piece was gripped between the two highly-polished platen plates by applying a light spring force provided for this purpose. The transducer core was screwed into a threaded axial hole in the silver steel rod under the nut, in such a way that the reading on the transducer conditioner was close to zero, and then the transducer holding plate was tightened to avoid any movement of the transducer.

To check the temperature of the test specimen, and presence of any temperature gradient inside the oil bath, a thermocouple was attached to a potentiometer. The oil bath was raised until the entire sample loading part was completely submerged in oil by rotating the square threaded rod. The oil bath was switched ON and set to the required test temperature and left for a few hours so that the whole assembly/system should acquire the same test temperature.

For the required stress level, the calculated weight was put in the load pan by taking into account the lever arm ratio, and this weight was held by the hydraulic jack. The Computer was switched ON and data acquisition software ”Windmill” was loaded.

The test was started in Windmill software, and load was applied on the test piece from the hydraulic jack by loosing its oil bleed valve knob. With the application of load the creep deformation was displayed by the transducer conditioner in digits and recorded by the Windmill software on the hard disk according to the test sequence file. A very small amount of deformation (up to 4 digits after decimal) could be seen on the transducer conditioner every second from the start to the end of the test and was recorded by the software. The data recorded by software was in the form of time versus strain. Most of the experiments were conducted to a minimum creep deformation of 1 % whereas in some tests and in some materials at higher temperatures and stresses, a creep strain was recorded of more than 10 % in a very short time (10 minutes). This data could be seen at any time on the computer and copied for further analysis.

The most important factor in creep testing was axial alignment of the loading system and specimen. Misalignment could have significantly influenced the test results, especially those at very low strains because misalignment affects the average stress at which the transition from elastic to nonelastic deformation occurs. The test piece temperature should also remain constant throughout the creep test and the applied load should not be varied during the test.

The thermocouple should normally be in contact with the surface of the test specimen so that any temperature gradient could be recorded correctly, but in this application the whole bath was closely controlled to a selected temperature, and significant time allowed before testing, to achieve equilibrium.

4.3.4 Calibration of Transducer

The transducer was held in a small plate especially designed for its calibration as shown in *Figure 22* and then dipped in oil at calibration temperature and was kept at least 20

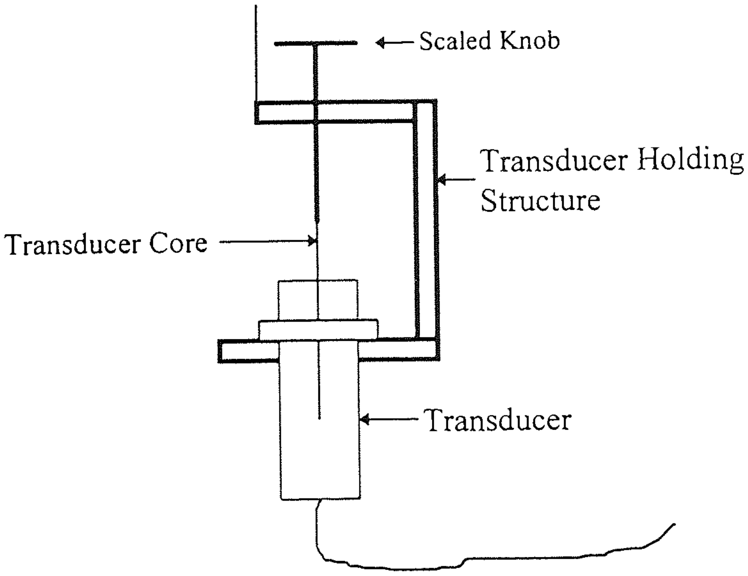

Figure 22. U-Shape metal structure used in Calibration of Transducer

minutes to settle to the calibration temperature. The rod in which the transducer core was fitted had a pitch diameter of 1mm. It was rotated clockwise for 2.5 rotations and anti-clockwise for -2.5 rotations and the displayed values on the transducer conditioner were listed in *Table 10* The multiplication factors were obtained for each temperature in order to measure the actual amount of creep contraction.

Table 10. The calibrated values obtained at different temperatures:

Temperature (°C)	Clockwise Rotation	Anti-Clockwise Rotation
70	+2.46	-2.49
100	+2.39	-2.48
130	+2.31	-2.45
160	+2.27	-2.40

Multiplication factors were obtained from these values for tests performed at different temperatures from 70 to 160°C. These multiplication factors were :

Table 11. Multiplication factors for different temperatures

Temperature (°C)	Multiplication Factor
70	1.01
100	1.03
130	1.05
160	1.07

4.3 Load Relaxation Testing

All zinc-based alloys and LM25 were also used for load-relaxation testing. These tests were carried out at temperatures of 80°C, 100°C and 120°C using an initial preload of 6kN. All load relaxation tests were done in duplicate but some of them were done thrice to better understand the behaviour of the alloys when double was not sufficient.

4.4.1 Load Relaxation Testing Equipment

The load relaxation testing equipment consisted of a load monitoring cell, oil bath and data acquisition system.

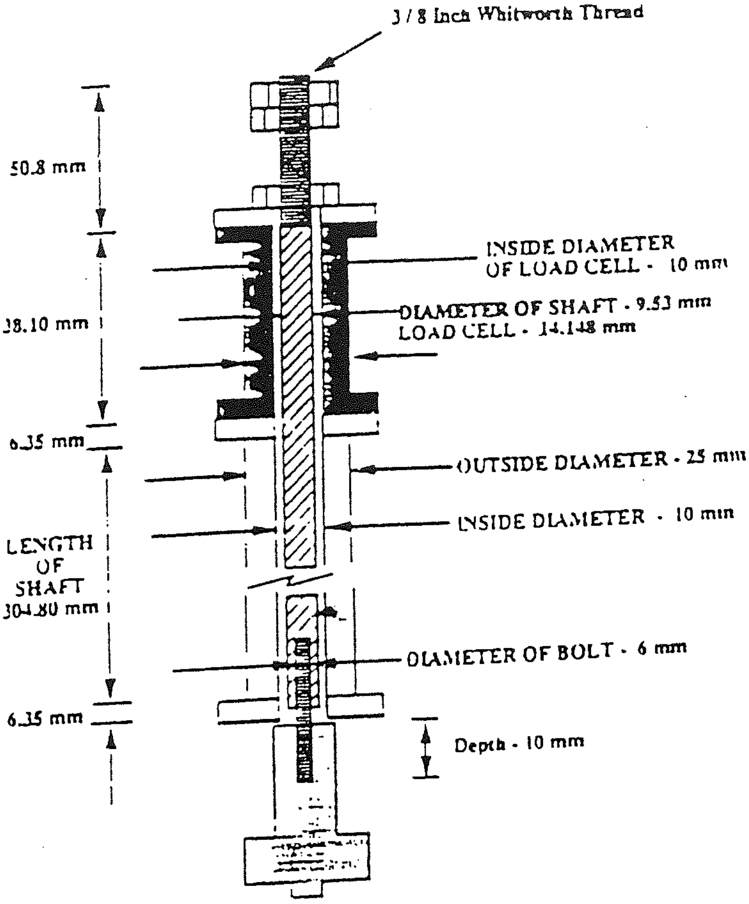

Figure 23. Load monitoring cell

The load monitoring cell (*Figure 23*) was used for the continuous monitoring of load in the commercial fasteners used. It consisted of a short tension rod to which the head of a fastener is attached, transmits tensile stress in the fastener through a compression load cell. When the casting was screwed onto the fastener, it simulated the effect of inserting a screw into a hole. The load cell (doughnut shaped) was a purchased item, used to measure the tensile force exerted on the fastener screw and thread of a casting. The maximum non-linearity was +/-0.5 % F.S., and its operating temperature range was -

54°C to 121°C. The housing material was stainless steel and it was said to be safe for a 50% overload.

The data acquisition system used to record the results of load relaxation tests was called "Translog 500", which is a comprehensive hardware and software package for the retrieval, recording, alarm monitoring and computation of data from transducers of many kinds. It was manufactured by RDP Electronics Ltd. U.K. and had a modular construction which was easily expandable. There were 8 to 64 channels per 19 inch rack and could be expanded to 256 channels. The system had digital filtering for high resolution and could scan very fast. i.e. 100 channels/s. Calibration facilities including push button zero setting, and auto-scaling in engineering units had been provided.*

The system had a host computer data logging programme which could be used with any IBM compatible computer having the necessary RS232 serial interface, and could be linked with spreadsheets such as Lotus 123. Thirty two software comparators each with high (HI) and low (LO) set points could be used to monitored transducer channels and operated relays. There were input/output modules for set point or programmed commands. Variable speed logging was another useful feature provided by the programme. This allowed the user to program the data logging speed to suit the application , e.g. at the start of a logging RUN, it was often necessary to take lots of data readings, and then slow down as the RUN progressed.

Data logging could be directed to a floppy disk, hard disk, RAM disk, or printer, and data storage was only limited by the disc capacity. The system was suitable for short and long term data-logging.

* *All information about (Translog 500) the data acquisition system was provided by RDP Electronic Ltd.*

The oil bath with a stirrer which circulated the oil to maintain the uniform temperature throughout the bath, was used to heat the test specimen and maintain the test temperature throughout the test. The oil bath has a capacity of 30 litres and the maximum working temperature was 150°C. The oil used was Vitrea 32. Seven test specimens could be loaded at one time. The temperature controller attached to the oil bath showed the oil temperature in digital form and also controlled the test temperature with an accuracy of +/-0.1°C.

4.4.2 Load Relaxation Testing Procedure

A 6mm diameter and 1mm pitch ISO Metric threaded fastener screw (M6x1) was locked in the tension rod and a test piece screwed over it to a depth of 16mm. The assembly was kept at constant testing temperature in an oil bath and immersed for two hours before the test commenced so that whole assembly acquired the same temperature.

The load was applied on the test piece by tightening the nut on the top of the rod, and this load was monitored continuously on the computer screen till it reached 6kN. The data acquisition system started to record data with the application of load on the test piece.

The residual load was continuously monitored for a period of up to 576 ks at each temperature. The test temperature was kept constant with a variation of +/-0.5°C.

The data recorded by the data acquisition system was in the form of time (min) versus retained load (N). The time interval for data recording was 0.5 minutes in the beginning and was gradually increased to a maximum of 4 hours interval.

All tests were carried out duplicate and if appreciable scatter was found in the results, some additional tests were also performed at those particular temperatures. The average values of the results were used to represent the load relaxation resistance/behaviour of these zinc-base alloys.

4.5 Metallography

4.5.1 Metallographic Specimen Preparation

The different steps followed in the preparation of metallographic specimens were: Specimens were cut in longitudinal and cross sectional sections from the samples, as-cast condition, and after test, with a jeweler's saw, using slow strokes and light pressure. They were mounted in bakelite using a hydraulic mounting press, and ground on silicon carbide paper from 120m to 1200m grades under light hand pressure. Water was used to cool the specimens frequently to prevent overheating. They were rinsed in acetone and polished using diamond abrasive to a final finish of 1μm to get a scratch free surface.

4.5.2 Scanning Electron Microscopy

Samples from each alloy in the as-cast condition and after tests (creep and load relaxation), were examined by scanning electron microscopy to study the structures and the effect of creep and load relaxation on microstructures.

To obtain better resolution than with light optical microscopy and to take advantage of the big difference between the atomic numbers of the two main constituents (zinc and aluminium) of the alloys, back-scattered electron scanning microscopy was adopted as the general investigation method. By using back scattered electrons, contrast could be obtained from the difference in average atomic number (Z) of various phases in the sample. Higher Z regions have more nuclear charge and hence give rise to a greater number of back scattered and smaller number of absorbed electrons than low Z regions. For this work, the scanning electron microscope, Cambridge Instruments SEM fitted with a special large area, back-scattered electron detector was used. The voltage used in the SEM for this work was 25 kV.

CHAPTER 5

5.0 EXPERIMENTAL RESULTS

5.1 Creep Results of Zinc-based Alloys

For each compressive creep experiment of zinc-based alloys the variation of creep strain was presented in the form of graphs plotted as percentage of creep strain (ε) versus time in seconds (s). In all cases, the curves showed the same general form of the creep curve, i.e. a primary creep stage which exhibited the steadily decreasing strain rate, followed by a linear steady-state region (secondary creep).

Most of the creep experiments were performed to produce a minimum creep strain of 1%, which was usually reached in the secondary creep region. In some tests, which were conducted at high stress (100 MPa) and high temperature (160°C), the creep strain reaches more than 10 % in a very short time. The tests were not generally allowed to proceed into the tertiary creep region. However, some curves showed a tertiary region when the alloys were tested at high stress and temperature, as seen in the cases of ZA8, ZA12 and ZA27 at 100 MPa and 160°C.

Some tests showed 1% creep strain at a rather early stage of creep, either in the primary or in early stages of the secondary creep region, due to which it was difficult to determine the exact secondary creep rate. Such experiments were therefore extended to obtain a reliable secondary creep data, until well defined secondary creep regions were obtained.

To investigate the compressive creep behaviour of alloys, more than 150 tests were performed at different stress and temperature conditions. Some examples of creep curves were selected to show the characteristic time-creep strain behaviour of the alloys as seen in *Figures 24 to 29*.

To examine the alloys more clearly some graphs were also drawn from average values to examine their comparative creep strength as shown in *Figures 30 to 35*.

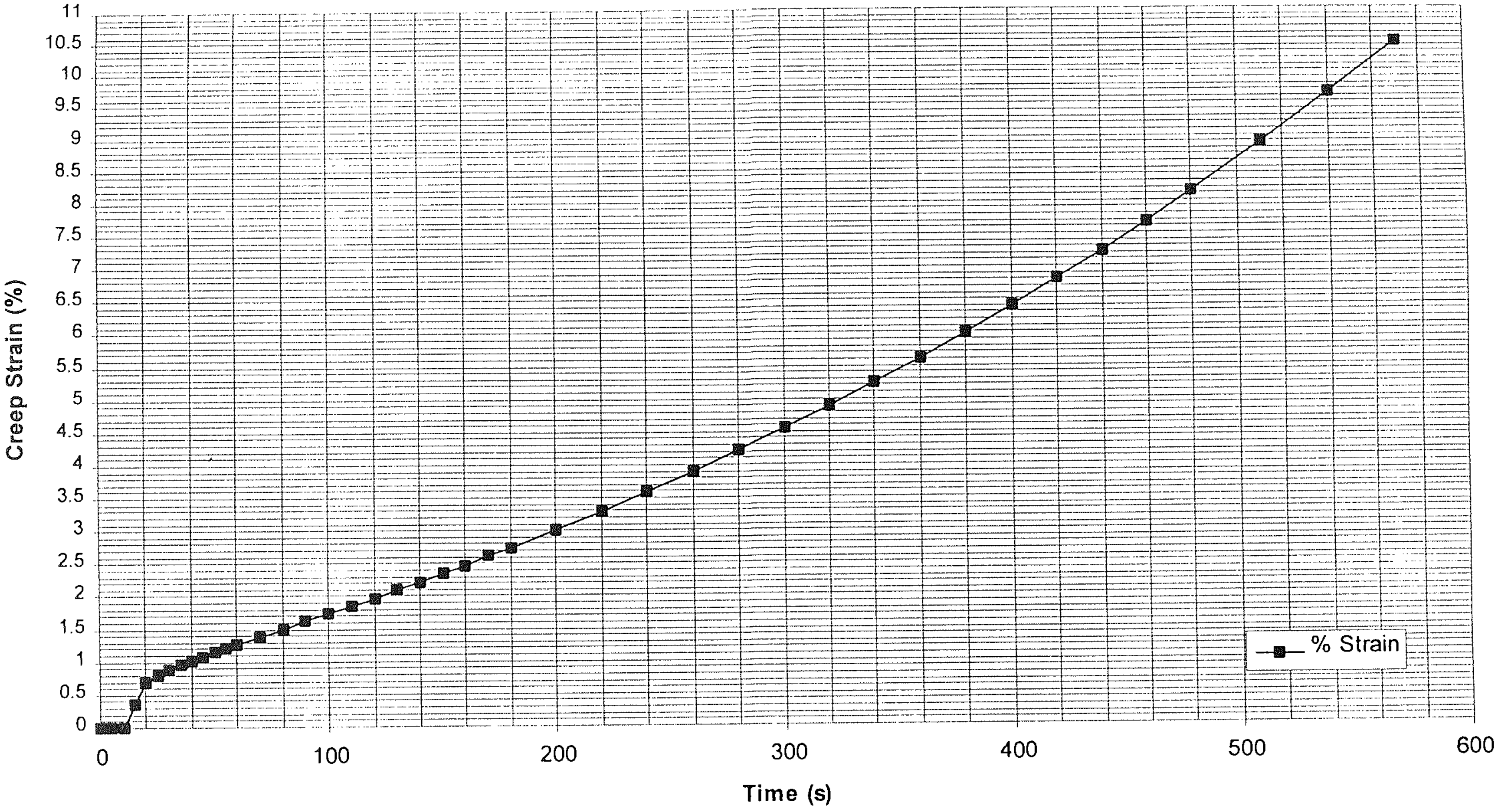

Figure 24. Creep curve of alloy ZA8 at 100 MPa and 160°C.

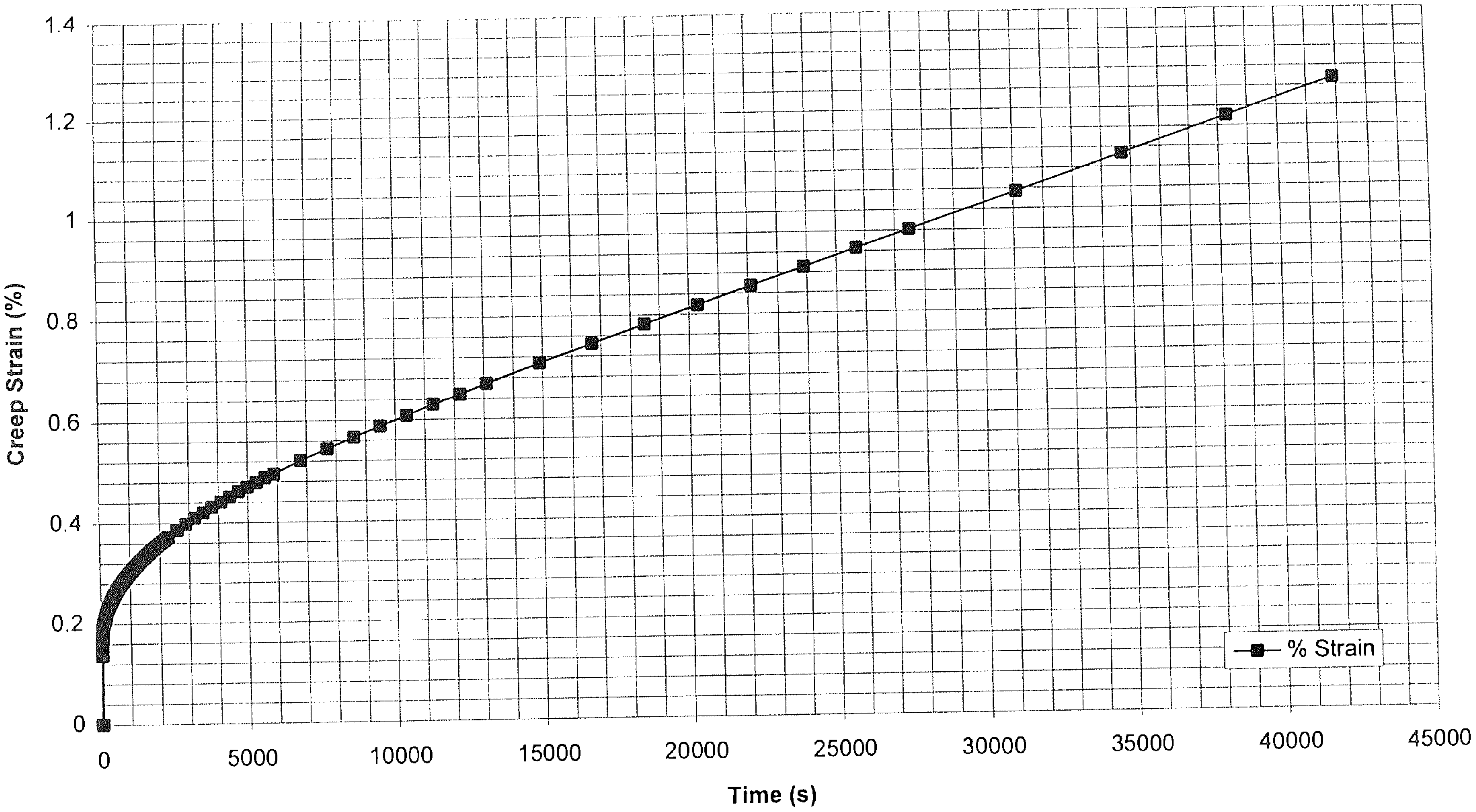

Figure 25. Creep curve of alloy ZA12 at 40 MPa and 130°C.

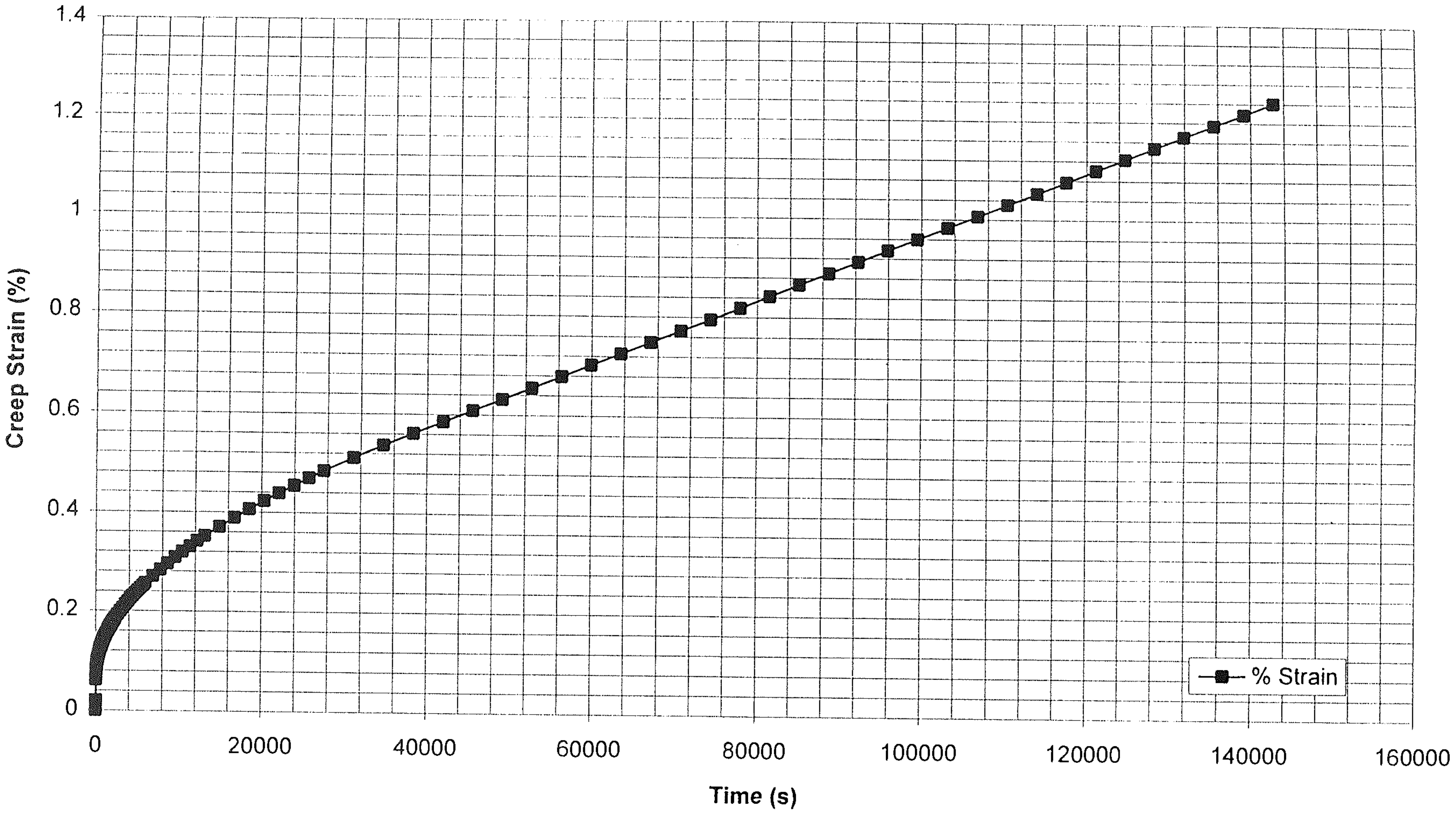

Figure 26. Creep curve of alloy ZA27 at 20 MPa and 130°C.

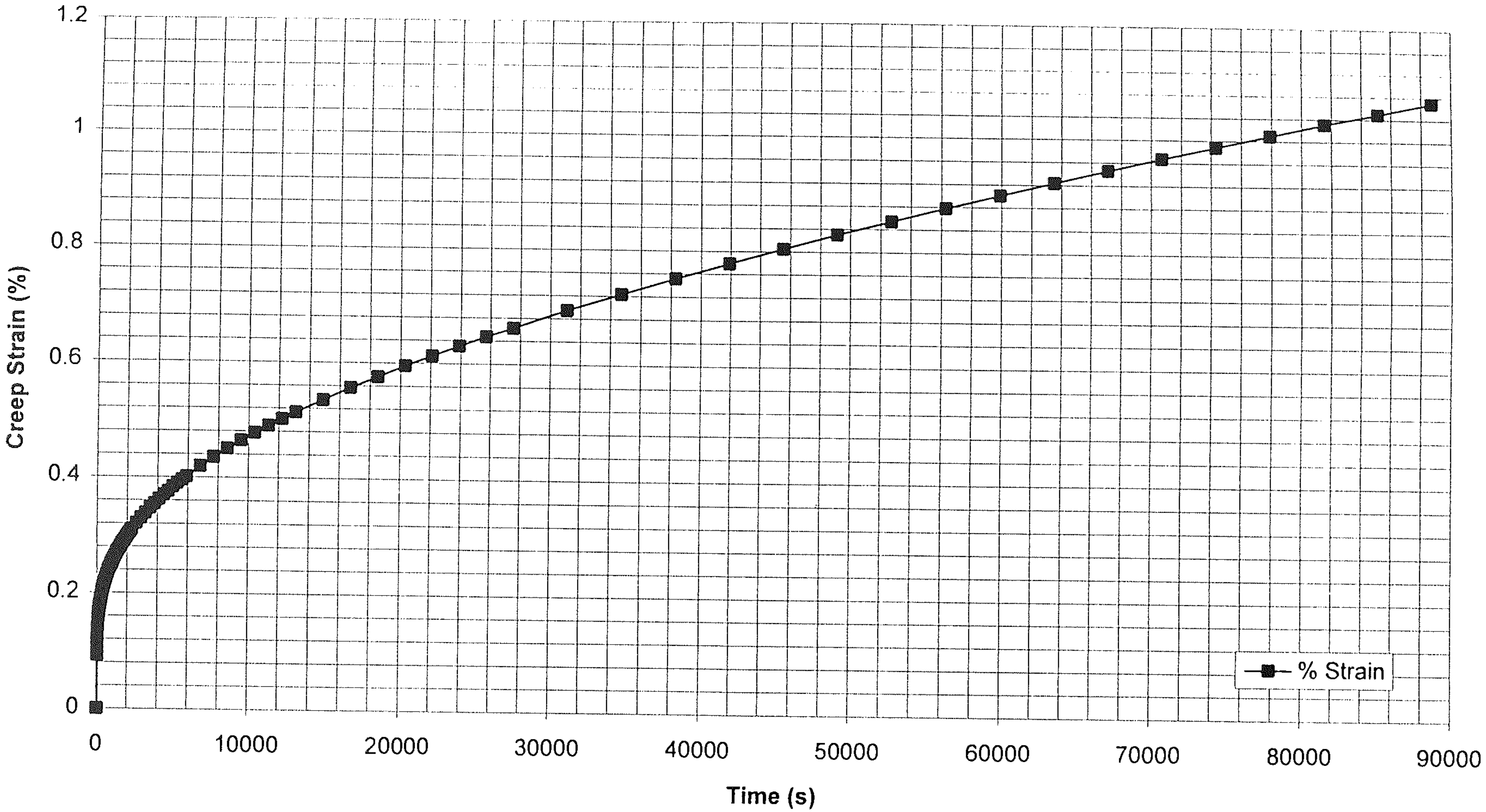

Figure 27. Creep curve of alloy ZA27 at 40 MPa and 100°C.

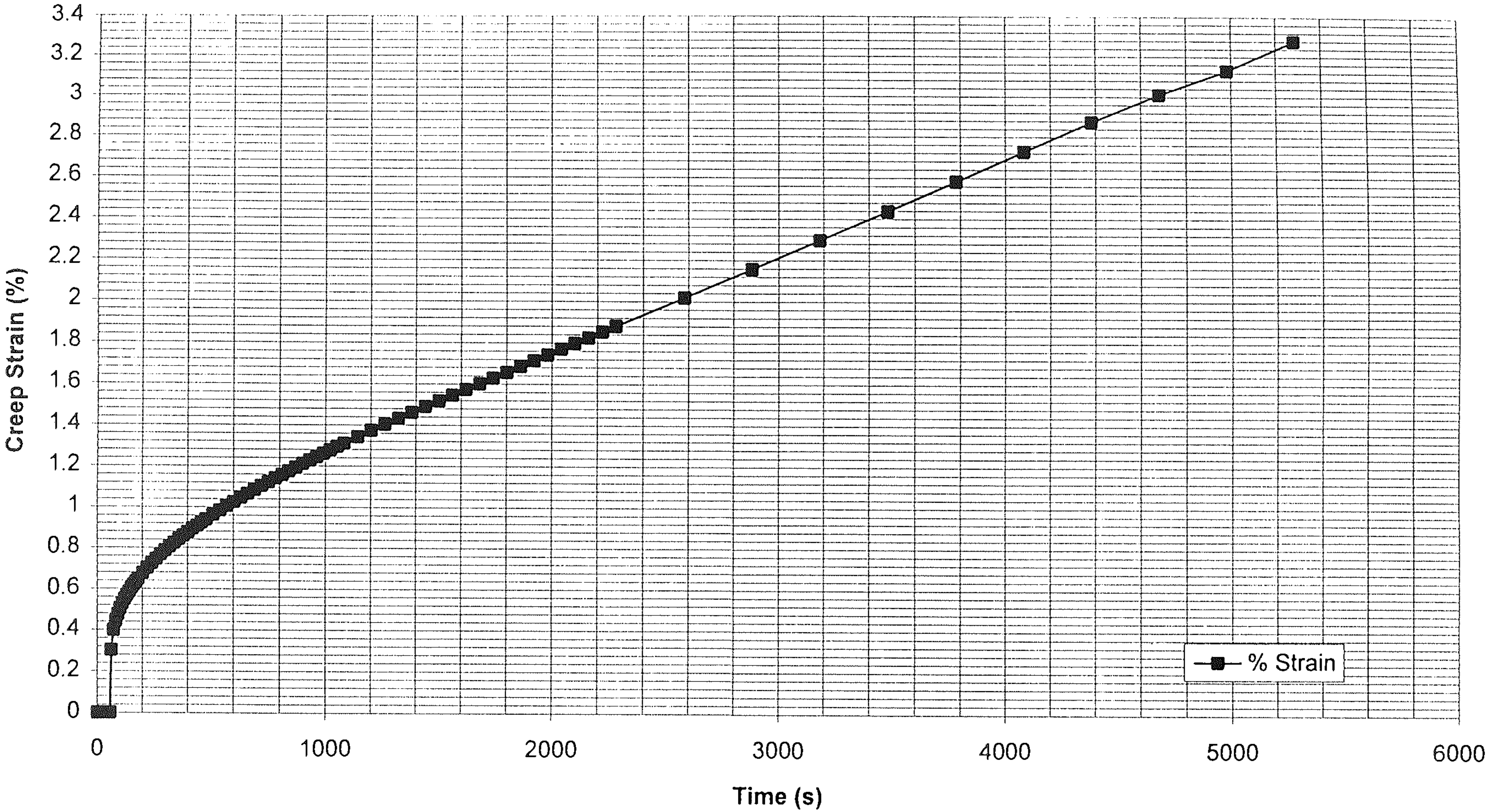

Figure 28. Creep curve of alloy Cosmal at 60 MPa and 160°C.

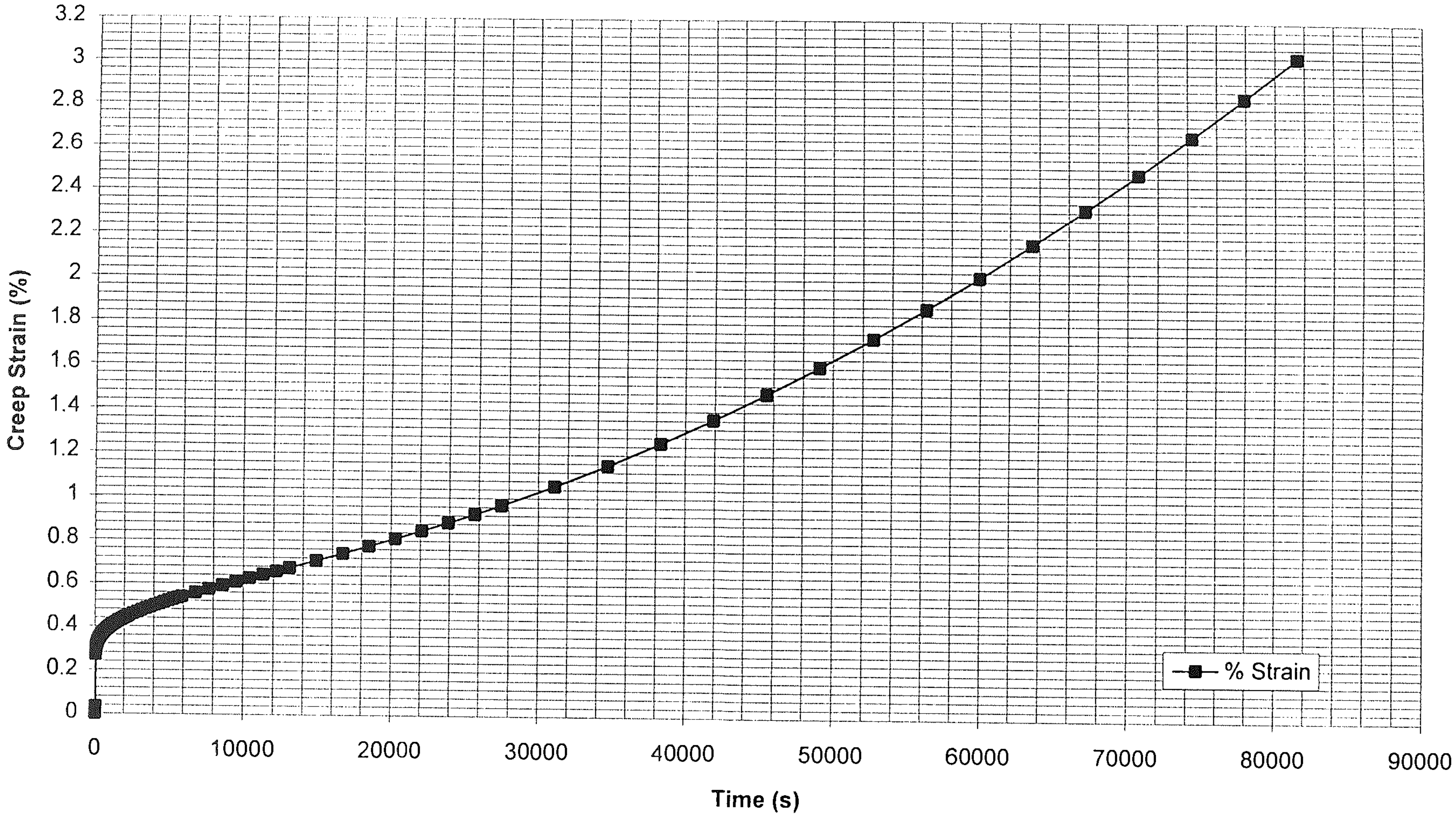

Figure 29. Creep curve of alloy Supercosmal at 100 MPa and 160°C.

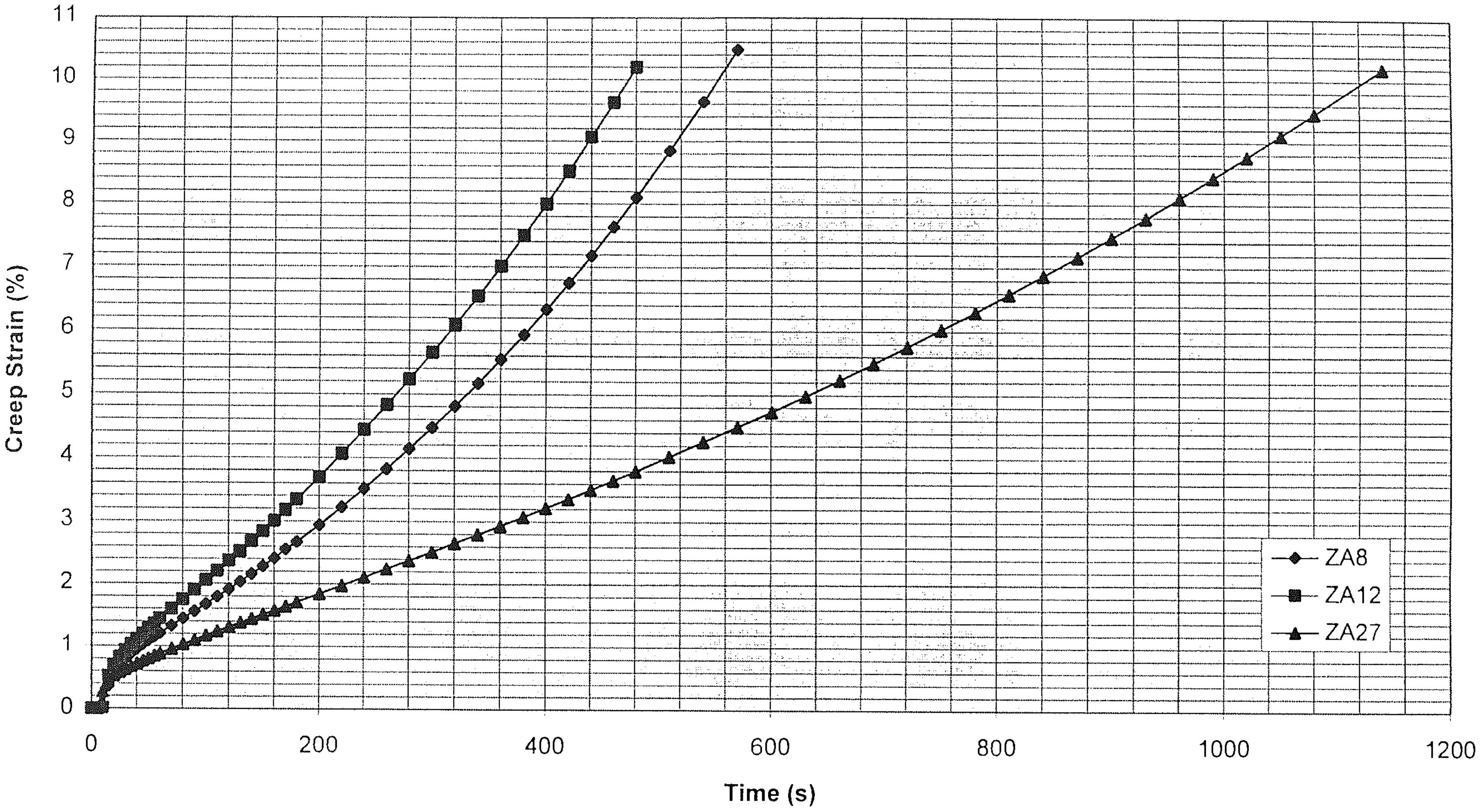

Figure 30. Creep curve of alloy ZA8, ZA12 and ZA27 at 100 MPa and 160°C (average values).

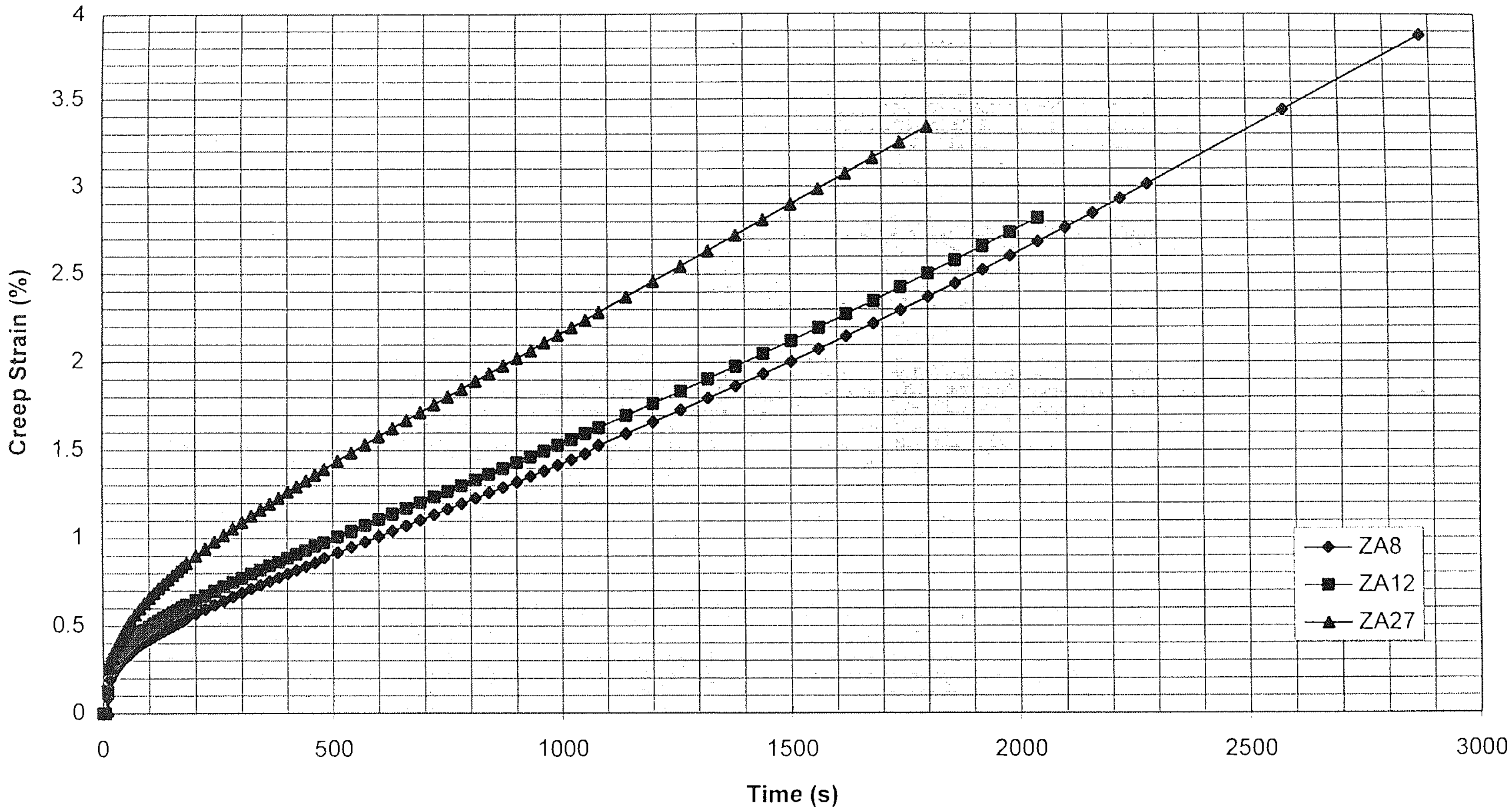

Figure 31. Creep curve of alloy ZA8, ZA12 and ZA27 at 60 MPa and 160°C (average values).

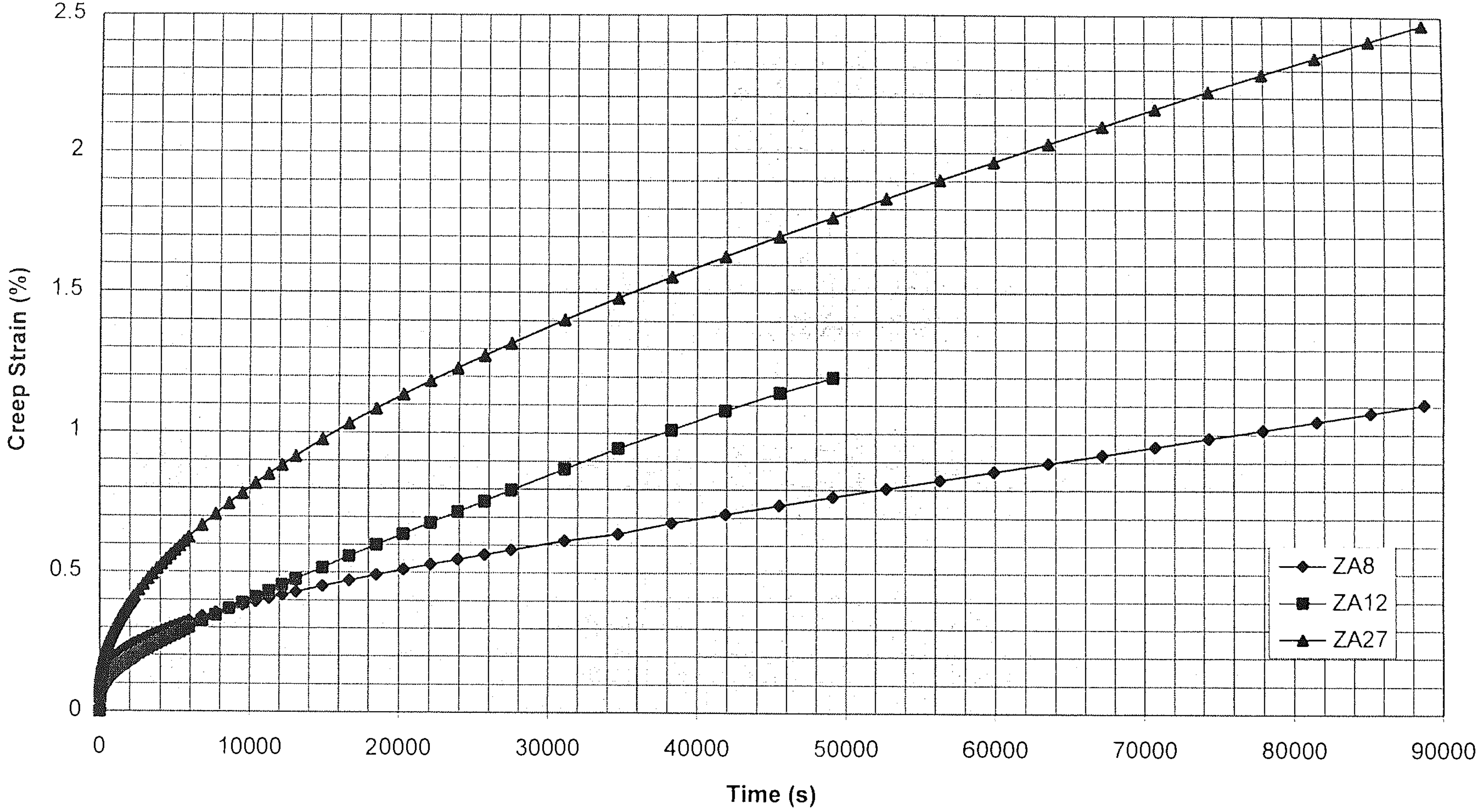

Figure 32. Creep curve of alloy ZA8, ZA12 and ZA27 at 20 MPa and 160°C (average values).

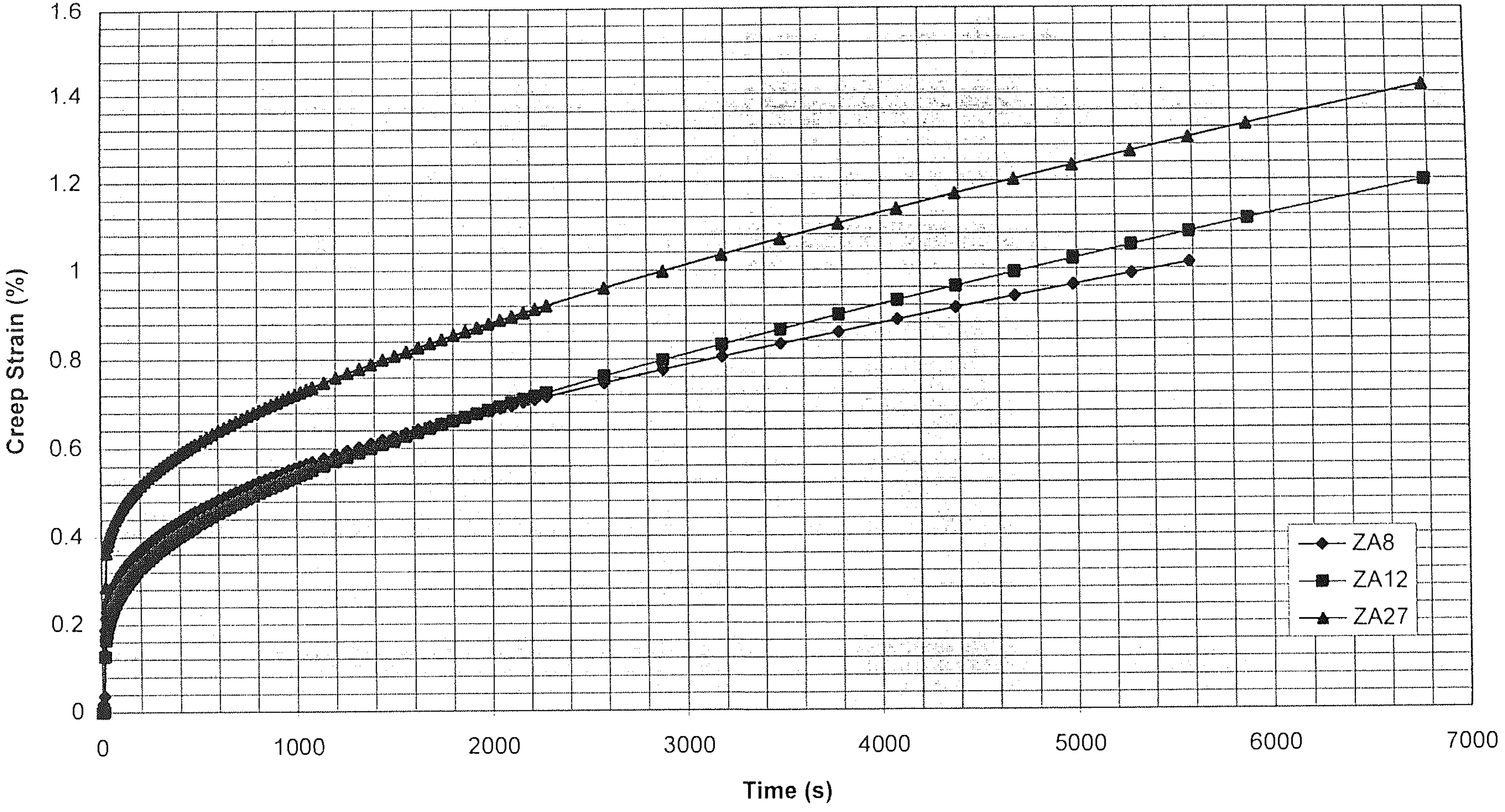

Figure 33. Creep curve of alloy ZA8, ZA12 and ZA27 at 100 MPa and 100°C (average values).

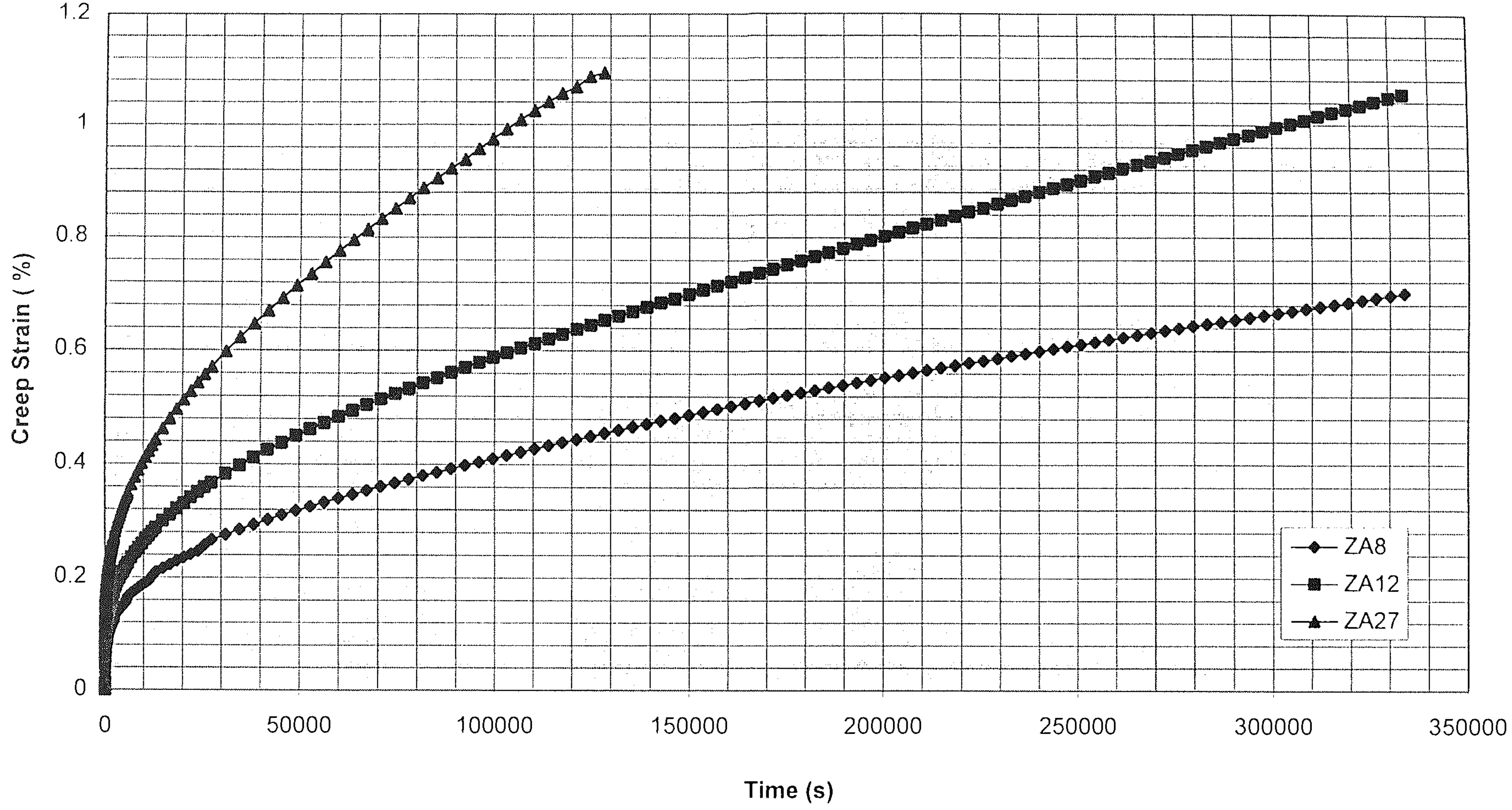

Figure 34. Creep curve of alloy ZA8, ZA12 and ZA27 at 40 MPa and 100°C (average values).

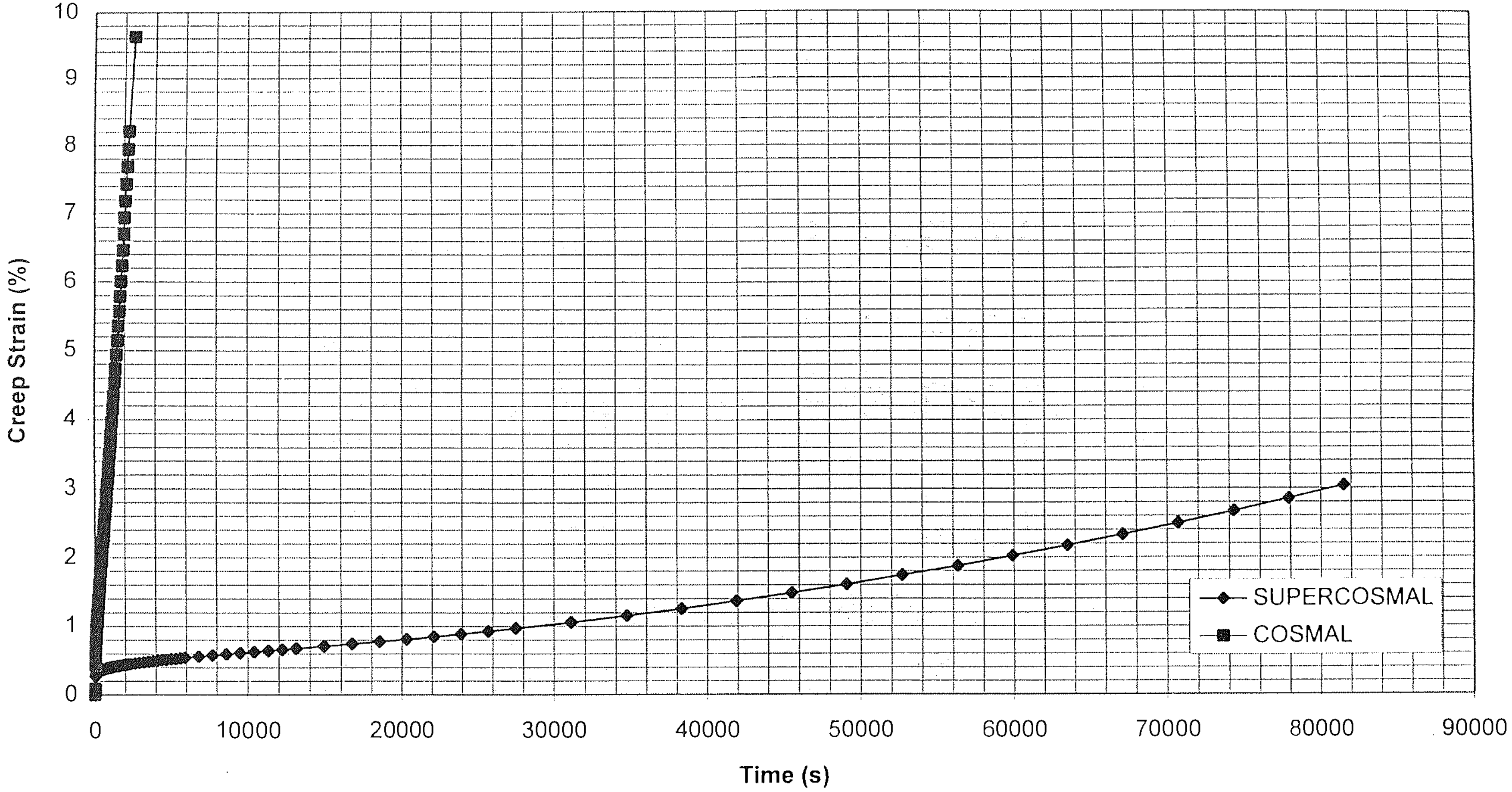

Figure 35. Creep curve of Cosmal and Supercosmal at 100 MPa and 160°C (average values).

In general, it was observed that alloy ZA8 had the least primary creep among the commercial zinc-base alloys and ZA27 the greatest. The overall creep strength of ZA27 was less than ZA8 at low stress and temperature conditions but it had more creep strength than ZA8 and ZA12 at high temperature (160°C and 130°C) and high stress (100MPa), *Figure 30* While secondary creep regions of alloy ZA27 were comparatively longer than alloy ZA8, and ZA12 has the least.

Among the high damping capacity alloys, Cosmal and Supercosmal, the Supercosmal had less primary creep and longer secondary creep regions. Supercosmal had the lowest minimum creep rate among all the tested materials. Due to its higher creep strength it was tested at higher temperature and stress to obtained 1% or more creep strain, while at lower stress and temperature conditions less than 1% creep strain was obtained. In order to get the 1% or more creep strain in Supercosmal at lower stress and temperature, a couple of months or even a couple of years may have been required as it is clear from its data that it has almost no creep at low stress and temperature conditions. The creep data of these alloys are tabulated in *Appendix A*.

The aluminium alloy LM 25 was tested at max. stress, 100 MPa and max. temperature 160°C but virtually no creep was found during an experiment which was run for one week.

Secondary creep rates (ε_s) were calculated from the steady-state parts of the creep curves, using linear regression analysis. The slope of the regression was taken to be the value of the secondary creep rate and the intercept of the slope on the strain ordinate at zero time, the primary creep strain including instantaneous creep strain.

To obtain the relative creep performances of the alloys to a selected total creep elongation, the times to produce a creep strain of 1%, 0.8%, 0.6%, 0.4% & 0.2% were also calculated from these curves. The creep data of the alloys tested at different test conditions are tabulated in *Appendix A*.

5.1.1 Primary Creep Contraction

The values of primary creep contraction were obtained by extrapolating the linear secondary creep portion of the curves back to zero time. The values of primary creep (%) were calculated for all alloys and are tabulated in *Appendix A*.

5.1.1.1 Primary Creep of Commercial Zinc-based Alloys

It is clear from the results of average primary creep, *Figure 36*, that temperature has a definite effect on primary creep contraction in commercial zinc-base alloys at any stress. The values of primary creep contraction at different temperatures are minimum in ZA8 and maximum in ZA27 with the one exception that ZA12 has less primary creep than ZA8 at 160°C. The temperature dependence of the primary creep contractions for alloys ZA8, ZA12 and ZA27 are plotted in *Figure 36* at one temperature against all stress conditions. In general it is also clear that in ZA8 and ZA12 the primary creep decrease with increase of temperature from 70°C to 160°C. Alloy ZA27 has anomalously high primary creep at 160°C.

The creep results also showed that primary creep of commercial zinc alloys was dependent on the applied stress, and increased with the increase of stress, *Figure 37*. The average primary creep at 20 MPa was much lower than at a higher stress, 100 MPa i.e. in ZA8 it was 0.37% at 20 MPa which increased to 0.53% at 100 MPa and the same behaviour was observed for ZA12 and ZA27.

It was also observed that the average primary creep of alloy ZA27 was much higher than the other two commercial alloys, ZA8 and ZA12 at all testing conditions.

5.1.1.2 Primary Creep of High Damping Capacity Alloys (Cosmal and Supercosmal)

In high damping capacity alloys, Cosmal and Supercosmal, the primary creep increased with the increase of stress as shown in *Figure 37*. The alloy Cosmal has maximum primary creep at 100 MPa which is 0.72% and minimum at 20 MPa. The Alloy Supercosmal has less primary creep at all stresses than Cosmal.

Temperature has an inverse effect on primary creep of high damping alloys. Unlike the commercial ZA alloys, primary creep in high damping alloys, in general, increases with temperature, *Figure 36* and Cosmal has more primary creep than Supercosmal at all temperatures.

The primary creep results of the alloys yielded another important fact that the primary creep of commercial zinc alloys increased with increasing aluminum content. From the results, the average values of primary creep plotted against the aluminum content of the alloys as shown in *Figure 38* which yielded an almost linear relationship between the primary creep and the aluminum content within the composition range of commercial zinc alloys and with further increase of aluminum content, as in Cosmal and Supercosmal, it reduces with a linear relationship. Maximum primary creep at 27 % is 0.64% which reduces to 0.59% at 40 % aluminum and 0.52% at 60 % aluminum.
The mean value of the contribution of primary creep to total creep strain for each alloy was calculated and found to be 0.46, 0.49, 0.64, 0.58 and 0.53% for alloys ZA8, ZA12, ZA27, Cosmal and Supercosmal respectively and is plotted against aluminum content in *Figure 38.*

5.1.2 Secondary Creep Rate

Secondary creep rates ($\dot{\varepsilon}_s$) of all the ZA alloys and high damping capacity alloys were calculated from the linear portion of the creep curves and were plotted in the form of $\ln\varepsilon_s$ (1/s) versus ln stress (σ), as shown in *Figures 39, 40, 41 and 42.* According to the power law equation, the plot should yield straight lines with a constant slope at a constant test temperature.

The figures showed the reasonably good correlation with constant slopes for all alloys tested over much of the stress and temperature range but deviation from the constant slope was observed in Cosmal at high temperature (160°C) and low stress (20MPa). The average value of stress exponent (n) calculated from these slope lines were as follows:

Table 12. The average value of stress exponent (n).

Alloy	Stress Exponent (n)
ZA8	4.52
ZA12	4.26
ZA27	3.50
Cosmal	4.43

An increased slope was observed in Cosmal at high temperature and low stress conditions, its value was 7.12.

From these graphs, the secondary creep rates at fixed 40 MPa for the temperature range of 70°C to 160°C were obtained and were tabulated in *Table 13.*

Table 13. Secondary Creep Rates (1/s) of the alloys at 40 MPa.

Temperature (°C)	70	100	130	160
ZA8	8.50×10^{-8}	1.17×10^{-6}	2.14×10^{-5}	1.58×10^{-4}
ZA12	6.82×10^{-8}	1.51×10^{-6}	2.14×10^{-5}	2.61×10^{-4}
ZA27	1.59×10^{-7}	3.72×10^{-6}	$3 .53 \times 10^{-5}$	5.53×10^{-4}
Cosmal	2.05×10^{-8}	1.30×10^{-7}	3.20×10^{-6}	2.14×10^{-5}

Using these values of secondary creep rates, the graphs of ln ($\dot{\varepsilon}_s$) versus the reciprocal of the test temperature (K) were plotted, *Figure 43*, at different stresses 20, 40, 60 and 100 MPa for all the alloys.

According to the Arrhenius-type equation such a plot should yield a straight line of slope (Q_c/R) and therefore the activation energy for creep at a constant stress.

It was seen that good straight lines were obtained for each alloy. The activation energies were calculated from these slope lines and listed in *Table 14*. The average value of activation energy for these alloys was 106±10.7kj/mole.

Table 14. The Calculated Activation Energies (Q_c) of Alloys.

Alloy	Activation Energy (kJ/mole)
ZA8	104
ZA12	112
ZA27	109
Cosmal	98

5.1.3 Total Creep Contraction

From the creep curves, the times to produce 0.2%, 0.4%, 0.6% , 0.8% and 1.0% creep strain were obtained and plotted as a function of ln (σ) at each temperature. These plots are shown for alloys ZA8, ZA12, ZA27 and Cosmal in *Figures 44, 45, 46 and 47* respectively. These graphs were found to be linear with a constant slope and yielding a stress exponent approximately independent of the stress.

Deviation from this slope was observed in Cosmal at low stress (20 MPa) and high temperature (160°C).

Average secondary creep rate and average time to 1 % creep strain for ZA alloys has been shown in *Figures 48 and 49.*

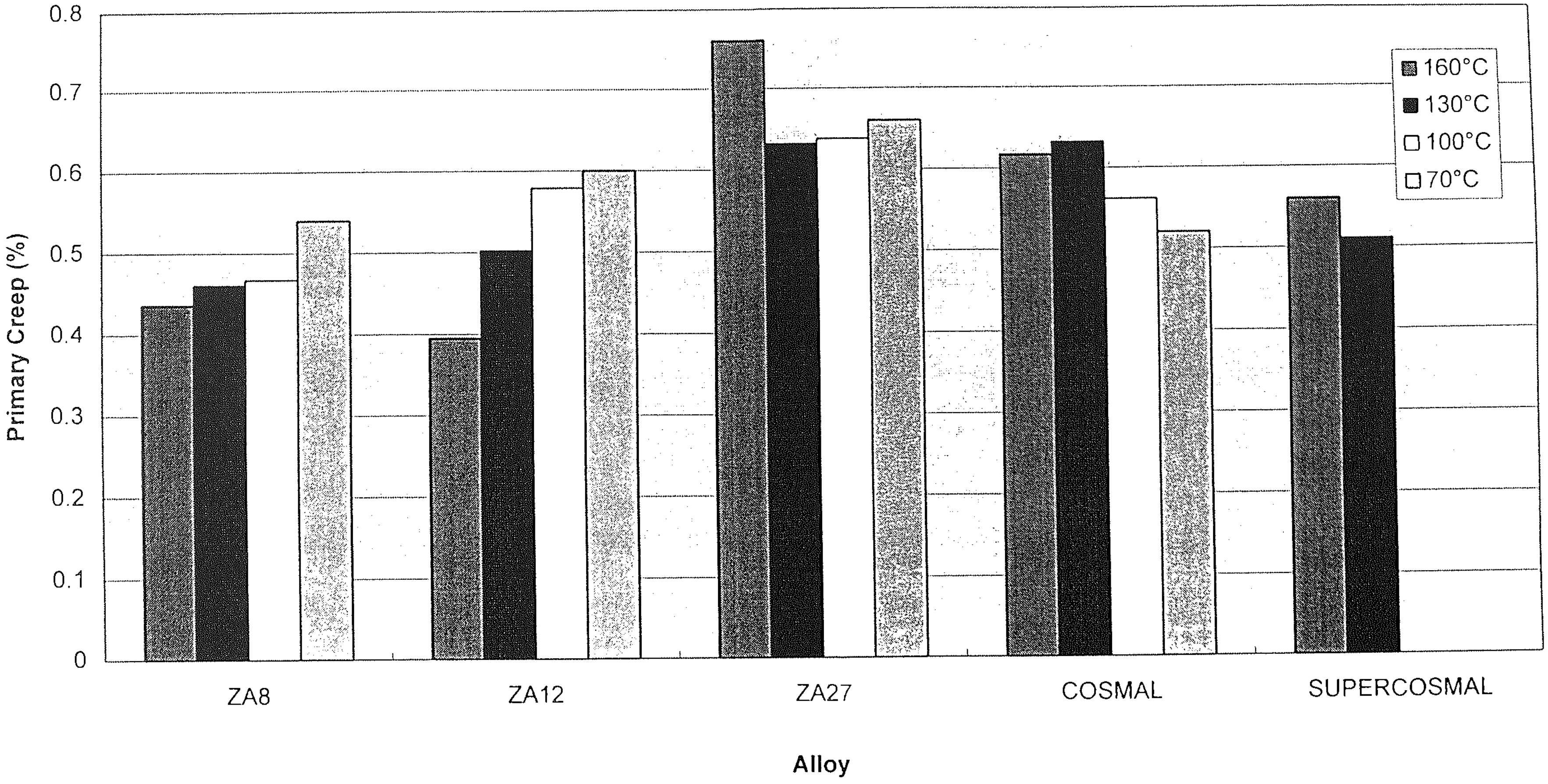

Figure 36. Variation of average primary creep contraction of the experimental alloys with temperature.

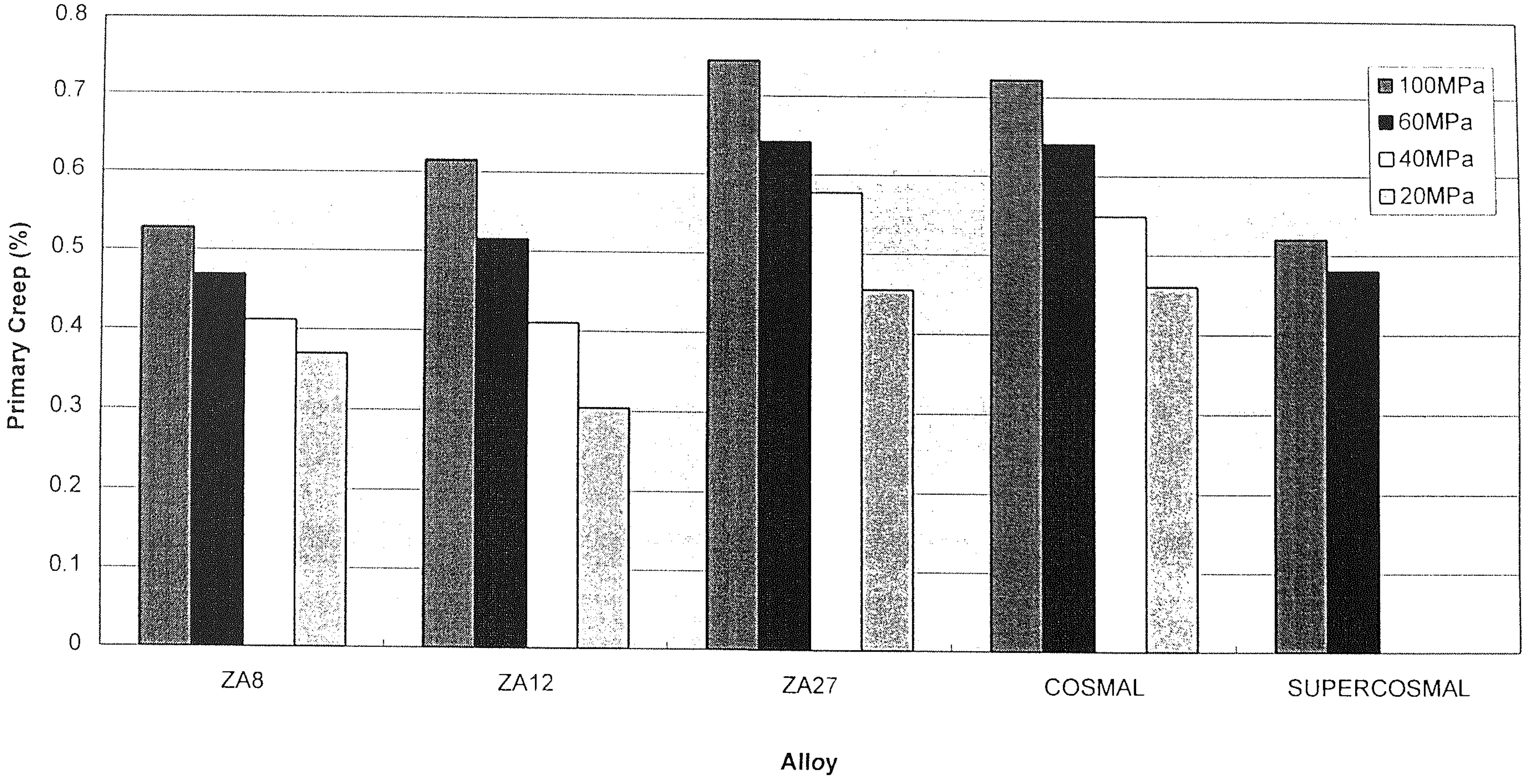

Figure 37. Variation of average primary creep contraction of the experimental alloys with stress.

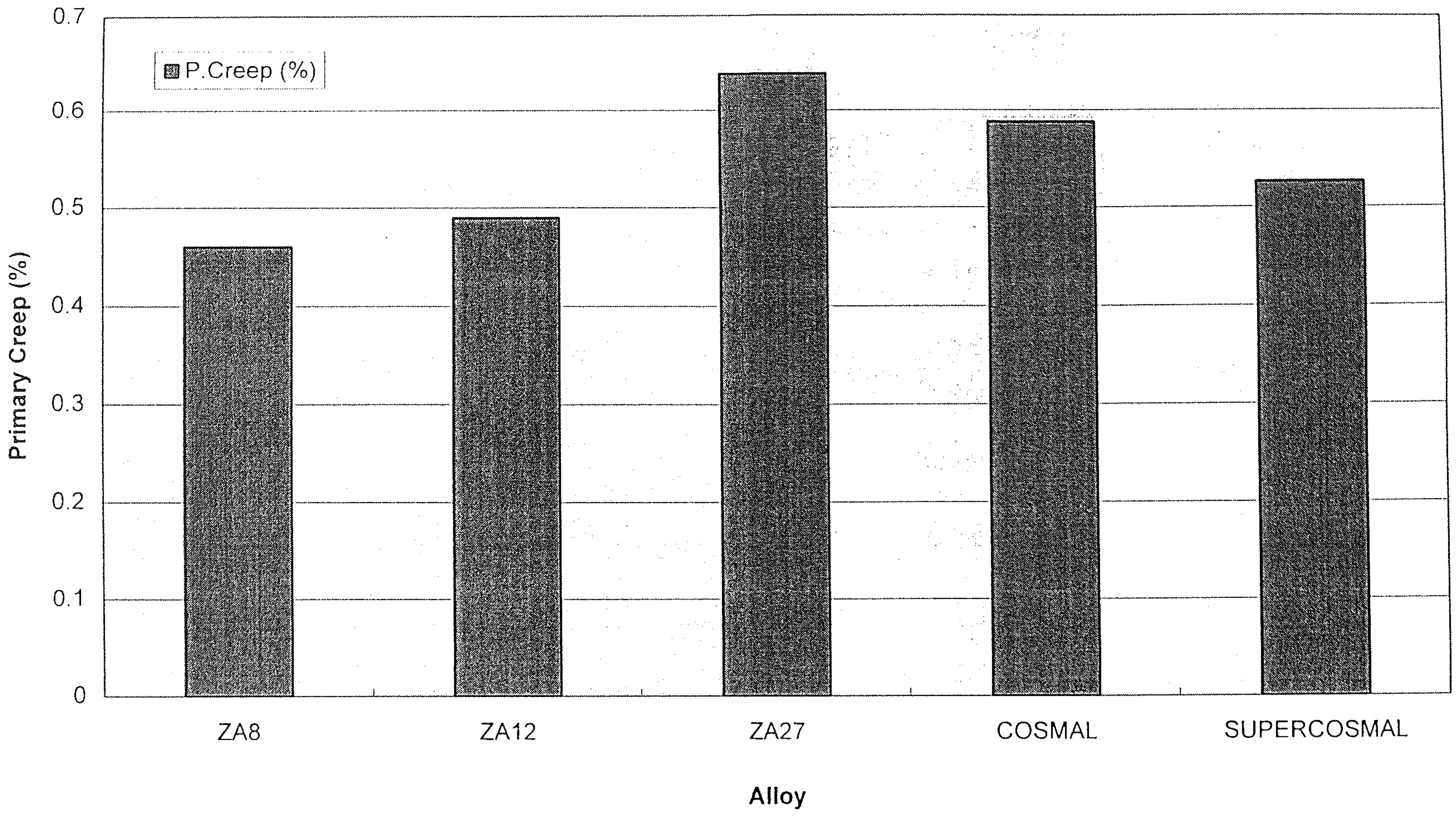

Figure 38. Variation of average primary creep contraction of the alloys with increasing aluminum content.

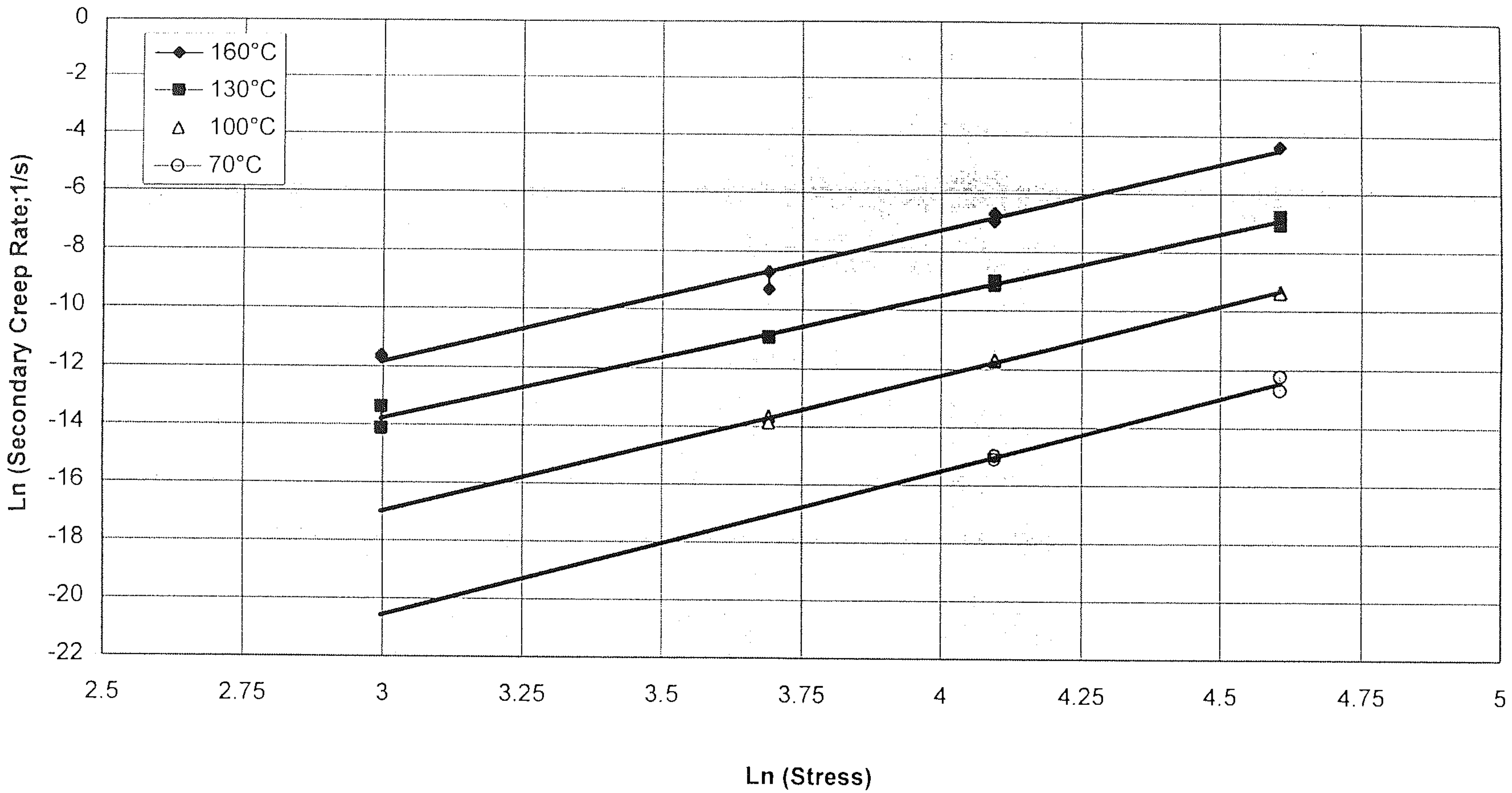

Figure 39. Variation of secondary creep rates of the alloy ZA8 with applied stress at different temperatures.

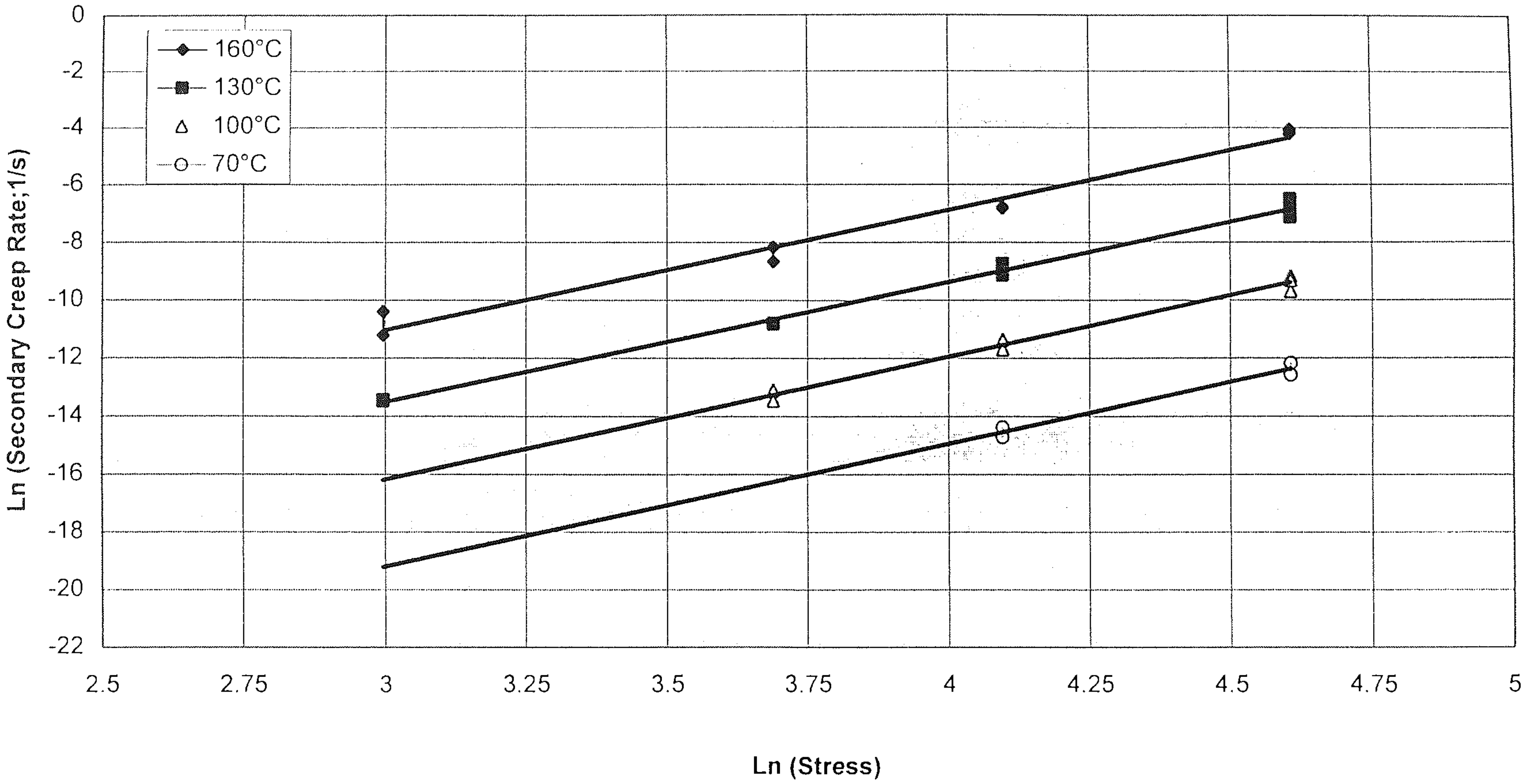

Figure 40. Variation of secondary creep rates of the alloy ZA12 with applied stress at different temperatures.

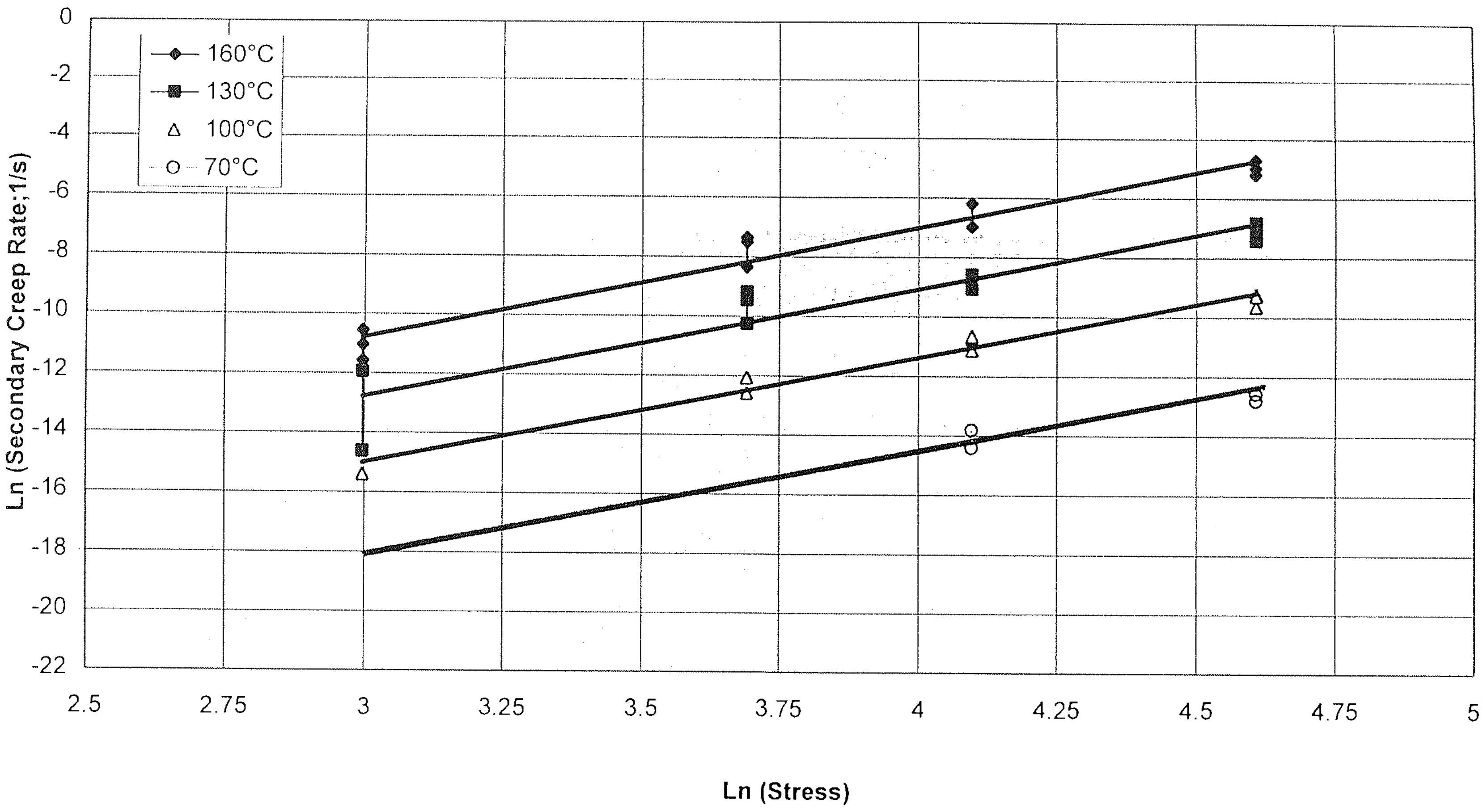

Figure 41. Variation of secondary creep rates of the alloy ZA27 with applied stress at different temperatures.

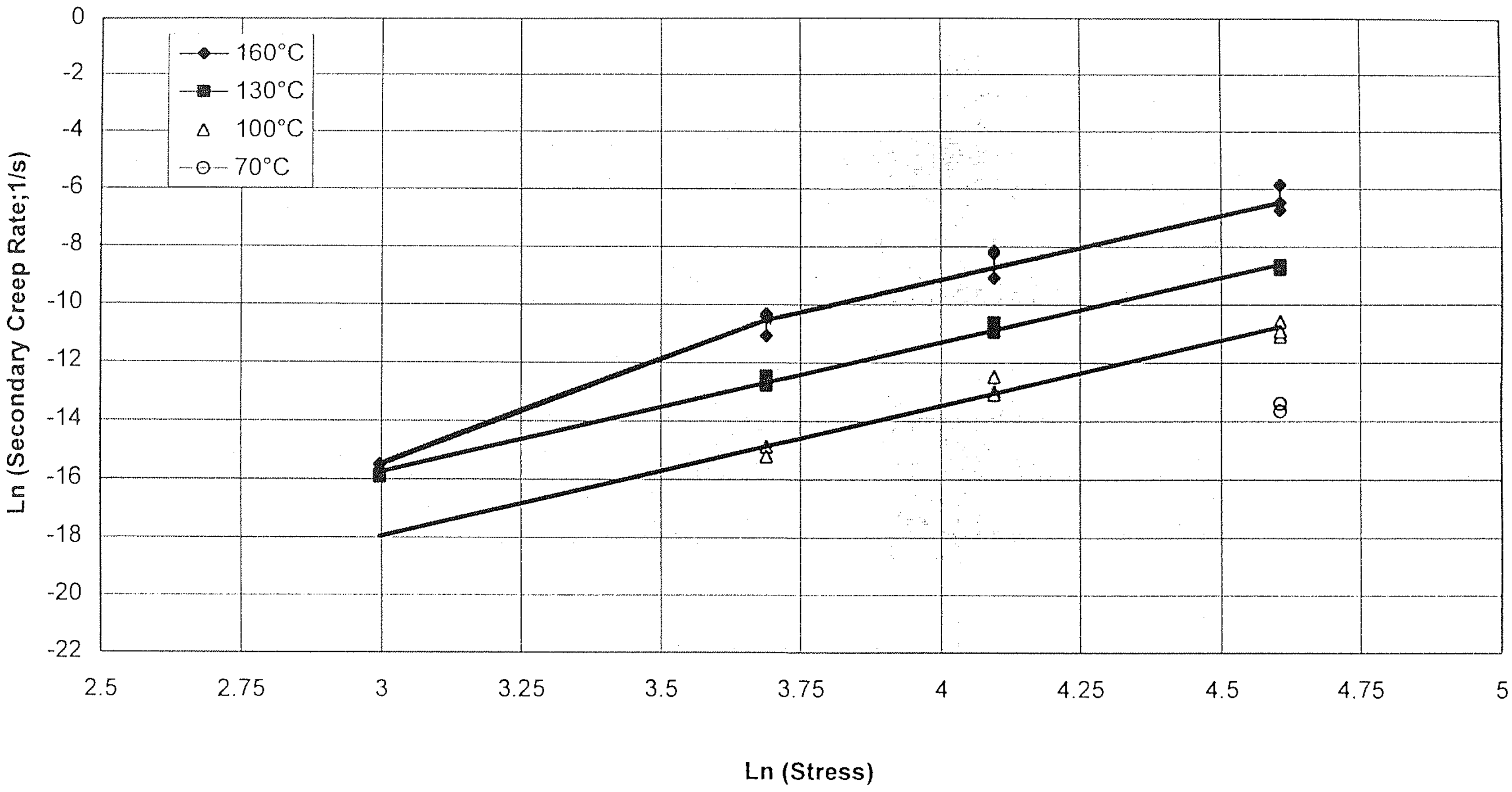

Figure 42. Variation of secondary creep rates of the Cosmal with applied stress at different temperatures.

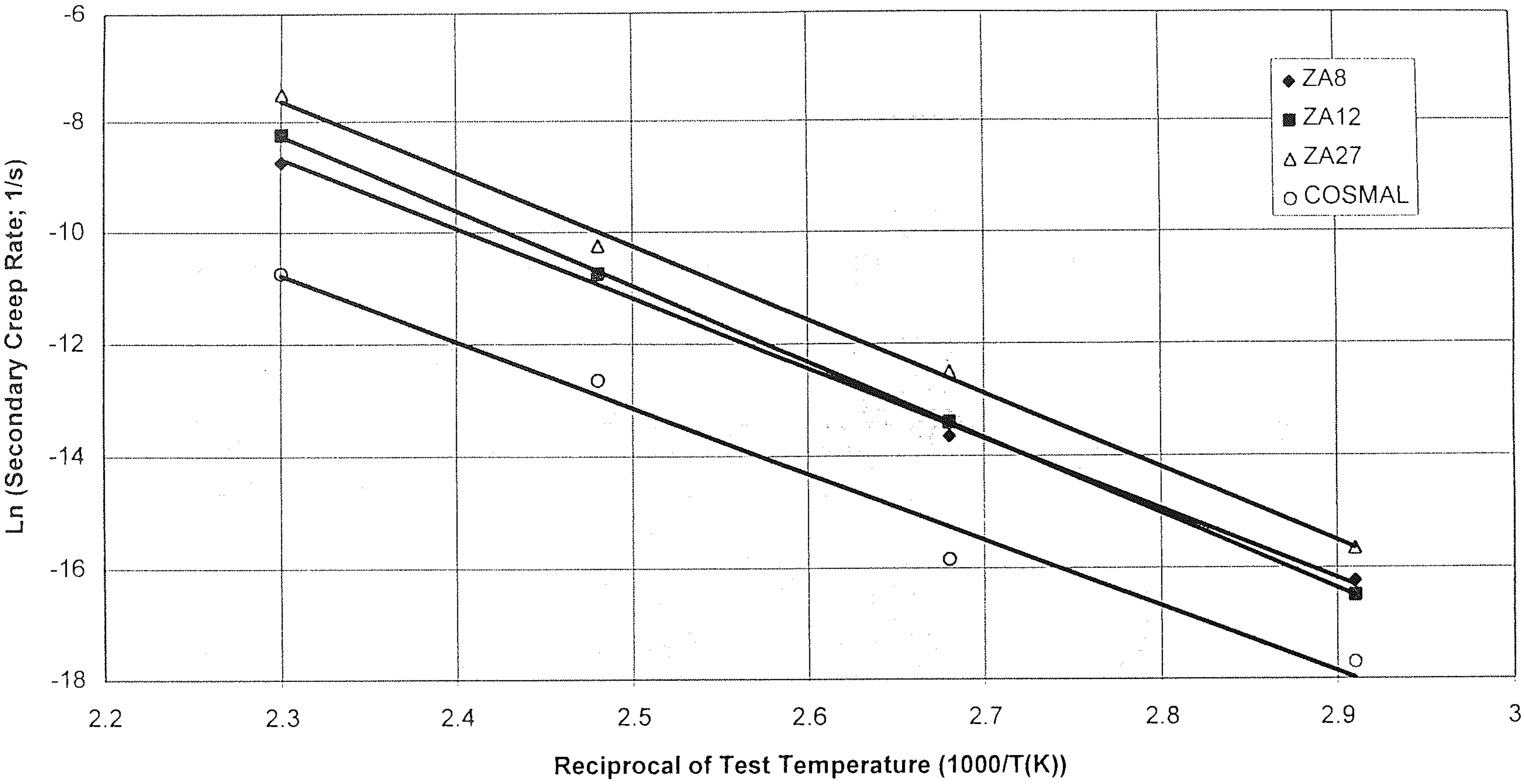

Figure 43. Variation of secondary creep rates of the alloys with the reciprocal test temperatures at 40 MPa.

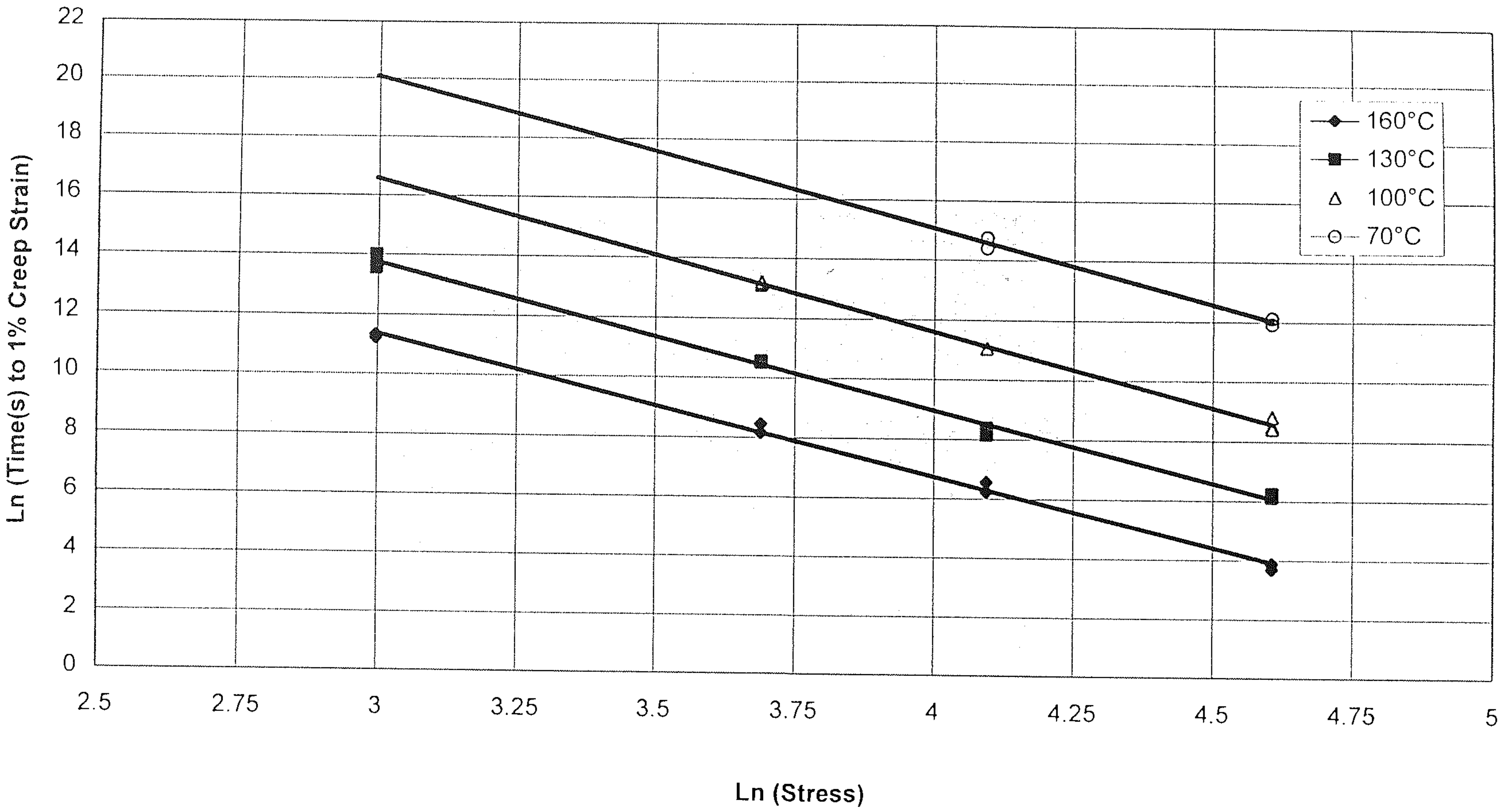

Figure 44. Variation of time to 1 % creep strain of the alloy ZA8 with applied stress at different temperatures.

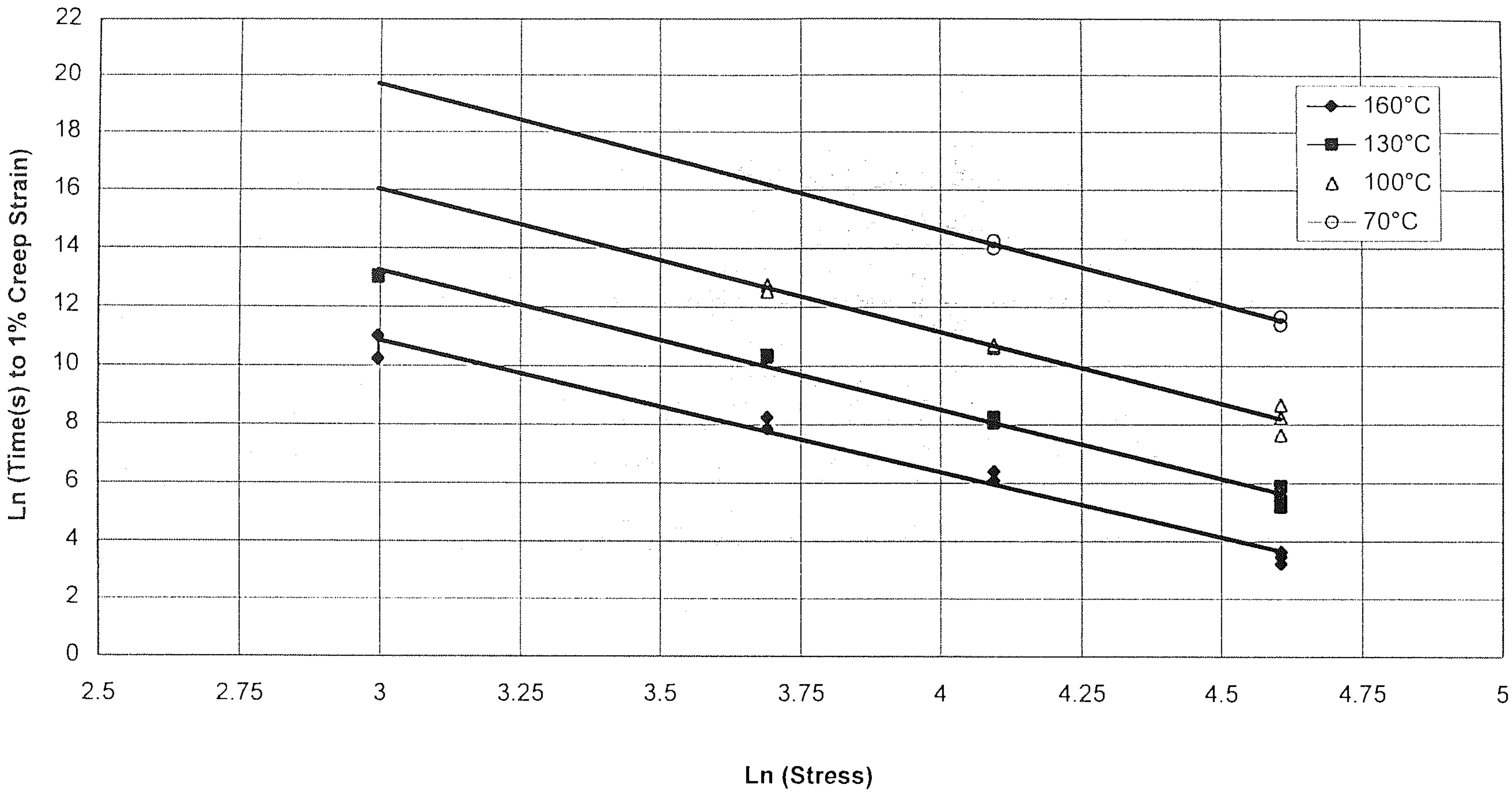

Figure 45. Variation of time to 1 % creep strain of the alloy ZA12 with applied stress at different temperatures.

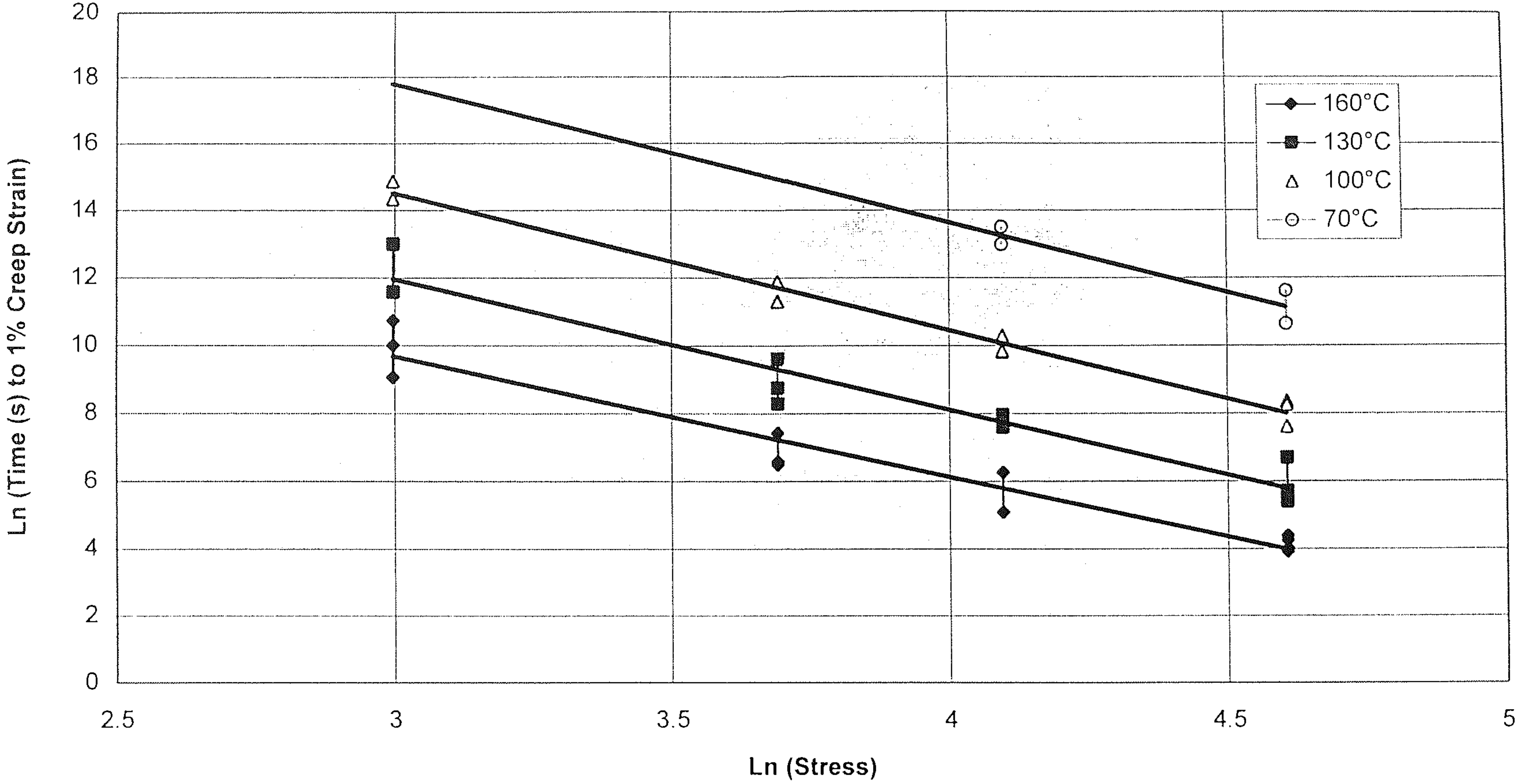

Figure 46. Variation of time to 1 % creep strain with applied stress at different temperatures for alloy ZA27.

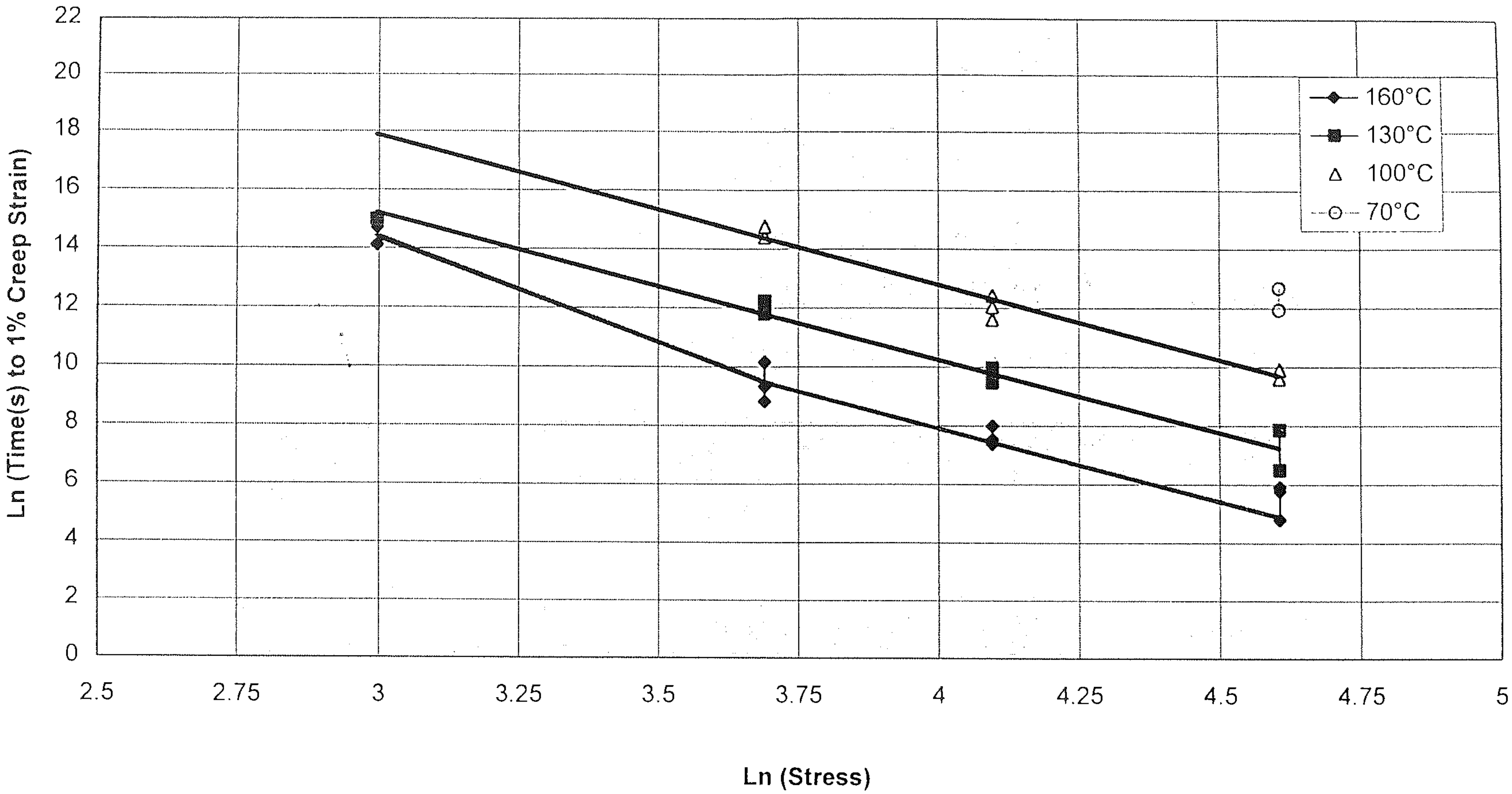

Figure 47. Variation of time to 1 % creep strain of Cosmal with applied stress at different temperatures.

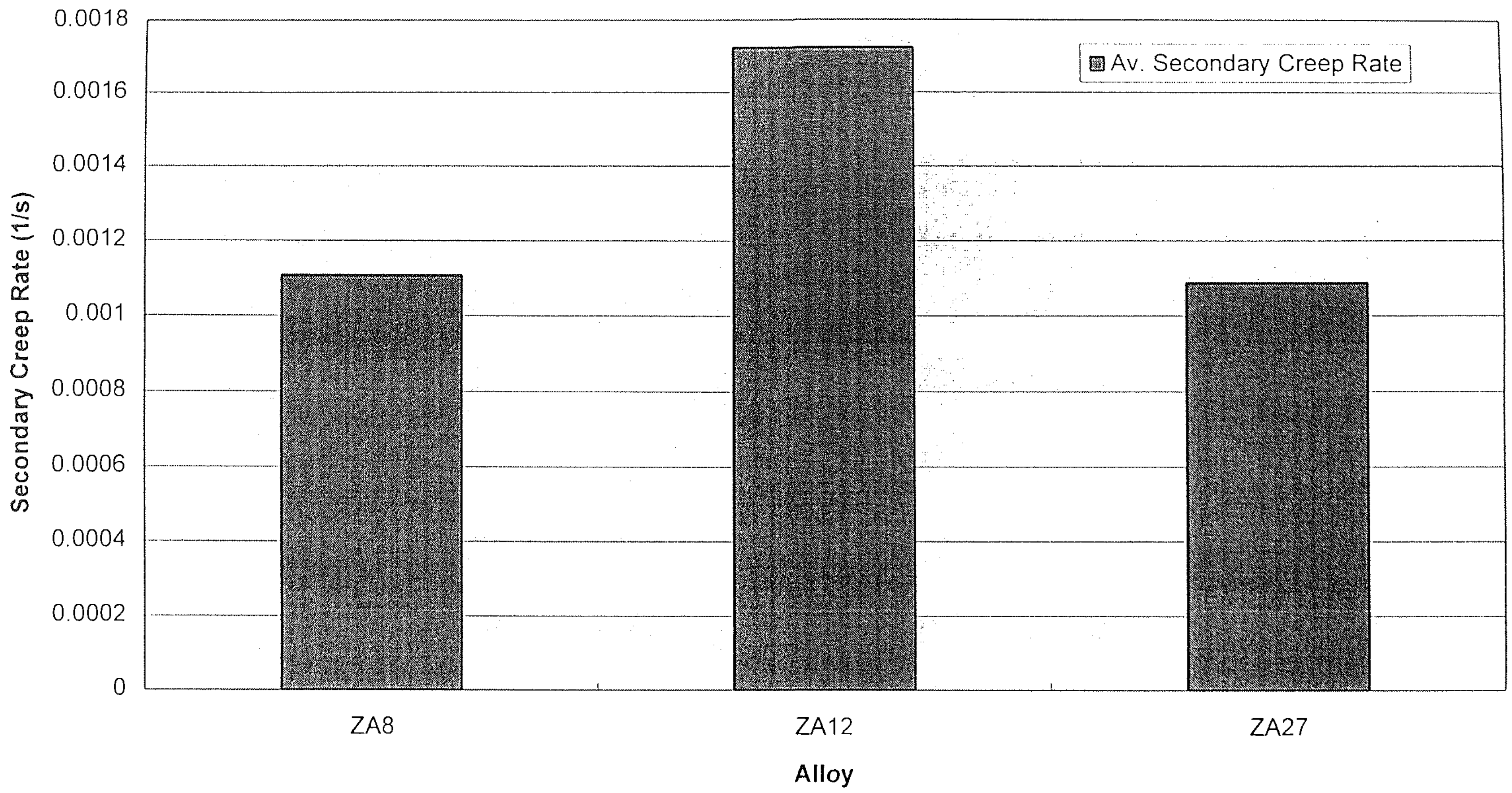

Figure 48. Variation of average secondary creep rates of the alloys ZA8, ZA12 and ZA27.

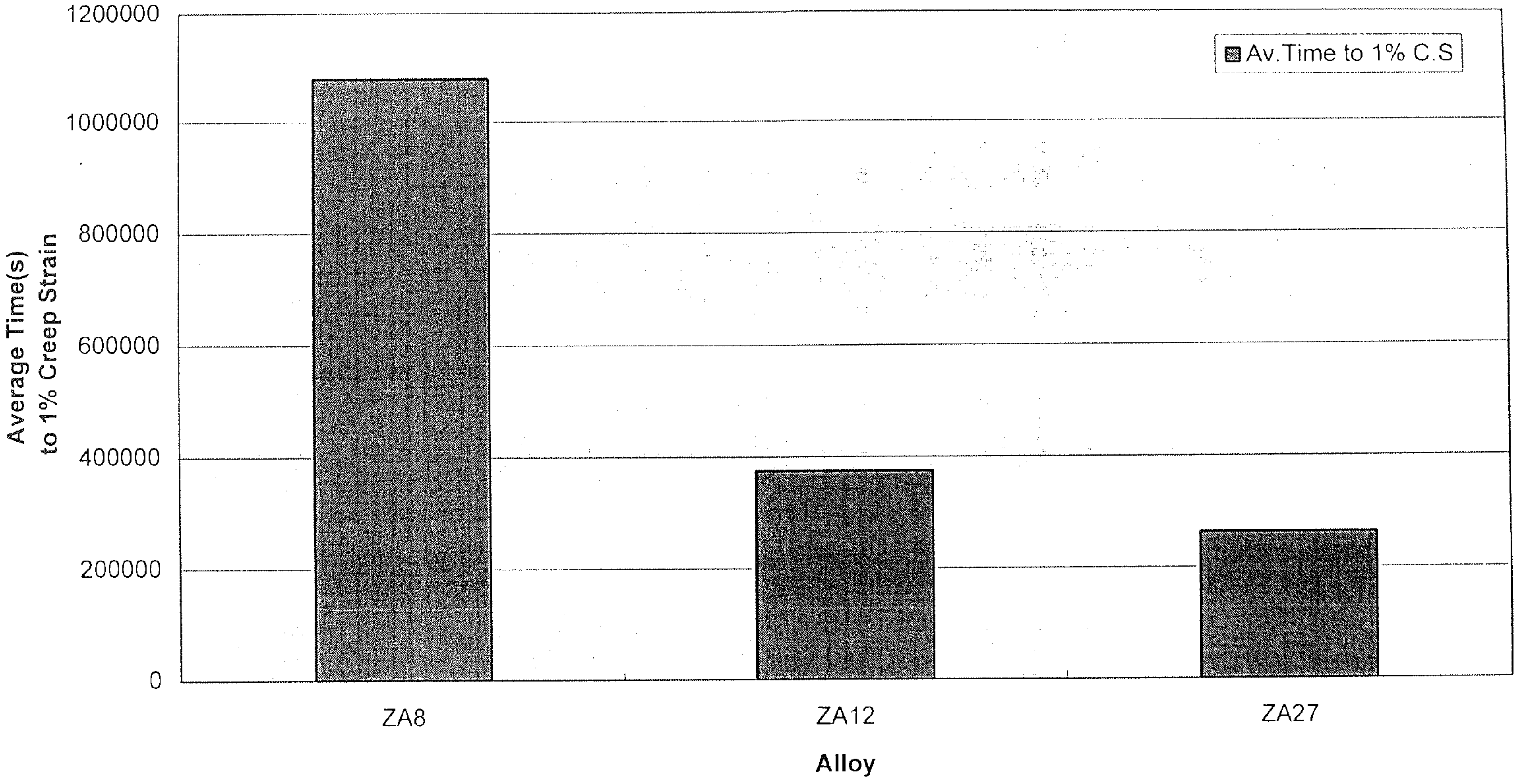

Figure 49. Variation of average times to 1 % creep strain of the alloys ZA8, ZA12 and ZA27.

5.2 Results of Load Relaxation Tests

The retained load versus time data from the load relaxation tests were used to plot the relaxation curves of *Figures 50 to 52*. These showed the relaxation behaviour of all the alloys at temperature of 80, 100, and 120°C respectively. It was observed that the amount of load loss increased rapidly with test temperature, and almost all of the curves approximated to a logarithmic decay of preload with time.

5.2.1 Results of Commercial ZA Alloys

The results of ZA alloys showed approximately the same load loss at 80°C and 100°C; only ZA12 was slightly better than ZA8 and ZA27, while at 120°C ZA8 had the worst position and ZA27 the best. At this temperature of 120°C, initially ZA12 had better creep resistance to load loss than ZA27, but with the passage of time ZA27 improved its performance while the other got worse as seen in *Figure 52*. From the load relaxation test data, it was observed that the final relaxed load recorded at 80°C was 33320 N for ZA8, 3476N for ZA12 and 3359N for ZA27. From these values of relaxed load, it was clear that no remarkable difference could be noted and it was difficult to say which one was superior or inferior in load loss. At 120°C ZA12 and ZA27 showed a clearly better creep resistance to load loss than ZA8 as could be seen from the recorded data at this temperature i.e. 1639N for ZA8, 2060N for ZA12 and 2067N for ZA27. In all results, the initial load loss was high, decreasing gradually with time, but not ceasing.

5.2.2 Results of High Damping Capacity Alloys

High damping capacity alloys had much better resistance to load loss than ZA alloys. From these two alloys, Supercosmal was much better in resistance than Cosmal at all test conditions as seen from comparison graphs, *Figures 50 to 52*. In both alloys load loss was increased with the increase of temperature. i.e. the load loss in Cosmal and Supercosmal at 80°C was 32% and 15% respectively while at 120°C this loss was 56% and 28 % respectively.

5.2.3 Results of LM25

LM25 had the best resistance to load loss among all six alloys tested at all conditions. Load loss in LM25 was 7%, 9% and 12% at 80°C, 100°C and 120°C respectively.

5.2.4 Comparison of Load Relaxation Results of Commercial ZA Alloys, High Damping Capacity Alloys and LM25

The comparative load relaxation graphs in the form of retained load (N) versus time (Min.) at 80, 100 and 120°C have been shown in *Figures 50 to 52.* When the results of load relaxation for ZA alloys were compared with those of high damping capacity alloys and LM25 it was observed that high damping alloys were more resistant to load loss than alloys ZA alloys at all test temperatures and LM25 had more resistance than high damping capacity alloys. Percentage of load loss of all six alloys at three temperatures is tabulated in *Table 15.*

Table 15. Percentage of load loss at different temperatures

Alloy	ZA8	ZA12	ZA27	Cosmal	Supercosmal	LM25
80°C	45	42	44	32	15	7
100°C	59	57	58	42	20	9
120°C	73	66	66	55	29	12

Therefore, on the basis of the results of these load relaxation tests, it can be concluded that high damping capacity alloys and LM25 are more suitable for higher temperature applications where load relaxation is an important factor.

5.2.5 Short and Long term Load Relaxation Tests

From the experimental data, graphs were drawn to show the variation of retained load after 50, 100 and 150 hours with reciprocal temperature for all six alloys, as shown in *Figures 53, 54 and 55* respectively. These plots should yield straight lines with constant slope at a constant temperature, and they showed that good correlation with constant slopes were obtained over much of the test conditions for all alloys. From these plots, the effect of short term, 50 hours, and long-term, 150 hours, load relaxation tests can be observed.

From 50 hours to 150 hours it was observed that LM25 had the best resistant to load loss and ZA8 the worst, whereas Supercosmal and Cosmal were on second and third position respectively among these alloys. ZA12 and ZA27 were slightly better than ZA8 but much weaker than Cosmal.

Retained Load (N) vs ln time (min) graphs are shown in *Figures 56, 57, 58, 59, 60, and 61* and they yield straight lines with constant slope.

Graphs of ln retained load (N) versus ln time (min) were also drawn at three different temperatures, i.e. 80, 100 and 120°C as shown in *Figures 62, 63, 64, 65, 66 and 67*. At a constant temperature, these plots should yield straight lines with a constant slope. The Figures showed that good correlation with constant slopes were obtained for alloys at all temperatures.

5.2.6 The Effect of Aluminium Content on Load Relaxation Behaviour of Experimental Alloys

Aluminum contents have a clear effect on load relaxation. Load loss was decreased with the increase of aluminium at all temperatures. It has been shown graphically in *Figure 68.*

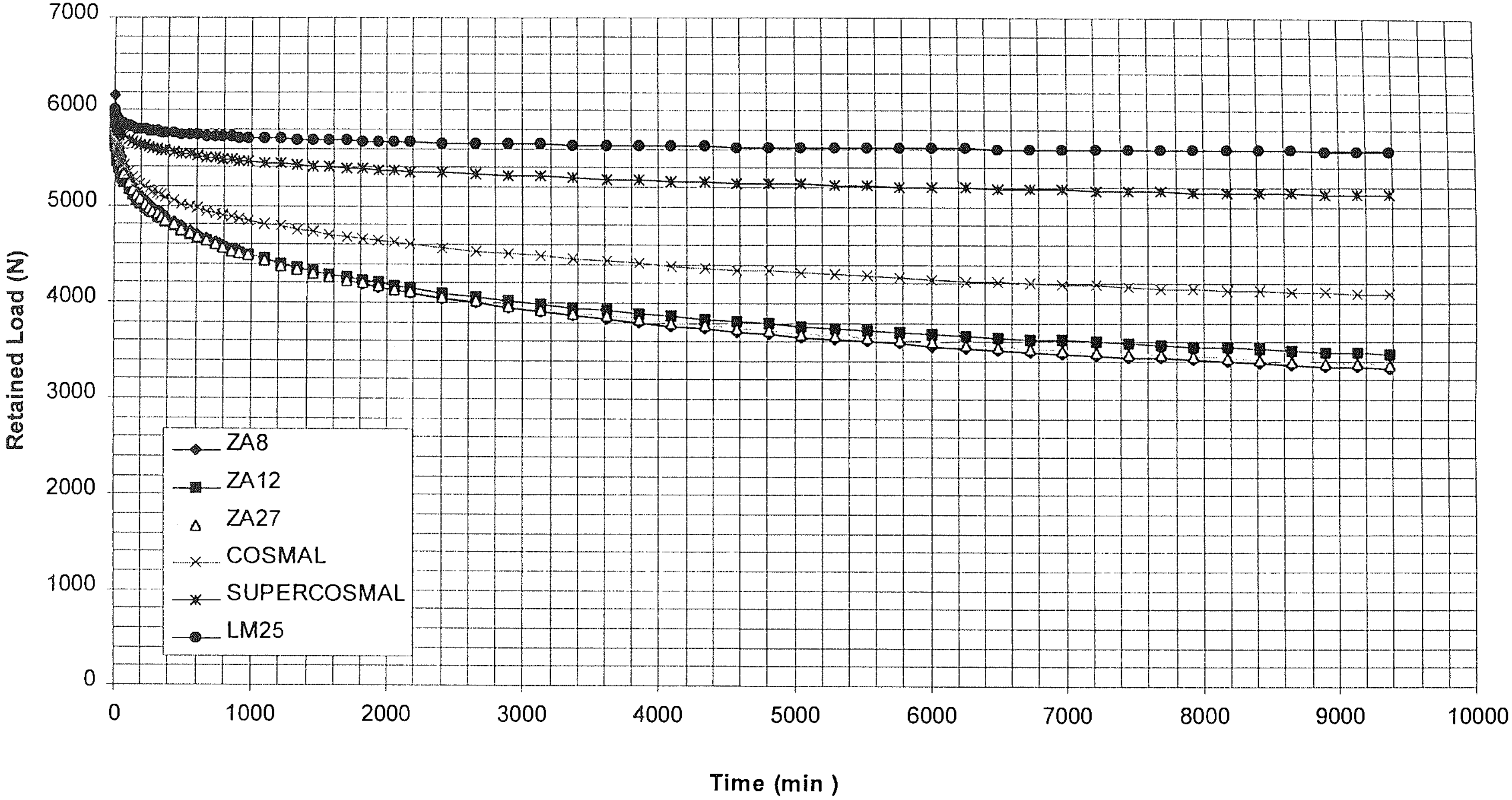

Figure 50. Variation of load-relaxation with time at 80°C.

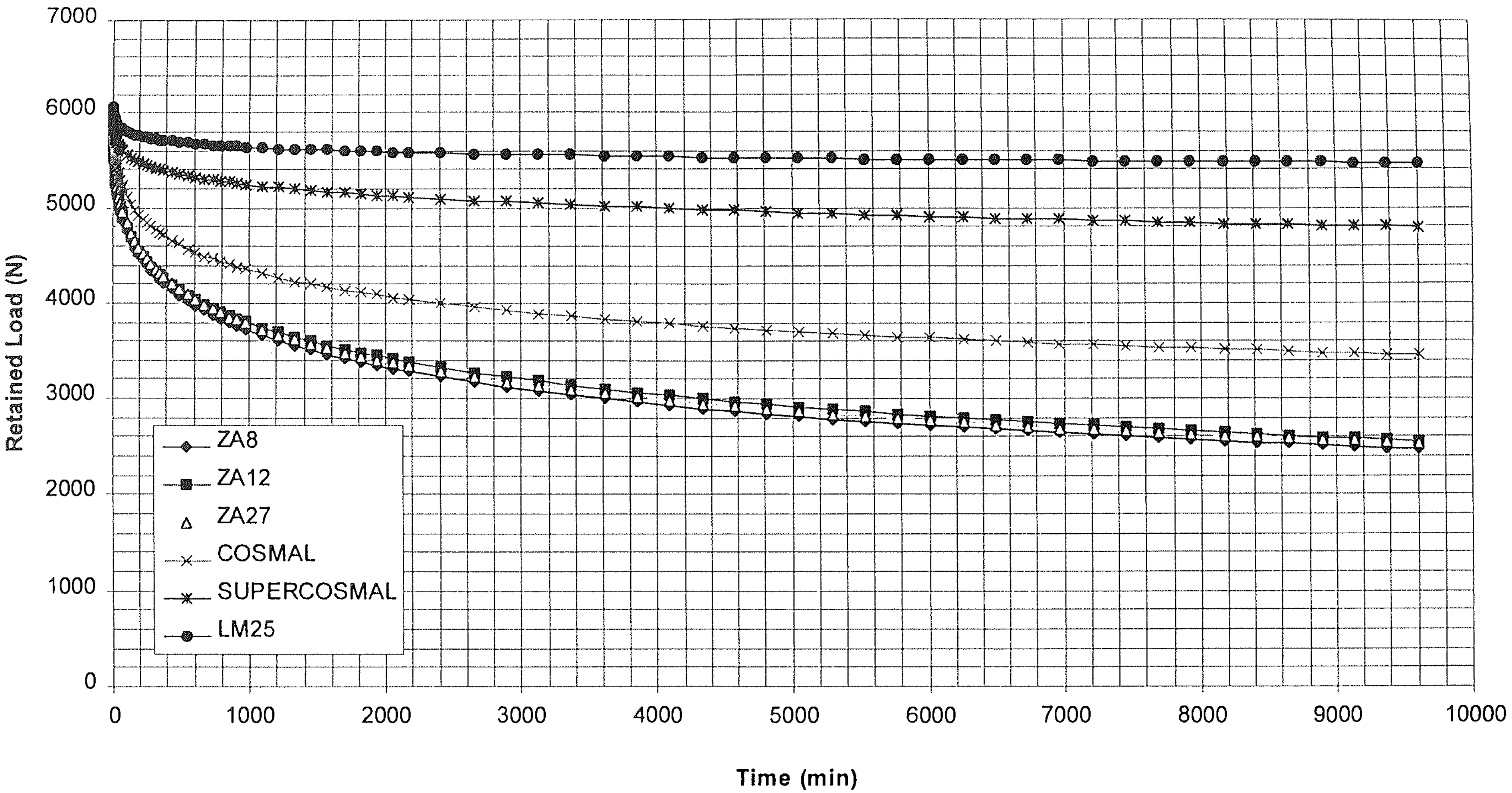

Figure 51. Variation of load-relaxation with time at 100°C.

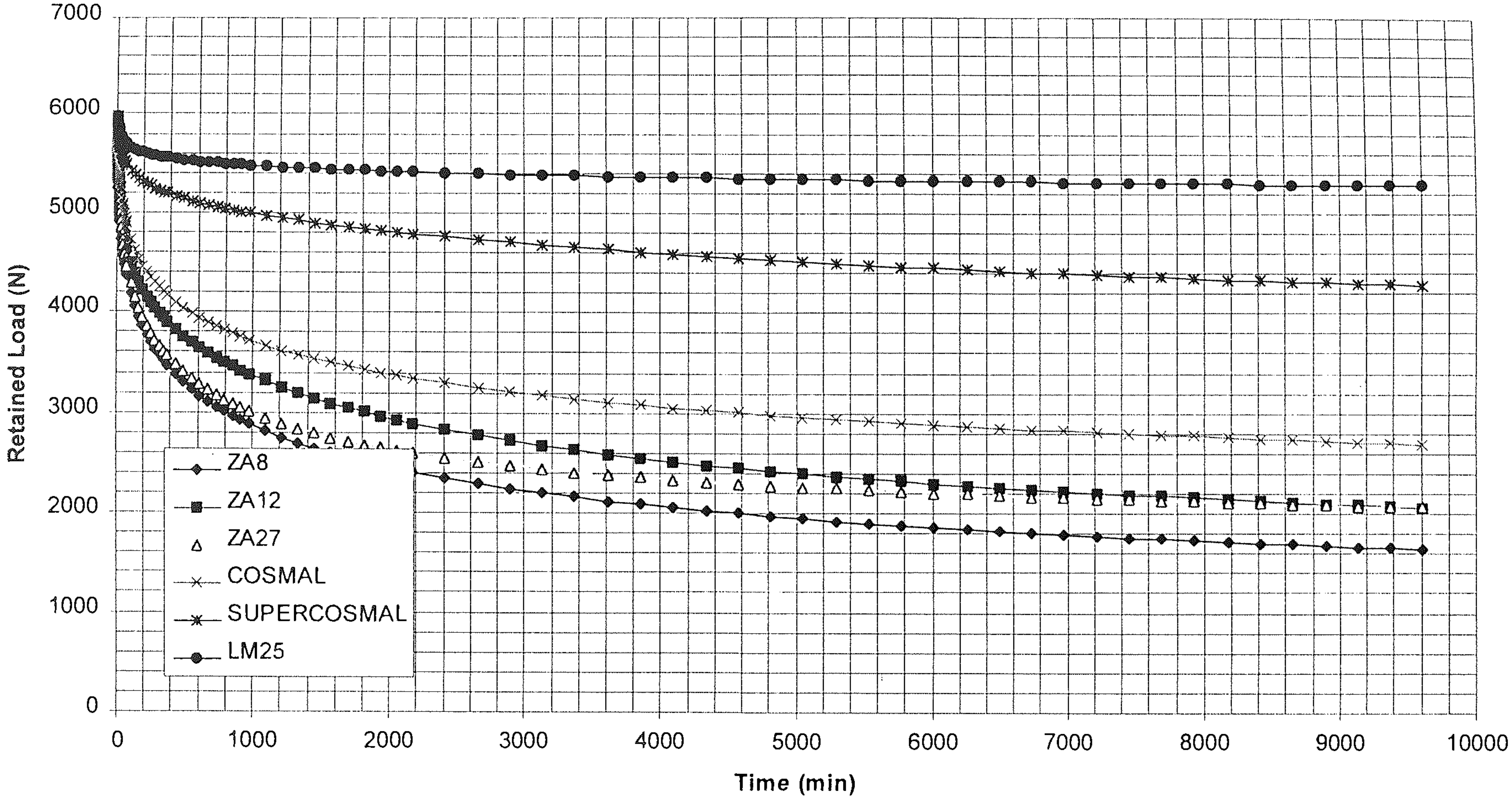

Figure 52. Variation of load-relaxation with time at 120°C.

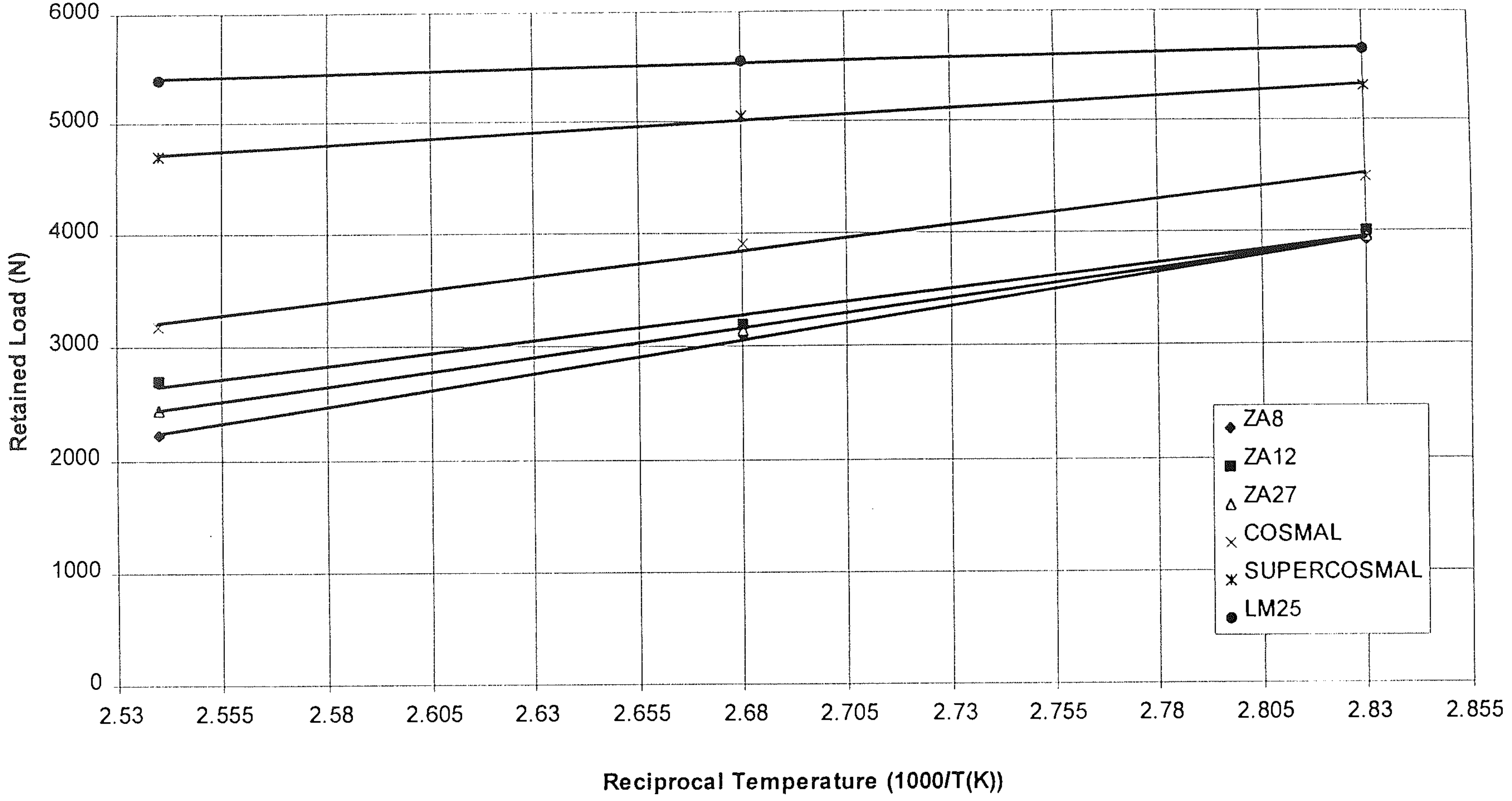

Figure 53. Variation of 50 hour load with reciprocal temperature for alloys ZA8, ZA12, ZA27, Cosmal, Supercosmal and LM25.

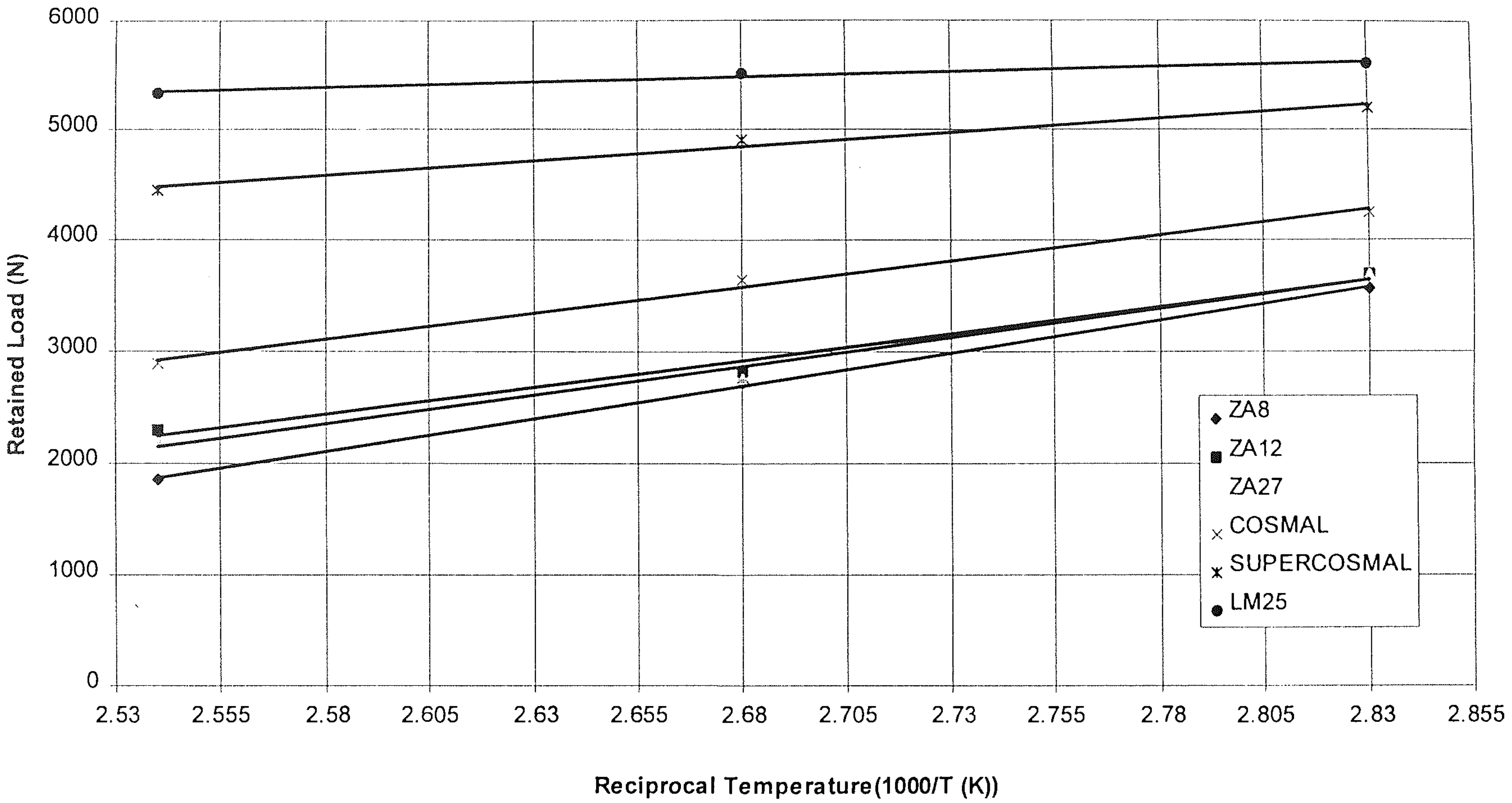

Figure 54. Variation of 100 hour load with reciprocal temperature for alloys ZA8, ZA12, ZA27, Cosmal, Supercosmal and LM25.

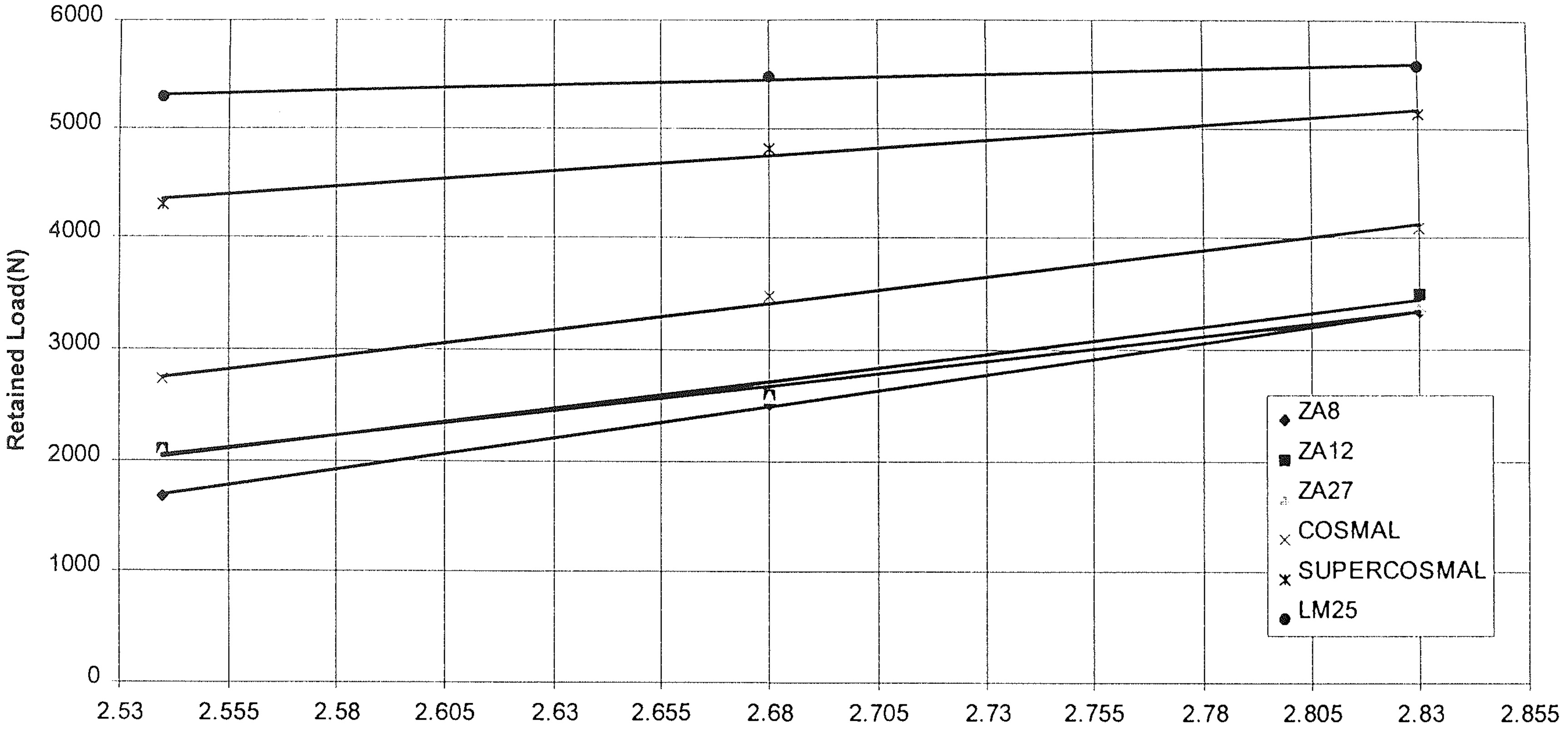

Figure 55. Variation of 150 hour load with reciprocal temperature for alloys ZA8, ZA12, ZA27, Cosmal, Supercosmal and LM25.

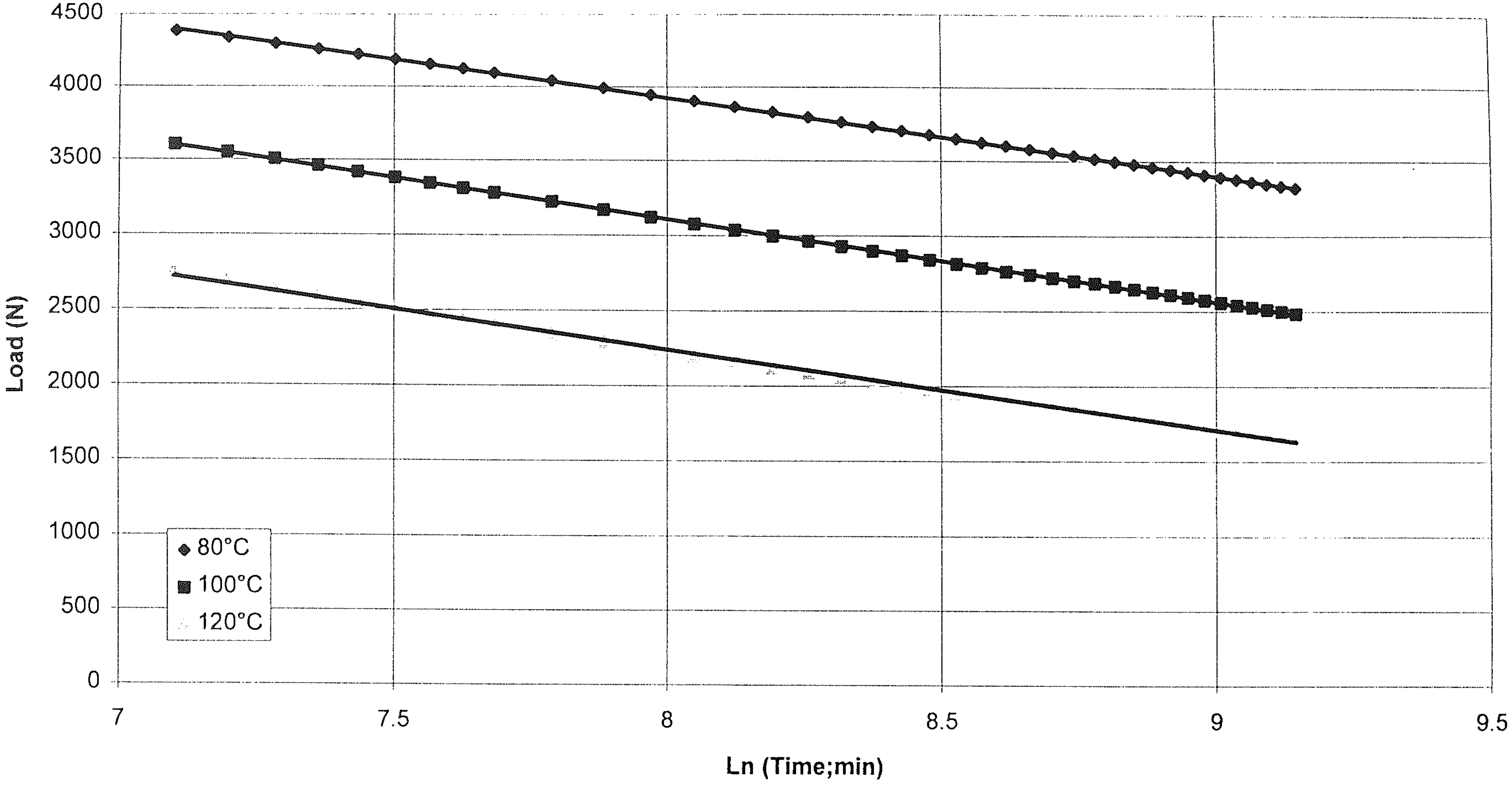

Figure 56. Variation of load-relaxation against ln time for ZA8.

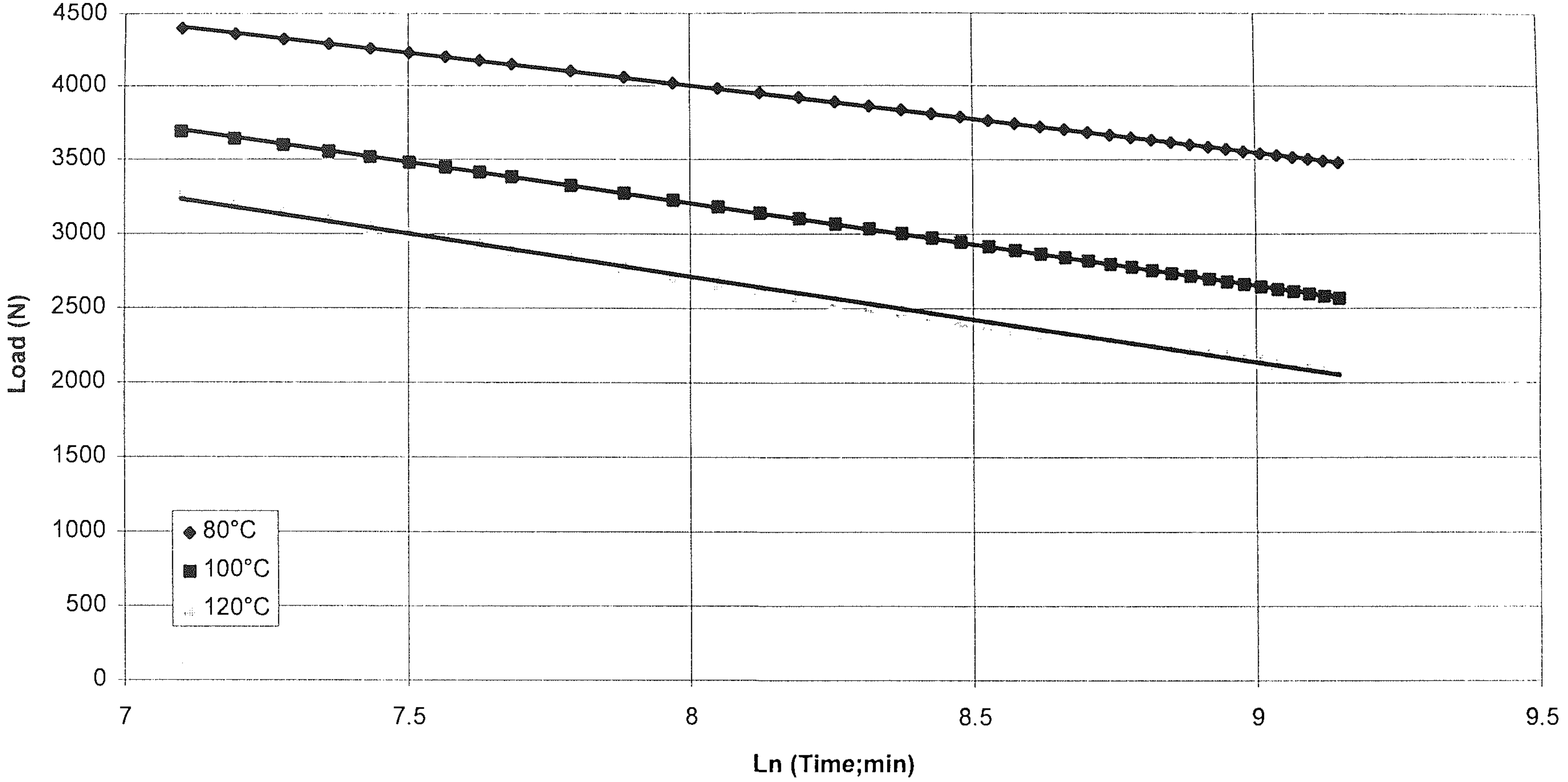

Figure 57. Variation of load-relaxation against ln time for ZA12.

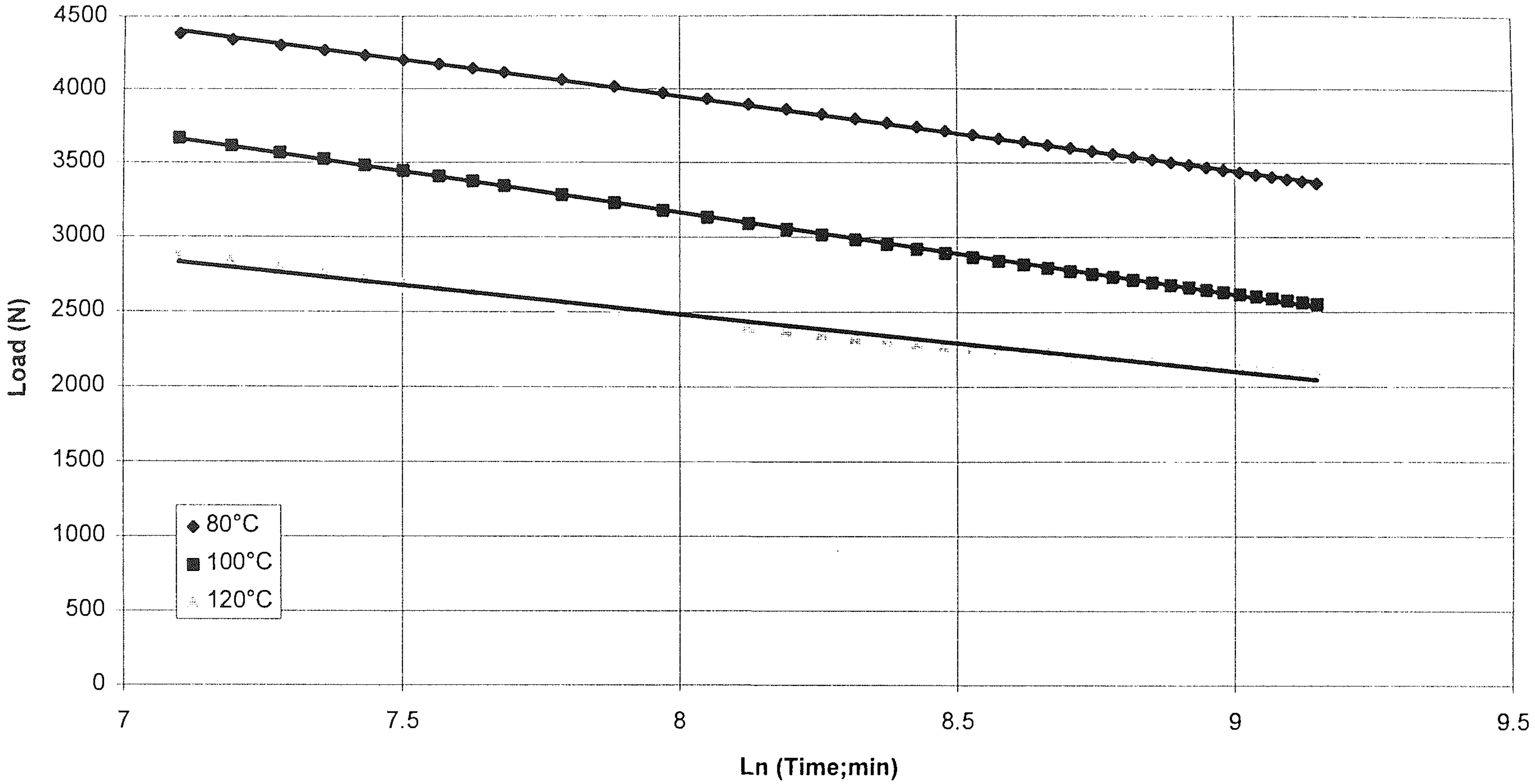

Figure 58. Variation of load-relaxation against ln time for ZA27.

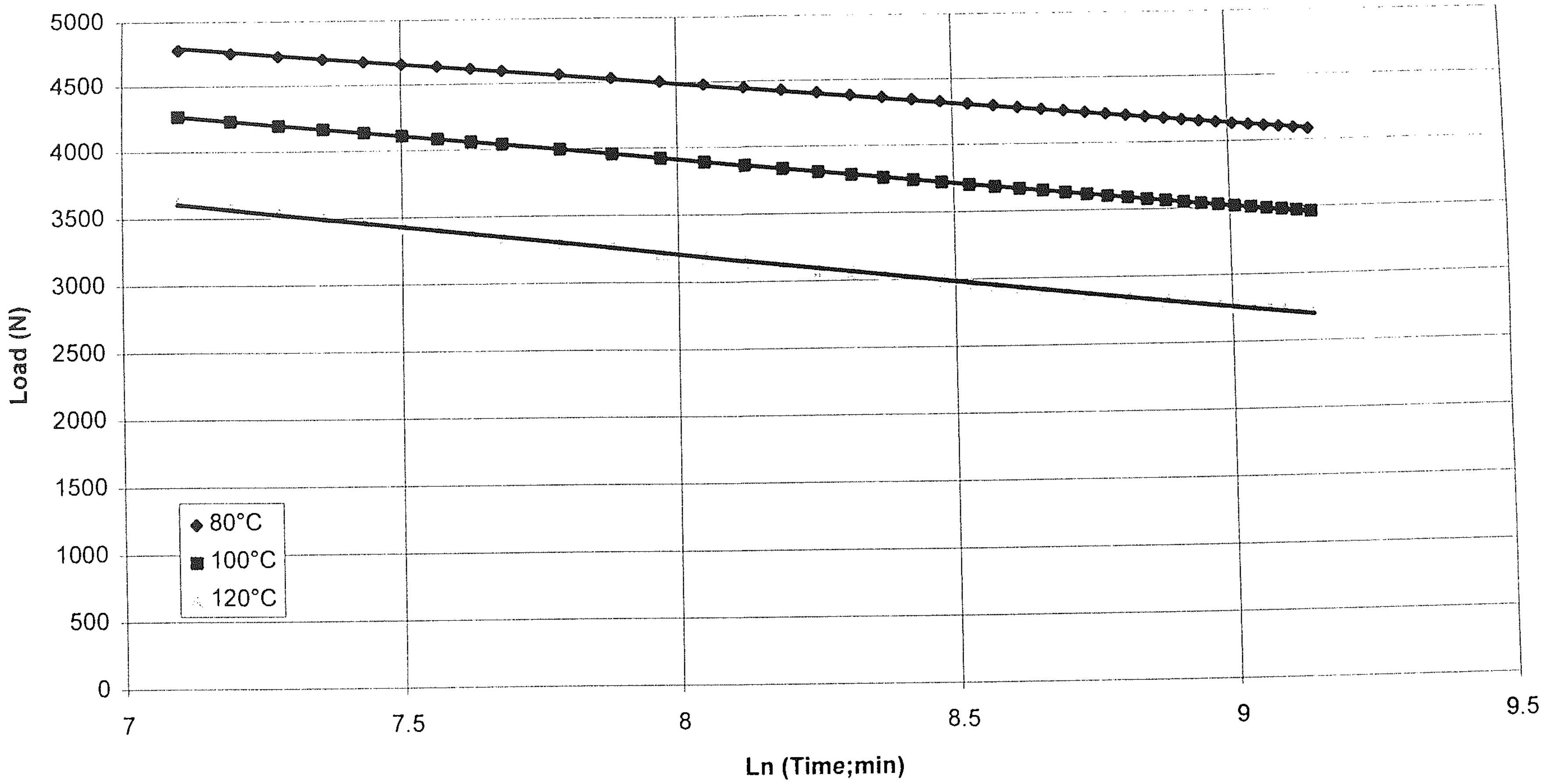

Figure 59. Variation of load-relaxation against ln time for Cosmal.

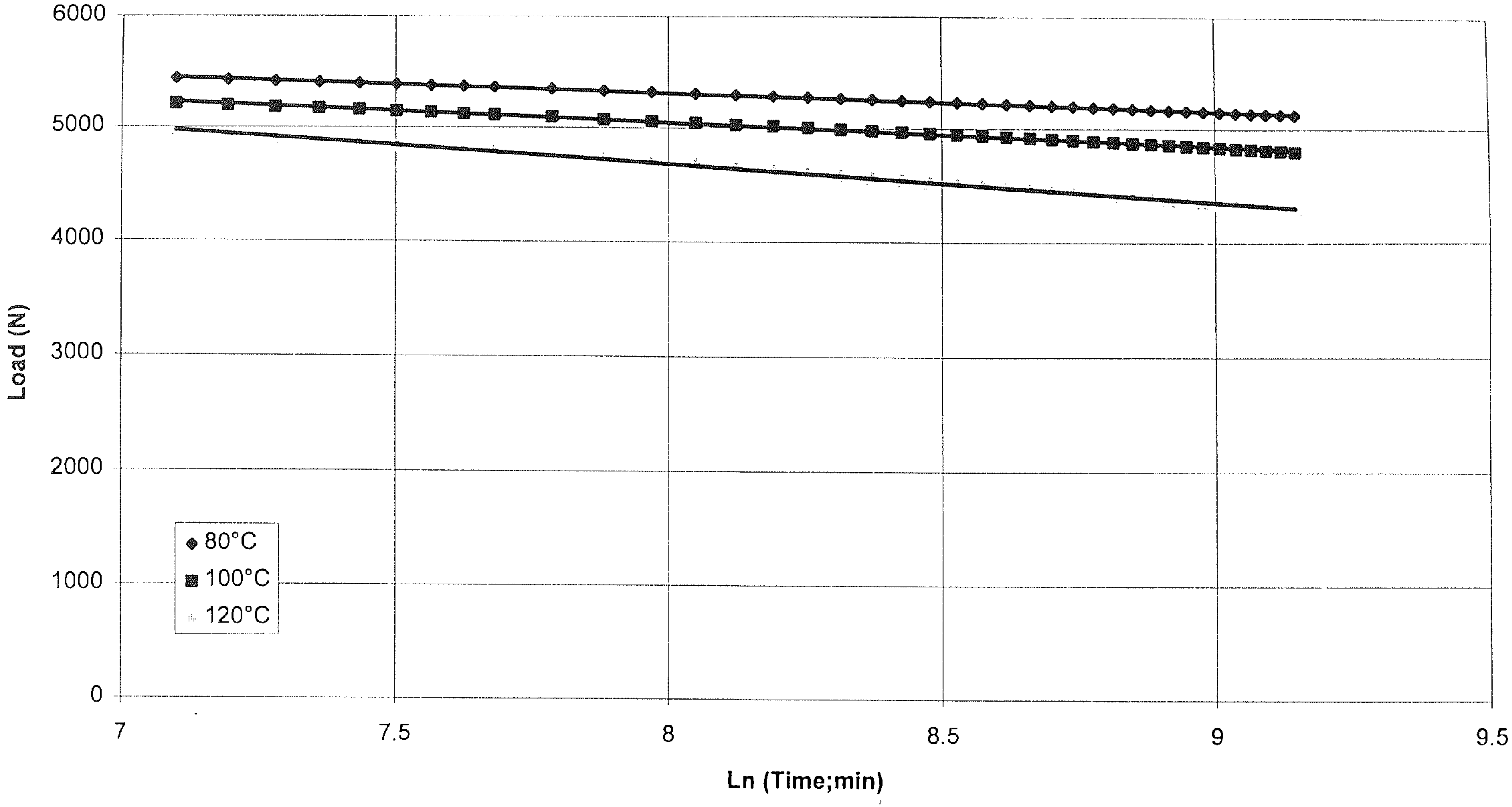

Figure 60. Variation of load-relaxation against ln time for Supercosmal.

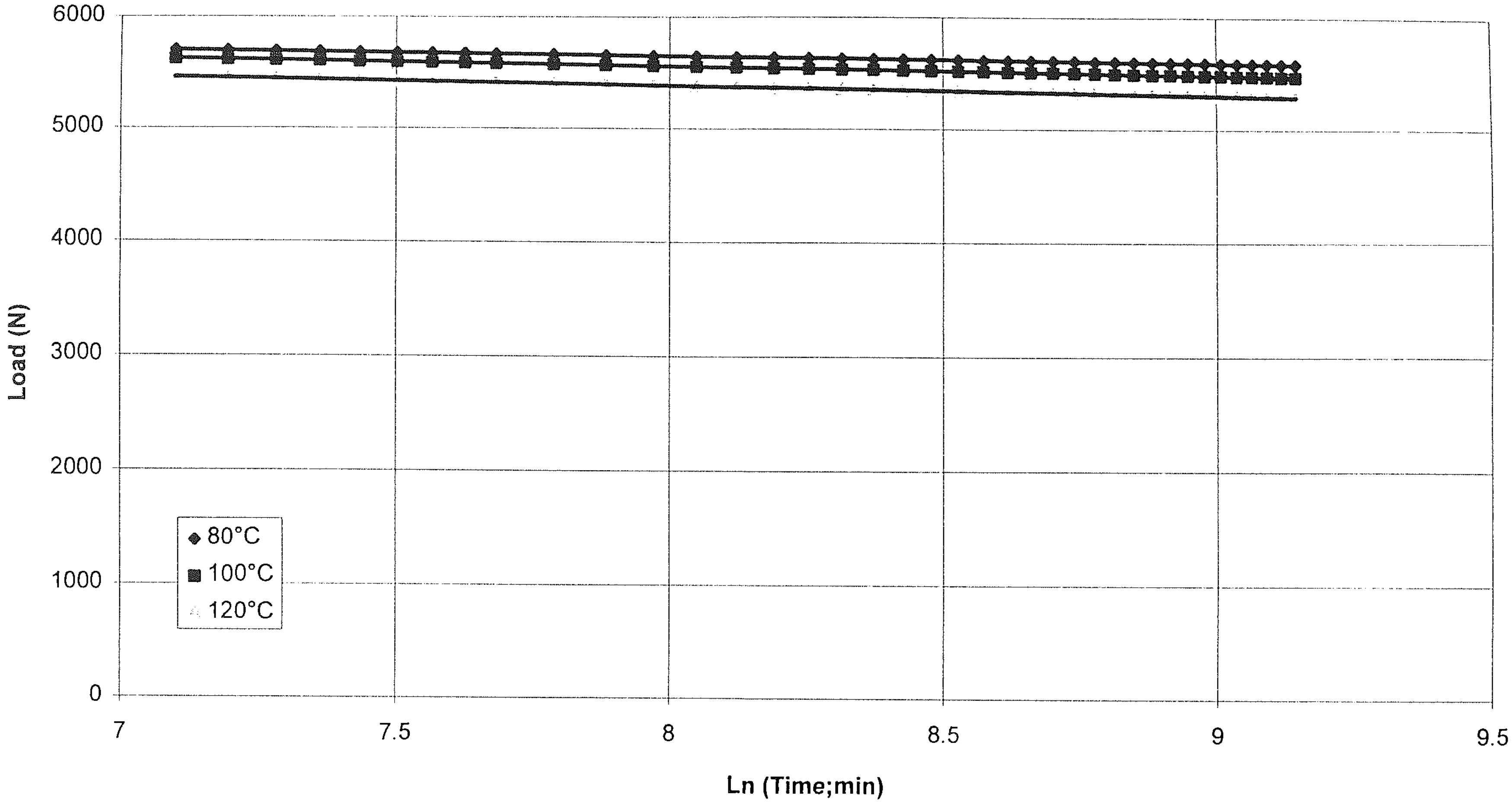

Figure 61. Variation of load-relaxation against ln time for LM25.

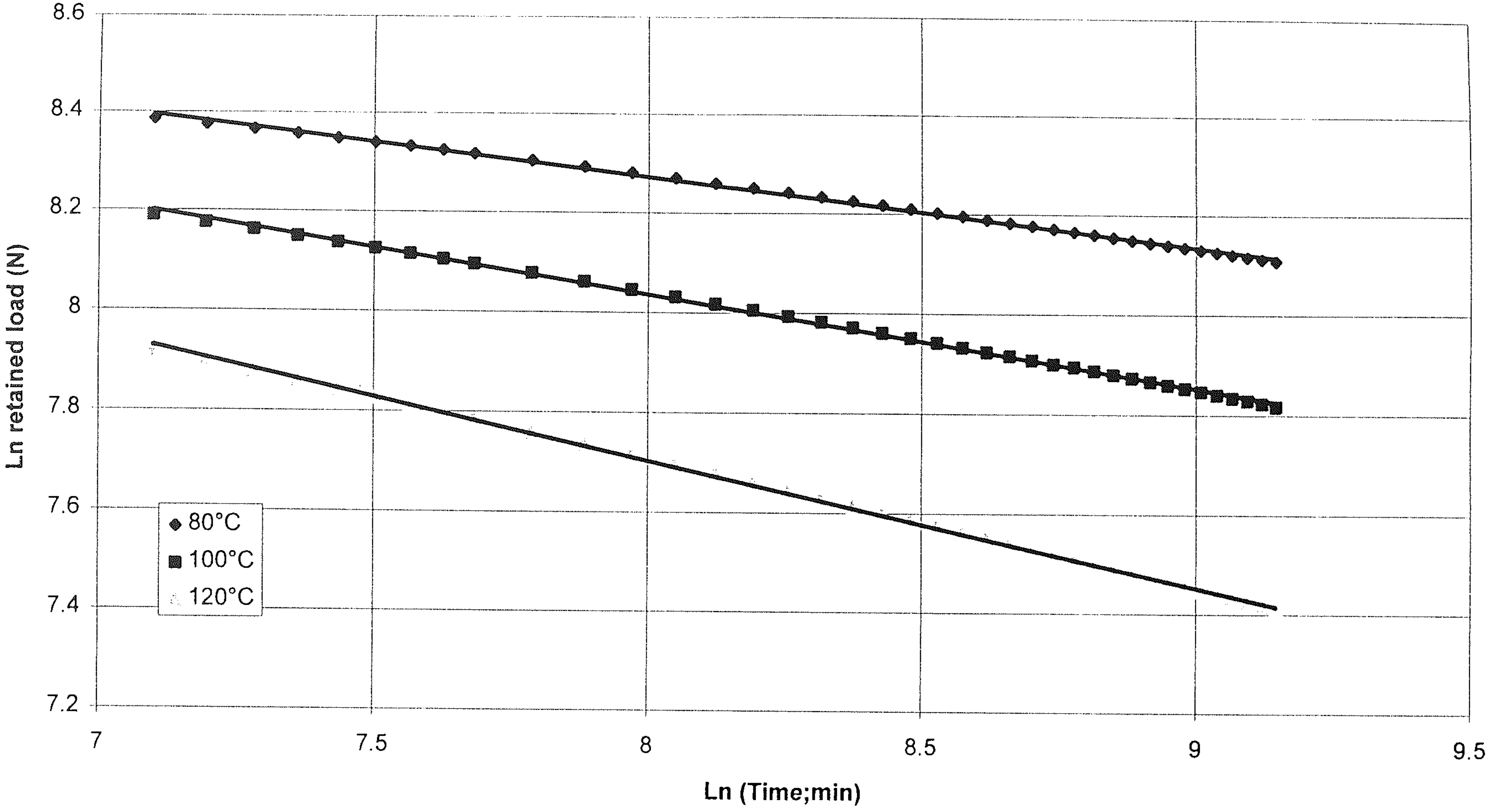

Figure 62. Ln retained load against ln time for ZA8.

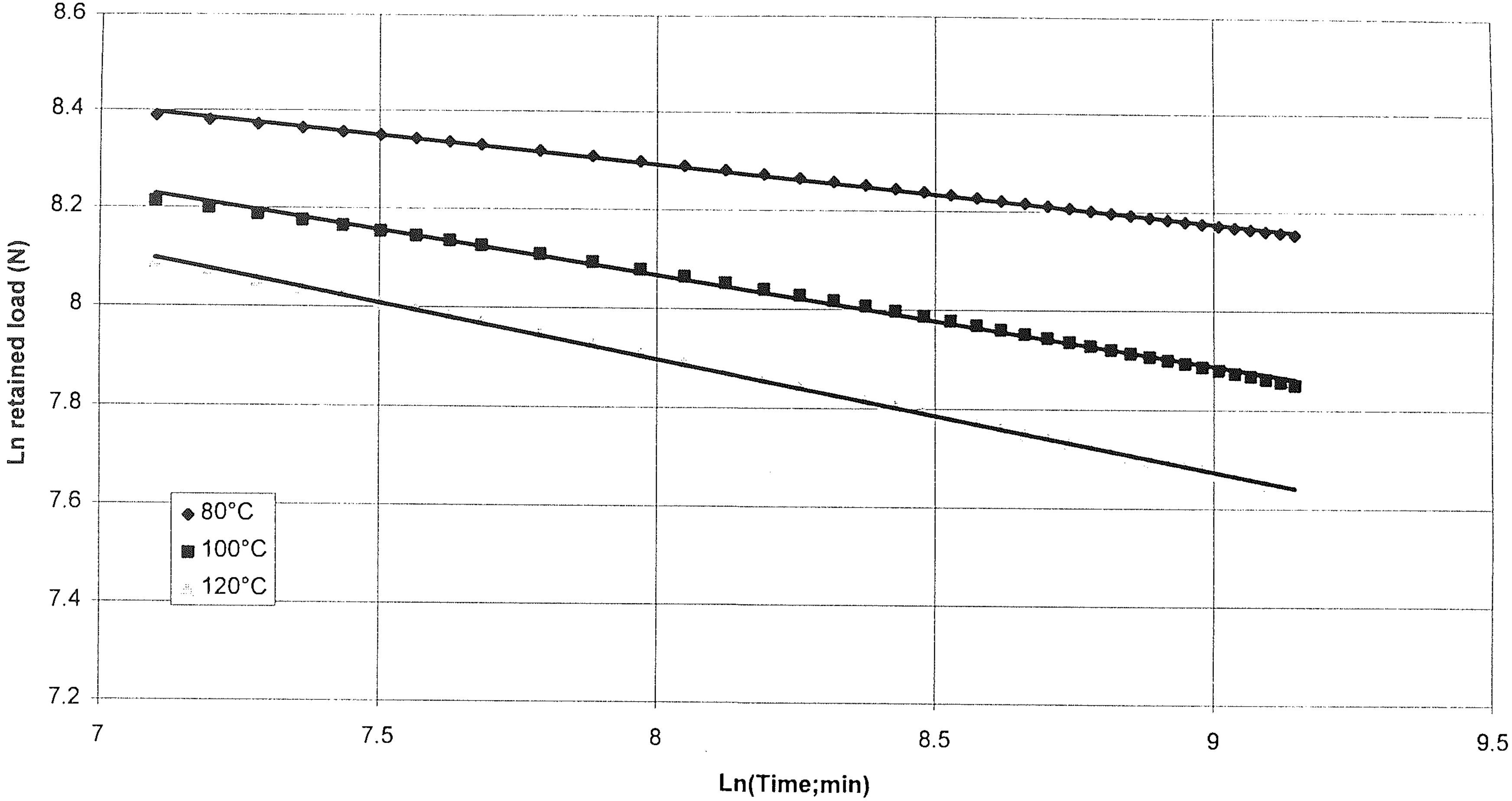

Figure 63. Ln retained load against ln time for ZA12.

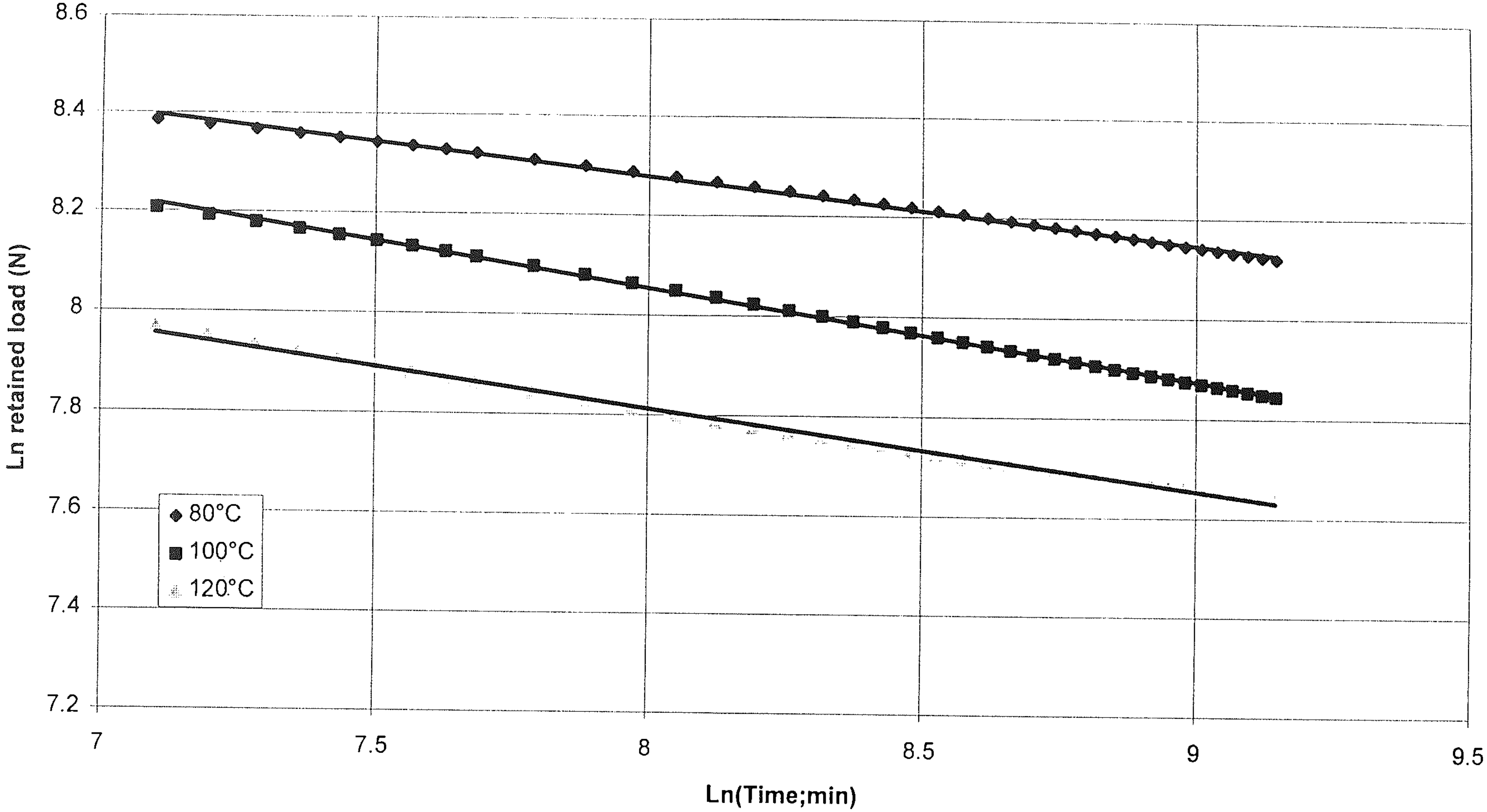

Figure 64. Ln retained load against ln time for ZA27.

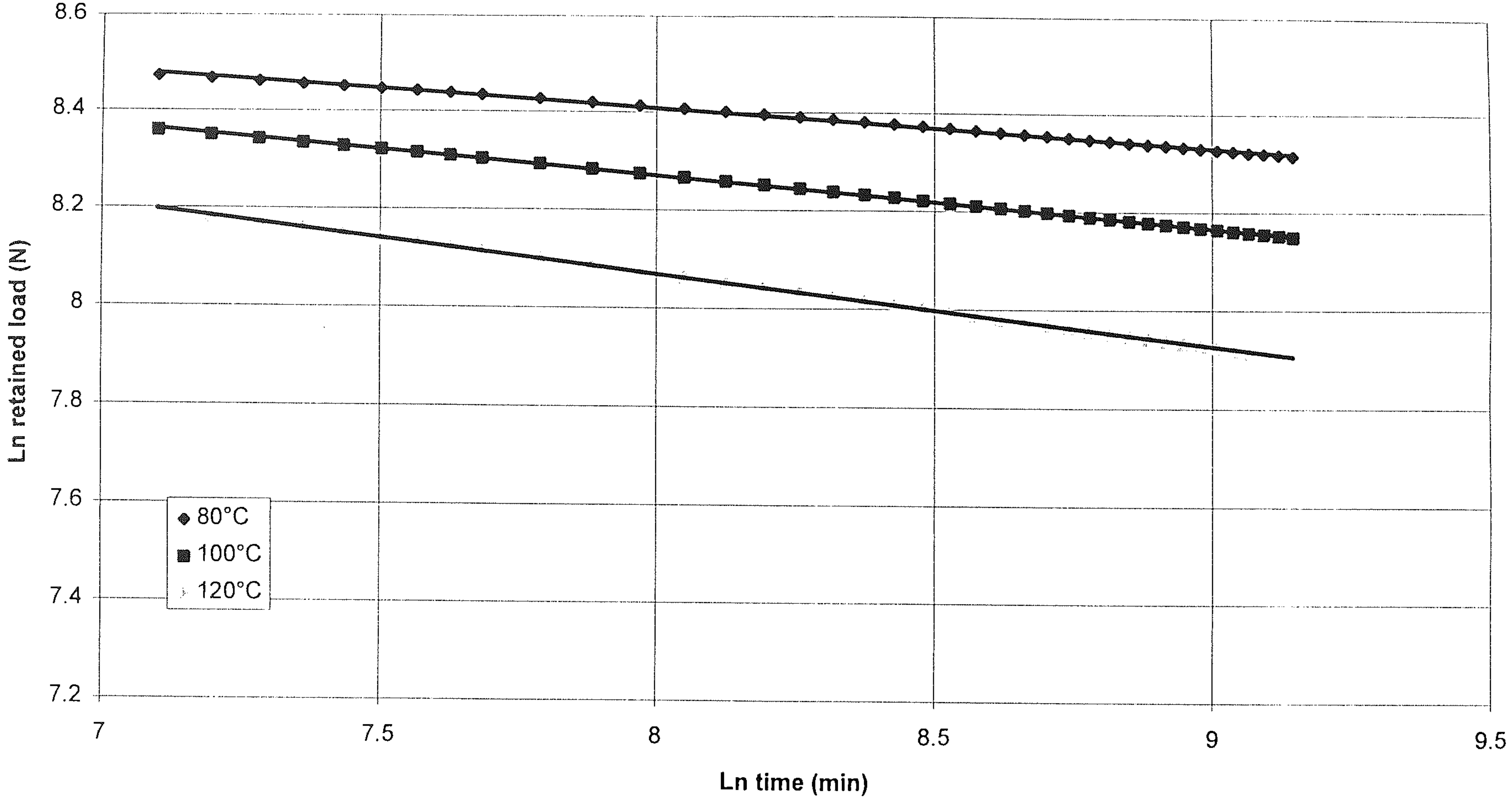

Figure 65. Ln retained load against ln time for Cosmal.

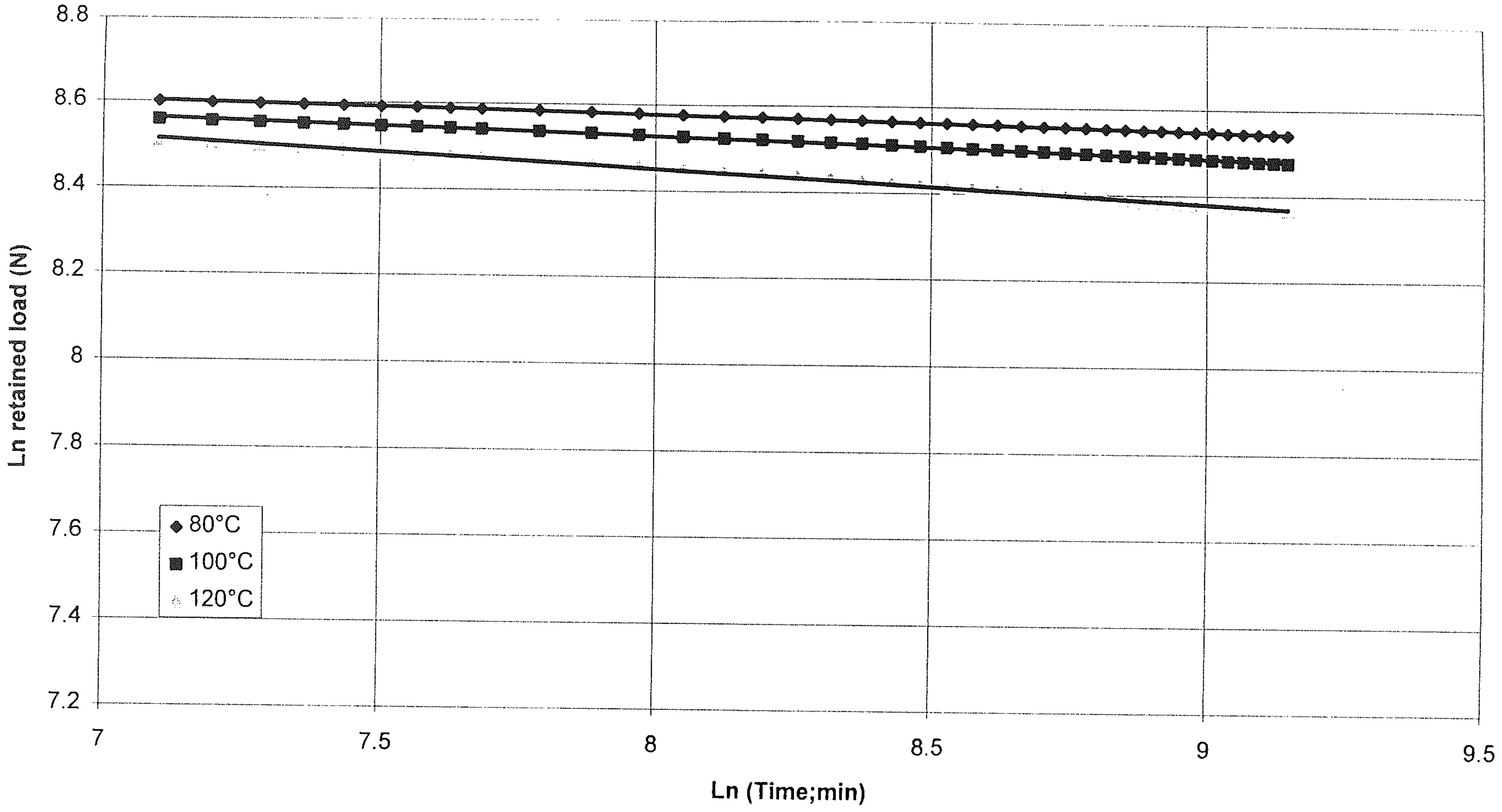

Figure 66. Ln retained load against ln time for Supercosmal.

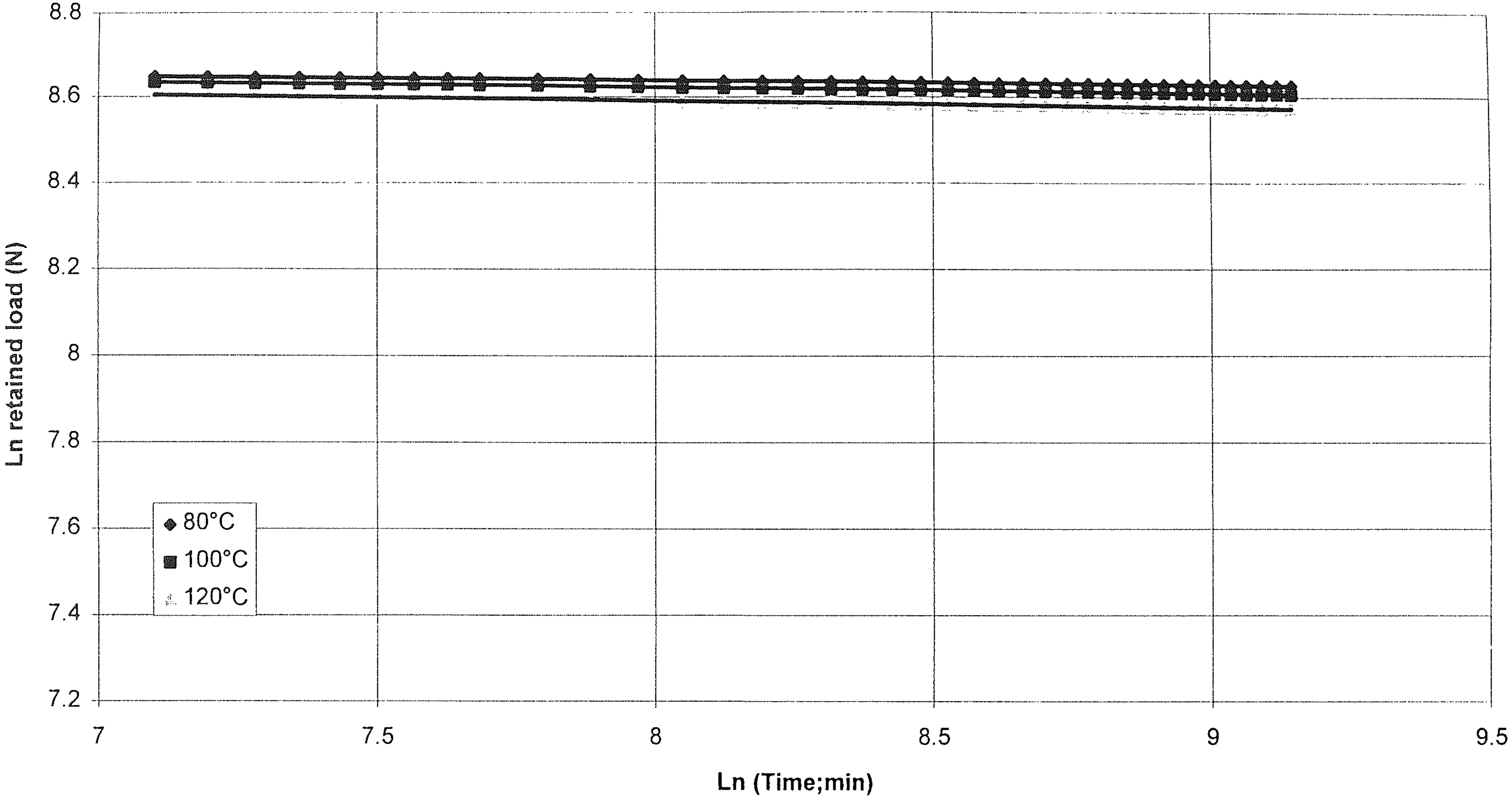

Figure 67. Ln retained load against ln time for LM25.

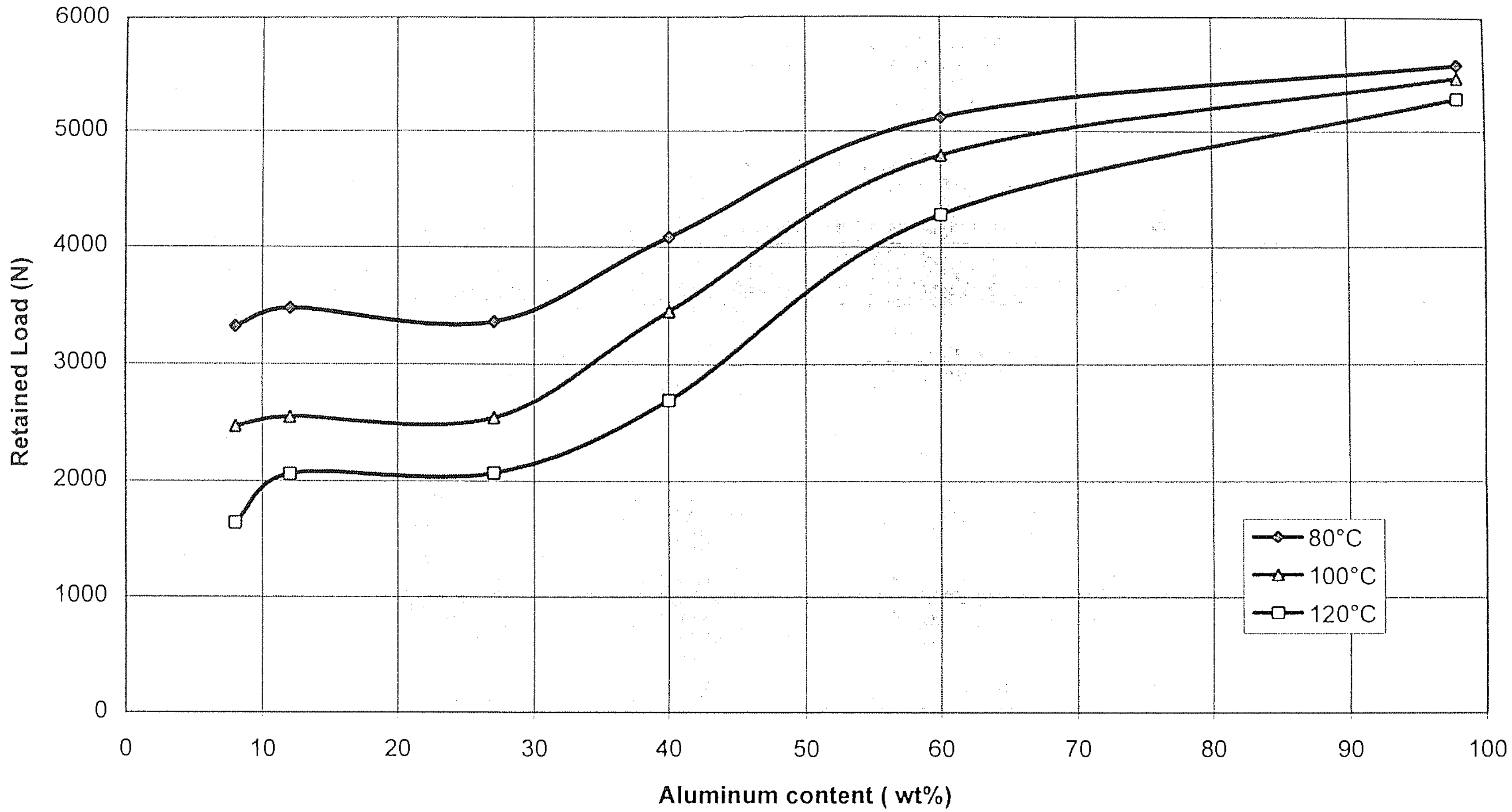

Figure 68. Variation of 150 hour load with aluminum content for alloys ZA8, ZA12, ZA27, Cosmal, Supercosmal and LM25.

5.3 Metallography of the Experimental Alloys

Samples were examined by scanning electron microscopy (SEM) before and after testing to study the microstructure of these experimental alloys. The contrast in the electron microscope images depends almost entirely on the average atomic number of the different phases present in the structure of the alloys. Therefore, in the back-scattered electron SEM micrographs of these alloys, zinc-rich phases appeared light and aluminium-rich phases dark, since the high-atomic-number zinc-rich phase had more electron scattering power than the aluminium-rich phase, although the shade of contrast could be adjusted by varying electronically the sensitivity of the electron detector to the atomic number.

5.3.1 Alloy ZA8

The as-cast structure of alloy ZA8 has been shown in *Figures 69, 70 and 71* at three different magnifications. The figures showed that the dendrites set in the eutectic were well developed due to the slow cooling rate of the casting. The primary phase was β set in an eutectic matrix. The β particles had decomposed and formed lamellae usually in the central portion of the grains with a coarser mixture of the phases at the edges. The lamellar regions in the dendrites interiors evidently had different orientations in small regions.

The microstructure of a creep test specimen of ZA8 was also checked tested at 100 MPa and 160°C by SEM as shown in *Figures 72, 73 and 74* . The test was of very short duration and no clear change in microstructure was observed except a network of zinc in β particles. As seen from the figures, the primary β particles did not change their shape, and no coarsening of the fine decomposed products was observed. The fine lamellae were little altered but the zinc network had developed at the boundaries of the regions of different orientations and at the junction with the particulate material at the edges of the dendrites.

The microstructure of load relaxation test samples have been shown in *Figures 75, 76 and 77.* This was similar to the creep tested samples, except that the zinc network was absent.

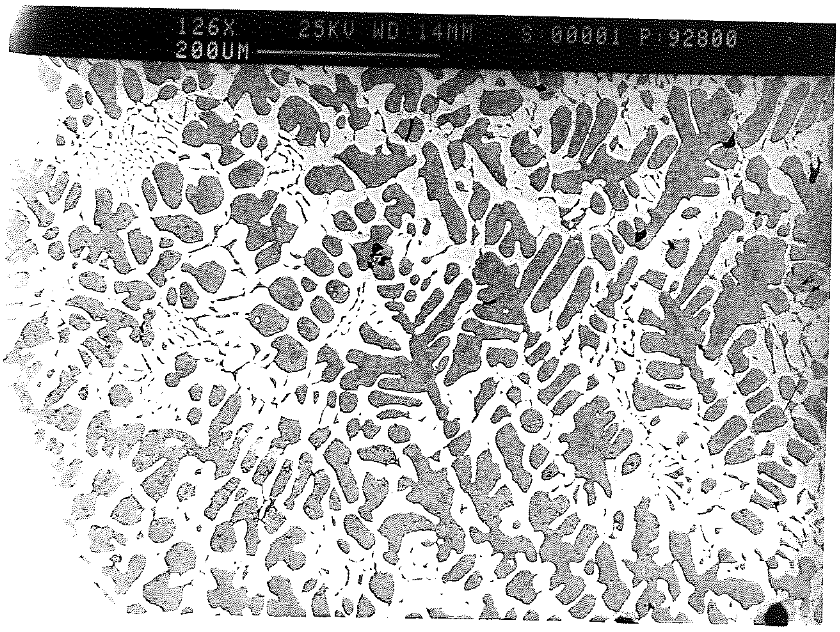

Figure 69. SEM. As cast structure of Alloy ZA8 showing the dendrites of primary β *phase in the irregular eutectic matrix.*

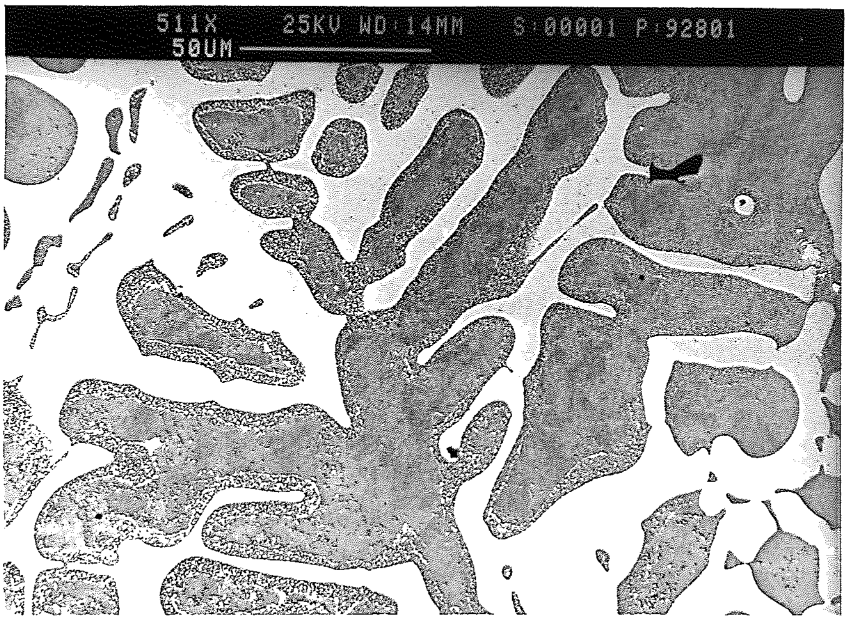

Figure 70. SEM. As cast structure of Alloy ZA8 at medium magnification showing the decomposed β.

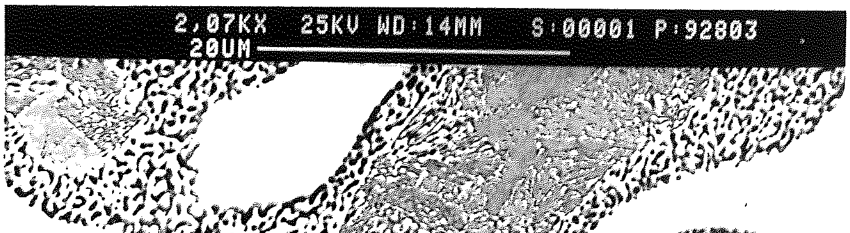

Figure 71. SEM. As cast structure of Alloy ZA8 at high magnification showing the decomposition of β *into particles at the edges, with fine lamellae in the centre.*

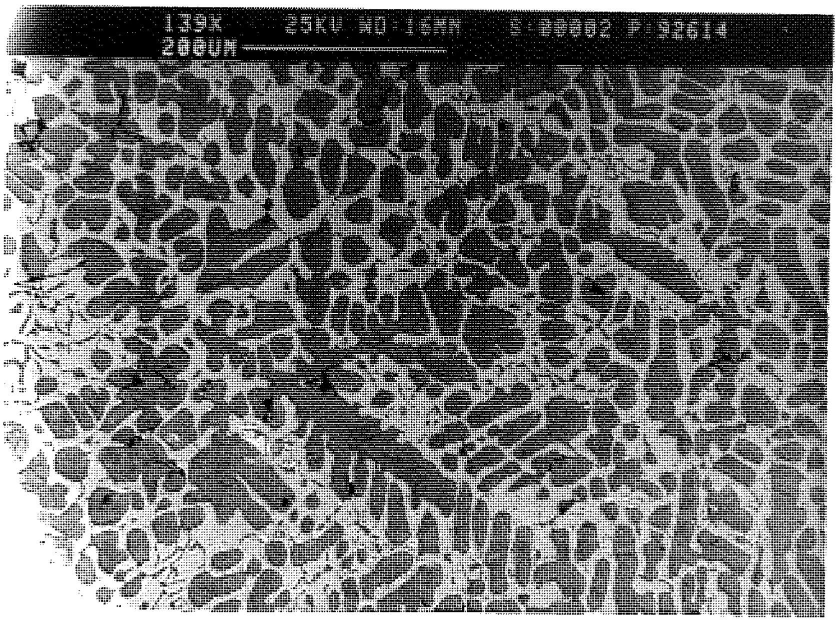

Figure 72. Alloy ZA8 tested at 100MPa and 160°C

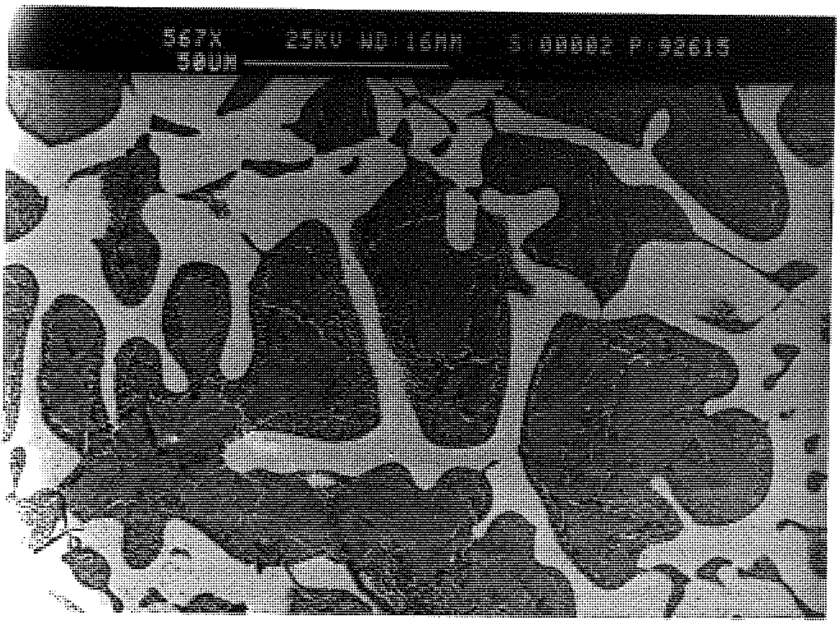

Figure 73. Alloy ZA8 tested at 100MPa and 160°C showing a zinc network in β particles at medium magnification.

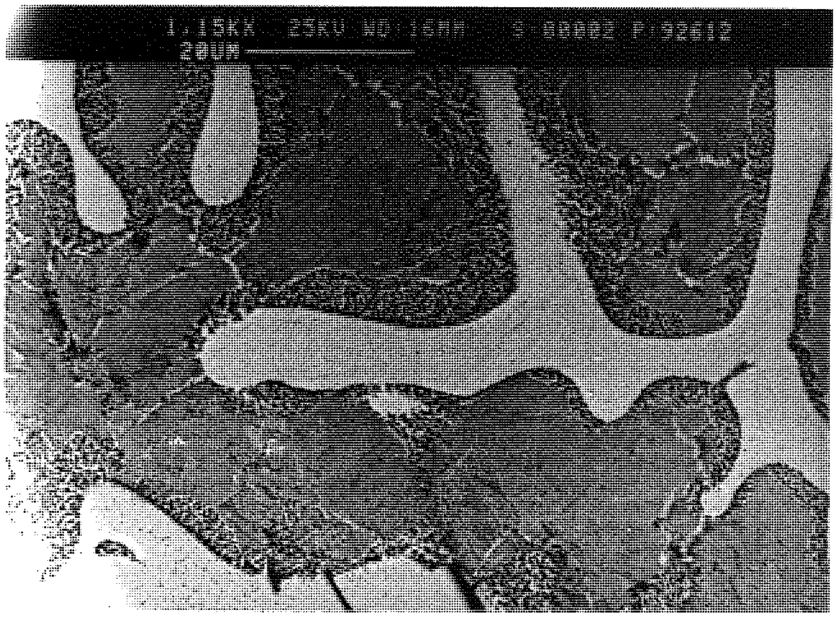

Figure 74. Alloy ZA8 tested at 100MPa and 160°C.

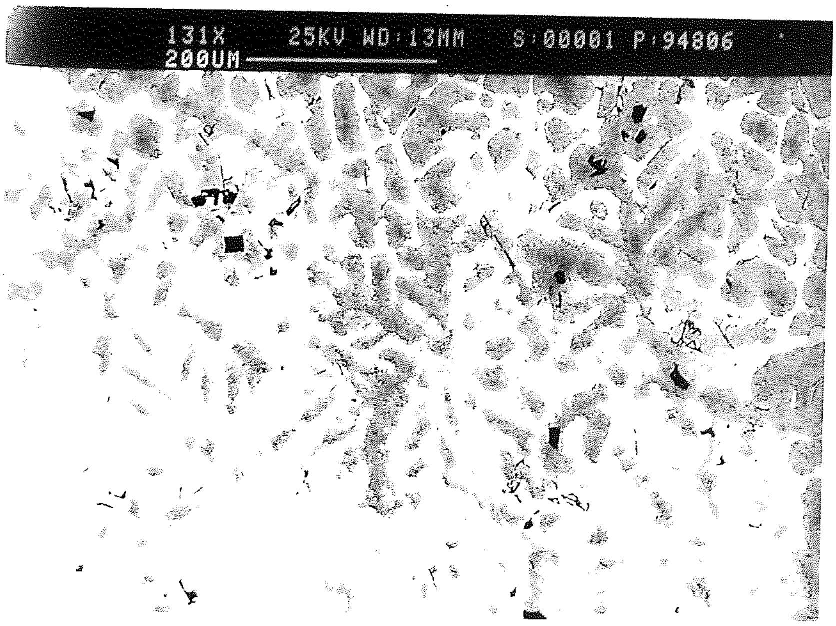

Figure 75. Alloy ZA8 tested at 120°C for load relaxation at low magnification.

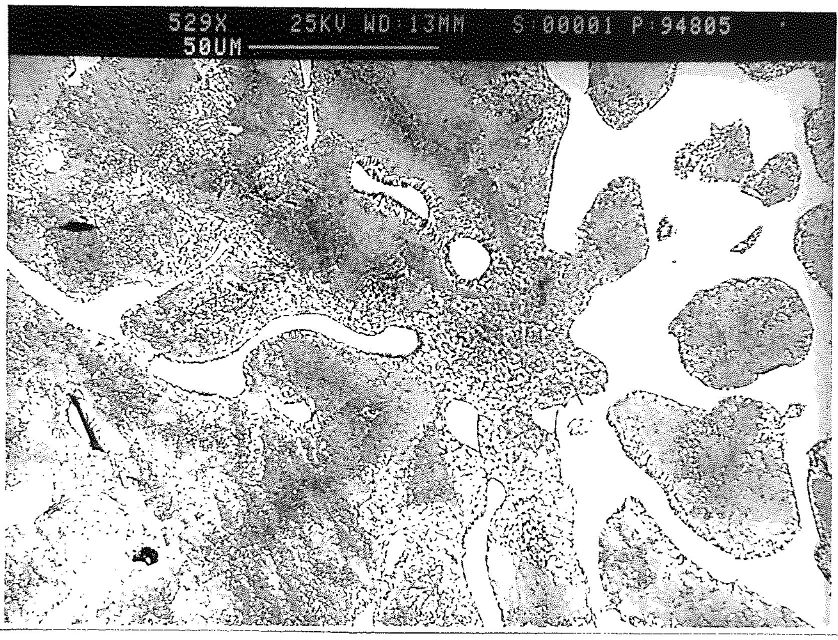

Figure 76. Alloy ZA8 tested at 120°C for load relaxation at medium magnification.

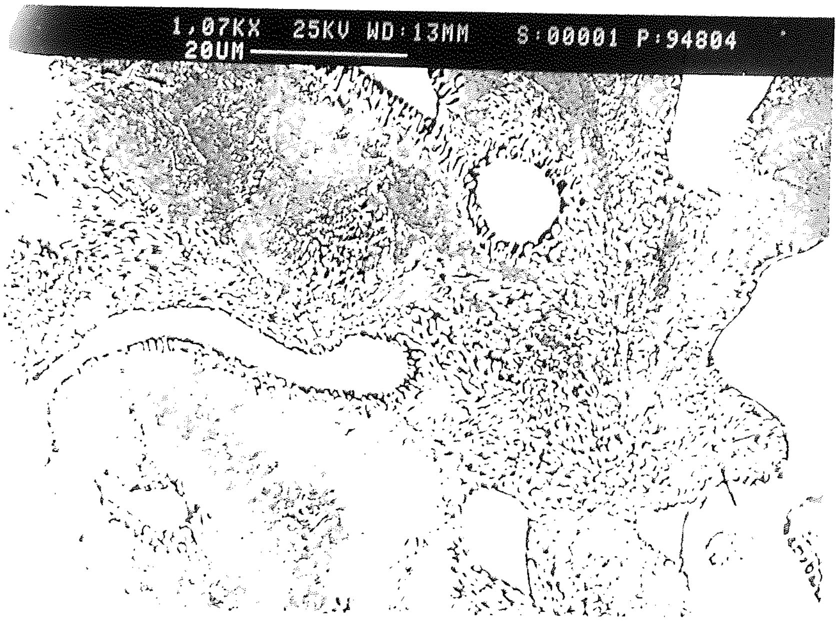

Figure 77. Alloy ZA8 tested at 120°C for load relaxation at high magnification

5.3.2 Alloy ZA12

Alloy ZA12 was also checked as cast and after creep test at 100 MPa and 160°C by SEM. The scale of the structure was similar to that of alloy ZA8 and microstructure was also very close to that of ZA8 except that there was more β and no eutectic matrix was found *(Figures 78, 79 and 80)*. It had dendrites of β particles which had decomposed at the edges like ZA8.

The creep tested samples showed a more distinct network of zinc in β particles *(Figures 81, 82 and 83)* but load relaxation samples showed no such network, *Figures 84, 85 and 86.* although there was a slight zinc enrichment at the inner boundary of the particulate layer.

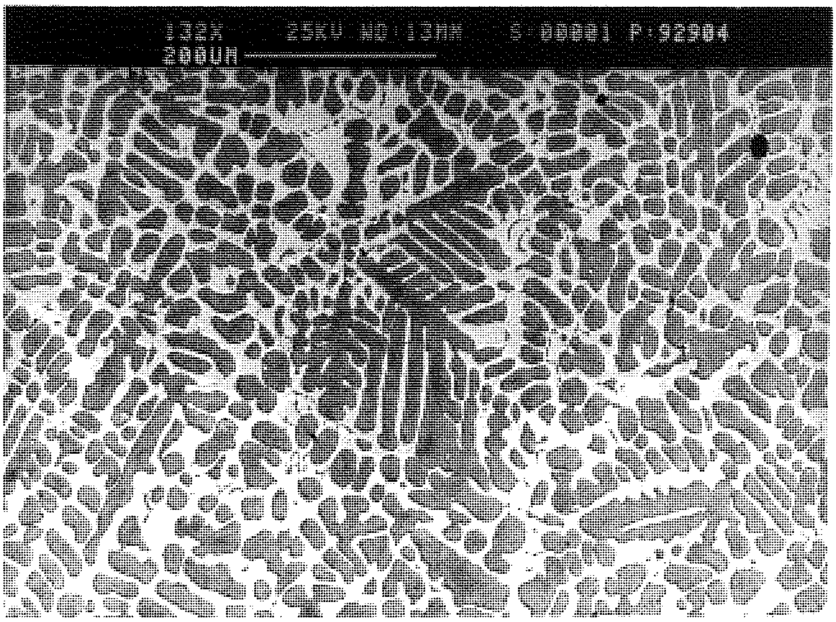

Figure 78. As cast structure of Alloy ZA12 showing the dendrites of primary β particles at low magnification.

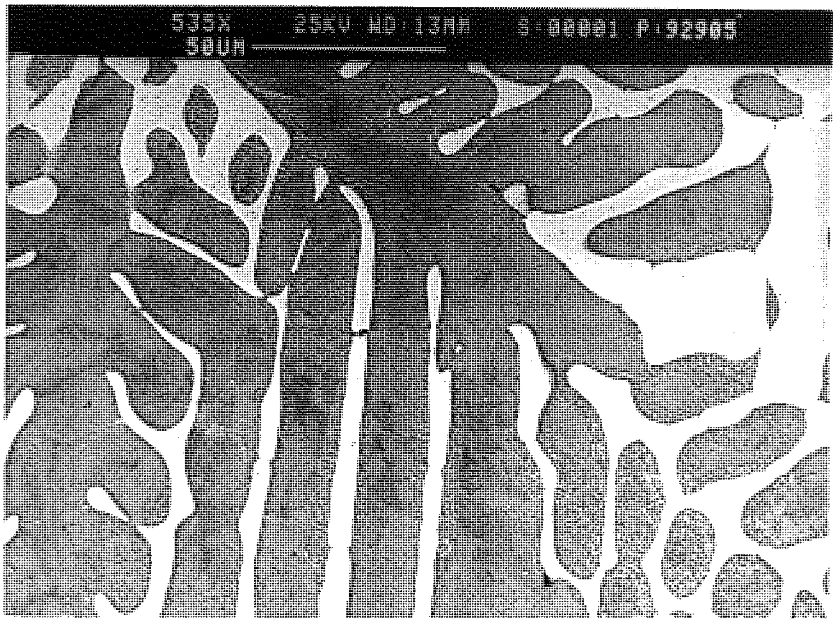

Figure 79. As cast structure of Alloy ZA12 at medium magnification showing the decomposed β.

Figure 80. As cast structure of Alloy ZA12 showing the decomposed β at high magnification.

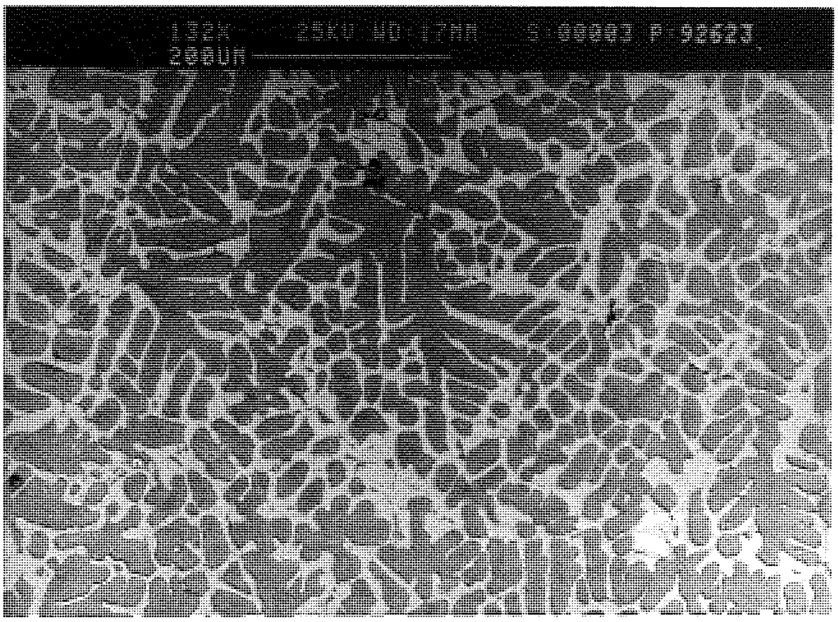

Figure 81. Alloy ZA12 tested at 100MPa and 160°C.

Figure 82. Alloy ZA12 tested at 100MPa and 160°C showing zinc network in β at medium magnification

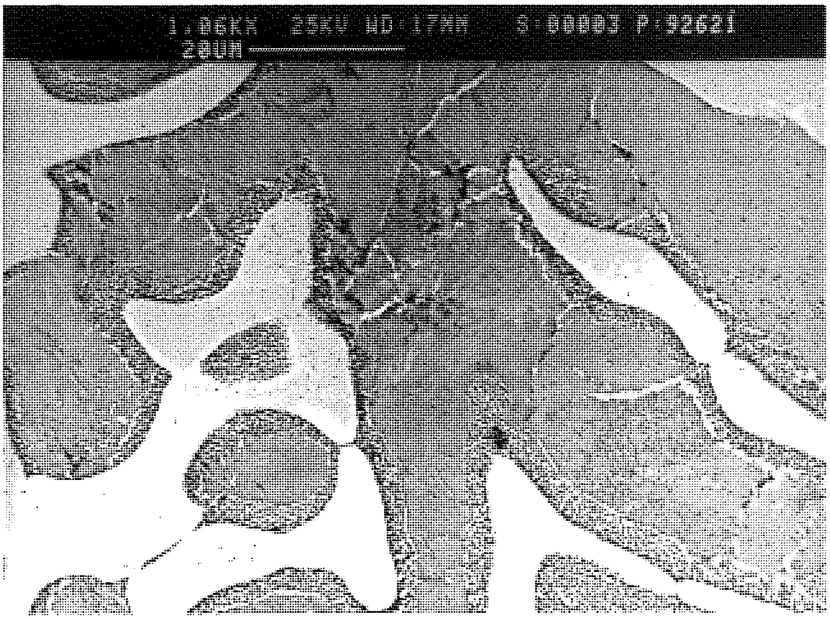

Figure 83. Alloy ZA12 tested at 100MPa and 160°C showing zinc network in β at high magnification

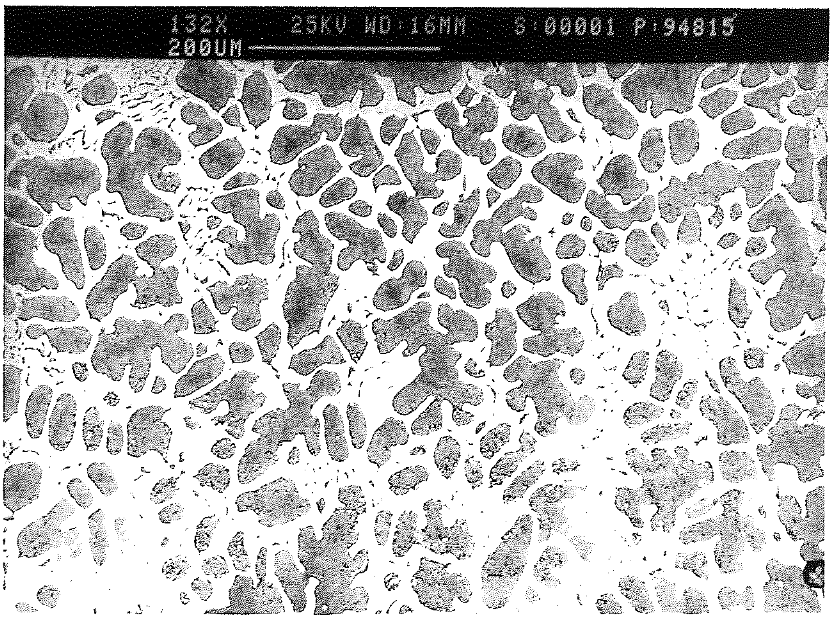

Figure 84. Microstructure of load relaxation sample of Alloy ZA12 tested at 120°C at low magnification showing β dendrites in the eutectic matrix.

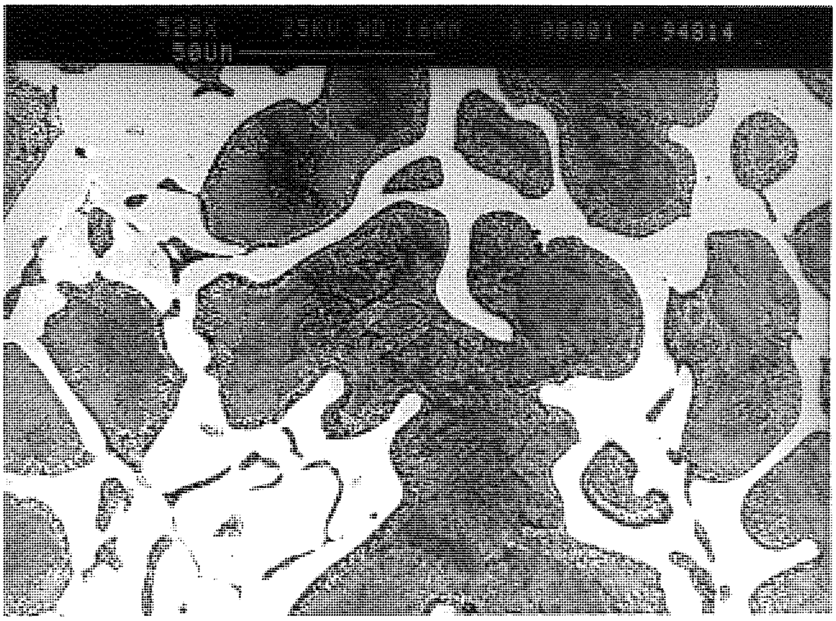

Figure 85. Microstructure of load relaxation sample of Alloy ZA12 tested at 120°C exhibiting the decomposition of β *into* α+η.

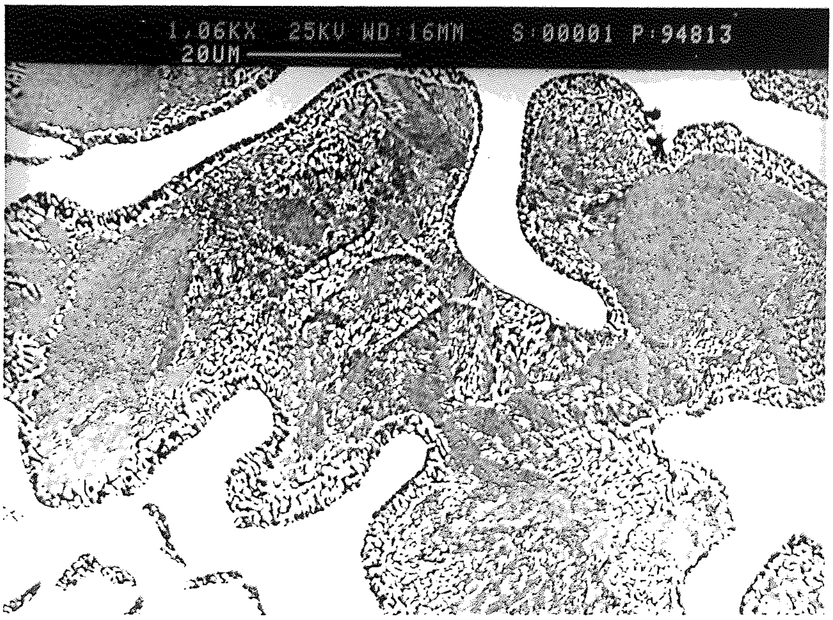

Figure 86. Microstructure of load relaxation sample of Alloy ZA12 tested at 120°C at high magnification.

5.3.3 Alloy ZA27

Alloy ZA27 with higher aluminum and copper content, had a more complex multiphase microstructure and a distinctly different structure from the previous one (ZA8 and ZA12). *Figures 87, 88 and 89* show a fine structure of dendrites in a mass of much smaller aluminum-rich particles with a network of interdendritic zinc. As appeared in *Figures 88 and 89* at higher magnification, solidification of this alloy had begun with the formation of aluminum-rich (α-α`) dendrities, and proceeded by precipitation of much more zinc-rich β phase. The latter formed around the primary dendrites through a peritectic reaction between the first formed α-phase and residual liquid. The cores decomposed in some parts into coarse, lamellar cellular products, and more frequently into a very fine mixture of zinc-rich phases. The β areas had subsequently decomposed into fine lamellar or irregular particles of α and η.

Precipitation of copper rich ε phase could not be differentiated from the zinc by atomic number contrast since it differs by only small fraction of an atomic number. The wide freezing range of this alloy makes it prone to micro-shrinkage and as a result porosity was observed which reduced the creep strength of this alloy.

The zinc network in tested samples was more prominent and in excess quantity in this alloy as compared to ZA8 and ZA12 and was accompanied by numerous small particles of aluminium. In some areas bands of particulate coarsening had resulted *(Figures 90, 91 and 92).*

Load relaxation samples have been represented in *Figures 93, 94 and 95.* These too showed development of particulate areas, although the zinc bands were few, but the scale of this effect was smaller than in the creep tested samples.

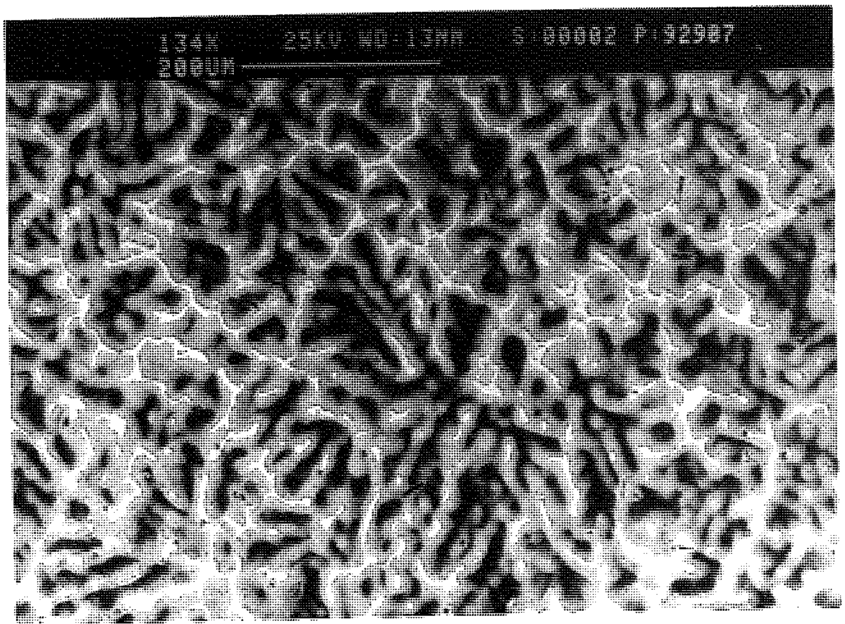

Figure 87. As cast structure of Alloy ZA27 showing α dendrites in β and η or η/ε network at low magnification. Shrinkage porosity is also evident in this figure.

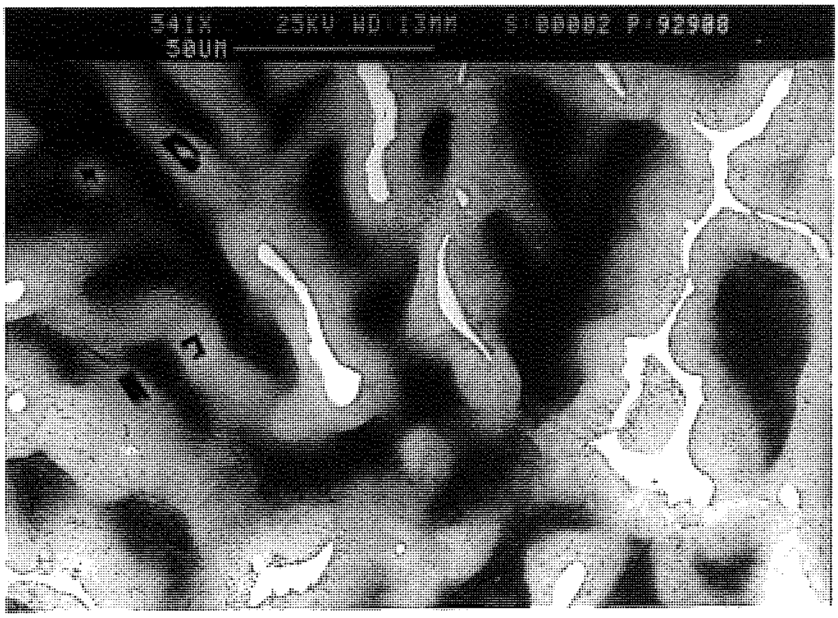

Figure 88. As cast structure of Alloy ZA27 showing the decomposition morphology of α dendrites at medium magnification. Dark angular phases are iron-rich phases with high aluminium contents.

Figure 89. As cast structure of Alloy ZA27 showing the equaixed structure of dark α dendrites surrounded by lighter decomposed β at high magnification.

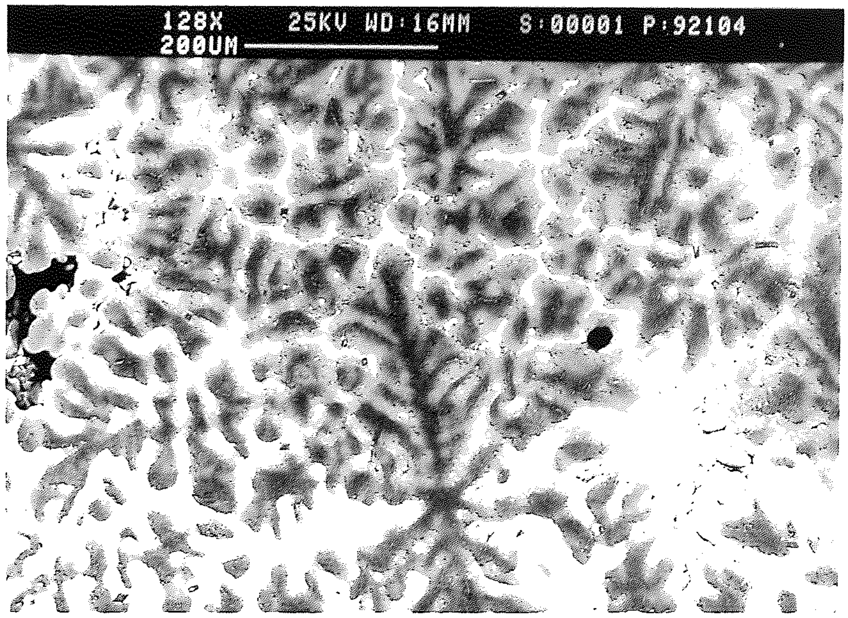

Figure 90. Micrograph of Alloy ZA27 tested at 100 MPa and 160°C at low magnification.

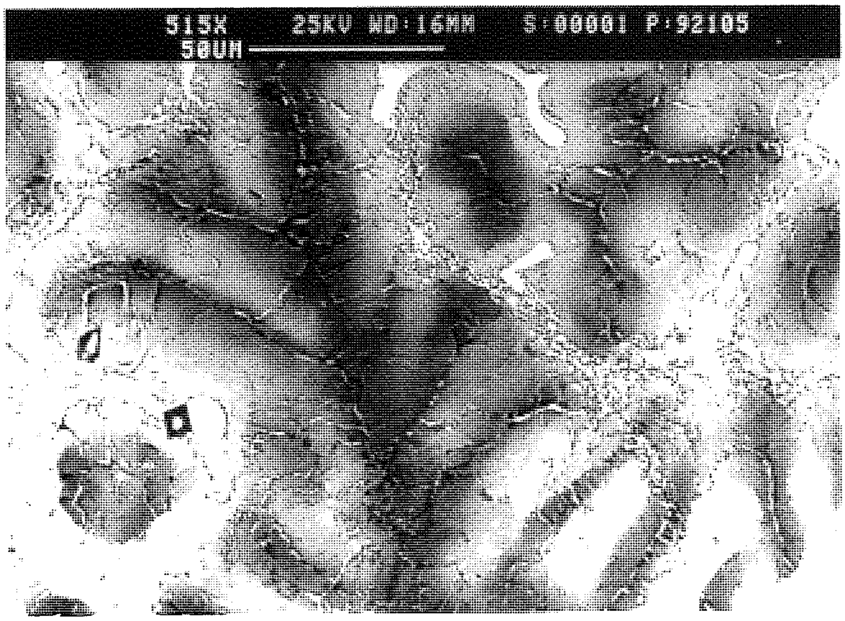

Figure 91. Micrograph of Alloy ZA27 tested at 100 MPa and 160°C showing the zinc network in α and β at medium magnification.

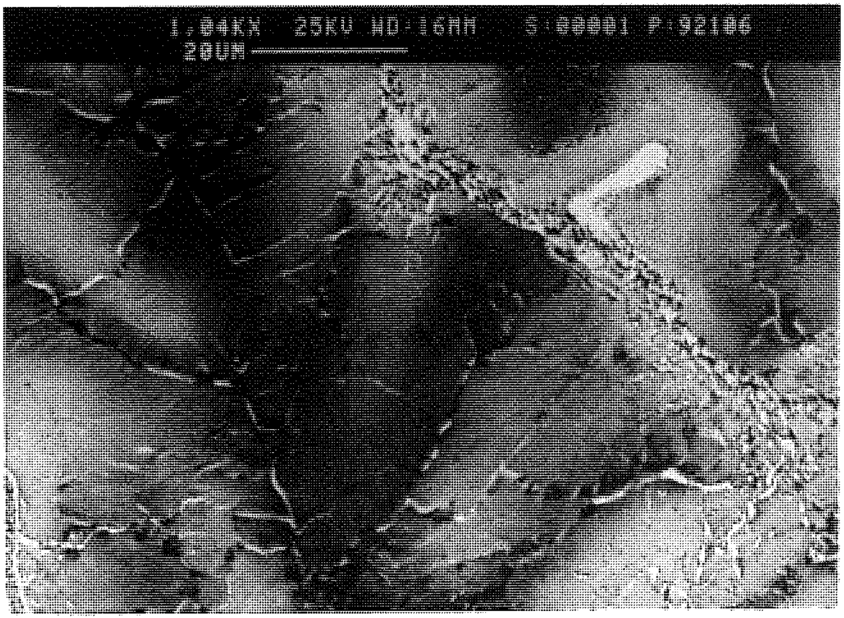

Figure 92. Micrograph of Alloy ZA27 tested at 100 MPa and 160°C at high magnification.

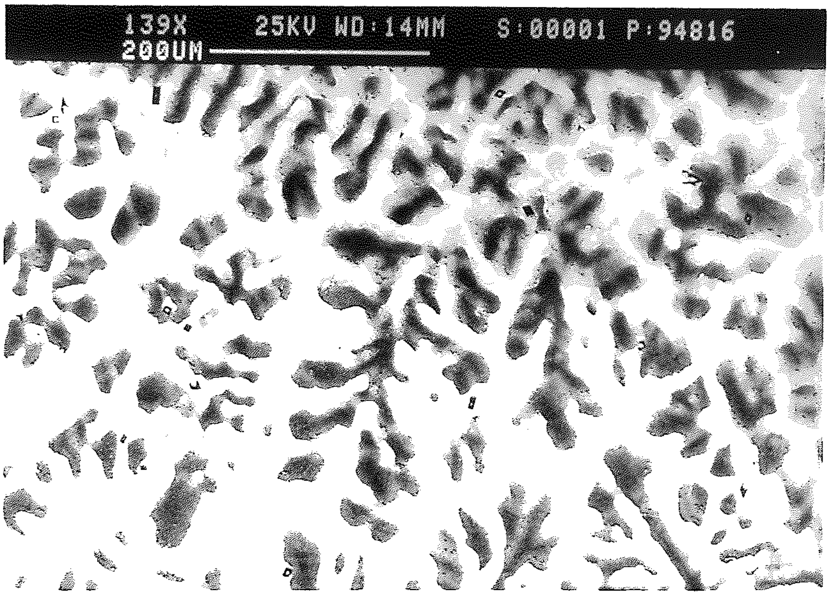

Figure 93. Micrograph of load relaxation sample of Alloy ZA27 tested at 120°C.

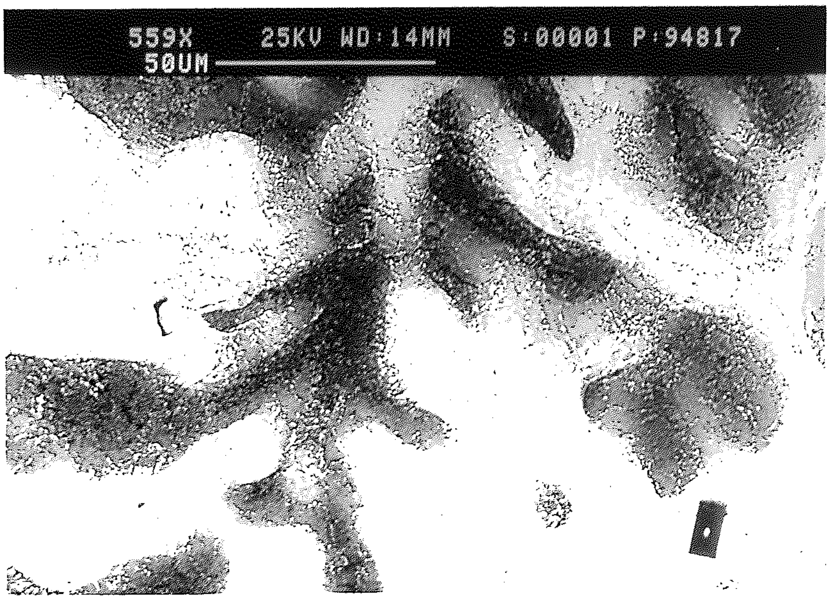

Figure 94. Micrograph of load relaxation sample of Alloy ZA27 tested at 120°C at medium magnification.

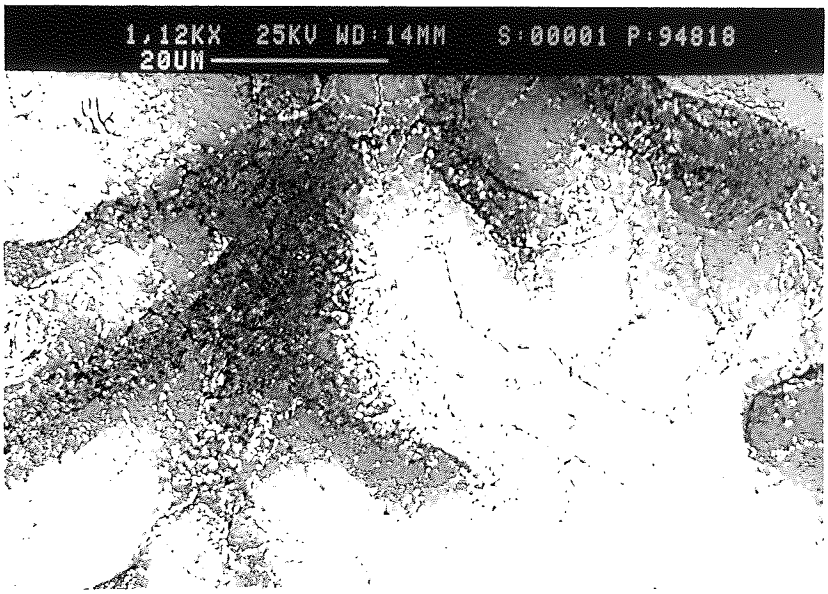

Figure 95. Micrograph of load relaxation sample of Alloy ZA27 tested at 120°C at high magnification.

5.3.4 Alloy Cosmal

As cast structure of Cosmal has been shown in *Figures 96, 97 and 98.* The first phase to solidify was evidently an eutectic mixture of α and Si, followed by β and ultimately η and Cu-rich phases. As silicon is almost insoluble in zinc and aluminium and has a high melting temperature, its crystals could be seen independently in the aluminium rich portion which solidified first. The α later broke down into two phases α and α' and both were in the form of a solid solution of zinc in aluminium with different percentages of zinc. *Figures 97 and 98* show a modest development of particulate decomposition in the α and β phases, possibly at sub-grain boundaries. The last liquid to solidify was not just η, but a mixture of phases, as many interdendritic η pools also contained many gray particles, which are probably the Cu-rich T' phase. Pale-gray laths present in the α or β are probably Mn-rich phases containing aluminium.

The tested sample at 160°C and 100 MPa shown in *Figures 99, 100 and 101*. Extensive development of zinc-bands and aluminium particles is shown by the medium and high magnification micrographs, even at the Si/α boundaries.

Micrographs of load relaxation samples of Cosmal have been shown in *Figures 102, 103 and 104*. These also showed areas of particulate development and some banding, but to a smaller extent than the creep test samples.

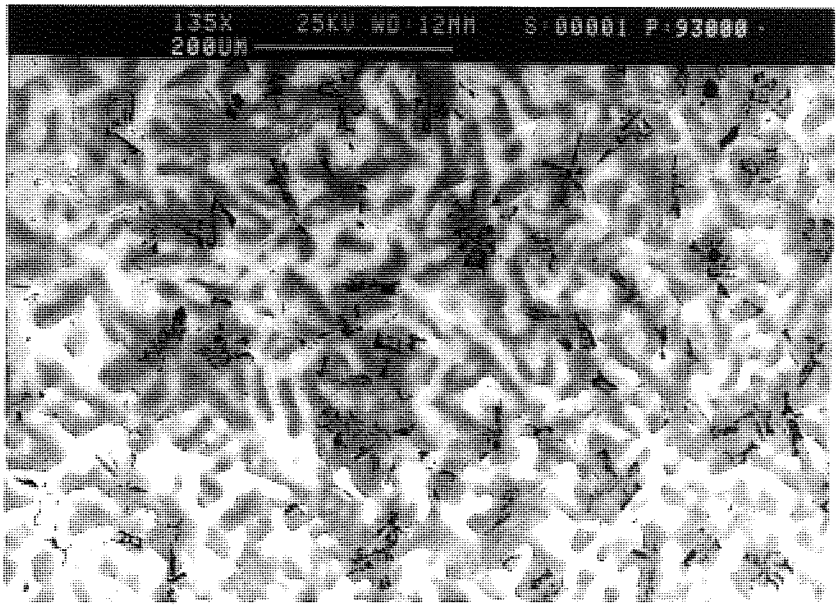

Figure 96. As cast structure of Cosmal showing the silicon crystals in α particles at low magnification.

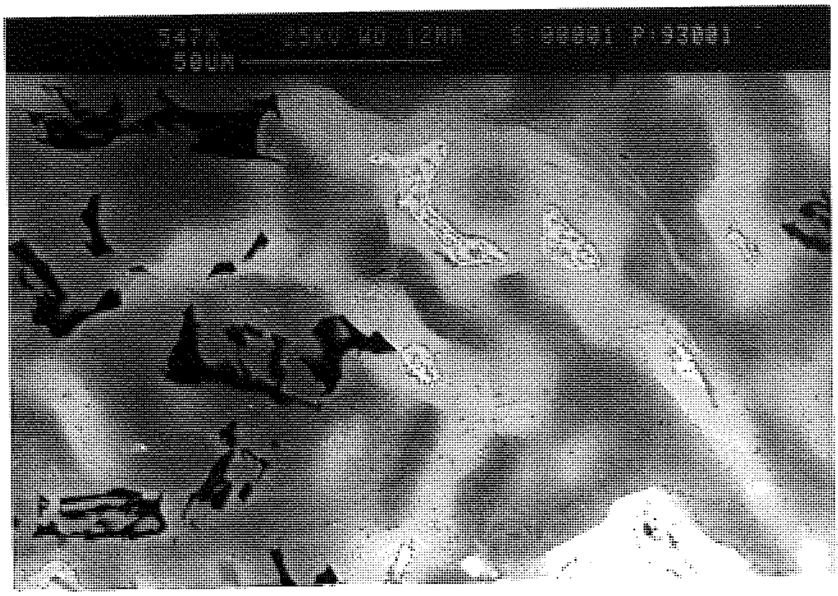

Figure 97. As cast structure of Cosmal showing the decomposition morphology of α *particles at medium magnification. The light-gray laths are probably Mn-rich phases, and the gray particulate phases in the* η *pools are probably T′ phase.*

Figure 98. As cast structure of Cosmal showing the decomposition of β *into* α+η *at high magnification.*

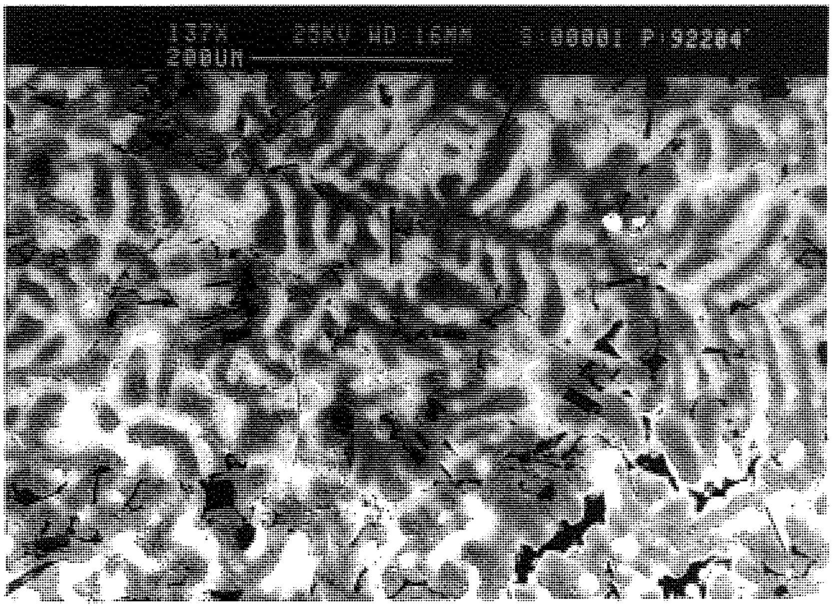

Figure 99. Micrograph of Cosmal tested at 100 MPa and 160°C at low magnification.

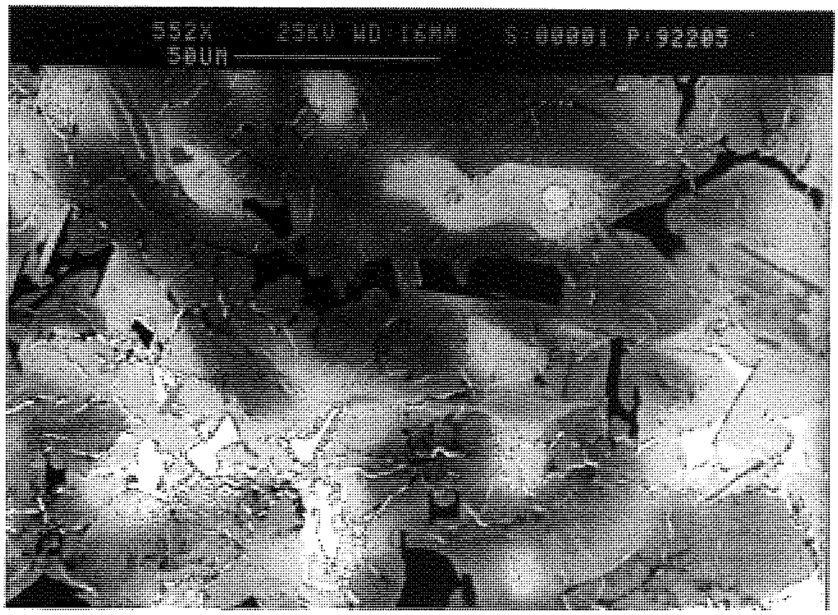

Figure 100. Micrograph of Cosmal tested at 100 MPa and 160°C at medium magnification

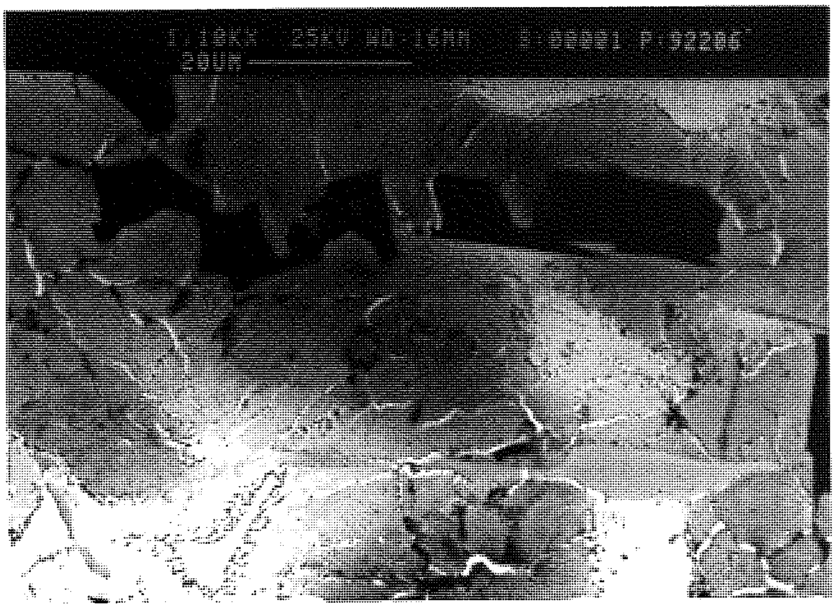

Figure 101. Micrograph of Cosmal tested at 100 MPa and 160°C at high magnification

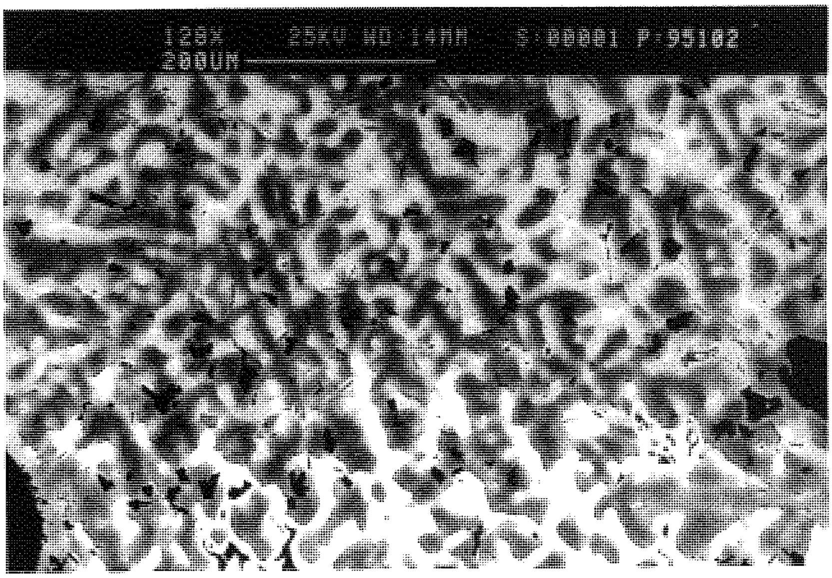

Figure 102. Micrograph of load relaxation sample of alloy Cosmal tested at 120°C at low magnification.

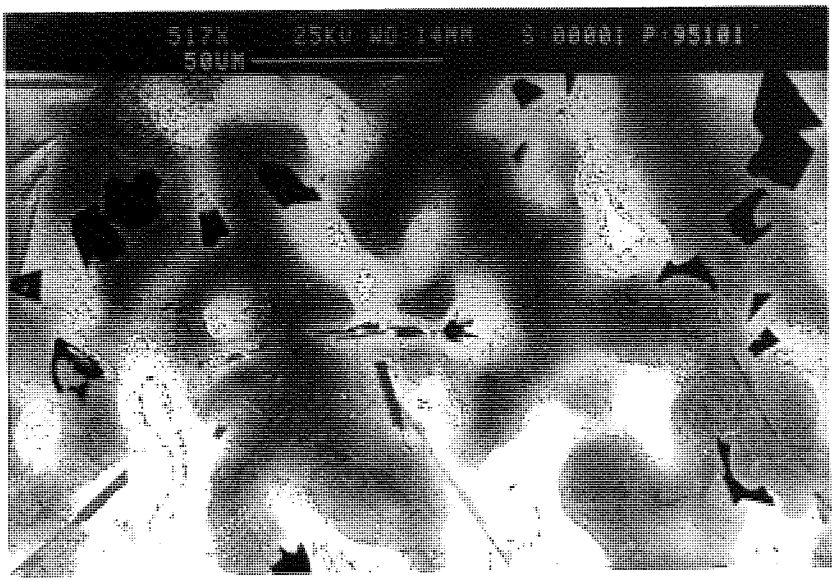

Figure 103. Micrograph of load relaxation sample of alloy Cosmal tested at 120°C at medium magnification.

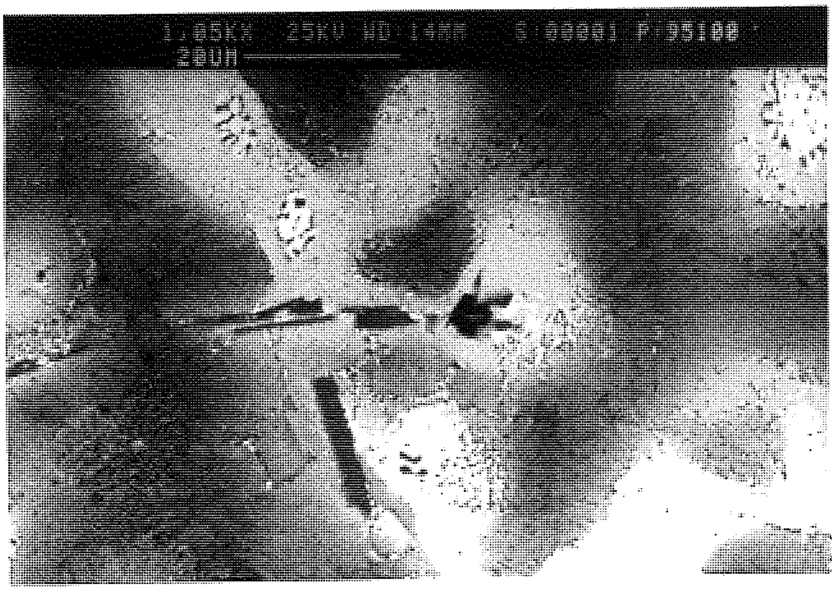

Figure 104. Micrograph of load relaxation sample of alloy Cosmal tested at 120°C at high magnification.

5.3.5 Alloy Supercosmal

Figures 105, 106 and 107 represent the as cast structure of Supercosmal with greater amount of silicon and aluminium contents as compared to alloy Cosmal. The first phase to solidify was evidently an eutectic mixture of α and Si, followed by β and ultimately η and Cu-rich phases. *Figures 106 and 107* show a modest development of particulate decomposition in the α and β phases, possibly at sub-grain boundaries. The last liquid to solidify was not just η, but a mixture of phases, as many interdendritic η pools also contained many grey particles, which are probably the Cu-rich T' phase. Grey clusters present in the α or β are probably Mn-rich phases containing aluminium.

Figures 108, 109 and 110 have been taken of a sample tested at 160°C and 100MPa which represent extensive development of zinc-bands and aluminium particles in the medium and high magnification micrographs, even at the Si/α boundaries.

Figures 111, 112 and 113 showed the micrograph of load relaxation sample of Supercosmal tested at 120°C. These also showed areas of particulate development and some banding, but to a smaller extent than the creep test samples.

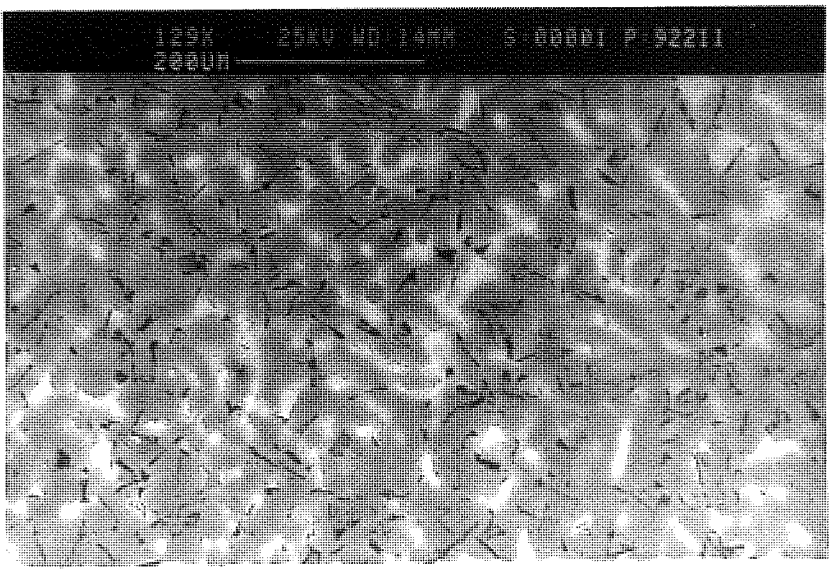

Figure 105. As cast structure of Supercosmal showing the silicon crystals in α particles at low magnification.

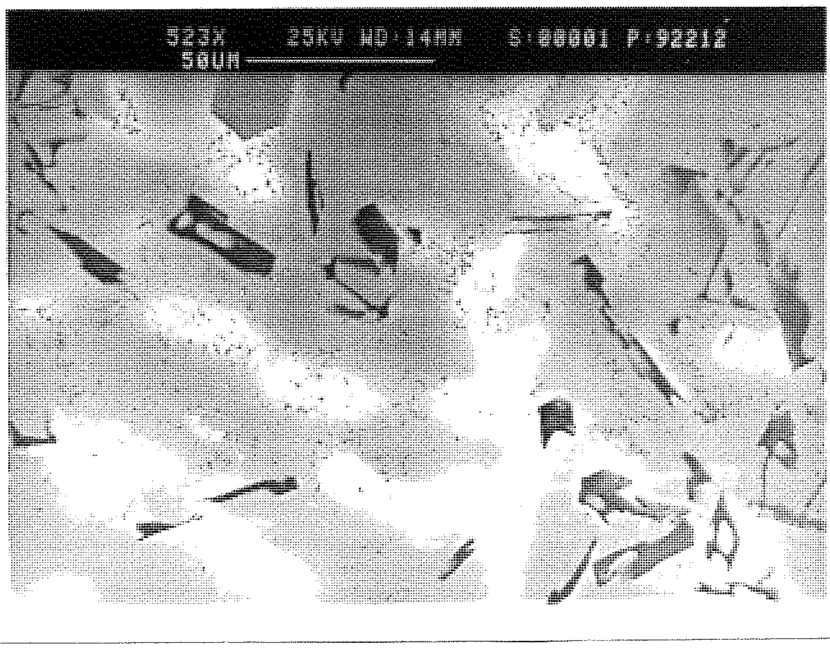

Figure 106. As cast structure of Supercosmal at medium magnification.

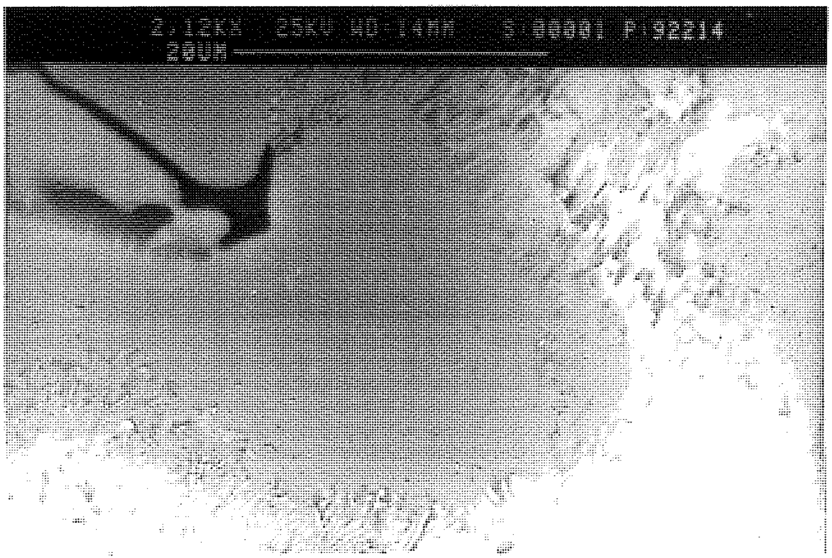

Figure 107. As cast structure of Supercosmal at high magnification.

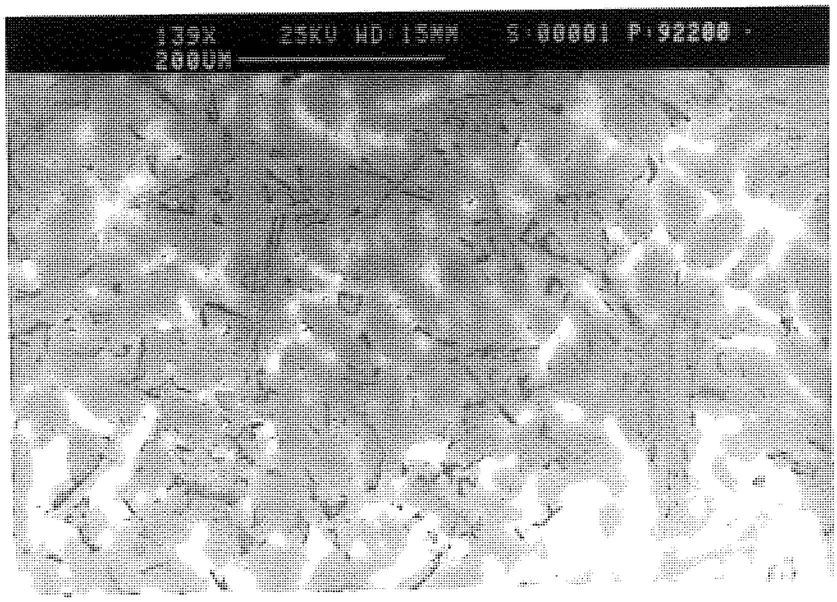

Figure 108. Micrograph of Supercosmal tested at 100 MPa and 160°C at low magnification

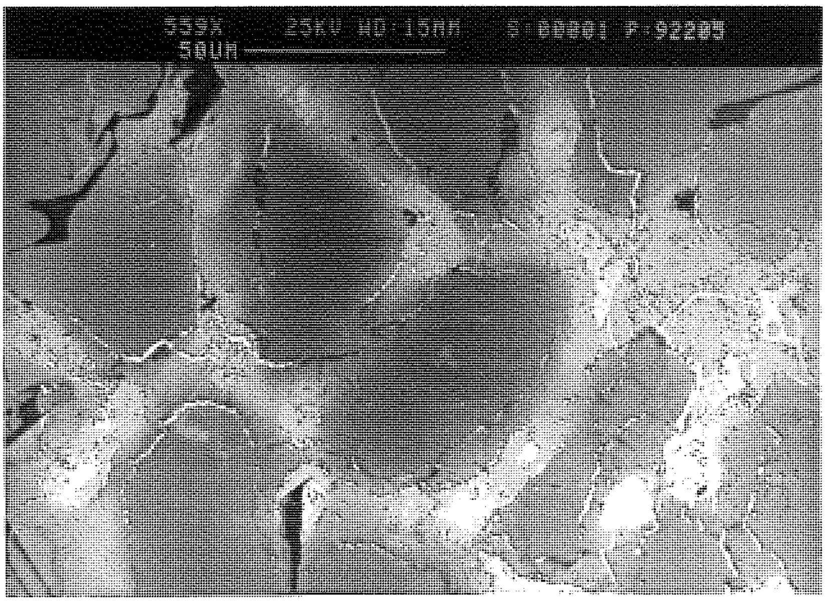

Figure 109. Micrograph of Supercosmal tested at 100 MPa and 160°C at medium magnification

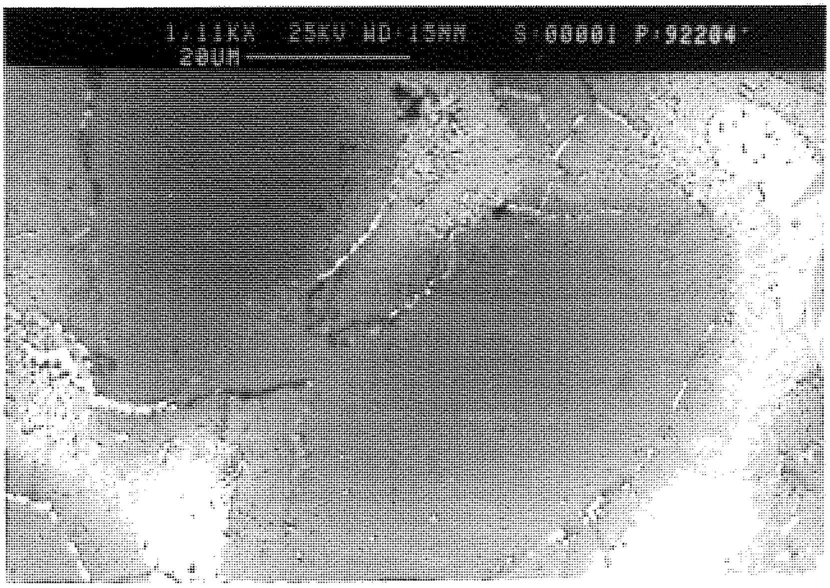

Figure 110. Micrograph of Supercosmal tested at 100 MPa and 160°C at high magnification

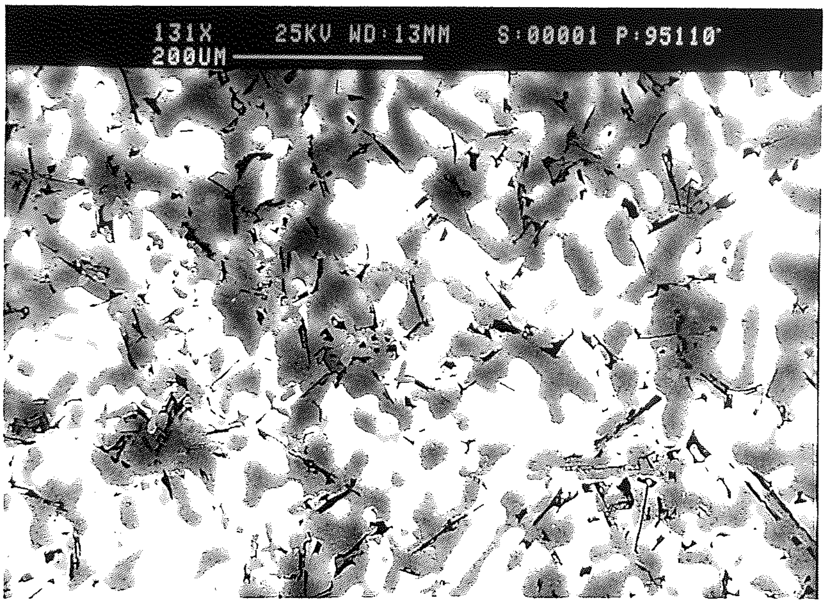

Figure 111. Micrograph of load relaxation sample of alloy Supercosmal tested at 120°C at low magnification.

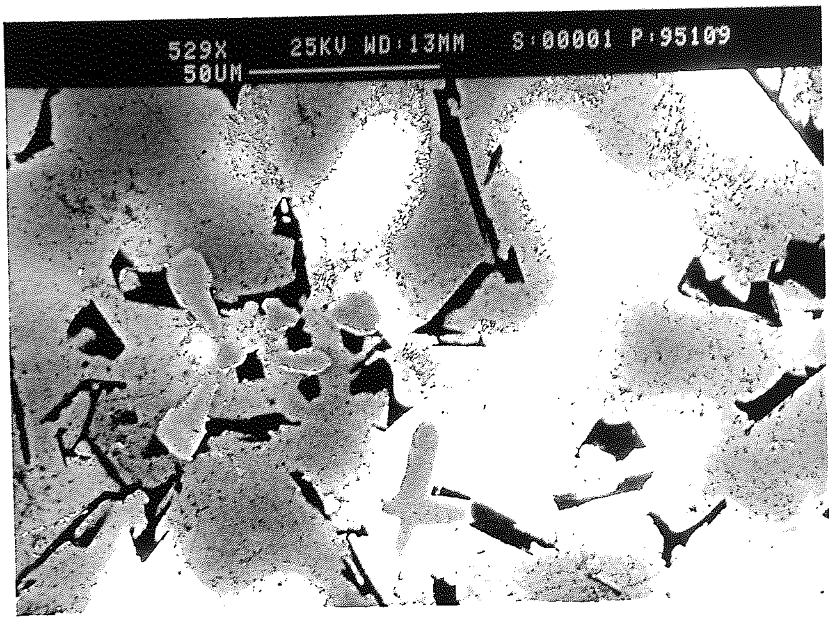

Figure 112. Micrograph of load relaxation sample of alloy Supercosmal tested at 120°C at medium magnification. Grey clustered phases are probably Mn-rich.

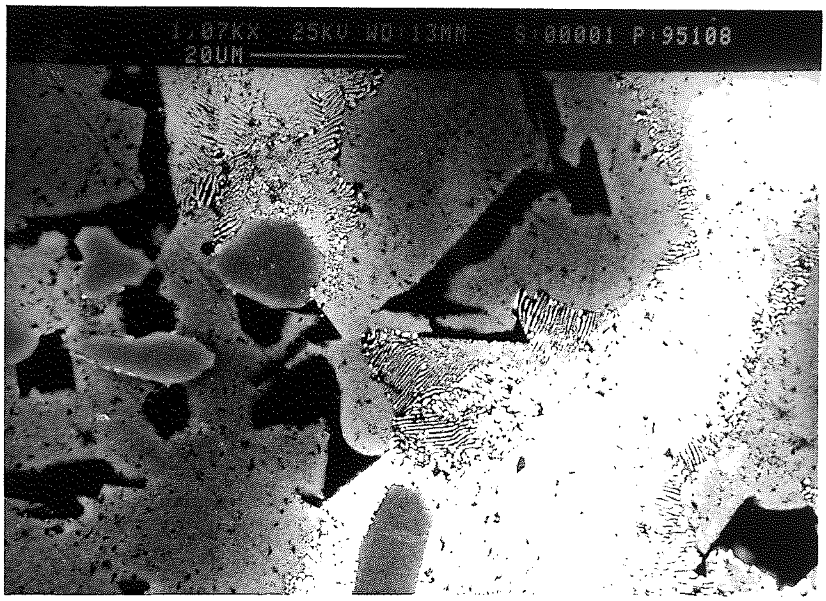

Figure 113. Micrograph of load relaxation sample of alloy Supercosmal tested at 120°C at high magnification.

5.3.6 Alloy LM25

The as cast structure of LM25 shown in *Figures 114, 115 and 116*. LM25 is a hypoeutectic alloy of Al and Si, and as cast structure consisted of primary α denderities in a small amount of AlSi eutectic. The eutectic form is very poor, and the silicon was mostly in the form of irregular laths with a slightly higher concentration in interdenderitic areas. This material showed almost no creep.

Micrographs of load relaxation tests of LM25 have been shown in *Figures 117, 118 and 119* and show structures unchanged from the as-cast alloy.

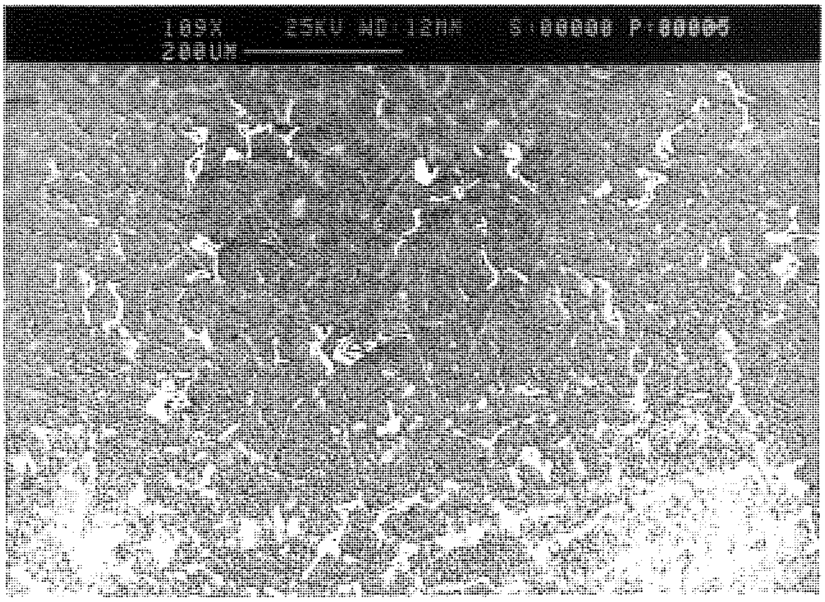

Figure 114. As cast structure of LM25 at low magnification.

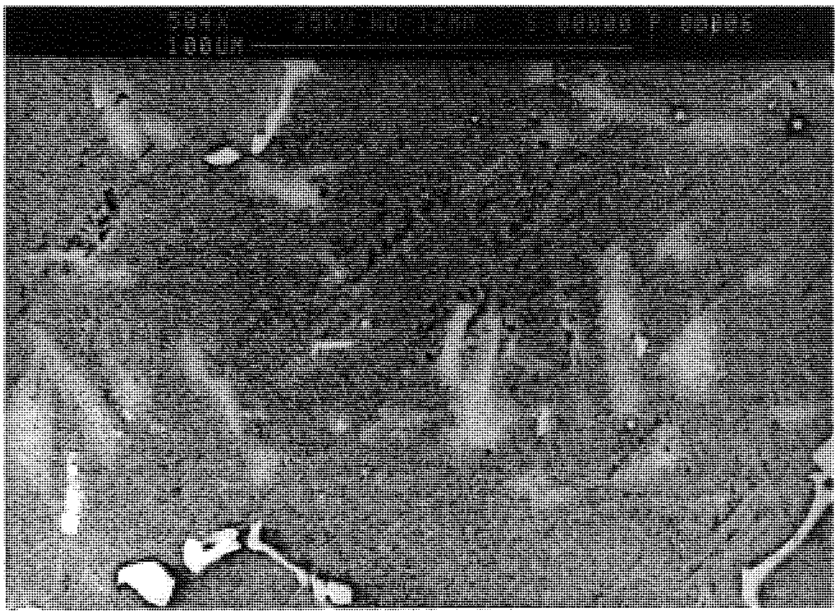

Figure 115. As cast structure of LM25 at medium magnification.

Figure 116. As cast structure of LM25 at high magnification.

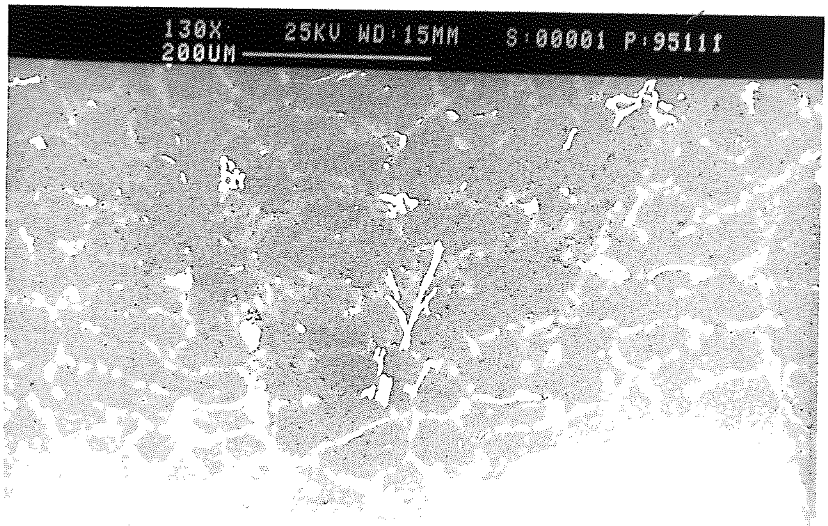

Figure 117. Micrograph of load relaxation sample of LM25 tested at 120°C at low magnification.

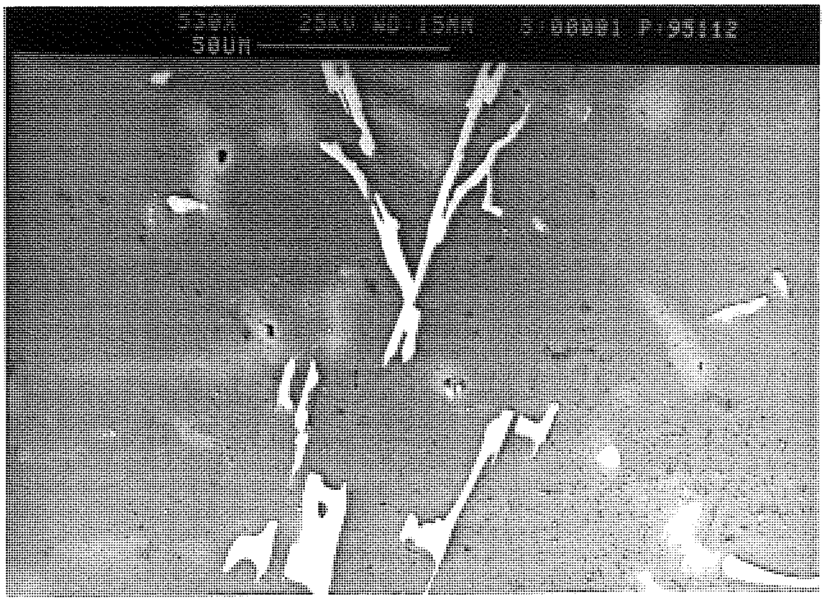

Figure 118. Micrograph of load relaxation sample of LM25 tested at 120°C at medium magnification.

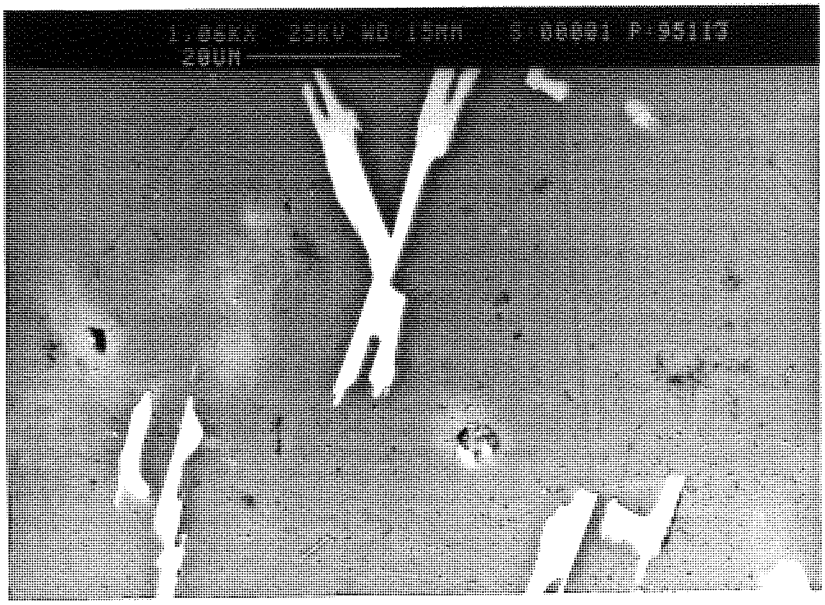

Figure 119. Micrograph of load relaxation sample of LM25 tested at 120°C at high magnification.

CHAPTER 6

6.0 DISCUSSION OF EXPERIMENTAL RESULTS

6.1 Correlation of Creep Data of the Experimental Zinc-Based Alloys

For any metal or alloy, simple graphical representations of the creep curves under certain stresses and temperatures are adequate to establish design data of creep such as the time to attain a prescribed creep strain. However, it has been recognised that the costs and duration of the tests required to obtain long-term design data are large. It is therefore essential for many practical and theoretical purposes to seek mathematical relationships which would satisfactorily correlate the creep data obtained from a limited number of relatively short duration experiments and allow a quantitative assessment of the creep behaviour of a material under different conditions.

Many empirical or semi-empirical mathematical relationships suggested in the literature are based on the secondary creep rate data, since steady-state creep behaviour is considered as the most important characterisation of creep behaviour of materials,(12) and offers numerous advantages. Therefore, secondary creep rates are generally used for detailed creep analysis of materials.

However, the relative importance of the primary, secondary and tertiary creep regions may vary significantly with variations in testing conditions, i.e. stress, temperature and / or metallurgical structure. As far as the metallurgical structure of alloys is concerned, the present investigation showed that generally the primary creep of alloys ZA8, ZA12 and ZA27 increased with increasing aluminium content but decreased in Cosmal and Supercosmal (*Figure 38)*. This figure showed that ZA27 has maximum primary creep among these alloys. Therefore, these results revealed that the primary creep of these experimental alloys increased with an addition of aluminium up to that of ZA27. The tests showed that the average primary creep of ZA alloys decreased with increasing temperature (*Figure 36*), with the exception that ZA27 has its maximum primary creep at 160°C while it increased with temperature in high damping capacity alloys. The primary creep contraction of all alloys was also increased with stress (*Figures 37)*.

Simultaneous work on tensile and compression creep tests on a complex nickel-chromium and an aluminium-copper alloy showed that the initial or primary creep deformation was larger in the compression than in the tension creep test(7).

When the primary creep contraction and the secondary creep rates (1/s) for ZA alloys of the current investigation were compared with those of the previous tensile creep tests(124) on the same alloy, it was revealed that in general, the primary creep was greater for compression tests at nearly similar test conditions which verified the above observations of Sully(7). It was also found that the resulting secondary creep rates were slower in tensile creep tests than in compression tests. A comparison of primary creep and secondary creep rates for alloy ZA8 in compression (current research) and tensile tests(124) of gravity cast has been shown in *Table 16*.

Table 16. Comparison of Creep data of compression (sand cast) and tensile (gravity cast) tests for alloy ZA8 at 40 MPa.

For Tensile:

Temperature (C°)	Primary Creep (%)	Secondary Creep Rate (%/s)	Time to 1% Creep Strain (s)
120	0.09	$2.59\text{x}10^{-7}$	107000
120	0.12	$1.71\text{x}10^{-7}$	135000
For Compression:			
130	0.33	$1.81\text{x}10^{-5}$	36680
130	0.35	$1.79\text{x}10^{-5}$	38280

The creep specimen used in this research work had L/D < 3 ratio, therefore specimens showed barrelling tested at higher stresses and temperatures, e.g. alloys ZA8, ZA12, ZA27 and Cosmal were barrelled at 100 MPa and 160°C.

The creep strain of about 10% was observed in ZA alloys in a few minutes at 100 MPa and 160°C and 1% creep strain was reached in early stages of the test i.e. some time in primary creep region. If it is recognised that the time to attain a specified creep strain, say 1%, is an essential requirement for many engineering design processes, any solution which is to be based on the secondary creep rate data of the experimental alloys would obviously lead to an inaccurate estimation of such strains.

The variation of creep properties in a material with temperature and with stress is of extreme practical importance, since without knowledge of the relation between creep and these variables it is impossible to use the results of the creep tests to predict the creep behaviour at stresses and temperatures other than those at which the tests are carried out. Several empirical relationships between creep rate or creep strain and stress and temperature have been suggested(12,111,112,122) to predict the creep behaviour of different materials.

A linear relationship was observed between the logarithms of applied stress and secondary creep rate in *Figures 39, 40, 41 and 42* for alloys ZA8, ZA12, ZA27 and Cosmal respectively which indicated that secondary creep rates were a simple power law function of the applied stress, and implied that the total creep deformation of zinc alloys could be correlated by *Equation 2.35* which was used by Murphy and Savaskan (111,112) to correlate the experimental creep data of gravity cast zinc alloys of near-eutectoid composition. Later, Murphy and Durman(122,138) used *Equation 2.35* to correlate the total creep elongation (up to 1%) of zinc-rich alloys No3, ZA8 and ZA27 with the testing conditions, where $n = 3.5$ and $Q = 106$ kJ/mole for all three alloys tested. *Equation 2.35* was as follows:

$$f(\varepsilon) = A\, t\, \sigma^n \exp(-Q/RT)$$

where A is a constant which takes into account the effects of composition and metallurgical structure, σ the nominal stress, n the stress exponent, t the creep time, Q an effective activation energy for creep, R the universal gas constant, T the absolute test temperature, and $f(\varepsilon)$ an undefined function of the creep strain ε, and when A, σ, n, Q and T are constant, f (ε) represents the shape of the creep strain versus time curve. Taking logarithms and rearranging:

$$\ln t = \ln f(\varepsilon) - \ln A - n(\ln \sigma) + Q/RT$$

but for a fixed creep strain:

$$\ln t = C' - n(\ln \sigma) + Q/RT$$

where C' is a new constant which incorporates A and ε.

The parametric plots for the alloys have shown that the total creep (up to 1%) can be related to the applied stress, temperature and the time of these tests by using the above derived equation. If this final relationship is obeyed for zinc alloys studied here, a plot of ln time to any fixed creep strain against ln stress (MPa) at constant temperature should be linear with a slope of (-n), with an intercept ($C' + Q/RT$), or a plot of ln time to any fixed creep strain versus 1/T at constant stress should be linear with a slope of Q/R, and an intercept of [$C' - n(\ln \sigma)$].

Such plots, as shown in *Figures 44 to 47*, plotted as ln time to 1% strain versus ln stress were in fact all linear with constant slopes over the majority of temperatures and stresses used. Deviations from these constant slopes were observed for Cosmal at 160°C and lower stresses. The value of n obtained from these graphs was 4.74, 4.71, 3.85 and 5.11 for ZA8, ZA12, ZA27 and Cosmal respectively.

The plots of ln time to 1% creep strain versus 1/T at constant stresses shown in *Figures 120 to 123* for all alloys were also linear with a good correlation of the data, giving the activation energy for creep (Q) of 112, 109, 102 and 101 kJ/mole for ZA8, ZA12, ZA27 and Cosmal respectively.

Therefore, it was obvious that all of the above linear plots were in accordance with the form of the single equation used and thus the creep behaviour of the alloys could be related to the testing conditions by this single relationship over all stress and temperature ranges. Once the values of n and Q are known, the constant C', which is a characteristic for each alloy and the chosen % strain, can be calculated from the intercept ($C' + Q/RT$).

Such a parametric plot therefore should allow the total creep strain to be calculated for any combination of temperature, applied stress and time.

However, a considerable degree of extrapolation is required to obtain C' in this way. Instead, C' is obtained and correlation of the data is given more clearly by a parametric plot of $[(Q/RT) - n \ln \sigma]$ against ln time to a given % contraction, which should give linear plots of 'unit slope' and intercept, a characteristic constant for the alloy and the chosen % strain. The differences in creep behaviour between the alloys are derive solely from differences in the values of this constant (C').

The plots of ln time to produce creep strain of 0.2, 0.4, 0.6, 0.8 and 1% versus the above creep parameter $[(Q/RT) - n \ln \sigma]$ for alloys ZA8, ZA12, ZA27 and Cosmal have been shown in *Figures 124, 125, 126 and 127,* respectively, using the unsmoothed original experimental data from individual creep curves (Appendix A) and excluding the data at lower stress levels at 160°C for alloy Cosmal where the greatly increased creep resistance was almost certainly due to structural coarsening which occurred during the lengthy, high temperature creep test. From these plots the intercepts (C') were obtained for all alloys and listed in *Table 17.* This table shows that although there is a great deal of scatter in the 0.2% plots, where differences between individual creep tests are significant, a very good correlation of the data is obtained in general by the parametric plots for 0.4, 0.6, 0.8 and 1% total creep contraction, indicating that this parameter together with the corresponding values of Q and n, may be used to estimate the creep behaviour of the experimental alloys with high confidence.

For general use of the *Equation 2.35,* values of the creep constant C' in *Table 17* were plotted against % creep contractions in *Figure 128* for all alloys. This plot yielded a linear relationship, with a good correlation of the data, so that the value of C' can be calculated from the plot easily for any given % creep contraction and using the *Equation*

2.35, such data can be used to calculate the permissible combinations of stress, temperature and creep life for any total creep strain within the range of 0.2 to 1.0%.

Table 17. Values of creep constant C' for alloys ZA8, ZA12, ZA27 and Cosmal

Strain(%)	0.20	0.40	0.60	0.80	1.00
Alloy ZA8	-9.63	-7.92	-6.43	-5.85	-5.43
ZA12	-8.66	-6.66	-5.79	-5.00	-4.68
ZA27	-11.38	-8.37	-7.75	-6.83	-6.55
Cosmal	-5.56	-2.45	-0.88	0.14	0.49

After finding the values of stress exponent (n), the activation energy (Q) and creep constant (C$'$), the maximum continuous design stresses which produce 0.2%, 0.4%, 0.6%, 0.8% and 1.0% creep strains in 100,000 hours (11.4 years) at different test temperatures were calculated in order to compare the relative creep performances of the alloys. The service life of 100,000 hours was used on the basis of ASME Boiler Code, according to which the maximum allowable design stress based on creep is that stress which produces strain of 1% in 100,000 hours. For zinc alloys a creep life may be 2000 hours, such as the running life of a motor car, would be more appropriate. However 100,000 hours life is used in zinc industry specifications. These values of design stresses are listed in *Table 18*.

The results of the calculations are plotted as a family of curves in *Figures 129, 130, 131 and 132* for the alloys which enable the total creep strain within the range of 0.2 to 1.0% to be determined from any combination of stress and temperature for service lives of 100,000 hours (11.4 years).

On the basis of calculated design stresses, it was found that Cosmal had better creep performance than all other alloys at all strain levels. As it is clear from the *Table 18* for

1% creep strain at 70°C , the design stresses for ZA8, ZA12, ZA27 and Cosmal are 20, 19, 12 and 24 MPa while at 160°C these design stresses are reduced to 4, 3.5, 2 and 6 MPa respectively for service life of 100,000 hours.

Table 18. Maximum continuous design stresses (MPa) to produce indicated % age strain in 100,000 hours for ZA8, ZA12, ZA27 and Cosmal

Alloy	Strain(%)	70°C σ	100°C σ	130°C σ	160°C σ
ZA8	0.2	8.14	4.18	2.37	1.45
	0.4	11.68	6.00	3.40	2.08
	0.6	16.00	8.21	4.66	2.85
	0.8	18.08	9.28	5.26	3.23
	1.0	19.76	10.14	5.75	3.53
ZA12	0.2	8.11	4.22	2.42	1.50
	0.4	12.40	6.45	3.70	2.29
	0.6	14.92	7.77	4.45	2.76
	0.8	17.65	9.18	5.27	3.26
	1.0	18.89	9.83	5.64	3.49
ZA27	0.2	3.37	1.60	0.84	0.48
	0.4	7.38	3.49	1.85	1.07
	0.6	8.67	4.10	2.17	1.25
	0.8	11.01	5.21	2.76	1.59
	1.0	11.84	5.61	2.97	1.71
COSMAL	0.2	7.29	4.17	2.60	1.72
	0.4	13.40	7.67	4.77	3.17
	0.6	18.23	10.44	6.49	4.31
	0.8	22.28	12.76	7.93	5.27
	1.0	23.83	13.64	8.49	5.64

In a comparison of ZA alloys for 0.2% to 1.0% creep strain, overall ZA8 had more creep strength than ZA12 which in turn was better than ZA27. At 160°C and 100MPa the ZA alloys are similar up to 1% but away from this ZA27 is becoming stronger and stronger than ZA8 and ZA12 *(Figure 30)* but contrary to this at lower stresses and 160°C it becomes weaker than other two alloys *(Figure 31 and 32).*

The net average values of stress exponent n and activation energy Q is 4.6 and 106k J/mole respectively for all testing alloys. Using these values of n and Q the calculated design stresses are shown in *Table 19.* These values are less than those as calculated above in *Table 18* for all alloys but are increased for alloy ZA27.

Table 19. Maximum continuous design stresses (MPa) to produce indicated % age strain in 100,000 hours for ZA8, ZA12, ZA27 and Cosmal using average values of n and Q

	Strain (%)	70°C	100°C	130°C	160°C
		σ	σ	σ	σ
ZA8	0.2	6.17	3.22	1.85	1.15
	0.4	9.08	4.74	2.73	1.69
	0.6	12.61	6.58	3.79	2.35
	0.8	14.34	7.49	4.31	2.67
	1.0	15.78	8.24	4.74	2.94
ZA12	0.2	6.92	3.61	2.08	1.29
	0.4	10.71	5.59	3.22	2.00
	0.6	12.94	6.76	3.89	2.41
	0.8	15.37	8.02	4.62	2.87
	1.0	16.51	8.62	4.96	3.08
ZA27	0.2	5.12	2.67	1.54	0.95
	0.4	13.23	6.91	3.97	2.47
	0.6	15.98	8.34	4.80	2.98
	0.8	19.56	10.21	5.87	3.65
	1.0	20.97	10.95	6.30	3.91
COSMAL	0.2	7.57	3.95	2.27	1.41
	0.4	12.05	6.29	3.62	2.25
	0.6	18.49	9.65	5.55	3.45
	0.8	19.78	10.33	5.94	3.69
	1.0	21.20	11.07	6.37	3.95

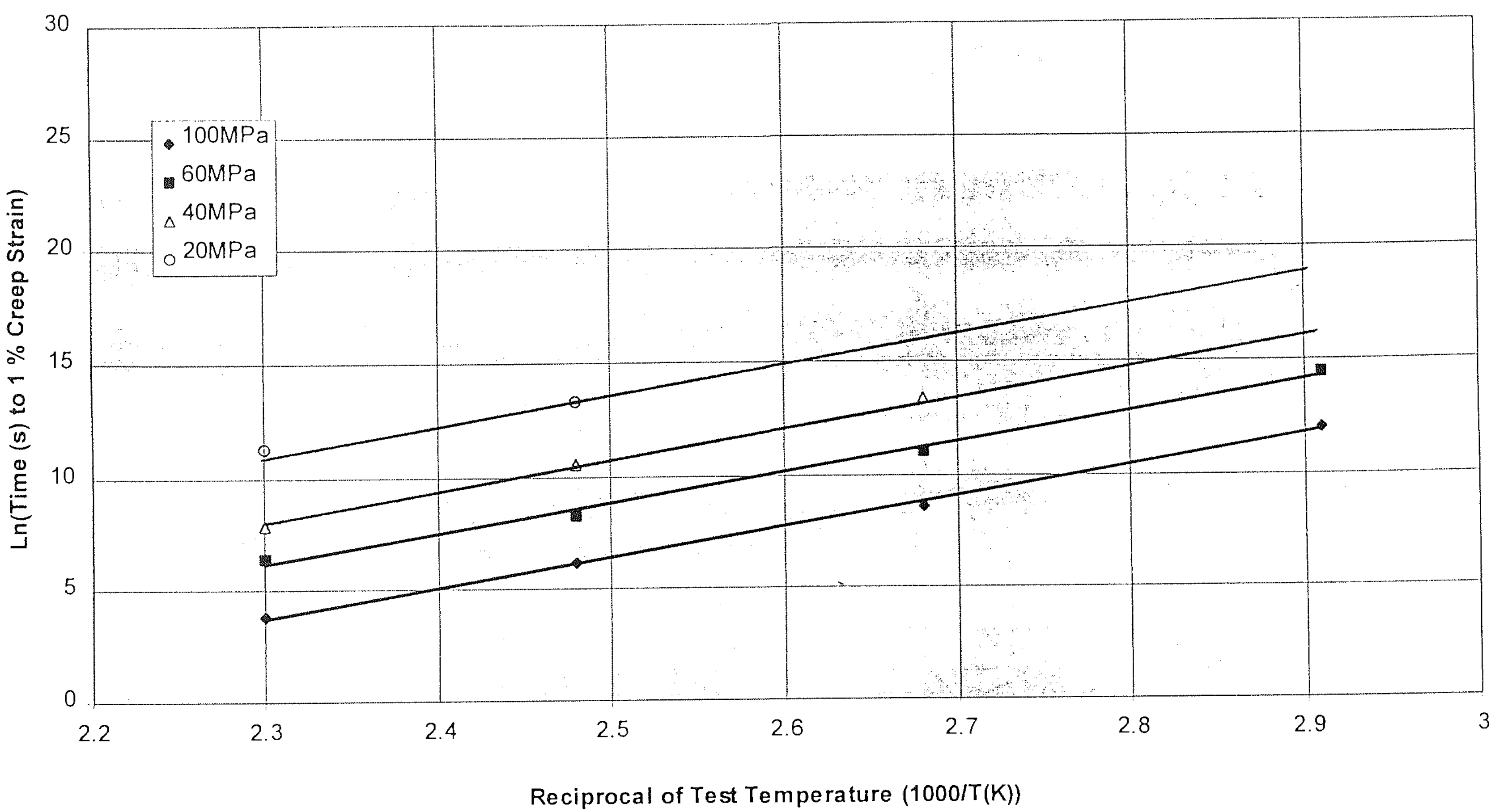

Figure 120. Ln times (s) to 1 % creep strain versus reciprocal of test temperatures at 100, 60, 40, and 20MPa for ZA8.

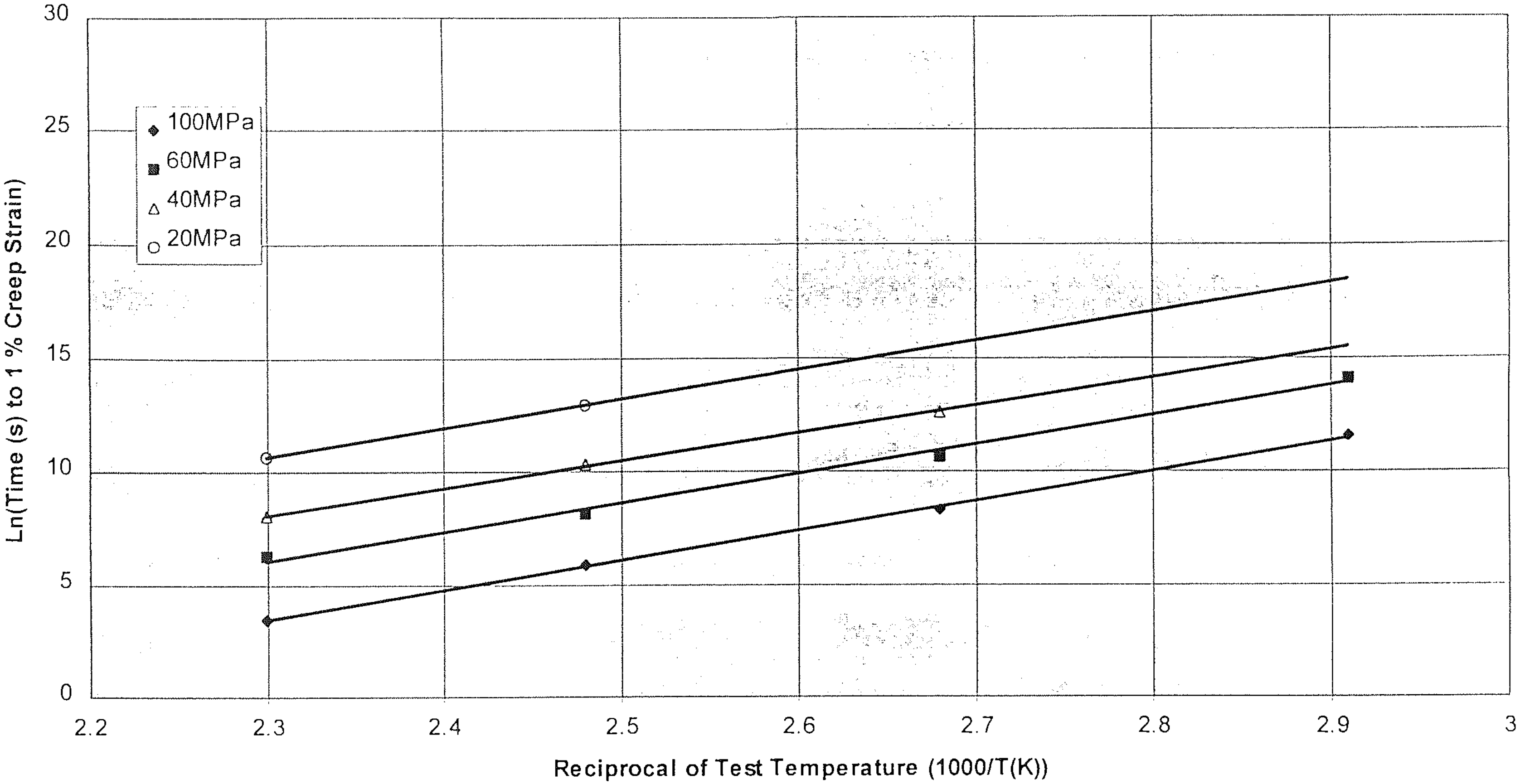

Figure 121. Ln times (s) to 1 % creep strain versus reciprocal of test temperatures at 100, 60, 40, and 20MPa for ZA12.

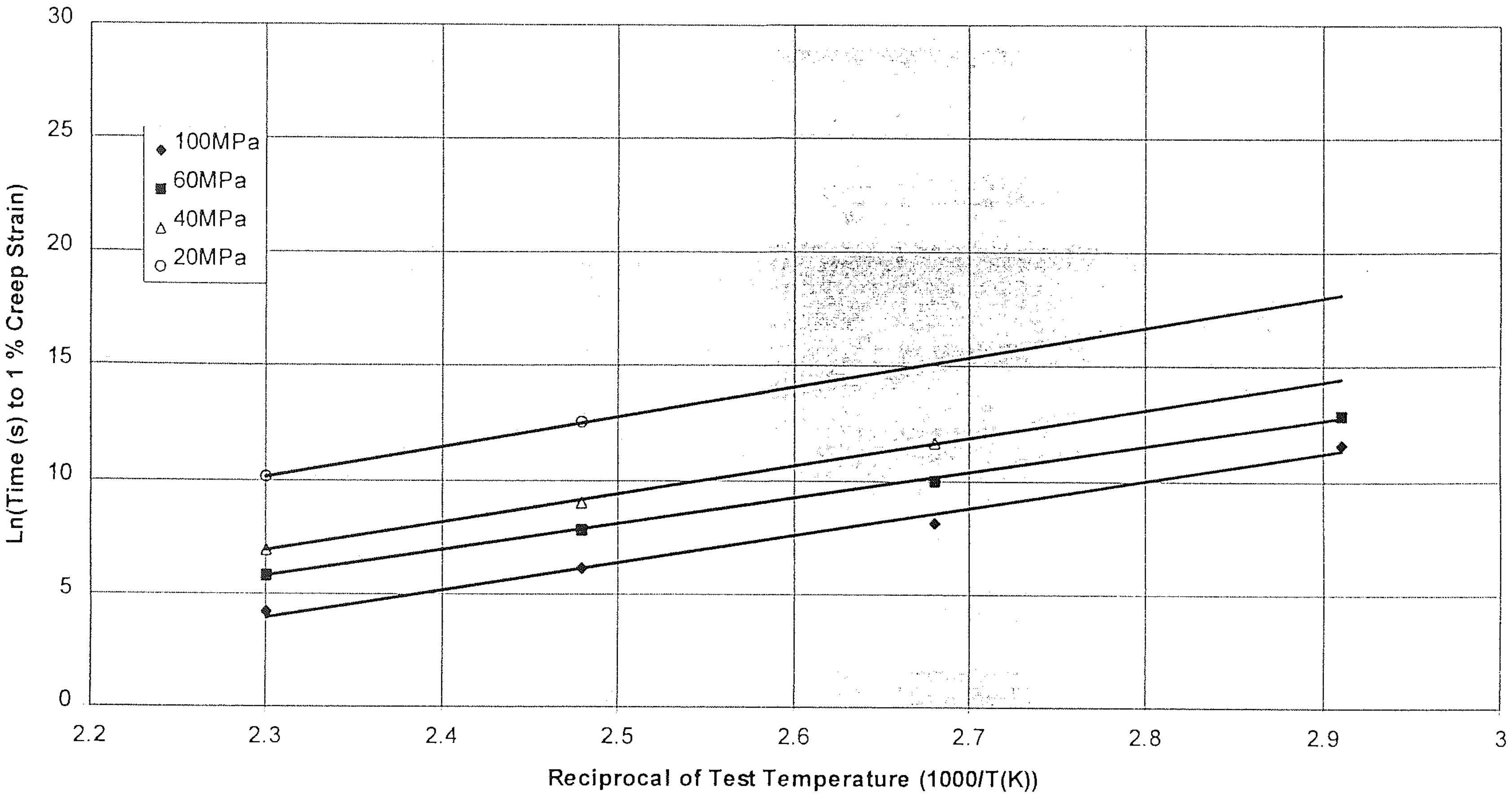

Figure 122. Ln times (s) to 1 % creep strain versus reciprocal of test temperatures at 100, 60, 40, and 20MPa for ZA27.

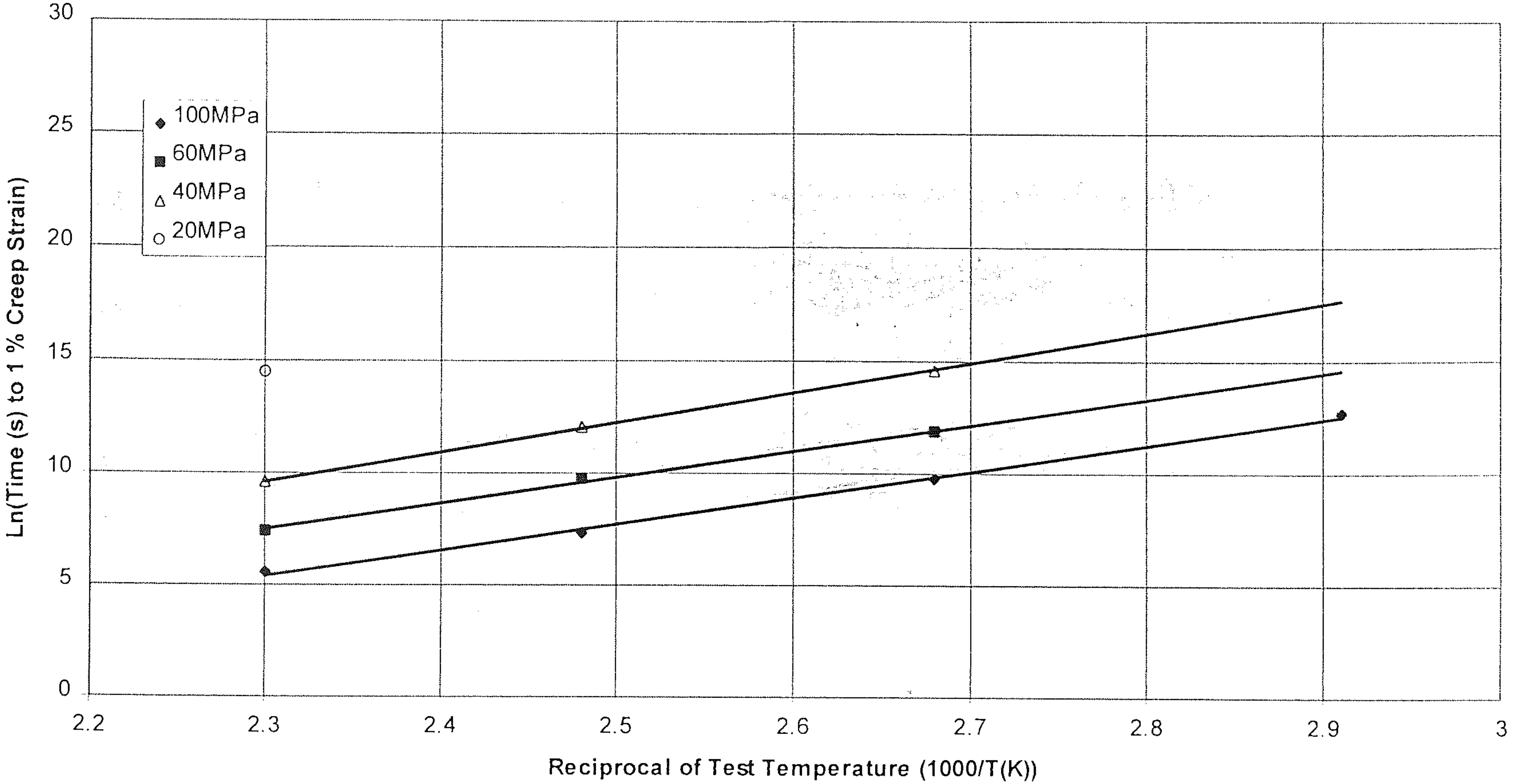

Figure 123. Ln times (s) to 1 % creep strain versus reciprocal of test temperatures at 100, 60, 40, and 20MPa for Cosmal.

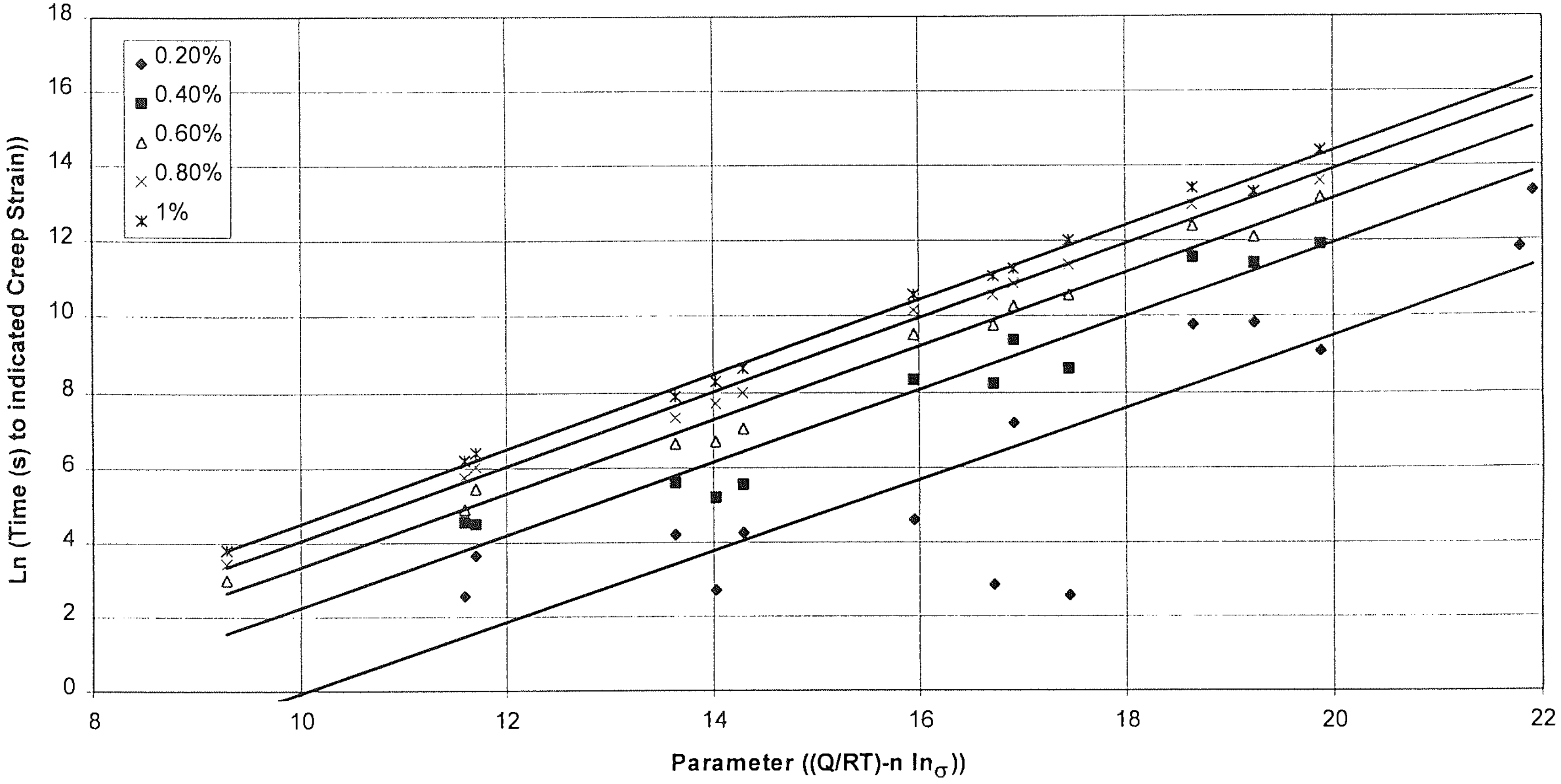

Figure 124. Ln times (s) to various creep strains versus creep parameter for alloy ZA8.

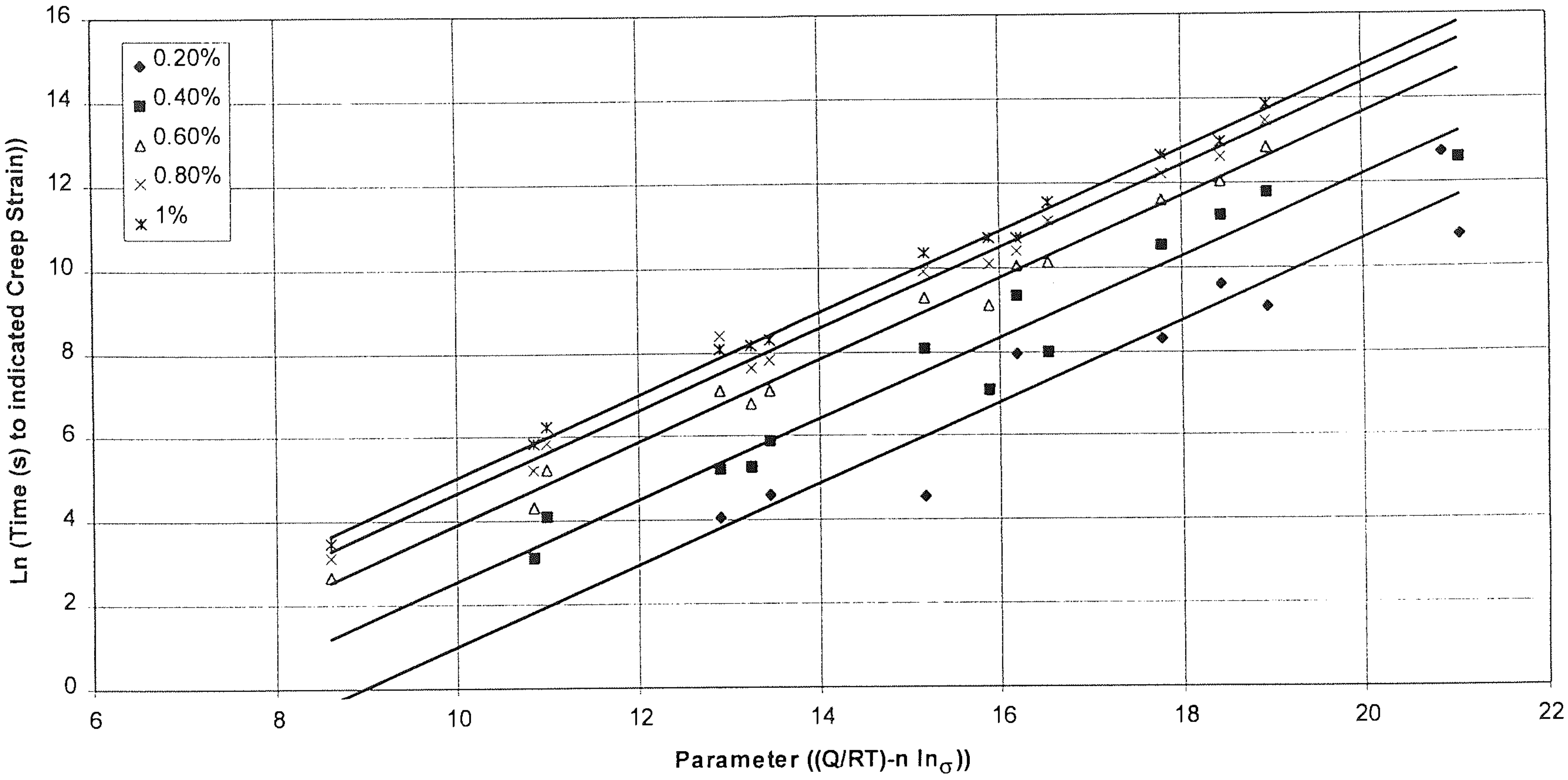

Figure 125. Ln times (s) to various creep strains versus creep parameter for alloy ZA12.

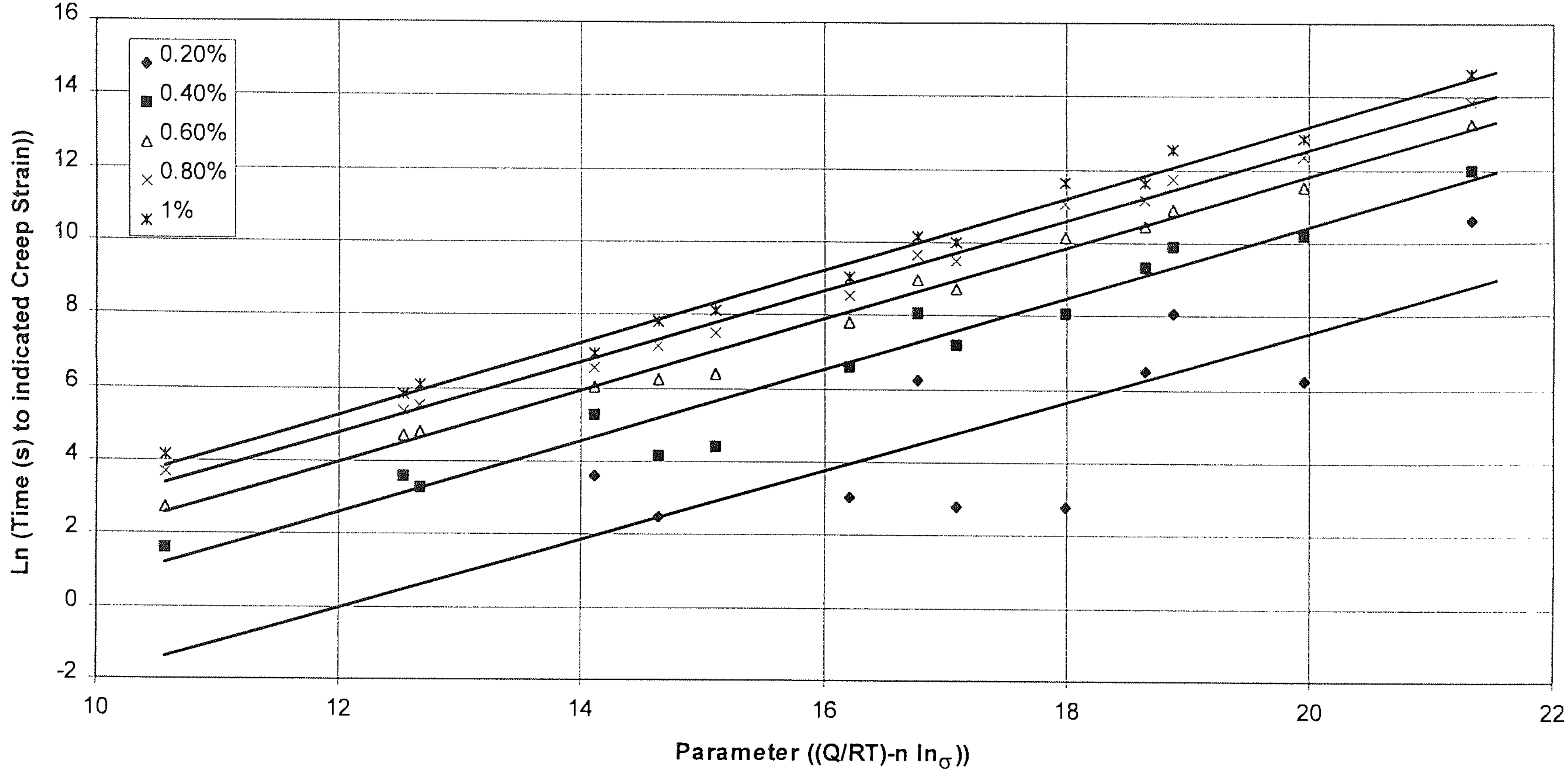

Figure 126. Ln times (s) to various creep strains versus creep parameter for alloy ZA27.

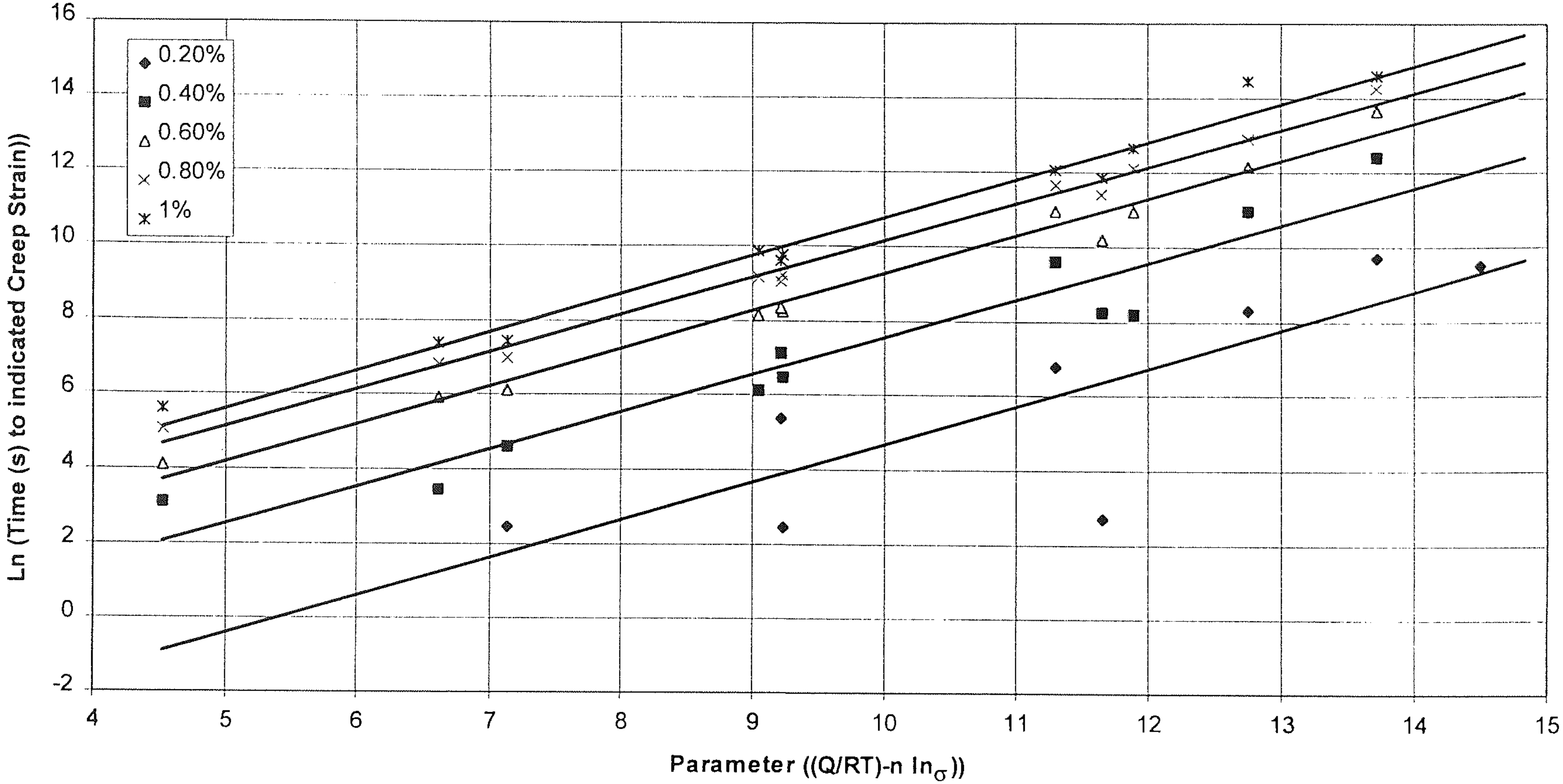

Figure 127. Ln times (s) to various creep strains versus creep parameter for alloy Cosmal.

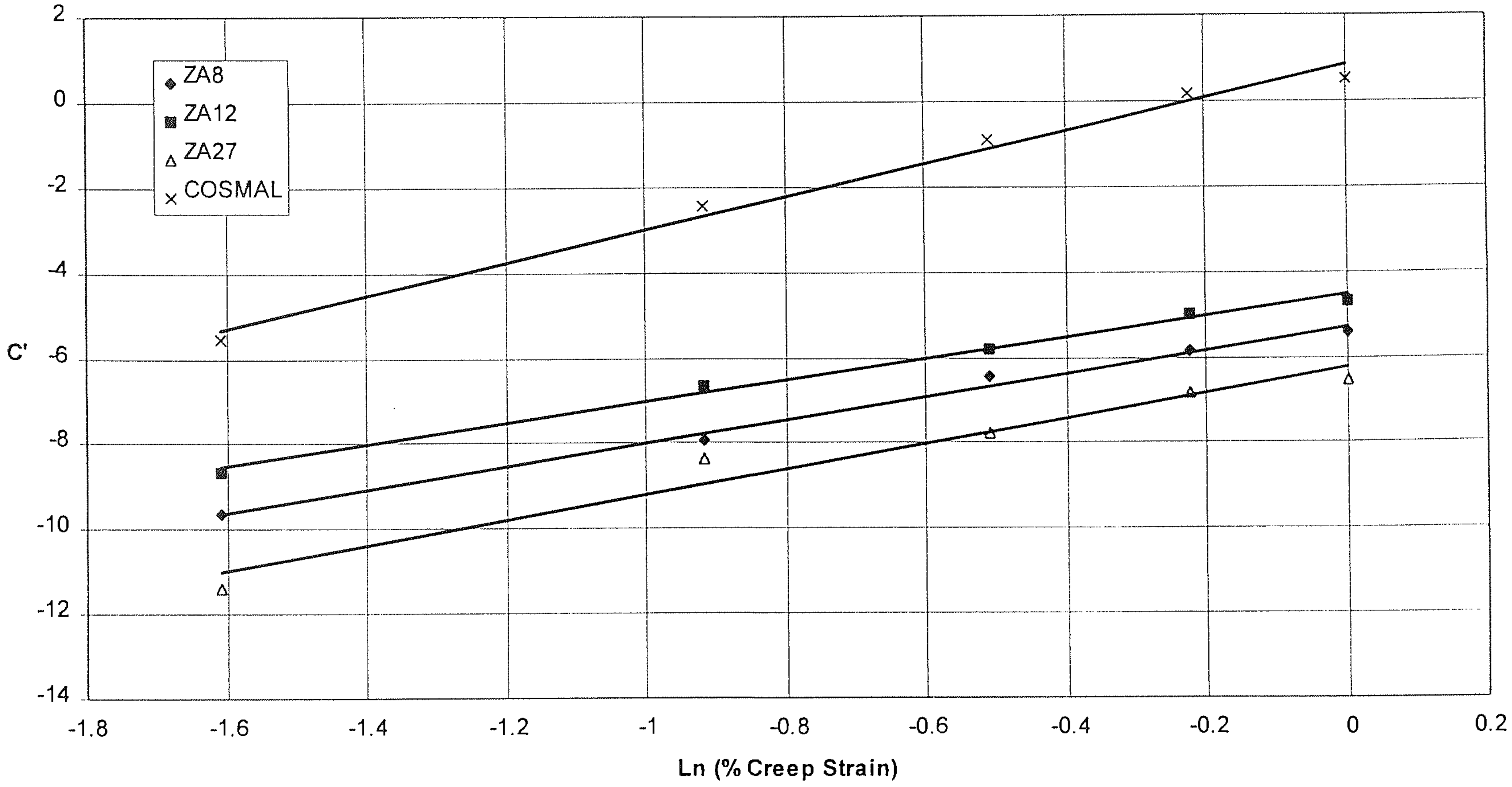

Figure 128. Variation of constant C' with creep elongations for alloys ZA8, ZA12, ZA27 and Cosmal.

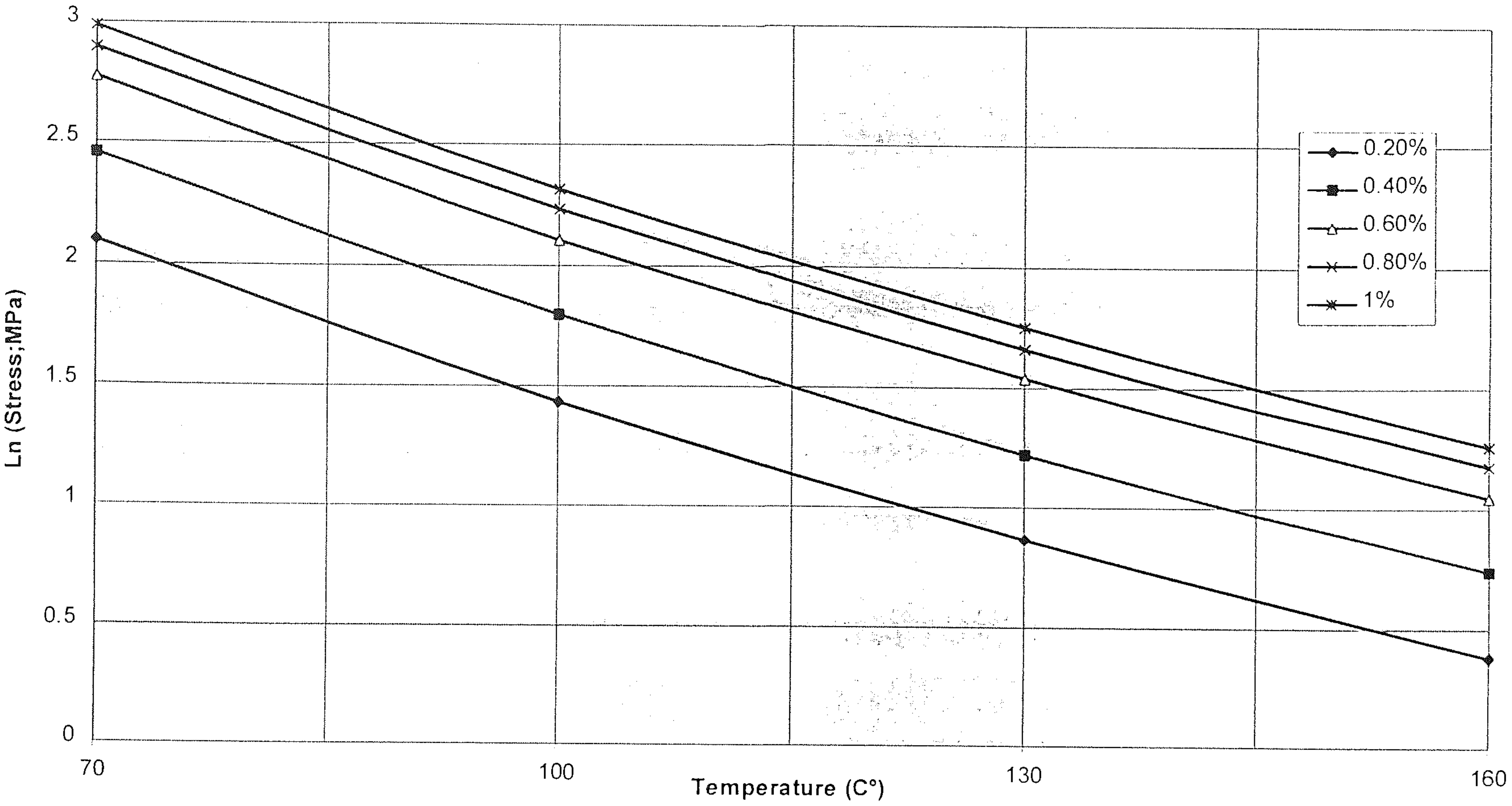

Figure 129. Maximum continuous design stress for allowable creep strains in 100,000 hours design life for alloy ZA8.

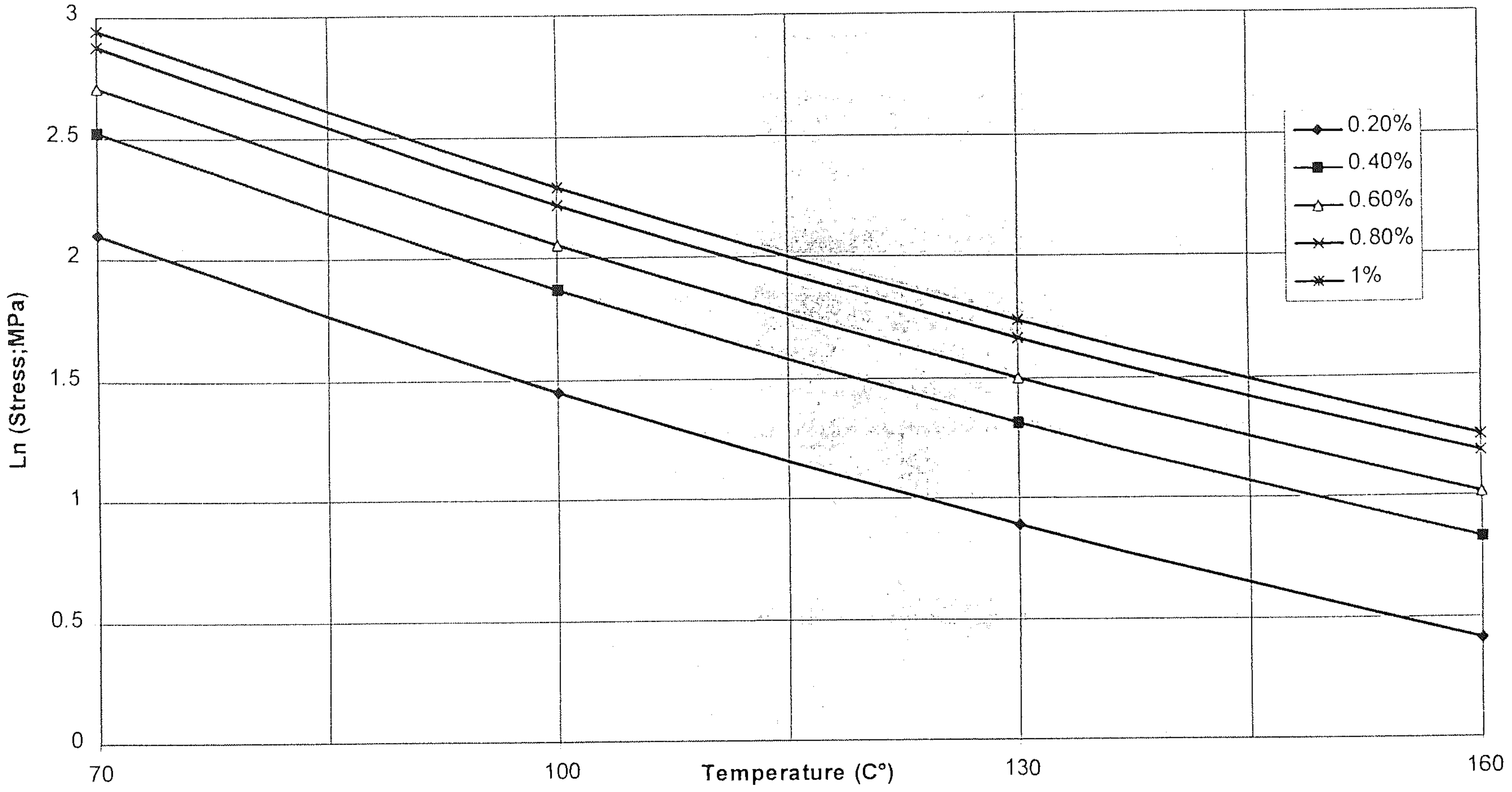

Figure 130. Maximum continuous design stress for allowable creep strains in 100,000 hours design life for alloy ZA12.

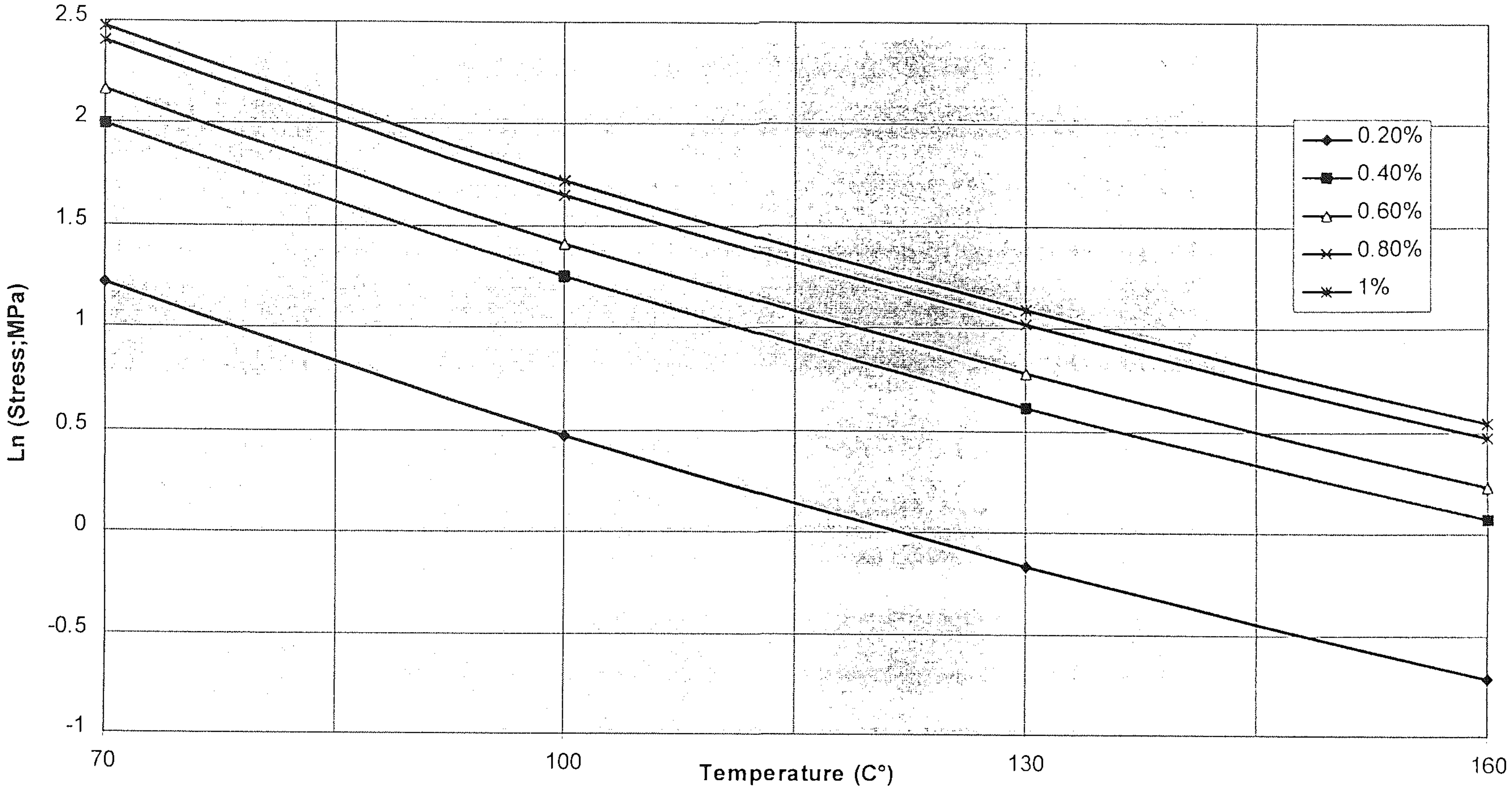

Figure 131. Maximum continuous design stress for allowable creep strains in 100,000 hours design life for alloy ZA27.

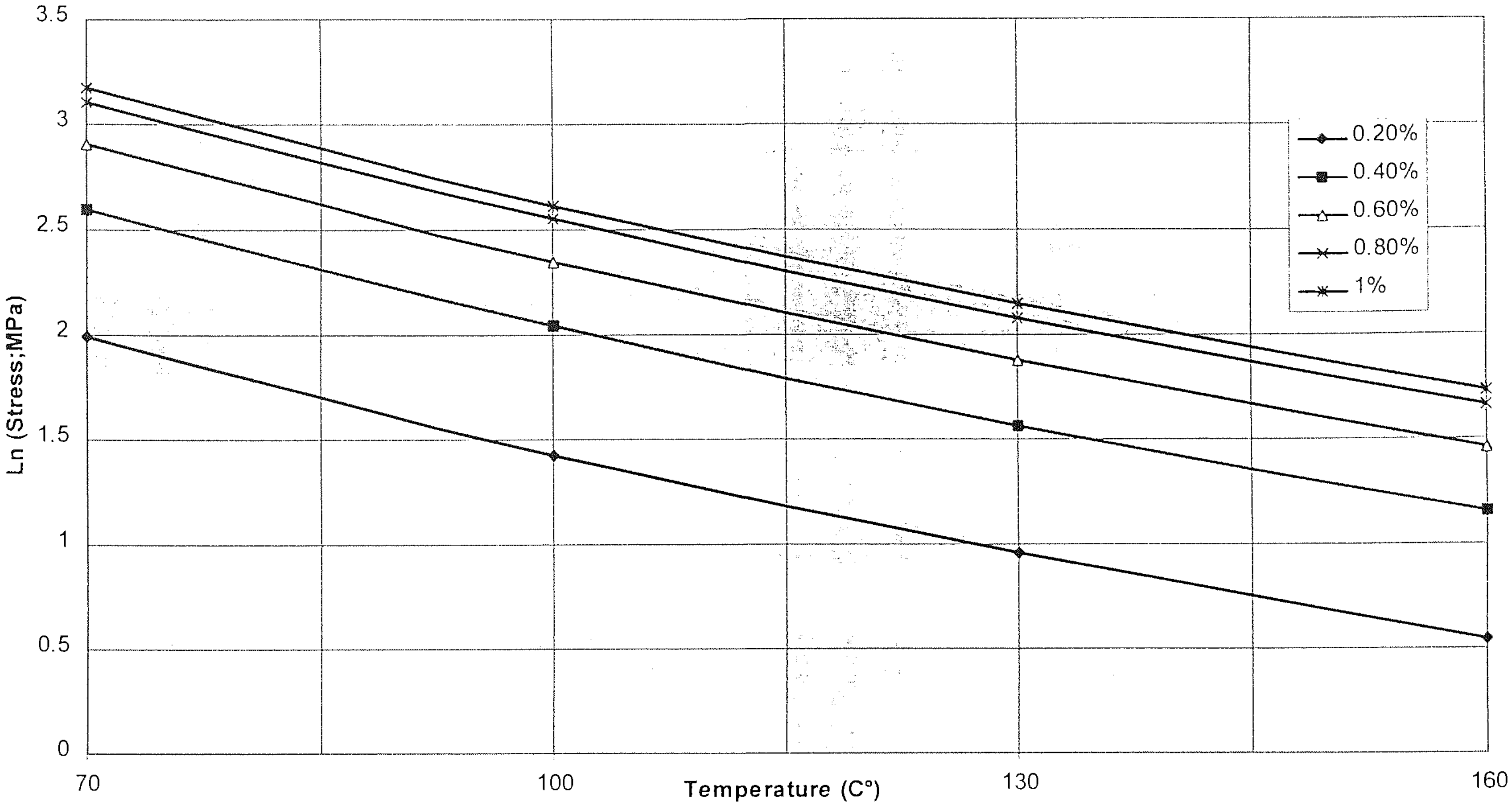

Figure 132. Maximum continuous design stress for allowable creep strains in 100,000 hours design life for alloy Cosmal.

6.2 Discussion of Load Relaxation Tests

The residual load was measured continuously and was plotted as time (min) versus preload (N) as shown in *Figures 50, 51 and 52* for all alloys at different temperatures. The results showed that initially load was lost rapidly but then diminished with time without ceasing. Results also showed that load loss increased with temperature and almost all of the curves approximated to a logarithmic decay of preload with time.

The results of ZA alloys showed a very small difference in load loss at 80°C and 100°C; only ZA12 was slightly better than ZA8 and ZA27, while at 120°C ZA8 had the worst position and ZA27 the best. At this temperature of 120°C, initially ZA12 had better creep resistance to load loss than ZA27, but with the passage of time ZA27 improved its performance while the other got worse as seen in *Figure 52.*

High damping capacity alloys (Cosmal and Supercosmal) and LM25 had much better resistance to load loss than ZA alloys. Among these two alloys, Supercosmal was much better in resistance than Cosmal under all test conditions as seen from comparison graphs, *Figures 50, 51 and 52.* In both alloys load loss increased with the increase of temperature. LM25 had the best resistant to load loss among all six alloys tested under all conditions.

Retained load (N) vs ln time (min) graphs are shown in *Figures 56, 57, 58, 59 60, and 61* and they yield straight lines with constant slope.

Graphs of ln retained load (N) versus ln time (min) were also drawn at three different temperatures, i.e. 80, 100 and 120°C as shown in *Figures 62, 63, 64, 65, 66, and 67.* These plots also yielded straight lines with a constant slope. The figures showed that a good correlation of data could be obtained using either a simple or logarithmic load, so that either could be used to correlate the data.

6.3 Theoretical Consideration of Creep Tests

The prime purpose of creep testing is, ordinarily, to determine the stress values at the temperatures involved, upon application of which the amount of deformation is limited to tolerance values over a period of time comparable to the anticipated working life of the member to be designed and manufactured. It is recognised that secondary creep rate is the most important characterisation of creep which is widely used as a measure of relative creep resistance and also a basis for theoretical interpretation that how it varies with temperature and stress. So on this basis, secondary creep rates have been shown in *Figures 39 to 42* and a comparison of tested alloys at 40 MPa against different temperatures shown in *Figure 43* which showed that Cosmal had substantially lower secondary creep rate than ZA alloys. Alloy ZA27 had maximum creep rate among these while ZA8 and ZA12 had not much difference.

As seen from creep curves that overall creep contractions of the alloys were very much affected by the primary creep contribution. A comparison of creep strain (%), taken from average values have been shown in *Figures 30 to 35* which showed that at higher stress and temperature conditions, Alloy ZA27 had better creep performance than other two ZA alloys and became weaker at lower stress and temperature.

Alloy ZA8 had less primary creep than ZA27 *(Figures 36 to 38)* and thus showed a considerably overall better creep resistance.

Activation energies, based on secondary creep rate, were found to be 109kJ/mole for ZA8 and ZA12, 106kJ/mole for ZA27 and 102kJ/mole for Cosmal and these values are similar obtained from empirical *Equation 2.35.*

The values for self diffusion in polycrystalline zinc was found in the range of 91-110kJ/mole by various workers(133-135) so these values have a good agreement with these values. The values of activation energy published in literature are varied and are in the range of 87 to 152 kJ/mole(136,137). However, the activation energy within small temperature and stress ranges reported by the above workers varied from 87 to 109kJ/mole. Thus the calculated activation energies for the experimental alloys suggest that creep rate in the experimental alloys is controlled by diffusion in zinc rich phase and the rate controlling process for creep might also be the rate controlling process for lattice diffusion in zinc.

This type of correlation between activation energy and that for self-diffusion is consistent with the observations manifested for almost all pure metals and solid solutions in high temperature creep region (68) and strongly support the suggestion first made by Weertman(14,16) that the most likely mechanism in such cases is that of dislocation climb. He proposed two different models predicting stress exponents of 3 and 4.5 respectively. The values of stress exponent of the experimental alloys was found 4.52, 4.26, 3.5 and 4.43 for ZA8, ZA12, ZA27 and Cosmal respectively which have indeed excellent agreement with the values proposed by Weertman. The stress exponent 3, proposed for first model was later reported to be limited to fcc metals.

ZA8, ZA12 and ZA27 are similar alloys differing primarily in AL contents, so the decline in stress exponent reflects some change linked to zinc-aluminium ratio. With increase of aluminium contents the amount of α-phase becomes proportionally greater. Thus more than one rate limiting processes may be acting concurrently in the α and η phases. The measured stress exponent may thus be some average value depending on zinc-aluminium ratio. The influence is that fcc α-phase has a lower associated stress exponent than cph η-phase.

The Cosmal and Supercosmal alloys are based on different chemical compositions to ZA alloys so the stress exponent does not continue to change with aluminium contents in the same way.

It is also assumed that climb and glide are sequential processes and the rate controlling process would be related to the slowest of the two. For the viscous glide model Weertman suggested a stress exponent 3 but it was found to be in the range of 3 to 3.5 for any solid alloys, forming class I-type solid solution(68). The other important aspect of class I-type of alloys is that they had very little primary creep whereas alloys which form Class II-type solid solutions show large primary creep(68) and come under the dislocation climb law having stress exponent 4.5. In view of these theoretical considerations it is believed that creep in the experimental alloys studied here was controlled by a dislocation climb process.

Despite this, the process of creep in these zinc-based alloys is undoubtedly affected to some degree by changes which occurred in the metallurgical structure during testing especially at the highest temperature. Such changes as the development of zinc banding, and breakdown of some regions into masses of particles must have greatly affected creep process. So any theoretical model for creep, a constant structure is assumed, and clearly these changes must render any single model invalid.

6.4 Comparison of Creep and Load Relaxation Tests

The difference in creep and relaxation phenomenon is very important . This problem has great importance in theory and practice because many machine parts work under relaxation of stresses and methods for calculation in designing these parts have not yet been invented.

Creep is time dependent deformation, generally under constant stress, but creep can also be caused by a stress which changes with time. Thus, at every given instant, creep would be due to the stress acting at that instant so here the history of the previous deformation of the sample is of great importance with respect to the subsequent deformation.

Stress/load relaxation is a phenomenon that occurs due to the elastic and plastic deformation that takes place in a sample and relaxation is usually represented by the conditions i.e.

$$\varepsilon_o = \varepsilon_e + \varepsilon_p = \text{constant}$$

where ε_o is initial elastic deformation and ε_e and ε_p are the elastic and plastic components of deformation at some subsequent time. As long as the size of the sample remains constant during relaxation, this process represents the transition from elastic to plastic deformation. So one can say that elastic deformation changes into plastic deformation only when all the dimensions of the relaxing sample or of machine parts remain constant.

However, when one dimension is fixed, the creep occurs in the other directions only when the stress varies. Hence above condition may be replaced by

$$\varepsilon_o = \varepsilon_e x + \varepsilon_p x$$

Change in stress/load in time is proportional to the increase in plastic strain when a sample is given initial constant deformation. Therefore, relaxation is not considered only a transition from elastic to plastic deformation but an increase in plastic deformation for a simultaneous and equal decrease in elastic deformation.

Stress/load, during relaxation, decreases because of the growth of the plastic deformation and growth of plastic deformation in time is creep.

Keeping in view the *Figures 56 to 61*, as they have a good agreement with the data, the retained load could be related by a simple relationship and could be represented by

$$P = A - \alpha \ln t$$

where P is a retained load after time t at given temperature and A and α are constants.

The retained load could also be approximated by a power law kinetic relationship with time *(Figures 62 to 67)* of the form:

$$P = A\,t^{-\alpha}$$

Where P is retained load after time t. A and α are constants.

There are different factors which affect the preload relaxation in any casting that include:

i) Type of threads and the method to produce these threads

ii) Thread engagement

iii) Size of the testing sample

iv) Size of thread pitch

The geometry of the screws and the methods used to produce threads in the castings had a great effect on load relaxation. The worst resistance to load loss was found in self-tapping screw in a plain hole of casting and best results obtained from cutting tap action (132) whereas threads produced by roll-forming tap gave an improved performance than self tapping method.

Variation in thread engagement was also studied by Murphy and Goodwin in Zn-Al alloys and found an increase in retained load with increase of thread engagement from 10 to 15mm. Increasing the thread pitch from 0.75 to 1.25mm gave a minor improvement in preload loss so it may contribute in load loss along with type of thread and thread engagement.

Preload relaxation is due to the compressive stress on the surface of the test specimen under the fastener and compressive or shear-related effects along the threads. Keeping the second factor constant, Murphy and Goodwin(132) studied the effect of compressive stress by changing the boss size and found a linear relationship between retained load and compressive stress and this relation was:

$$P = B - n\sigma$$

where P is retained load after time t, B and n are constant and σ the boss compressive stress.

The investigation showed that 50% increase of the compressive stress on the surface under the fastener resulted only 20% increase in an average load reduction in Alloy 3 (132). This showed that preload relaxation is mostly a thread-related effect rather than compressive stress on the surface area under the fastener.

The behaviour of different alloys studied here in current investigation for compressive creep and load relaxation was as follows:

For compressive creep the alloys are in the order of LM25, Supercosmal, Cosmal, ZA8, ZA12 and ZA27. However at higher stresses and temperatures ZA27 was better than ZA8 and ZA12, *Figures 30 and 31.*
For load relaxation the alloys are in the order LM25, Supercosmal, Cosmal, ZA12, ZA27 and ZA8. (Note however that at higher temperature ZA27 improved its performance compared with ZA12 with the passage of time, *Figure 52*).

So the investigation showed that the experimental alloys behaved in the same manner in compressive creep and load relaxation with the exception of ZA8. Overall, that alloy was better in compressive creep than ZA12 and ZA27, but showed the worst position in load relaxation.

CHAPTER 7

7.0 CONCLUSIONS

1) The designed equipment offers an easy and precision method of compressive creep testing. The axial strain could be measured directly off a gauge length with a data acquisition system. Another important aspect of this equipment is that it could be used for tensile creep testing with minor changes in the loading and unloading part of the equipment.

2) The total creep contraction of sand cast experimental alloys was shown to be correlated by a creep equation:

$$f(\varepsilon) = A\,t\,\sigma^n \exp(-Q/RT)$$

where $n = 4.52$ for ZA8, 4.26 for ZA12, 3.5 for ZA27 and 4.43 for Cosmal.

$Q = 109$kJ/mole for ZA8 and ZA12; 106kJ/mole for ZA27 and 102kJ/mole for Cosmal.

3) Deviations from the creep kinetics were observed in Cosmal at 160°C and 20 MPa which were probably due to structural coarsening.

4) The average primary creep contraction of all experimental alloys increased with stress. In general, primary creep increased with temperature for ZA alloys but decreased with temperature for Cosmal and Supercosmal.

5) Primary creep increased with increasing aluminium contents up to the composition of ZA27, but further increase of aluminium progressively reduced the primary creep.

6) LM25 had almost no creep at 160°C and 100MPa.

7) Creep resistance was in the order ZA8, ZA12 and ZA27, except for 160°C/100MPa and 130°C/100MPa where ZA27 was best.

8) High damping capacity alloys had a lower secondary creep rate than ZA alloys under all testing conditions. Supercosmal was marginally better than Cosmal under all conditions, e.g. about 20x at 160°C and 100 MPa. Secondary creep rates of ZA8 were found to be substantially lower than those of ZA12 and ZA27.

9) The stress exponents (n) calculated from secondary creep rates varied from 3.5 to 4.52 for experimental alloys, very close to the values established for the rate controlling mechanism of dislocation climb. In ZA alloys n decreased with increase of aluminium contents. The Cosmal alloys with different chemical compositions behaved differently. Deviation in Cosmal at low stress and high temperature indicate a change in creep mechanism possibly due to structural coarsening.

10) The primary α and β phases in the as-cast structures decomposed to lamellar phases on cooling, with some particulates at dendrite edges and grain boundaries. Further breakdown into particulate bodies occurred during creep testing, and zinc bands developed at the highest test temperature of 160°C.

11) During load relaxation tests all experimental alloys suffered a rapid initial loss in load which diminished with time. This loss in load increased with test temperature.

12) LM25 was found to have the best resistance to load loss among the alloys tested from 80°C to 120°C, followed by Supercosmal and then Cosmal. The load loss in ZA alloys was approximately the same with minor differences at 80 and 100°C, but at higher temperature (e.g.120°C) ZA8 had poorer resistance to load loss than ZA27. At this temperature initially ZA12 had the better resistance to load loss than ZA27, but with the passage of time ZA27 improved its relative performance.

13) The retained load could be related by a simple kinetic relationship:

$$P = A - \alpha \ln t$$

or by a power law relationship of the form:

$$P = A\, t^{-\alpha}$$

Where P is retained load after time t. A and α are constants.

14) During load relaxation the experimental alloys behaved in the same order as for compressive creep testing i.e. LM25, Supercosmal, Cosmal, ZA8, ZA12 and ZA27 with the exception of ZA8. Overall, ZA8 was better in compressive creep than ZA12 and ZA27 but showed a worse position in load relaxation.

CHAPTER 8

7.0 SUGGESTIONS FOR FURTHER WORK

1. Under certain conditions of stress and temperature ZA27 changed its creep resistance relative to the other alloys. More work needs to be done at different stresses and temperatures for a better understanding of its compressive creep and load relaxation behaviour.

2. The SEM work on the experimental alloys was carried out to understand creep in terms of their metallographic structures. The metallographic study was carried out on as cast and some tested alloys but more SEM work on creep specimens would be useful to understand the creep mechanisms involved in the alloys (especially in high damping capacity alloys) more clearly at high temperature and low stress.

3. Casting conditions determine the detailed microstructure of as-cast alloys, so the effect of different casting procedures on creep should be examined.

4) A preliminary equation for load relaxation was derived but a more detailed study in this field may give a better theoretical expression for load relaxation.

REFERENCES

1. Engineering Properties of Zinc Alloys. *Lead Zinc Research Organisation Inc., 3rd Ed., New York, 1988.*

2. **Sully A.H.** Metallic Creep and Creep Resistant Alloys. London, *1949.*

3. Characterisation of high temperature materials. *The Institute of Metals, 1988.*

4. **Dowling N.E.** Mechanical Behaviour of Materials. *Prentice-Hall Int., Inc., New Jersey, 1993.*

5. **Conrad H.** Mechanical Behaviour of Materials at Elevated Temperatures. *Editor : Dorn J.E., McGraw-Hill Book Company, Inc., New York, 1961.*

6. **Tweeddale J.G.** Materials Technology. *Vol. 1, Butterworths & Co. Ltd., London, 1973.*

7. **Sully A.H.** Creep Testing in Compression for Simple Creep Assessment. *Product Engineering, Vol. 24, 150-153, 1953.*

8. **Oding I.A., Ivanova V.S., Burdukskii V.V. and Geminov, V.N.** Creep and Stress Relaxation in Metals. *English Editor : Kennedy A.J. 1st Edition, Oliver and Boyd, London, 1965.*

9. **Weertman J. and Weertman J.R.** Physical Metallurgy, Part II. *Editors : Cahn R.W. and Haasen P., North-Holland Physics Publishing, Amsterdam, 1983.*

10. **Smallman R.E.** Modern Physical Metallurgy. *3rd Edition, Butterworth & Co. Ltd., Scotland, 1970.*

11. **Greenfield P.** Creep of Metals at High Temperatures, *Mills & Boon Ltd., London, 1972.*

12. **Garofalo F.** Fundamentals of Creep and Creep-Rupture in Metals. *The MacMillan Company, New York, 1965.*

13. **Ahmadieh A. and Mukherjee A.K.** Stress-Temperature-Time Correlation for High Temperature Creep Curves. *Mat. Sci. & Eng., Vol. 21, 115-124, 1975.*

14. **Weertman J.** Theory of Steady State Creep Based on Dislocation Climb. *J. Applied Physics, Vol. 26, 1213-1217, 1955.*

15. **Mukherjee A.K., Bird J.E. and Dorn J.E.** Experimental Correlations for High Temperature Creep. *Trans. ASM, Vol. 62, 155-179, 1969.*

16. **Weertman J.** Steady State Creep Through Dislocation Climb. *J. Applied Physics, Vol. 28, 362-364, 1957.*

17. **Lagneborg R.** Dislocation Mechanisms in Creep. *Int. Metall. Rev., Vol. 17, 130-146, 1972.*

18. **Evans R.W. and Wilshire B.** Creep of Metals and Alloys. *The Inst. of Metals, London, 1985.*

19. **Weertman J.** Dislocation Climb Theory of Steady State Creep. *Trans. ASM, Vol. 61, 681-694, 1968.*

20. **Weertman J.** Creep of Indium, Lead and Some Other Alloys with Various Metals. *Trans. Metall. Soc., AIME, Vol. 218, 207-218, 1960.*

21. **Mohamed F.A. and Langdon T.G.** The Transition from Dislocation Climb to Viscous Glide in Creep of Solid Solution Alloys. *Acta Metall., Vol. 22, 779-788, 1974.*

22. **Murty K.L., Mohamed F.A. and Dorn J.E.** Viscous Glide, Dislocation Climb and Newtonian Viscous Deformation Mechanisms of High Temperature Creep in Al-3Mg. *Acta Metall., Vol. 20, 1009-1018, 1972.*

23. **Lagneborg R.** Creep and Fatigue in High Temperature Alloys. *Editor : Bressers J., Applied Science Publishers Ltd., London, 1981.*

24. **Sellars C.M. and Quarrell A.G.** The High Temperature Creep of Gold-Nickel Alloys. *J. Inst. Met., Vol. 90, 329-336, 1961-62.*

25. **Nix W.D. and Barrett C.R.** A Model for Steady State Creep Based on the Motion of Jogged Screw Dislocations. *Acta Metall., Vol. 13, 1247-1258, 1965.*

26. **Holmes J.J.** Diffusion Controlled Motion of Jogged Screw Dislocations. *Acta Metall., Vol. 15, 570-571, 1967.*

27. **Gibbs G.B.** Diffusion Controlled Motion of Jogged Screw Dislocations. *Scripta Metall., Vol. 1, 135-137, 1967.*

28. **McLean D.** The Physics of High Temperature Creep in Metals. *Reports on Progress in Physics, Vol. 29, 1-33, 1969.*

29. **Lagneborg R.** Development and Refinement of the Recovery Creep Theory. *Met. Sci. J., Vol. 3, 161-168, 1969.*

30. **Lagneborg R.** A Modified Recovery Creep Model and its Evaluation. *Met. Sci. J., Vol. 6, 127-133, 1972.*

31. **Barrett C.R., Ahlquist C.N. and Nix W.D.** Interpretation of the Recovery/Work-Hardening Model of Creep. *Met. Sci. J., Vol. 4, 41-46, 1970.*

32. **Nabarro F.R.N.** Deformation of Crystals by the Motion of Single Ions. *Report of a Conference on the Strength of Solids. Phy. Soc., 75-90, London, 1948.*

33. **Herring C.** Diffusional Viscosity of a Polycrystalline Solid. *J. Applied Physics, Vol. 21, 437-445, 1950.*

34. **Coble R.L.** A Model for Boundary Diffusion Controlled Creep in Polycrystalline Materials. *J. Applied Physics, Vol. 34, 1679-1682, 1963.*

35. **Burton B. and Greenwood G.W.** Analysis of Coble Creep in Cylindrical and Cubic Crystals. *Mat. Sci. & Technology, Vol. 1, 1029-1032, Dec. 1985.*

36. **Ansell G.S. and Weertman J.** Creep of a Dispersion-Hardened Aluminium Alloy. *Trans. Metall. Soc., AIME, Vol. 215, 838-843, 1959.*

37. **Lagneborg R.** Recovery Creep in Materials Hardened by a Second Phase. *J. Mat. Sci., Vol. 3, 596-602, 1968.*

38. **Urie V.M. and Wain H.L.** Plastic Deformation of Coarse-Grained Aluminium. *J. Inst. of Metals, Vol. 81, 153-159, 1952-53.*

39. **Carreker R.P. and Hibbard W.R.** Tensile Deformation of High-Purity Copper as a Function of Temperature, Strain Rate, and Grain Size. *Acta Metall., Vol. 1, 654-663, 1953.*

40. **Hanson D. and Wheeler M.A.** The Deformation of Metals under Prolonged Loading. Part1.- The Flow and Fracture of Aluminium. *J. Inst. of Metals, Vol. 45, 229-257, 1931.*

41. **McLean D. and Farmer M.H.** The Relation During Creep between Grain Boundary Sliding, Sub-Crystal Size, and Extension. *J. Inst. of Metals, Vol. 85, 41-50, 1956-57.*

42. **Weinberg F.** Grain Boundary Shear in Aluminium. *Trans. AIME, Vol. 212, 808-817, 1958.*

43. **Rhines F.N., Bond W.E. and Kissel M.A.** Grain Boundary Creep in Aluminium Bicrystals. *Trans. ASM, Vol. 48, 919-945, 1956.*

44. **Tung S.K. and Maddin R.** Shear Along Grain Boundaries in Aluminium Bicrystals. *Trans. AIME, Vol. 209, 905-910, 1957.*

45. **Fazan B., Sherby O.D. and Dorn J.E.** Some Observations on Grain Boundary Shearing During Creep. *Trans. AIME, Vol. 200, 919-922, 1954.*

46. **Suery M. and Mukherjee A.K.** Creep Behaviour of Crystalline Solids. Editors : Wilshire B. and Evans R.W., *Pineridge Press, Swansea, 1985.*

47. **Valiev R.Z. and Kaybyshev O.A.** Mechanism of Superplastic Deformation in a Magnesium Alloy. *Phy. Stat. Sol., Vol. 9, 65-76, 1977.*

48. **McLean D.** Grain Boundary Slip During Creep of Aluminium. *J. Inst. of Metals, Vol. 81, 293-300, 1952-53.*

49. **Harper J.G., Shepard L.A. and Dorn J.E.** Creep of Aluminium under Extremely Small Stresses. *Acta Metall., Vol. 6, 509-518, 1958.*

50. **Martin J.A., Herman M. and Brown N.** Grain Boundary Displacement Vs Grain Deformation as The Rate-Determining Factor in Creep. *Trans. AIME, Vol. 209, 78-81, 1957.*

51. **McLean D. and Farmer M.H.** Grain Boundary Movement, Slip, and Fragmentation During Creep of Aluminium-Copper, Aluminium-Magnesium, and Aluminium-Zinc Alloys. *J. Inst. of Metals, Vol. 83, 1-10, 1954-55.*

52. **Gibbs G.B.** The Sliding Contribution to the Total Strain of a Polycrystalline Aggregate. *Met. Sci., Vol. 11, 65-67, 1977.*

53. **Edington J.W., Melton K.N. and Cutler C.P.** Superplasticity. *Prog. Mat. Sci., Vol. 21, 61-170, 1976.*

54. **Mukherjee A. K.** Deformation Mechanisms in Superplasticity. *Ann. Rev. Mat. Sci., Vol. 9, 191-217, 1979.*

55. **Edington J.W.** Microstructural aspects of superplasticity. *Metall. Trans. Vol.13A, 703-715, 1982.*

56. **Langdon T.G.** The Mechanical Properties of Superplastic Materials. *Metall. Trans., Vol. 13A, 689-701, 1982.*

57. **Chaudhari P.** Deformation Behaviour of Superplastic Zn-Al Alloys. *Acta. Metall., Vol. 15, 1777-1786, 1967.*

58. **Farghalli A.M., Mohamed M.I.A. and Langdon T.G.** Factors Influencing Ductility in the Superplastic Zn - 22% Al Eutectoid. *Metall. Trans., Vol. 8A, 933-938, 1977.*

59. **Arieli A., Yu A.K.S. and Mukherjee A.K.** Low Stress and Superplastic Creep Behaviour of Zn - 22% Al Eutectoid *Metall. Trans., Vol. 11A, 181-191 1982.*

60. **Livesey D.W. and Ridley N.** Investigation of Stress-Strain Rate Curve at Low Strain Rates for Superplastic Zn - 22% Al Alloy. *Scripta Metall., Vol 16, 165-168, 1982.*

61. **Keybyshev O.A., Kazachkov I.V. and Rodionov B.V.** Influence of Structure and Composition on the Superplasticity of Zinc-Aluminium Alloys. *Fiz. Metal Metalloved., Vol. 39, No. 2, 338-346, 1975.*

62. **Cook R.C. and Risebrough N.R.** *Superplasticity in Dilute Zinc-Aluminium Alloy. Scripta Metall., Vol. 2, 487-490, 1968.*

63. **Surey M. and Mukherjee A.K. Superplasticity** Correlation Between Structure and Properties, Creep Behaviour of Crystalline Solids. *Editors: Wilshire B. and Evans R.W., Vol. 3 in the Series Progress in Creep and Fracture, 137-200 Pinerigde Press, Swansea, 1985.*

64. **Chen I.W.** Migration Assisted Diffusional Creep by Grain Boundary Diffusion. *Acta Metall., Vol. 30, 1317-1323, 1985.*

65. **Ashby M.F. and Verrall R.A.** Diffusion Accommodated Flow and Superplasticity. *Acta Metall., Vol. 21, 149-163, 1973.*

66. **Novikov I.I., Portnoy V.K. and Levchenko V.J.** Investigation of Structural Changes During Superplastic Deformation of Zn - 22% Al Alloy by Replica Locating Technique . *Acta Metall., Vol. 29, 1077-1090, 1981.*

67. **Shariat D., Vastava R.B. and Langelo T.g.** An Evaluation of the Roles of Intercrystalline and Interphase Boundary Sliding in Two-Phase Superplastic Alloys. *Acta Metall., Vol. 30, 285-296, 1982.*

68. **Sherby O.D. and Burke P.M.** Mechanical Behaviour of Crystalline Solids at Elevated Temperatures. *Prog. Mat. Sci., Vol. 13, 325-390, 1966-67.*

69. **Garofalo F.** An Empirical Relation Defining the Stress Dependence of Minimum Creep Rate in Metals. *Trans. AIME, Vol. 227, 351-356, 1963.*

70. **Blum W. and Reppich B.** Creep Behaviour of Crystalline Solids. *Editors : Wilshire B. and Evans R.W., Pineridge Press, Swansea, 1985.*

71. **Horiuchi R. and Otsuka M.** Mechanism of High Temperature Creep of Aluminium-Magnesium Solid Solution Alloys. *Trans. Jap. Inst. Metals, Vol. 13, 284-293, 1972.*

72. **Evans W.J. and Harrison G.F.** The Development of a Universal Equation for Secondary Creep Rates in Pure Metals and Engineering Alloys. *Met. Sci., Vol. 10, 307-313, 1976.*

73. **Haung H.I.L., Sherby O.D. and Dorn J.E.** Activation Energy for High Temperature Creep of High Purity Aluminium. *Trans. AIME, Vol. 206, 1385-1388, 1956.*

74. **Tietz T.E. and Dorn J.E.** Creep of Copper at Intermediate Temperatures. *Trans. AIME, Vol. 206, 156-162, 1956.*

75. **Sherby O.D., Lytton J.L. and Dorn J.E.** Activation Energies for Creep of High-Purity Aluminium. *Acta Metall., Vol. 5, 219-227, 1957.*

76. **Garofalo F., Richmond O., Domis W.F. and Gemmingen F.V.** Strain-Time, Rate-Stress and Rate-Temperature Relations During Large Deformations in Creep. *Joint Int. Conf. on Creep. The Inst. of Mech. Eng., London, 1963.*

77. **Howard E.M., Barmore W.C., Mote J.D. and Dorn J.E.** On the Thermally-Activated Mechanism of Prismatic Slip in the Silver-Aluminium Hexagonal Intermediate Phase. *Trans. AIME, Vol. 227, 1061-1068, 1963.*

78. **Poirier J.P.** Is Power-Law Creep Diffusion-Controlled? *Acta Metall., Vol. 26, 629-637, 1978.*

79. **Wachtman J.B.J.** Creep and Recovery. *American Society for Metals, Cleveland, 1957.*

80. **Brinson G. and Argent B.B.** The Creep of Niobium. *J. Inst. of Metals, Vol. 91, 293-298, 1962-63.*

81. **Davies P.W., Dennison J.P. and Evans R.W.** The High-Temperature Creep and Fracture of Polycrystalline Gold. *J. Inst. Metals, Vol. 92, 409-412, 1963-64.*

82. **Conway J.B. and Mullikin M.J.** Techniques for Analyzing Combined First- and Second-Stage Creep Data. *Trans. Met. Soc. AIME, Vol. 236, 1629-1632, 1966.*

83. **Evans W.J. and Wilshire B.** Transient and Steady-State Creep Behaviour of a

Copper-15at.- % Aluminium Alloy. *Met. Sci. J., Vol. 4, 89-94, 1970.*

84. **Sidey D. and Wilshire B.** Mechanisms of Creep and Recovery in Nimonic 80A. *Met. Sci. J., Vol. 3, 56-60, 1969.*

85. **Evans W.J. and Wilshire B.** Transient and Steady-State Creep Behaviour of Nickel, Zinc, and Iron. *Trans. Met. Soc. AIME, Vol. 242, 1303-1307, 1968.*

86. **Davies P.W., Evans W.J., Williams K.R. and Wilshire B.** An Equation To Represent Strain/Time Relationships During High Temperature Creep. *Scripta Metall., Vol. 3, 671-674, 1969.*

87. **Evans W.J. and Wilshire B.** The High Temperature Creep and Fracture Behaviour of 70-30 Alpha-Brass. *Met. Trans., Vol. 1, 2133-2139, 1970.*

88. **Evans R.W., Parker J.D. and Wilshire B.** Recent Advances in Creep and Fracture of Engineering Materials and Structures. *Editors : Wilshire B. and Owen D.R.T., Pineridge Press, Swansea, 1982.*

89. **Evans R.W., Beden I. and Wilshire B.** Proc. 2nd. Int. Conf. on Creep and Fracture of Engineering Materials and Structures. *Editors : Wilshire B. and Owen D.R.T., Pineridge Press, Swansea, 1984.*

90. **Evans R.W. and Wilshire B.** Proc. 3rd. Int. Conf. on Creep and Fracture of Engineering Materials and Structures. *Editors : Wilshire B. and* Evans R.W., *Pineridge Press, Swansea, 1987.*

91. **Murray J.L.** The Al-Zn System. *Bulletin of Alloy Phase Diagrams, Vol. 4, No. 1, 55-73, 1983.*

92. **Hanson D. and Gayler M.L.V.** Further Study of the Alloys of Aluminium and Zinc. *J. Inst. Metals, Vol. 27, 267-306, 1922.*

93. **Tanabe T.** Studies in the Aluminium-Zinc System. *J. Inst. Metals, Vol. 32, 415-453, 1924.*

94. **Isihara T.** On the Equilibrium Diagram of the Aluminium-Zinc System. *J. Inst. Metals, Vol. 33, 73-90, 1925.*

95. **Owen E.A. and Pickup L.** X-ray Study of Aluminium-Zinc Alloys at Elevated Temperatures. *Phil. Mag., Vol. 20, 761-777, 1935.*

96. **Ellwood E.C.** An X-ray Study of the Constitution of Aluminium-Zinc Alloys of High Purity Above 275°C, with a Description of a New High Temperature X-ray

Camera. *J. Inst. Metals, Vol. 66, 87-96, 1940.*

97. **Ellwood E.C.** The Solid Solutions of Zinc in Aluminium. *J. Inst. Metals, Vol. 80, 217-224, 1951-52.*

98. **Fink W.L. and Willey L.A.** Equilibrium Relations in Aluminium-Zinc Alloys of High Purity, II. *Trans. Amer. Inst. Min. Met. Eng., Vol. 122, 244-265, 1936.*

99. **Gayler M.L.V. and Sutherland E.G.** The Constitution of Aluminium-Zinc Alloys of High Purity, the Nature of the Thermal Change at 443°C. *J. Inst. Metals, Vol. 63, 123-147, 1938.*

100. **Hansen M. and Anderko K.** Constitution of Binary Alloys. *2nd. Ed., McGraw Hill Book Company Inc., USA, 1958.*

101. **Presnyakov A.A., Gorban Yu A. and Chervyakova V.V.** The Aluminium-Zinc Phase Diagram. *Russian Journal of Physical Chemistry, Vol. 35, No. 6, 632-633, 1961.*

102. **Goldak G.R. and Parr J.G.** A High Temperature X-ray Diffractometer Study of the Zinc-Aluminium System in the Region 40-75 wt. % Zinc. *J. Inst. Metals, Vol. 92, 230-233, 1963-64.*

103. **Mondolfo L.F.** Aluminium Alloys - Structure and Properties. *Butterworth, London, 1976.*

104. **Greaves R.H. and Wrighton H.** Practical Microscopical Metallography. 4th Ed., *Chapman & Hall, London, 1957.*

105. **Pearson W.B.** A Handbook of the Lattice Spacings and Structures of Metals and Alloys. *Vol. 2, Pergamon Press, London, 1967.*

106. **Metal s Handbook.** Phase Diagrams of Binary Alloy Systems. *8th Ed., Vol. 8, American Society for Metals, Ohio, 1973.*

107. **Naziri H. and Pearce R.** The Influence of Copper Additions on the Superplastic Forming Behaviour of the Zn-Al Eutectoid. *Inst. J.Mech. Sci., Vol. 12, 513-521, 1970.*

108. **Nuttall K.** Effect of Some Ternary Additions on the Mechanical Properties of the Zn-Al Eutectoid Alloy. *J. Inst. Metals, Vol. 101, 329-333, 1973.*

109. **Mulvania L.E., Weltzin R.D. and Talcott P.A.** A Superplastic Zn-Al Alloy

with Creep Resistance. *Met. Eng. Quarterly, Vol. 14, 55-60, 1974.*

110. **Savaskan T.** The Structure and Properties of Zinc-Aluminium Based Bearing Alloys. *Ph.D. Thesis, The University of Aston in Birmingham, 1980.*

111. **Savaskan T. and Murphy S.** Creep Behaviuor of Zn-Al-Cu Bearing Alloys. *Z. Metallkunde, Vol. 74, 76-82, 1983.*

112. **Murphy S., Savaskan T. and Hill J.** The Creep Kinetics of Zinc-Aluminium Based Alloys. *Presented at 24th Ann. Conf. Of Metallurgists, CIM, Vancouver, Canada, 1985.*

113. **Mae Y. and Sakono-oka A.** New Die Casting Alloys With High Damping Capacity. *Metall. Soc. AIME, Paper No. A85-18, 1985.*

114. **Gervais E., Levert H. and Bess M.** Development of a Family of Zinc Based Foundry Alloys. *Presented at the 84th Casting Congress and Exposition, and Published in the Transactions of the American Foundrymen's Society, St. Louis, Missouri, U.S.A., April 21-25, 1980.*

115. **Loong C.A., Gervais E. and Lefebvre M.** Properties and Die-Casting ZA Alloys. *Trans. 13th SDCE Int. Die-Casting Congress and Exposition, Paper No. G-T85-055, June 3-6, Milwaukee, USA, 1985.*

116. **Apelian D., Paliwal M. and Herrschart D.C.** Casting with Zinc Alloys. *J. Metals, Vol. 33, 12-20, Nov. 1981.*

117. **Calayag T. and Ferres D.** High Performance High Aluminium Zinc Alloys for Low Speed Bearings and Bushings. *SAE Technical Paper Series, Earthmoving Industry Conf., Peoria, Illinois, April 19-21, 1982.*

118. Mazak Zinc Alloys for Pressure Die-Castings. *A Booklet for Designers, Mazak Ltd., Bristol, U.K., 1972.*

119. **Balliett R.W.** Mechanical Properties of Creep Resistant Zinc Die-Casting Alloys. *Paper No. G575-OB, 8th SDCH Int. Die-Casting Exposition and Congress, Detroit, Michigan, March 17-20, 1975.*

120. **Rennhack E.H. and Conard G.P.** Creep Deformation of Rolled Zn-Ti Alloys. *Trans. Metall. Soc. AIME, Vol. 236, 1441-1444, 1966.*

121. **Rennhack E.H. and Conard G.P.** Structural Aspects of Fibering in Rolled Zn-Ti Alloys and their Relation to Creep. *Trans. Metall. Soc. AIME, Vol. 236, 1441-1444, 1966.*

122. **Murphy S., Hill J. and Durman M.** Creep Behaviour of Commercial Pressure Die Cast Zinc Alloys. *Presented at 12th Int. Pressure Diecaster Conf., Florence, Italy, 1987.*

123. **Loong C.A.** Temperature and Ageing and Thickness Effects on Die-Casting Alloys. *Proc. 25th CIM Conf., 157-170, Toronto, Canada, 1986.*

124. **Durman M.** The Creep Behaviour of Pressure Die Cast Zinc-Aluminium Based Alloys. *Ph.D. Thesis, The University of Aston in Birmingham, 1989.*

125. **Hanna M.D., Carter J.T. and Rashid M.S.** Sliding Wear and Friction Characteristics of Six Zn-Based Die-Casting Alloys. *Wear 203-204, 11-21, 1997.*

126. **Hanna M.D. and Rashid M.S.** ACuZinc: Improved Zinc Alloys for Die Casting Applications. *SAE Technical Paper Series, International Congress and Exposition, Detroit, Michigan, March 1-5, 1993.*

127. Stress Relaxation Testing. Editor: Fox A., *ASTM Special Technical Publication 676, A Symposium Sponsored by ASTM, Kansas City, Mo., 24-25 May, 1979.*

128. **Johnson A.E.** Creep and Relaxation of Metals at High Temperatures. *Engineering, Vol. 168, 237-239, 1949.*

129. **Henderson J. and Ferguson F.R.** Creep Relaxation in Components. *NEL Report No. 625, Glasgow, Nov. 1976.*

130. **Solberg J.K. and Thon H.** Stress Relaxation and Creep of Some Aluminium Alloys. *Mat. Sci. & Eng., Vol. 75, 105-116, 1985.*

131. **Murphy S. and Haines C.W.** Preload Relaxation of Threaded Fasteners in Zinc Alloy Pressure Die Castings. *Advances in Science, Technology and Applications of Zn-Al Alloys, Edited by: Villasenor G.T., Zhu Y.H. and Pina C., Mexico, 1994.*

132. **Murphy S. and Goodwin F.E.** Preload Relaxation of Steel Fasteners in Zinc Alloy Pressure Die Castings - Some Engineering Solutions. *SAE Technical Paper Series, International Congress and Exposition, Detroit, Michigan, Feb. 26-29, 1996.*

133. **Shirn G.A., and Wajda E.S. and Huntington N.B.** Self Diffusion in Zinc. *Acta Metall., Vol. 1, 515-518, 1953.*

134. **Hilliard J.E., Averbach B.L. and Cohen M.** Self and Inter Diffusion in Al-Zn Alloys. *Acta Metall., Vol. 7, 86-92, 1959.*

135. **Sherby O.D. and Tegart W.J.M.** Activation Energies for High Temperature Creep of Polycrystalline Zinc. *Phil. Mag., Vol. 5, 1287-1296, 1985.*

136. **Sherby O.D., Orr R.L and Dorne J.E.** Creep Correlation of Metals at Elevated Temperatures. *Trans. AIME, J. Metals, Vol. 200, 71-80, 1954.*

137. **Flinn J.E and Munson D.E.** Stress-Dependence of the Transition Behaviour in Multi-Mechanism Creep Reactions: with Special Reference to Zinc. *Phil. Mag., Vol. 11, 861-870, 1967.*

138. **Murphy S., Durman M. and Hill J.** Kinetics of Creep in Pressure Diecast Commercial Zinc-Aluminium Alloys. Z. Metallkunde, Vol. 79, 243-247, 1988.

139. **Mott, N.F.,** *Phil. Magzine Vol. 43, 1151, 1952; Vol. 44, 741, 1953.*

140. **Crossland I.G. and Jones R.B.** Dislocation Creep in Magnesium. *Met. Sci. J., Vol. 6, 162-166, 1972.*

APPENDICES

APPENDIX A

CREEP TEST DATA OF THE ALLOYS ZA8, ZA12, ZA27, COSMAL AND SUPERCOSMAL

Creep Test Data of Alloy ZA8 at 160°C

Stress (MPa)	Primary Creep %	Secondary Creep Rate (%/s)	Time to 0.2% Creep Strain (s)	Time to 0.4% Creep Strain (s)	Time to 0.6% Creep Strain (s)	Time to 0.8% Creep Strain (s)	Time to 1.0% Creep Strain (s)
100	0.55	1.24×10^{-2}	-	-	18	27	40
100	0.4	1.25×10^{-2}	-	-	22	34	48
60	0.38	1.24×10^{-3}	15	77	190	350	510
60	0.36	9.40×10^{-4}	60	105	280	490	700
40	0.61	9.08×10^{-5}	70	440	1200	2580	4680
40	0.5	1.64×10^{-4}	60	380	990	2040	3480
20	0.29	8.91×10^{-6}	1860	14880	34680	57280	81480
20	0.4	8.20×10^{-6}	780	8580	23880	45480	74280

Creep Test Data of Alloy ZA8 at 130°C

Stress (MPa)	Primary Creep %	Secondary Creep Rate (%/s)	Time to 0.2% Creep Strain (s)	Time to 0.4% Creep Strain (s)	Time to 0.6% Creep Strain (s)	Time to 0.8% Creep Strain (s)	Time to 1.0% Creep Strain (s)
100	0.44	1.14×10^{-3}	13	35	150	325	510
100	0.63	8.53×10^{-4}	-	35	120	280	460
60	0.56	1.07×10^{-4}	15	30	780	2380	4380
60	0.57	1.25×10^{-4}	15	100	780	1980	3480
40	0.33	1.81×10^{-5}	15	3180	12480	23880	36680
40	0.35	1.79×10^{-5}	180	5180	14880	25680	38280
20	0.36	1.54×10^{-6}	22080	85880	109480	201080	437480
20	0.43	7.37×10^{-7}	14880	95880	257880	949080	776280

Creep Test Data of Alloy ZA8 at 100°C

Stress (MPa)	Primary Creep %	Secondary Creep Rate (%/sec)	Time to 0.2% Creep Strain (s)	Time to 0.4% Creep Strain (s)	Time to 0.6% Creep Strain (s)	Time to 0.8% Creep Strain (s)	Time to 1.0% Creep Strain (s)
100	0.59	8.36×10^{-5}	-	90	780	2580	4980
100	0.45	8.75×10^{-5}	70	600	1860	3780	6780
100	0.62	8.47×10^{-5}	-	80	700	2220	4600
60	0.48	8.12×10^{-6}	10	2680	16780	39280	63680
60	0.46	8.51×10^{-6}	25	4780	18680	40080	63580
40	0.25	1.18×10^{-6}	27480	142680	297480	477880	671880
40	0.42	9.60×10^{-7}	6780	70680	193080	369480	661080
20	-	-	247080	-	-	-	-
20	-	-	1498080	-	-	-	-

Creep Test Data of Alloy ZA8 at 70°C

Stress (MPa)	Primary Creep %	Secondary Creep Rate (%/sec)	Time to 0.2% Creep Strain (s)	Time to 0.4% Creep Strain (s)	Time to 0.6% Creep Strain (s)	Time to 0.8% Creep Strain (s)	Time to 1.0% Creep Strain (s)
100	0.56	3.03×10^{-6}	13	5580	38280	86080	149880
100	0.51	2.69×10^{-6}	18	9480	59880	106680	182280
60	0.47	2.14×10^{-7}	4680	153480	527880	1319880	1794080
60	0.52	1.72×10^{-7}	16680	171480	555880	1597080	2545980
40	-	-	200280	-	-	-	-
40	-	-	88680	-	-	-	-

Creep Test Data of Alloy ZA12 at 160°C

Stress (MPa)	Primary Creep %	Secondary Creep Rate (%/s)	Time to 0.2% Creep Strain (s)	Time to 0.4% Creep Strain (s)	Time to 0.6% Creep Strain (s)	Time to 0.8% Creep Strain (s)	Time to 1.0% Creep Strain (s)
100	0.4	1.52×10^{-2}	-	-	17	27	38
100	0.51	1.69×10^{-2}	-	-	16	23	32
100	0.65	1.47×10^{-2}	-	-	11	17	25
60	0.52	1.09×10^{-3}	-	45	130	260	440
60	0.36	1.14×10^{-3}	-	75	240	420	600
40	0.36	1.72×10^{-4}	90	660	1500	2580	3780
40	0.359	2.81×10^{-4}	28	320	930	6120	2580
20	0.18	3.02×10^{-5}	1680	7680	14880	20280	27480
20	0.21	1.34×10^{-5}	3780	14880	31080	45480	59880

Creep Test Data of Alloy ZA12 at 130°C

Stress (MPa)	Primary Creep %	Secondary Creep Rate (%/s)	Time to 0.2% Creep Strain (s)	Time to 0.4% Creep Strain (s)	Time to 0.6% Creep Strain (s)	Time to 0.8% Creep Strain (s)	Time to 1.0% Creep Strain (s)
100	0.69	1.50×10^{-3}	-	13	45	115	220
100	0.72	8.10×10^{-4}	-	15	60	175	360
100	0.61	9.93×10^{-4}	-	40	125	260	440
60	0.66	1.09×10^{-4}	-	90	570	1680	3180
60	0.42	1.61×10^{-4}	-	300	1200	2400	3780
40	0.4	2.04×10^{-5}	90	3180	10380	20280	31080
40	0.39	2.01×10^{-5}	100	3180	10480	20080	30480
20	0.35	1.46×10^{-6}	14880	81480	182280	304680	448680
20	0.37	1.39×10^{-6}	16680	85080	189480	311880	455880
20	0.41	1.55×10^{-6}	11280	59880	139080	277080	380080

Creep Test Data of Alloy ZA12 at 100°C

Stress (MPa)	Primary Creep %	Secondary Creep Rate (%/s)	Time to 0.2% Creep Strain (s)	Time to 0.4% Creep Strain (s)	Time to 0.6% Creep Strain (s)	Time to 0.8% Creep Strain (s)	Time to 1.0% Creep Strain (s)
100	0.62	1.03×10^{-4}	-	120	780	2100	3780
100	0.87	6.20×10^{-5}	-	80	600	1150	2110
100	0.48	9.00×10^{-5}	100	870	2160	4080	5880
60	0.65	8.42×10^{-6}	-	110	5280	18480	41480
60	0.48	1.16×10^{-5}	-	2280	12180	28480	45480
40	0.51	1.42×10^{-6}	4380	38280	117480	221880	347880
40	0.44	2.03×10^{-6}	3480	34680	95880	182280	279480
20	-	-	45480	-	-	-	-
20	-	-	45480	283080	-	-	-

Creep Test Data of Alloy ZA12 at 70°C

Stress (MPa)	Primary Creep %	Secondary Creep Rate (%/s)	Time to 0.2% Creep Strain (s)	Time to 0.4% Creep Strain (s)	Time to 0.6% Creep Strain (s)	Time to 0.8% Creep Strain (s)	Time to 1.0% Creep Strain (s)
100	0.6	3.43×10^{-6}	-	2880	24880	65480	117480
100	0.63	3.01×10^{-6}	-	3780	25680	74280	128280
60	0.51	4.56×10^{-7}	8580	128280	376680	718680	1071480
60	0.56	3.97×10^{-7}	11280	146280	401880	740280	1100280

Creep Test Data of Alloy ZA27 at 160°C

Stress (MPa)	Primary Creep %	Secondary Creep Rate (%/s)	Time to 0.2% Creep Strain (s)	Time to 0.4% Creep Strain (s)	Time to 0.6% Creep Strain (s)	Time to 0.8% Creep Strain (s)	Time to 1.0% Creep Strain (s)
100	0.44	6.85×10^{-3}	-	-	12	50	80
100	0.65	5.53×10^{-3}	-	-	-	45	70
100	0.58	8.90×10^{-3}	-	5	20	35	55
100	0.72	8.10×10^{-3}	-	-	15	30	50
60	0.86	2.02×10^{-3}	-	27	52	95	160
60	0.5	9.31×10^{-4}	-	45	165	330	520
40	0.73	5.43×10^{-4}	20	85	220	420	660
40	0.66	6.34×10^{-4}	10	80	230	450	720
40	0.61	2.35×10^{-4}	80	410	780	1200	1680
20	0.6	9.33×10^{-6}	1050	5880	13880	27480	45480
20	1.2	2.60×10^{-5}	140	990	2880	5280	8580
20	0.67	1.61×10^{-5}	320	2580	6780	13080	22080

Creep Test Data of Alloy ZA27 at 130° C

Stress (MPa)	Primary Creep %	Secondary Creep Rate (%/s)	Time to 0.2% Creep Strain (s)	Time to 0.4% Creep Strain (s)	Time to 0.6% Creep Strain (s)	Time to 0.8% Creep Strain (s)	Time to 1.0% Creep Strain (s)
100	0.52	6.02×10^{-4}	-	46	230	480	810
100	0.85	9.03×10^{-4}	-	10	50	105	220
100	0.84	1.09×10^{-3}	-	25	90	180	300
60	0.72	1.16×10^{-4}	-	41	510	1450	2880
60	0.66	1.86×10^{-4}	12	85	490	1150	1990
40	0.53	7.89×10^{-5}	14	410	1800	3780	6330
40	0.48	3.56×10^{-5}	38	1330	4580	9080	14880
40	0.59	1.02×10^{-4}	10	400	1000	2400	4000
20	0.31	6.53×10^{-6}	2880	18480	45000	77000	106680
20	0.81	4.50×10^{-7}	3480	22080	67080	175080	441480

Creep Test Data of Alloy ZA27 at 100°C

Stress (MPa)	Primary Creep %	Secondary Creep Rate (%/s)	Time to 0.2% Creep Strain (s)	Time to 0.4% Creep Strain (s)	Time to 0.6% Creep Strain (s)	Time to 0.8% Creep Strain (s)	Time to 1.0% Creep Strain (s)
100	0.58	9.75×10^{-5}	-	120	870	2280	4300
100	0.75	6.55×10^{-5}	-	100	760	2160	3900
100	0.97	9.36×10^{-5}	-	25	200	900	2040
60	0.63	2.18×10^{-5}	25	1300	5380	11280	18480
60	0.58	1.48×10^{-5}	12	1380	7480	16680	29480
60	0.54	2.37×10^{-5}	11	1440	5440	11380	19000
40	0.5	3.42×10^{-6}	990	16680	49090	94880	146280
40	0.55	5.75×10^{-6}	320	5880	22080	45480	81480
20	0.52	2.15×10^{-7}	31080	139080	337080	1075080	2216280
20	-	-	20280	175080	794280	-	-

Creep Test Data of Alloy ZA27 at 70°C

Stress (MPa)	Primary Creep %	Secondary Creep Rate (%/s)	Time to 0.2% Creep Strain (s)	Time to 0.4% Creep Strain (s)	Time to 0.6% Creep Strain (s)	Time to 0.8% Creep Strain (s)	Time to 1.0% Creep Strain (s)
100	0.66	3.511×10^{-6}	16	3180	25680	65480	110280
100	0.65	3.68×10^{-6}	12	2220	18480	38280	92280
60	0.62	1.00×10^{-6}	510	27480	103080	225480	445880
60	0.5	3.68×10^{-7}	1840	301080	477480	592680	729480

Creep Test Data of Alloy Cosmal at 160°C

Stress (MPa)	Primary Creep %	Secondary Creep Rate (%/s)	Time to 0.2% Creep Strain (s)	Time to 0.4% Creep Strain (s)	Time to 0.6% Creep Strain (s)	Time to 0.8% Creep Strain (s)	Time to 1.0% Creep Strain (s)
100	0.51	1.53×10^{-3}	-	-	60	190	320
100	0.68	2.82×10^{-3}	-	-	30	70	120
100	0.58	1.18×10^{-3}	-	22	95	220	370
60	0.81	1.12×10^{-4}	12	148	735	1810	2980
60	0.51	2.83×10^{-4}	12	90	280	850	1870
60	0.58	2.64×10^{-4}	-	70	360	900	1600
40	0.71	3.09×10^{-5}	210	1200	3280	6780	11280
40	0.86	3.23×10^{-5}	-	220	1200	3180	6780
40	0.62	1.55×10^{-5}	220	2220	7680	14880	25680
20	0.88	1.52×10^{-7}	4980	85080	279480	549480	2421747
20	0.76	1.85×10^{-7}	2880	25680	99480	257880	1342440

Creep Test Data of Alloy Cosmal at 130°C

Stress (MPa)	Primary Creep %	Secondary Creep Rate (%/s)	Time to 0.2% Creep Strain (s)	Time to 0.4% Creep Strain (s)	Time to 0.6% Creep Strain (s)	Time to 0.8% Creep Strain (s)	Time to 1.0% Creep Strain (s)
100	0.61	1.54×10^{-4}	-	55	540	1440	2580
100	0.9	1.75×10^{-4}	-	10	210	415	660
60	0.71	2.43×10^{-5}	-	280	2580	7480	13080
60	0.66	1.77×10^{-5}	12	1020	4880	12000	21080
40	0.49	3.88×10^{-6}	1320	12480	38280	81580	131880
40	0.42	2.87×10^{-6}	460	16780	74280	142680	203880

Creep Test Data of Alloy Cosmal at 100°C

Stress (MPa)	Primary Creep %	Secondary Creep Rate (%/s)	Time to 0.2% Creep Strain (s)	Time to 0.4% Creep Strain (s)	Time to 0.6% Creep Strain (s)	Time to 0.8% Creep Strain (s)	Time to 1.0% Creep Strain (s)
100	0.63	2.56×10^{-5}	-	380	3180	7680	14880
100	0.71	1.54×10^{-5}	-	800	3800	9000	20000
100	0.64	1.84×10^{-5}	-	180	3180	10380	20280
60	0.6	3.84×10^{-6}	15	3180	24000	60180	110280
60	0.61	2.31×10^{-6}	-	4208	29380	120280	168880
60							247780
40	0.38	3.48×10^{-7}	4680	214680	740280	1269480	1795080
40	0.36	2.50×10^{-7}	27480	257880	963480	1766280	2565480

Creep Test Data of Alloy Cosmal at 70°C

Stress (MPa)	Primary Creep %	Secondary Creep Rate (%/s)	Time to 0.2% Creep Strain (s)	Time to 0.4% Creep Strain (s)	Time to 0.6% Creep Strain (s)	Time to 0.8% Creep Strain (s)	Time to 1.0% Creep Strain (s)
100	0.58	1.34×10^{-6}	-	3480	57280	175080	315480
60	-	-	13080	-	-	-	-
40	-	-	886880	-	-	-	-

Creep Test Data of Alloy Supercosmal at 160°C

Stress (MPa)	Primary Creep %	Secondary Creep Rate (%/sec)	Time to 0.2% Creep Strain (s)	Time to 0.4% Creep Strain (s)	Time to 0.6% Creep Strain (s)	Time to 0.8% Creep Strain (s)	Time to 1.0% Creep Strain (s)
100	0.46	3.48×10^{-5}	-	300	4080	9880	16580
100	0.42	2.00×10^{-5}	-	1040	9080	20180	31080
100	0.7	1.28×10^{-5}	-	200	2400	10800	22080
60	0.71	8.25×10^{-7}	4580	35680	96280	185800	355080
60	0.86	5.90×10^{-7}	1050	10380	23880	106680	238080
40	-	-	2220	135480	808680		
20	-	-	153480				

Creep Test Data of Alloy Supercosmal at 130°C

Stress (MPa)	Primary Creep %	Secondary Creep Rate (%/s)	Time to 0.2% Creep Strain (s)	Time to 0.4% Creep Strain (s)	Time to 0.6% Creep Strain (s)	Time to 0.8% Creep Strain (s)	Time to 1.0% Creep Strain (s)
100	0.55	2.40×10^{-6}	10	70	25680	103080	187580
60	-	-	23880	445080	-	-	-
40	-	-	106680	-	-	-	-

APPENDIX B

LOAD RELAXATION DATA OF THE ALLOYS ZA8, ZA12, ZA27, COSMAL, SUPERCOSMAL AND LM25

Load Loss With Time at 80°C

TIME(MIN)	ZA8	ZA12	ZA27	COSMAL	SUPERCOSMAL	LM25
0						
0.5	6147					
1	6014		6015	5888		
1.5	5959		5976	5844	5973	5999
2	5922	5811	5930	5815	5944	5979
2.5	5893	5766	5897	5793	5928	5968
3	5870	5735	5872	5775	5916	5960
3.5	5851	5710	5851	5761	5907	5955
4	5833	5690	5832	5749	5900	5952
4.5	5818	5673	5816	5738	5894	5948
5	5804	5657	5801	5727	5888	5945
5.5	5791	5644	5788	5718	5883	5942
6	5779	5631	5776	5709	5878	5939
6.5	5768	5620	5765	5701	5874	5937
7	5758	5610	5754	5694	5870	5934
7.5	5748	5600	5744	5687	5866	5932
8	5738	5590	5734	5680	5862	5930
8.5	5730	5582	5725	5674	5859	5928
9	5721	5573	5716	5668	5856	5926
9.5	5714	5566	5708	5662	5853	5924
10	5706	5559	5700	5656	5850	5923
11	5692	5544	5686	5646	5844	5919
12	5678	5531	5672	5636	5839	5916
13	5666	5520	5659	5627	5835	5914
14	5655	5508	5647	5619	5830	5912
15	5644	5498	5635	5610	5826	5909
16	5633	5488	5624	5603	5822	5906
17	5624	5478	5613	5596	5819	5904
18	5614	5470	5604	5589	5815	5902
19	5605	5461	5594	5582	5811	5901
20	5596	5453	5585	5576	5808	5898
25	5558	5418	5544	5548	5794	5890
30	5525	5388	5509	5524	5782	5883
35	5496	5361	5478	5502	5772	5877
40	5470	5338	5451	5484	5762	5871
45	5446	5316	5426	5467	5754	5866
50	5425	5297	5403	5452	5746	5862
55	5406	5279	5382	5437	5739	5858
60	5387	5263	5362	5424	5732	5854
65	5369	5247	5344	5411	5726	5850
70	5353	5233	5327	5400	5721	5847

100	5270	5160	5240	5341	5692	5830
130	5203	5102	5170	5296	5670	5818
160	5148	5054	5113	5257	5652	5808
190	5098	5012	5062	5224	5636	5799
220	5055	4974	5019	5195	5622	5792
250	5014	4940	4979	5169	5610	5786
280	4978	4909	4943	5145	5599	5779
310	4944	4880	4910	5123	5589	5774
340	4912	4854	4878	5103	5580	5769
370	4882	4828	4849	5084	5571	5764
430	4827	4780	4796	5049	5554	5756
490	4777	4738	4748	5017	5540	5749
550	4732	4698	4704	4989	5528	5742
610	4689	4662	4665	4964	5516	5736
670	4650	4628	4628	4940	5506	5731
730	4614	4597	4593	4917	5495	5727
790	4579	4567	4562	4897	5486	5722
850	4546	4538	4531	4876	5477	5718
910	4515	4512	4503	4858	5469	5714
970	4486	4487	4476	4840	5461	5710
1090	4432	4440	4426	4807	5447	5703
1210	4383	4397	4380	4777	5433	5698
1330	4337	4357	4338	4750	5421	5693
1450	4295	4320	4299	4724	5410	5687
1570	4256	4287	4263	4700	5399	5682
1690	4219	4255	4229	4676	5389	5678
1810	4185	4226	4196	4655	5380	5674
1930	4152	4198	4166	4635	5372	5670
2050	4122	4171	4137	4616	5363	5667
2170	4092	4145	4109	4597	5355	5663
2410	4038	4098	4058	4563	5340	5657
2650	3989	4056	4012	4531	5326	5651
2890	3943	4016	3969	4503	5315	5646
3130	3902	3980	3930	4476	5303	5642
3370	3863	3948	3892	4450	5292	5637
3610	3827	3916	3857	4427	5281	5634
3850	3793	3886	3824	4404	5271	5630
4090	3761	3859	3793	4382	5261	5626
4330	3730	3833	3765	4363	5253	5623
4570	3702	3807	3737	4344	5244	5620
4810	3675	3785	3710	4326	5236	5617
5050	3648	3762	3685	4308	5228	5614
5290	3624	3741	3660	4291	5220	5611
5530	3600	3720	3637	4275	5213	5608
5770	3577	3701	3615	4260	5206	5608

6010	3556	3682	3594	4246	5199	5606
6250	3535	3664	3573	4231	5193	5604
6490	3515	3646	3554	4218	5186	5601
6730	3496	3629	3534	4204	5180	5599
6970	3477	3613	3516	4191	5174	5597
7210	3459	3598	3498	4178	5167	5595
7450	3441	3583	3481	4167	5162	5593
7690	3425	3568	3463	4155	5156	5592
7930	3408	3553	3447	4144	5150	5590
8170	3393	3539	3431	4132	5145	5588
8410	3377	3526	3416	4122	5139	5585
8650	3362	3513	3401	4111	5134	5584
8890	3347	3500	3386	4102	5129	5583
9130	3333	3489	3372	4092	5125	5581
9370	3320	3476	3359	4082	5120	5579
9610						5578

Load Loss With Time at 100°C

TIME(MIN)	ZA8	ZA12	ZA27	COSMAL	SUPERCOSMAL	LM25
0						
0.5						
1		6031		6005		6055
1.5	5838	5874		5915	5936	6028
2	5738	5797		5867	5903	6012
2.5	5681	5744	5898	5831	5883	6000
3	5637	5704	5804	5804	5869	5992
3.5	5602	5670	5757	5781	5857	5985
4	5574	5641	5722	5761	5846	5979
4.5	5550	5615	5693	5743	5838	5974
5	5528	5591	5669	5726	5829	5968
5.5	5507	5570	5647	5712	5822	5964
6	5488	5552	5627	5698	5816	5960
6.5	5471	5533	5609	5686	5810	5956
7	5455	5517	5592	5674	5804	5953
7.5	5440	5501	5576	5662	5799	5949
8	5426	5487	5561	5652	5793	5946
8.5	5413	5473	5548	5641	5789	5943
9	5400	5460	5535	5632	5784	5940
9.5	5388	5447	5522	5623	5780	5937
10	5377	5435	5510	5614	5776	5935
11	5355	5413	5488	5598	5768	5929
12	5335	5392	5467	5582	5761	5925
13	5316	5372	5447	5568	5755	5921
14	5299	5354	5429	5554	5748	5916
15	5282	5337	5412	5542	5742	5913
16	5267	5321	5395	5530	5737	5910
17	5252	5306	5380	5518	5732	5906
18	5238	5291	5365	5507	5727	5903
19	5225	5277	5351	5496	5721	5900
20	5211	5264	5338	5486	5717	5897
25	5155	5205	5278	5441	5697	5884
30	5106	5155	5226	5403	5680	5873
35	5064	5111	5181	5369	5665	5864
40	5027	5072	5141	5339	5651	5856
45	4992	5037	5105	5312	5639	5849
50	4961	5006	5072	5288	5629	5842
55	4933	4976	5041	5265	5619	5836
60	4906	4949	5013	5243	5610	5831
65	4881	4923	4986	5223	5601	5825

70	4857	4899	4960	5204	5593	5820
100	4739	4779	4833	5110	5553	5797
130	4645	4685	4733	5036	5522	5780
160	4567	4608	4649	4976	5497	5765
190	4500	4541	4578	4925	5476	5753
220	4439	4481	4515	4879	5457	5743
250	4385	4429	4458	4838	5441	5734
280	4336	4381	4407	4801	5426	5727
310	4291	4338	4360	4767	5412	5720
340	4249	4297	4317	4736	5399	5713
370	4209	4259	4277	4707	5388	5707
430	4139	4192	4205	4654	5367	5696
490	4075	4132	4140	4608	5348	5687
550	4018	4078	4082	4566	5331	5678
610	3966	4028	4029	4528	5316	5670
670	3918	3984	3981	4493	5301	5664
730	3873	3942	3936	4461	5289	5658
790	3832	3903	3895	4432	5277	5652
850	3794	3867	3856	4404	5265	5646
910	3757	3833	3820	4378	5255	5642
970	3723	3802	3785	4353	5245	5637
1090	3660	3742	3722	4308	5226	5629
1210	3603	3689	3665	4266	5209	5620
1330	3551	3640	3613	4230	5194	5613
1450	3504	3596	3566	4195	5179	5608
1570	3460	3554	3522	4164	5166	5602
1690	3419	3516	3480	4136	5155	5596
1810	3380	3478	3442	4109	5143	5592
1930	3344	3444	3406	4083	5132	5587
2050	3310	3412	3372	4059	5121	5583
2170	3279	3381	3340	4037	5111	5578
2410	3220	3324	3280	3994	5092	5570
2650	3167	3272	3227	3955	5074	5563
2890	3118	3225	3177	3921	5058	5556
3130	3075	3181	3132	3890	5043	5551
3370	3033	3141	3091	3861	5029	5546
3610	2996	3103	3051	3833	5015	5540
3850	2960	3067	3015	3807	5002	5535
4090	2927	3034	2981	3783	4989	5530
4330	2895	3002	2950	3760	4978	5526
4570	2866	2973	2919	3740	4966	5523
4810	2838	2944	2891	3720	4956	5519
5050	2812	2916	2864	3700	4945	5515
5290	2786	2890	2839	3681	4934	5511
5530	2762	2865	2814	3664	4925	5507

5770	2740	2841	2792	3648	4915	5505
6010	2718	2819	2770	3632	4906	5502
6250	2697	2796	2750	3617	4897	5499
6490	2683	2775	2730	3602	4888	5496
6730	2663	2754	2711	3588	4879	5493
6970	2643	2734	2693	3574	4871	5490
7210	2625	2716	2676	3562	4863	5487
7450	2607	2697	2660	3549	4856	5486
7690	2590	2679	2645	3536	4848	5483
7930	2573	2661	2629	3525	4839	5480
8170	2557	2644	2615	3513	4832	5478
8410	2541	2627	2601	3502	4824	5475
8650	2526	2612	2588	3491	4817	5473
8890	2512	2596	2575	3481	4811	5471
9130	2498	2581	2563	3471	4804	5469
9370	2483	2566	2552	3461	4797	5466
9610	2469	2551	2541	3451	4790	5465

Load Loss With Time at 120°C

TIME(MIN)	ZA8	ZA12	ZA27	COSMAL	SUPERCOSMAL	LM25
0						
0.5						
1	5817	5725				
1.5	5837	5788	5281	5903	5978	
2	5708	5688	5820	5812	5934	5966
2.5	5624	5620	5735	5754	5904	5942
3	5559	5566	5674	5713	5882	5925
3.5	5505	5527	5624	5677	5863	5911
4	5460	5493	5581	5647	5847	5901
4.5	5421	5461	5544	5621	5833	5892
5	5385	5434	5510	5597	5820	5884
5.5	5353	5409	5480	5577	5809	5876
6	5324	5386	5452	5557	5798	5870
6.5	5296	5365	5426	5539	5789	5864
7	5272	5345	5401	5522	5780	5859
7.5	5248	5326	5378	5506	5772	5854
8	5226	5309	5356	5490	5764	5848
8.5	5205	5293	5335	5476	5756	5844
9	5185	5278	5315	5462	5749	5840
9.5	5166	5263	5297	5449	5742	5836
10	5148	5248	5279	5436	5736	5832
11	5114	5222	5245	5413	5724	5825
12	5083	5197	5213	5391	5713	5818
13	5054	5174	5185	5370	5703	5812
14	5028	5153	5156	5350	5694	5807
15	5003	5134	5131	5332	5685	5801
16	4979	5114	5106	5315	5677	5796
17	4956	5096	5083	5298	5669	5792
18	4934	5079	5061	5283	5661	5788
19	4914	5063	5040	5269	5655	5784
20	4894	5047	5020	5254	5647	5780
25	4807	4978	4930	5190	5618	5763
30	4734	4919	4853	5135	5593	5749
35	4670	4868	4787	5088	5571	5737
40	4613	4823	4727	5046	5552	5727
45	4563	4783	4674	5007	5535	5717
50	4517	4747	4625	4972	5519	5709
55	4474	4712	4581	4940	5506	5702
60	4434	4680	4540	4910	5493	5695
65	4397	4651	4501	4882	5481	5689

70	4363	4624	4465	4855	5469	5683
100	4190	4486	4286	4723	5414	5655
130	4057	4379	4149	4621	5372	5635
160	3947	4292	4038	4537	5337	5618
190	3853	4217	3944	4465	5308	5605
220	3771	4150	3862	4402	5282	5593
250	3698	4092	3790	4347	5260	5583
280	3633	4038	3725	4297	5239	5573
310	3573	3990	3667	4252	5221	5565
340	3519	3944	3614	4211	5203	5558
370	3469	3902	3566	4173	5187	5552
430	3379	3826	3479	4104	5159	5539
490	3299	3758	3403	4043	5133	5529
550	3229	3697	3335	3989	5110	5519
610	3166	3641	3275	3941	5089	5511
670	3108	3590	3221	3897	5070	5503
730	3056	3543	3172	3856	5051	5496
790	3007	3498	3126	3819	5035	5490
850	2962	3456	3084	3784	5019	5484
910	2920	3417	3046	3752	5004	5479
970	2881	3381	3009	3721	4990	5473
1090	2810	3312	2944	3666	4963	5464
1210	2746	3250	2887	3616	4940	5455
1330	2690	3194	2836	3572	4917	5447
1450	2638	3141	2790	3530	4896	5440
1570	2590	3093	2749	3493	4876	5434
1690	2547	3048	2711	3458	4857	5428
1810	2507	3005	2677	3427	4838	5422
1930	2470	2966	2646	3397	4821	5417
2050	2435	2929	2617	3369	4805	5412
2170	2402	2894	2591	3342	4789	5407
2410	2342	2829	2543	3294	4758	5398
2650	2289	2771	2502	3250	4730	5390
2890	2241	2718	2466	3211	4703	5384
3130	2197	2671	2435	3175	4678	5377
3370	2157	2626	2406	3142	4653	5371
3610	2119	2586	2380	3111	4631	5365
3850	2085	2548	2356	3083	4609	5360
4090	2057	2513	2335	3055	4588	5355
4330	2026	2480	2314	3030	4568	5350
4570	1998	2450	2296	3007	4549	5346
4810	1971	2420	2278	2985	4530	5342
5050	1945	2394	2262	2963	4512	5337
5290	1921	2368	2247	2943	4496	5334
5530	1899	2343	2232	2924	4479	5330

5770	1877	2321	2218	2906	4464	5327
6010	1859	2298	2206	2889	4448	5323
6250	1840	2277	2193	2872	4434	5320
6490	1821	2257	2182	2856	4420	5317
6730	1803	2238	2170	2841	4407	5314
6970	1787	2220	2160	2826	4394	5311
7210	1771	2203	2150	2812	4381	5308
7450	1755	2186	2140	2799	4370	5305
7690	1741	2176	2131	2786	4358	5303
7930	1725	2159	2122	2773	4347	5300
8170	1715	2143	2114	2760	4336	5298
8410	1701	2127	2105	2748	4326	5295
8650	1688	2113	2097	2737	4316	5293
8890	1676	2099	2090	2727	4306	5291
9130	1663	2085	2082	2715	4297	5289
9370	1651	2073	2075	2704	4288	5287
9610	1639	2060	2067	2694	4279	5284